DEVELOPMENT OF MICROBIAL SYSTEM TO REMEDIATE REINFORCED CONCRETE STRUCTURES

A Thesis

Submitted in fulfilment of the requirements for the award of the degree of

DOCTOR OF PHILOSOPHY

by

Kamal Anand

(Roll No. 901602007)

Under the Guidance of

Dr. Shweta Goyal
Professor
Department of Civil Engineering

Dr. M. Sudhakara Reddy
Professor
Department of Biotechnology

Department of Civil Engineering

Thapar Institute of Engineering and Technology, Patiala-147004

Punjab, India

CERTIFICATE

Certified that the thesis "**Development of microbial system to remediate reinforced concrete structures**" which is submitted by Mr. **Kamal Anand**, in fulfilment of the requirement for the award of the degree of **Doctor of Philosophy** in the Department of Civil Engineering, Thapar Institute of Engineering & Technology, Patiala, is a record of the candidate's own independent and original research work carried out by him under my supervision and guidance. The matter embodied in this thesis has not been submitted in part or full to any other University or Institute for the award of any degree.

Dr. Shweta Goyal
Professor
Department of Civil Engineering
Thapar Institute of Engineering & Technology

Dr. M. Sudhakara Reddy
Professor
Department of Biotechnology
Thapar Institute of Engineering & Technology

DECLARATION

I hereby declare that the work presented in the thesis entitled "**Development of microbial system to remediate reinforced concrete structures**" in the fulfilment of the requirement for the award of the Degree of **Doctor of Philosophy** in the Department of Civil Engineering, Thapar Institute of Engineering & Technology, Patiala, is an authentic record of my own work during the period July 2016 to January 2023, under the supervision of **Dr. Shweta Goyal**, Professor, Department of Civil Engineering, Thapar Institute of Engineering & Technology, Patiala and **Dr. M. Sudhakara Reddy**, Professor, Department of Biotechnology, Thapar Institute of Engineering & Technology, Patiala. The material embodied in this thesis has not been submitted in parts or full in any other university or institute for the award of any degree in India or Abroad.

Place: Patiala
Date: 16-June-2023

Kamal Anand
Department of Civil Engineering
Thapar Institute of Engineering
& Technology

ACKNOWLEDGEMENT

This thesis is the end of my journey in obtaining my PhD, probably the most stimulating activity of my life. It was a long and challenging yet very fulfilling journey that I completed. In pursuit of this academic endeavor, I have been exceptionally fortunate because inspiration, guidance, direction, cooperation, love and care came my way in abundance. I feel nostalgic when I look back on my journey and find it difficult to put into words the never-ending support and encouragement of everyone throughout these years.

First and foremost, I would like to bow to Almighty for blessing me so abundantly, far beyond what I deserve. With a deep gratitude, I acknowledge my PhD Supervisor, Professor Shweta Goyal, Department of Civil Engineering, TIET, Patiala for giving me this wonderful opportunity to be a part of her research team. Her guidance, motivation, enthusiasm and dedication for research rendered to me during my work, without which the present endeavor would not have achieved the same status. Her support and faith in my ability made me strive for excellence and nothing less.

I reckon this opportunity to express my regards and gratitude to my PhD co-supervisor, Professor M. Sudhakara Reddy, Department of Biotechnology, TIET. His valuable suggestions, proficient guidance and advice helped me successfully accomplish this difficult task. His constructive criticism and spirit of striving for excellence is commendable.

I am privileged to thank Prof. Prem Pal Bansal, Professor & Head, Department of Civil Engineering for providing excellent academic and lab facilities. I am thankful to doctoral committee members Dr. Rafat Siddique, Senior Professor & Dean of Research & Development Cell, Dr. N. Tejo Prakash, Professor & Associate Dean of Research & Development Cell and Dr. Heaven Singh, Assistant Professor, for their constant support and constructive criticism during my study. My heartfelt gratitude goes to Dr. Naveet Kaur, Bridge Engineering and

Structures (BES) Division, CSIR-CRRI, New Delhi, for teaching electromechanical impedance technique used in this study.

I thank colleagues Mr. Upender Bishnoi, Mr. Ashish Kumar Tiwari, Dr. Sumit Joshi and Ms. Navneet Sidhu for their continuous support. I would specially thank Dr. Kirti Vardhan for his unconditional support throughout these years and for many fruitful and refreshing discussions.

I owe special thanks to my lab mates Himanshu, Purnima, and Harvinder for stirring discussions and support. I owe a word of thanks to Mr. Soni Singh and Mr. Ram Simran.

I find it difficult to express in words, my sincere sense of indebtedness towards my parents, brother and sister-in-law. My unquestionable gratitude is for the never-ending love and support of my father Mr. Kewal Krishan and mother Mrs. Shashi Anand. My father is my backbone and my mother is the pillar of my strength. I consider myself lucky to have such supportive and loving parents. I extend my respect to my elder brother Mr. Ashish Anand and sister-in-law Mrs. Guncha Anand for their unconditional love and support.

Last but not least, I wish to acknowledge all those whose names have not been figured here but who helped me in any form during my research work.

Date: 16-June-2023

Place: Patiala

(Kamal Anand)

ABSTRACT

Utilization of microbially induced calcium carbonate precipitation (MICCP) via biomineralization process has been considered a novel method in self-healing of concrete structures in past decade. To develop MICCP as ready product for field scale construction, mineral-based inoculum of higher shelf life is required. The present study focuses on this aspect of field-based application of MICCP. In this study, mineral admixture (fly ash (FA), silica fume (SF), cement kiln dust (CKD) and rice husk ash (RHA)) based bacterial inoculum were developed to immobilize bacteria in concrete. The prepared inoculums were stored at varying temperatures (4°C and 25°C) and the survival of bacterial cells in carrier-based materials were tested on a weekly basis until 270 days of storage at both temperatures using the plate count method. The cell viability was found to be in the range of 4.5 to 6.0 log cfu/g in FA and SF based inoculum at both the storage temperature even till 180 days of storage. In case of CKD and RHA based inoculum, decline in cell concentration was noted within 90 days of storage at both temperatures indicating CKD and RHA are not suitable as carrier materials. Therefore, only FA and SF based inoculums stored at 4°C were incorporated in concrete to immobilize bacteria and tested for strength and permeation characteristics at the age of 7 and 28 days. In this study, bacterial carrier admixed and bacterial carrier spray treatment of concrete specimens was carried out using nutrient broth, urea and calcium chloride. Results revealed significant improvement of approximately 27% in the compressive strength at 28 days of testing. Also, remarkable reduction in the permeability was observed at 28 days with the incorporation of mineral inoculums.

Further, anti-corrosive aspects of FA and SF based inoculum were tested in the chloride environment. Reinforced concrete (RC) specimen containing FA and SF based inoculum as admixed and spray strategy were cast and cured for 28 days in respective curing. These test specimens were then subjected to accelerated current induced corrosion in the chloride

environment. The changes occurred due to the corrosion were monitored using well established electrochemical and newly emerging electromechanical impedance (EMI) technique. The results clearly suggested that the FA and SF based carrier material can be effectively used for the corrosion prevention in RC structures and the emerging EMI technique can efficiently monitor the corrosion process.

The developed inoculums were tested for the self-healing capabilities in the concrete. The prismatic concrete specimens of 500 × 100 × 100 mm were cast containing FA and SF based inoculum and the crack of approximately 0.5 mm width was generated at the time of casting. After 28 days of water curing, these specimens were dried and the artificial crack width of approximately 0.5mm was healed autonomously using a bacteria-based healing agent (nutrient broth, urea and calcium chloride). The healed cracked surface was examined through optical imaging to monitor the crack width reduction. Along with this, EMI technique was used to monitor the crack healing potential until the full healing of cracked surface was achieved. At the end of test, the healed specimens were subjected to bending failure to assess the strength regain. Significant regain was noticed in healed bacterial specimen (approximately 33 %) in comparison to the control. The healing mineral precipitated inside the cracks was examined through field emission scanning electron microscopy (FESEM), energy dispersive X-ray spectroscopy (EDX), X-ray diffraction (XRD) and thermogravimetric analysis (TGA) to evaluate its physicochemical attributes. The results give clear proof that the FA and SF-based carrier materials can be effectively used in healing the cracks in concrete.

Further, to repair existing cracks in concrete structure, bio-cementitious grout were developed using FA and SF inoculums and were tested for fresh and hardened properties. The best performing cementitious bio-grout was used to repair cracks in concrete structures. An attempt was made to develop a procedure for the remediation of cracks in three varying orientations, i.e. horizontal, vertical and inverted, to target actual cracks that might exist in the structures.

The performance of the repaired surface was assessed in terms of recovery in flexural strength and water tightness. The mineral composition of the healing product was examined by FESEM-EDX and XRD; results clearly indicated the presence of calcite crystals inside the pores. Also, to quantify the calcium carbonate precipitation in the bio-repaired specimens during curing, EMI technique was employed. Overall, it can be concluded that FA and SF based inoculum can effectively promote MICCP activity to seal the fractured crack of any orientation in existing concrete structures.

The best performing bio-grout was then used to repair cracks in actual concrete structures. The cracked location were identified and bio-grout was injected inside the cracked surface. The repaired surface was then cured using growth media supplemented with nutrients. To assess the MICCP activity, EMI technique was employed during the curing period and at the end samples were extracted for microstructural analysis. Results indicated the presence of calcite crystals responsible for the densification of pores.

LIST OF PUBLICATIONS

The following publications in peer reviewed journals are the outcome of the present research work:

1. **Anand K**, Goyal S, Reddy MS (2022) Long-term viable SF immobilized bacterial cells as sustainable solution for crack healing in concrete. **Structures**, 43: 1342-1355. Impact factor: **4.01**
2. **Anand K**, Goyal S, Reddy MS (2022) Crack healing in concrete by microbially induced calcium carbonate precipitation as assessed through electromechanical impedance technique. **European Journal of Environmental and Civil Engineering**, 1-21. Impact factor: **2.187**
3. **Anand K**, Goyal S, Kaur N, Reddy MS (2023) Viable FA based bacterial cells as sustainable solution for corrosion prevention in RC structures. **Construction and Building Materials**, 365: 130056. Impact factor: **7.693**
4. **Anand K**, Goyal S, Reddy MS (2023) Development of field applicable remediation procedure using bio-cementitious grout for concrete cracks in variable orientations. **Journal of Building Engineering**, 67: 106024. Impact factor: **7.144**
5. **Anand K**, Goyal S, Reddy MS (2023) Corrosion inhibition in reinforced concrete using silica fume immobilized bacterial cells. **Journal of Sustainable Cement-Based Materials**. Impact factor: **5.328 (Accepted)**

Paper under revision

1. **Anand K**, Goyal S, Reddy MS (2023) Development of bio-cementitious grout using silica fume based bacterial agent for remediation of cracks in concrete structures. Journal of Materials in Civil Engineering. Impact factor: 3.651

TABLE OF CONTENTS

LIST OF FIGURES

LIST OF TABLES

CHAPTER 1:
INTRODUCTION

1.0 GENERAL

With an estimated yearly utilization approaching 30 billion tonnes, concrete is the second most extensively consumed building material around the globe after water by mass (Monteiro et al. 2017). Concrete is the most suited construction material because of its availability and strength characteristics (Sidiq et al. 2019). Despite several benefits and prodigious demands, concrete faces major shortcomings of low tensile strength and poor cracking resistance, leading to premature failure under service life (Wang et al., 2019). Cracks are almost inevitable and can occur at any stage of the concrete service life (Gupta et al. 2017). Micro cracks permit the ingress of moisture, harmful agents like CO_2, SO_4^{2-} and Cl^- into concrete resulting in early corrosion of reinforcement in concrete (Basheer et al. 2001). The end products of rebar corrosion are expansive and produce tensile stresses in concrete, which further leads to widening of the cracks. Conversion of micro-cracks into macro cracks eventually compromises the structural integrity (Yang et al., 2010).

Various existing techniques for repairing the cracks include the manual application of chemicals (Sisomphon et al. 2012) and polymeric sealers (Araújo et al. 2018; Van Tittelboom et al. 2011). These techniques maintain the strength and durability of reinforced concrete to a certain extent, but require regular examination and maintenance post repairing. In the past two decades, the introduction of bacteria or microbes in concrete has emerged as a promising solution for increasing the strength and durability properties. The method that utilizes the capability of bacteria to precipitate calcium carbonate is named as microbially induced calcium carbonate precipitation (MICCP). MICCP has drawn much attention due to its sustainability, good compatibility with concrete and has proven to be a promising technique (De Belie et al. 2018; Kan et al. 2019; Seifan and Berenjian 2019).

1.1 MECHANISM OF MICCP

MICCP via urea hydrolysis is the simplest and most widely used method for the precipitation of carbonates for concrete applications (Bains et al. 2015). The majority of previously reported studies adopted ureolytic bacteria to precipitate calcium carbonate in concrete structures (Achal et al. 2011a; Alazhari et al. 2018a; Dhami et al. 2013c; Joshi et al. 2018a; Seifan et al. 2016). The precipitation of calcium carbonates via urea hydrolysis by ureolytic bacteria is the most straightforward and most easily controlled mechanism of MICCP, with potential to produce high amounts of carbonates in a short period of time (Dhami et al. 2013c). MICCP comprises of series of complex biochemical reactions. As part of metabolism, some bacterial species produce urease, which catalyzes urea to carbamate and ammonium, as shown in Equations (1.1) and (1.2).

$$\underset{\text{Urea}}{CO(NH_2)_2} + \underset{\text{Water}}{H_2O} \longrightarrow \underset{\text{Carbamate}}{NH_2COOH} + \underset{\text{Ammonia}}{NH_3} \qquad (1.1)$$

$$\underset{\text{Carbamate}}{NH_2COOH} + \underset{\text{Water}}{H_2O} \longrightarrow \underset{\text{Ammonia}}{NH_3} + \underset{\text{Carbonic Acid}}{H_2CO_3} \qquad (1.2)$$

These products formed in Equations (1.1) and (1.2); further equilibrate in water to form bicarbonate and 2 moles of ammonium and hydroxide ions, as shown in Equations (1.3) and (1.4), resulting in increase of pH.

$$\underset{\text{Ammonia}}{2NH_3} + \underset{\text{Water}}{2H_2O} \longleftrightarrow \underset{\text{Ammonium Ions}}{2NH_4^+} + \underset{\text{Hydroxide Ions}}{2OH^-} \qquad (1.3)$$

$$\underset{\text{Hydroxide Ions}}{2OH^-} + \underset{\text{Carbonic Acid}}{H_2CO_3} \longleftrightarrow \underset{\text{Bicarbonate Ions}}{CO_3^{2-}} + \underset{\text{Water}}{2H_2O} \qquad (1.4)$$

Since the cell wall of the bacteria is negatively charged, the bacteria draw cations from the environment, including Ca^{2+}, to deposit on their cell surface. The Ca^{2+} ions subsequently react with the $(CO_3)^{2-}$ ions, leading to the precipitation of $CaCO_3$ at the cell surface that serves as a nucleation site. The processes are represented by Equations (1.5) and (1.6).

$$Ca^{2+} + \text{Cell} \longrightarrow \text{Cell-}Ca^{2+} \quad (1.5)$$

Calcium Ions

$$\text{Cell-}Ca^{2+} + CO_3^{2-} \longrightarrow \text{Cell-}CaCO_3 \quad (1.6)$$

Bicarbonate Ions Calcium Carbonate

1.2 CHALLENGES ASSOCIATED FOR UPSCALING MICCP

The MICCP process results in the production of high amounts of ammonium which is detrimental to the environment (Wiktor and Jonkers 2011). Many investigators have used bacteria as a measure of an eco-friendly healing agent in concrete structures (Rong et al. 2020; Xu and Wang 2018). The results revealed that bacteria could produce calcium carbonate ($CaCO_3$) precipitation inside the cracks and block them, thus the mechanical properties of the concrete could be restored to a certain extent (Ramachandran et al. 2001). Researchers have reported using biomineralized material (bacteria) in sustainable and durable construction (Beatty et al. 2022). However, the survival of bacterial cells in the harsh alkaline environment of concrete is of significant concern (Lee and Park 2018; Wiktor and Jonkers 2011). Also, there is an extensive need for carrier materials to address this concern, which can provide an optimum environment for bacteria to safeguard against the high alkalinity of concrete.

Another major challenge associated with MICCP is its complex methodology which requires expensive lab facilities to grow bacterial culture. This limits its implementation to field engineering applications. Also, to make it commercially viable for large field applications, it is desired to use carrier material known to be synergistic with concrete. Various mineral

admixtures which have already shown engineering benefits can be used as potential carrier for bacteria in concrete.

1.3 GAPS IN THE RESEARCH AREA

MICCP has shown promising results in improving strength and durability at the laboratory scale. Implementation of the MICCP technique in new construction and as a remediation measure for repairing existing damages in concrete with economical alternatives of suitable bacterial carrier material with effective curing method is to be investigated. Previous studies documented various carrier materials to immobilize bacteria in the concrete. These include perlite (Alazhari et al. 2018a), polyurea (Zamani et al. 2020), diatomaceous earth (Wang et al. 2012a), hydrogel (Wang et al. 2014) and graphite nanoplatelets (Khaliq and Ehsan 2016). These carrier materials have proven to be productive for self-healing of concrete. But the shelf life of existing carrier materials is not defined prior to its application. Also, the high cost associated with these existing carriers limits its application. Hence a, thorough research is required to develop cost effective suitable carrier inoculums of high and defined shelf life for the construction industry. Based on these gaps, the objectives of the present work are finalized.

1.4 OBJECTIVES OF THE PROPOSED WORK

1) To investigate the effectiveness of CKD and fly ash as a carrier material for bacterial inoculum.
2) To investigate the efficiency of prepared bacterial inoculum as a surface treatment measure.
3) To use the bacterial inoculum for onsite remediation of damaged RC structures.

1.5 ORIENTATION OF THESIS

The thesis has been organized into six chapters. In the first chapter, an introduction about the topic is presented. The objectives of the present study have also been laid out in this chapter.

In the second chapter, a literature review regarding the application of MICCP technology in concrete has been presented. The use of various bacterial strains and their effect on the mechanical and durability properties of concrete has been presented. A thorough review of existing carrier materials reported for bacteria for MICCP application has been presented. The third chapter focuses on the development of various mineral inoculums and their testing to define the shelf life of the bacterial product. These developed mineral inoculums were immobilized in concrete to test their strength and permeation characteristics. The fourth chapter deals with the corrosion performance of mineral inoculum immobilized in RC under chloride environment. The RC specimens were subjected to impressed current-induced corrosion over the complete test exposure. The fifth chapter deals with the performance of mineral inoculums as crack repair measures in concrete structures. The sixth chapter deals with the relevant conclusions drawn from the present study. In the end, references cited in the entire work are presented.

CHAPTER 2: REVIEW OF LITERATURE

2.0 GENERAL

Concrete is the most widely used construction material around the globe due to its high strength and low price. Despite several benefits and considerable demand, concrete faces shortcomings leading to premature failure under service life (Rajczakowska et al. 2019; Wang et al. 2019a). This may include its low tensile strength, high brittleness and poor cracking resistance. Cracks are almost inevitable and can occur at any stage of the concrete service life (Joshi et al. 2017). Micro cracks permit ingress of water and chloride into concrete and cause early deterioration of concrete. During the exposure to environment and loadings, these micro crack leads to macro cracks which eventually compromises the structural integrity (Zamani et al. 2020). Therefore, it becomes imperative to repair these cracks as early as possible to extend the service life of concrete structures.

Various techniques for repairing the cracks are addressed in the literature including the manual application of chemical (Sisomphon et al. 2012), polymeric sealers (Issa and Debs 2007; Van Tittelboom et al. 2011) and surface treatments (Pan et al. 2017). Traditionally, polymeric sealers are found to be promising coating and improving the durability of concrete. Pan et al., (2017) reported many challenges associated with the failure of polymeric sealers. These include blistering, cracking, holes and peeling of coating. Thus, suitable alternative is required for effective repair of concrete structures. Researchers reported various surface treatment methods for protecting concrete structures against penetration of aggressive ions by forming a barrier layer. Based on chemical nature, surface treatment materials can be classified into two categories i.e. organic and inorganic protective agents. Organic materials are the protective agents which do not react with the concrete substrate during the application on the repair surface. Inorganic surface materials are reported to be mainly aqueous solutions of sodium silicate. Many studies reported the positive results of these organic and inorganic materials in

protecting the surface from the penetration of aggressive ions (Jiang et al. 2015; Pan et al. 2016). Still, many challenges need to be addressed related to the synthesis, service life and application cost, limiting its implementation at the field scale.

Recently, the innovative technique of using bacteria as bioagent to induce calcium carbonate precipitation has emerged as promising technique in the past two decades. This bio-based technique is known as microbially induced calcium carbonate precipitation (MICCP) (Achal et al., 2011a; Dhami et al., 2013; Kan et al., 2019; Zhang et al., 2017). MICCP has recently become an attractive topic of research in civil engineering. Researchers have explored various bacterial strains to enhance the mechanical, durability and crack healing of concrete in the past decade (Achal et al. 2011a; Alazhari et al. 2018b; Bhaskar et al. 2017; Chahal et al. 2012; De Muynck et al. 2008, 2010; Nguyen et al. 2019; Sierra-Beltran et al. 2014; Tripathi et al. 2019). Also the ecological benefits of MICCP in urban development has been explored (Achal et al. 2016). The sustainability of promising technology has been reported (Sierra-Beltran et al. 2014). Self-healing of cracks has shown significant results at micro-scale (Bergh et al. 2020; Jongvivatsakul et al. 2019) and still the strategies are required to be proposed for field-scale application. The major challenge associated with field implementation is bacteria survival in high alkaline pH environments (Jonkers et al. 2010). To tackle this issue, researchers reported many suitable carrier materials for bacteria to survive in harsh concrete environment (Khaliq and Ehsan 2016). The detrimental influence of bacterial carriers on the mechanical properties of concrete has been reported (Erşan et al., 2016). There is a need to select suitable mineral carrier for bacteria already known to be synergistic with the concrete. There is a need to address the proper shelf life of carrier material for MICCP application in the field. This chapter provides the state of art of MICCP activity in concrete, focusing on various bacterial strains reported for improvement in strength and durability properties, their mechanism, self-healing via biomineralization and field applications.

2.1 BACTERIAL STRAINS FOR MICCP ACTIVITY

Initially researchers isolated various bacterial strains and tested its efficiency to induce calcium carbonate precipitation in growth media supplemented with different dosage of calcium chloride and urea (Achal et al. 2010; Ersan et al. 2015; Ramachandran et al. 2001). The results indicated that bacteria were capable to produce urease, which has been responsible in calcium carbonate precipitation. Various bacterial strain reported in the literature has been tabulated in Table 2.1 which are found to be efficient for MICCP activity in cementitious composites. Majority of these reported bacterial strains found to be of bacillus species.

Table 2.1: Various bacterial strains reported in the literature

Microorganism	**Material**	**Reference**
B. sphaericus	Mortar, Concrete	(Pungrasmi et al. 2019), (Jongvivatsakul et al. 2019), (Gupta et al. 2018), (Snoeck et al. 2018), (Su et al. 2019)
B. megaterium	Concrete	(Nain et al. 2019), (Achal et al. 2011b)
Bacillus sp. CT-5	Concrete	(Joshi et al. 2018a), (Joshi et al. 2019), (Tripathi et al. 2019), (Achal et al. 2011a)
S. pasteurii	Mortar, Concrete	(Bergh et al. 2020), (Ksara et al. 2019), (Ruan et al. 2019), (Xu and Wang 2018), (Bhaskar et al. 2017), (Choi et al. 2017), (Rong et al. 2020)
B. subtilis	Concrete	(Nguyen et al. 2019), (Khushnood et al. 2020), (Nain et al. 2019), (Khaliq and Ehsan 2016)
*B. cohnii**	Concrete	(Jiang et al. 2020), (Zhang et al. 2017), (Jonkers et al. 2010), (Kumari et al. 2017)
*B. pseudofirmus**	Mortar, Concrete	(Zamani et al. 2020), (Alazhari et al. 2018a), (Jonkers et al. 2010), (Jonkers and Schlangen 2006)
B. cereus	Concrete	(Wu et al. 2019)
S. ureae	Concrete	(Bhaskar et al. 2017)
B. licheniformis	Soil	(Ramdas et al. 2020)
*B. halodurans**	Concrete	(Jonkers and Schlangen 2006)
B. aerius	Concrete	(Siddique et al. 2016)

*Non-ureolytic bacteria

2.2 MECHANISM OF MICCP

Based upon the literature survey, it has been found that mainly four types of microorganisms are involved in MICCP process. These are photosynthetic organisms (cyanobacteria), sulphate reducing bacteria, organisms utilizing organic acids and organisms involved in urea hydrolysis. Among all four types, MICCP via urea hydrolysis is simplest and most widely adopted for calcium carbonate precipitation. In this study, bacteria involved in urea hydrolysis was studied and only its mechanism is reported. MICCP via urea hydrolysis is an easily controlled mechanism in which high amounts of carbonates are produced by the ureolytic bacteria in short time period (Figure 2.1).

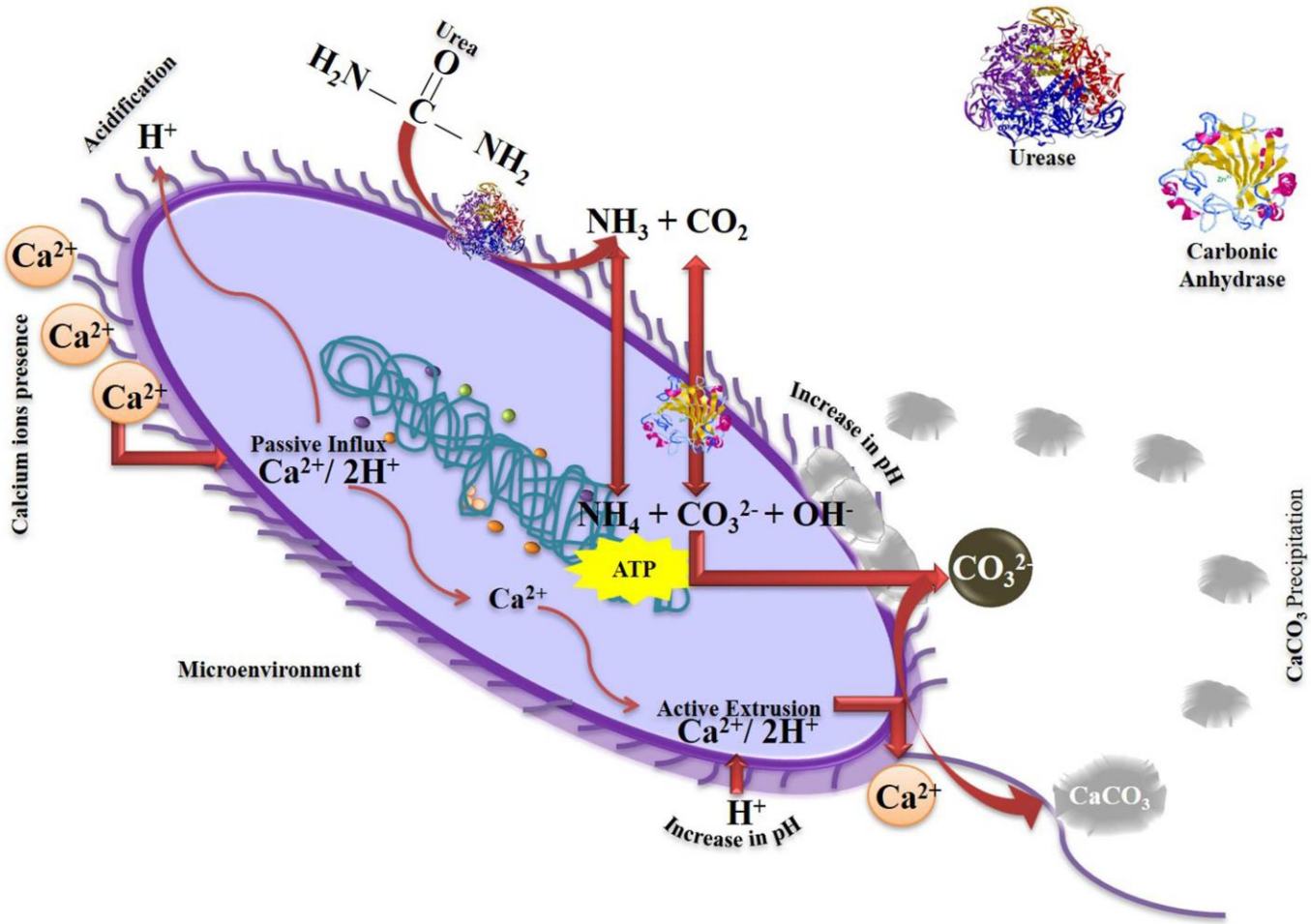

Figure 2.1: Schematic diagram of MICCP formation mediated by urease and carbonic anhydrase (Castro-Alonso et al. 2019)

2.3 APPLICATION OF MICCP IN CONCRETE

The following sections discuss literature related to mechanical and durability properties of microbial concrete. The section is further extended to discuss application of microbial concrete for corrosion resistance, remediation of cracks via biomineralization, field application and various challenges faced to upscale MICCP for field implementation.

2.3.1 Influence of MICCP on strength properties of concrete

The potential of employing MICCP in cementitious composites to improve early as well as later strength properties have been widely reported by researchers in past two decades. Initially, Ramachandran et al., (2001) reported that using *B. pasteurii* positively influences the performance of portland cement mortar. Achal et al., (2011a) studied the compressive strength of cement mortar made by using *B. megaterium* ATCC 14581, which was grown in the nutrient broth media containing urea. The compressive strength significantly increased for the mortar cubes containing microbial cells. Pei et al., (2013) used *B. subtilis* in the concrete specimens and concluded that the concrete specimen prepared with B. subtilis precipitated $CaCO_3$, thereby increasing the compressive strength. Krishnapriya et al., (2015) used *B. megaterium* MTCC 1684 in the concrete specimens and reported an improvement in compressive strength of 12.1% compared to control specimens. Joshi et al., (2018) investigated the efficiency of curing treatments (admixed and spray) in improving mechanical properties of concrete using the ureolytic bacterial strain *Bacillus sp. CT-5* and found an average increase of 29% and 8% in bacterial admixed and spray treated specimens compared to control specimens at 28 days of testing. Mondal and Ghosh (2018) fabricated concrete specimens with *B. Subtilis* having bacterial cell concentration of 10^5 cells/ml and noticed a 27% improvement in compressive strength at 28 days of testing compared to control specimens. Nain et al., (2019) tested concrete specimens prepared with *B. subtilis* and *B. megaterium* and found compressive strength improvement of 14.36% and 22.58% at 28 days of testing. A similar trend of improvement in

split tensile strength was noticed in bacterial specimens. Recently researchers reported the effect of non-ureolytic bacteria on the mechanical properties of mortar and concrete (Kumari et al. 2017; Nguyen et al. 2019; Su et al. 2019). Kumari et al., (2017) reported 49% increase in compressive strength by using non-ureolytic bacteria *B. cohnii* at the age of 28 days. Overall, it can be inferred that most of the reported studies used bacillus species to precipitate calcium carbonate inside the concrete matrix and found significant improvement in the strength properties of concrete.

2.3.2 Influence of MICCP on durability properties of concrete

The effectiveness of MICCP application in cementitious materials to enhance the permeability properties have been reported by various researchers. Achal et al., (2011b) reported fly ash concrete containing *B. megaterium* cells absorbed nearly 3.5 times less water than the control concrete. They also found that the permeability of the concrete with bacterial cells was lower than control concrete. De Muynck et al., (2008) reported the mortar specimens made with *B. sphaericus* found less permeable than control specimens due to precipitation of $CaCO_3$ resulted in pore refinement. Dhami et al., (2013) reported 40% reduction in water absorption and 31% reduction in porosity due to bio deposition of $CaCO_3$ on surface of specimens in comparison to control. This biogenic deposition of $CaCO_3$ acts as pore blocker and restrict the penetration of aggressive ions inside the concrete. Nosouhian et al., (2016) reported that the incorporation of *S. Pasteurii* and *B. Subtilis* improved the resistance of concrete to chloride permeation. Indeed, the average number of coulombs passed through the bacteria-containing concrete was 11.7% less than that of control concrete. In another research, Siddique et al., (2016) found that 10^5 cells/ml of *B. aerius* improved of about 22% the resistance of concrete to total charge passing through concrete prepared with 10% replacement of cement by rice husk ash and tested at 56 days. Joshi et al., (2018a) reported with the bacterial treatment the charge transfer is reduced drastically in rapid chloride penetration test. Similar observations of significant reduction in

permeability were reported by other researchers (Chahal et al. 2012; Joshi et al. 2018b; Kalhori and Bagherpour 2017; Sharma et al. 2022; Sidhu et al. 2022; Tripathi et al. 2019; Vahabi et al. 2015). The literature on performance of bacteria (without any protective material) on corrosion resistance is very limited reported. Achal et al., (2012) investigated the effectiveness of MICCP on reinforcement corrosion. RC specimens were treated with *Bacillus sp. CT-5* and subjected to accelerated current induced chloride corrosion. The results showed that bacterial-treated RC specimens reduced the corrosion rate four times more than the control specimens. Bisht et al., (2020) noted a similar observation of corrosion reduction. This is because microbial urea hydrolysis and aerobic oxidation of organic carbon require O_2 as final electron acceptor to initiate and/or to keep the microbial activity. This may result in oxygen consumption in the concrete, which may pose a limitation for rebar corrosion (De Belie 2016).

2.3.3 Challenges faced to upscale MICCP

Incorporating fresh bacterial culture in a liquid medium while preparing fresh concrete has significantly improved the mechanical and durability properties of concrete. However, in the long term, the primary concern regarding the utilization of MICCP in concrete has been the survival of bacteria in the highly alkaline concrete environment. This concern was well reported in the literature by Jonkers et al., (2010). To address this concern, researchers reported various protective carrier materials to immobilize bacteria and increase bacterial cell viability in concrete. Dzionek et al., (2016) reported the definition of good carrier material and suggested a carrier material should be insoluble, non-toxic; both for the immobilized material and the environment; easily accessible, inexpensive, stable and possess large surface area. Researchers used silica gel (Van Tittelboom et al. 2010), perlite (Alazhari et al. 2018b; Jiang et al. 2020), zeolite (Bhaskar et al. 2017), hydrogel (Wang et al. 2014), graphite nano platelets (Khaliq and Ehsan 2016), vermiculite (Soda et al. 2023) as potential carriers for bacteria in concrete. Other major concern is the dosage of carrier material to be used in the preparation of concrete. De

Belie (2016) reported these carrier materials will have detrimental influence on the compressive strength, especially if these are added in dosages exceeding 1% weight of cement. Moreover, use of supplementary cementitious materials (SCM) as carrier materials are encouraged, as they can be immobilized in high dosage. Other reason is SCM has positive influence on strength due to pozzolanic action (Khaliq and Ehsan 2016).

2.3.4 Remediation of cracks using bacteria via biomineralization

Several investigators have used bacteria as a measure of crack healing in the last decade (Bergh et al. 2020; Jiang et al. 2020; Jongvivatsakul et al. 2019; Khushnood et al. 2022; Nguyen et al. 2019; Rong et al. 2020; Sisomphon et al. 2012; Van Tittelboom et al. 2010; Zamani et al. 2020). Different bacterial strains, carriers, methodologies have been adopted by researchers to study the self-healing mechanism of cracks autonomously (Table 2.2). Initially the application of bacteria to remediate the cracks in cement mortar specimens was reported by Ramachandran et al., (2001). Crack was artificially generated of 3.125 mm width and depth of 25.4 mm. Authors reported the mineralization process was effective in shallow cracks than in deeper ones because the bacteria grow more actively in presence of oxygen. Wiktor and Jonkers (2011) generated crack of varying width from 0.05 to 1 mm in prismatic specimens of 40 × 40 × 160 mm. Bacterial based specimens showed promising results in crack filling at the curing age of 40 days. Luo et al., (2015) simulated cracks in mortar specimen using embedded nail method of different crack with varying from 0.1 to 1 mm. Spore-forming alkali-resistant bacteria healed specimen with crack width up to 0.8 mm. Algaifi et al., (2020) generated artificial crack using copper plate in mortar specimen of 30 mm (dia) and 50 mm (height) and they reported the complete healing of a 0.4 mm crack width was achieved after 70 days at the crack mouth. Vaezi et al., (2020) investigated the optimum bacterial concentration and calcium lactate content in mortars specimen containing recycled concrete aggregate as full replacement of natural fine aggregate.

Table 2.2: Overview of different bacteria, carriers, methodologies adopted by the researchers to study the self-healing mechanism of cracks

S.No.	Material	Bacteria	Carrier	Properties studied for crack healing	Reference
1.	Concrete	*B. cohnii*	Expanded perlite	Optical analysis, XRD and FESEM	(Jiang et al. 2020)
2.	Mortar	*B. pseudofirmus*	Polyurea	Microscopy, FESEM, EDX and TGA	(Zamani et al. 2020)
3.	Concrete	*B. Subtilis*	Recycled coarse aggregates and fine aggregates	FESEM, TGA, XRD and XRF	(Khushnood et al. 2020)
4.	Concrete	*B. cereus*	Direct	SEM, FTIR, XRD and DSC	(Wu et al. 2019)
5.	Concrete	*B. subtilis*	Direct	Optical microscopy, SEM, EDX and Raman analysis	(Nguyen et al. 2019)
6.	Mortar	*Lysinibacillus sp.*	Direct	Visual examination, XRD and FESEM	(Su et al. 2019)
7.	Mortar	*B. pseudofirmus*	Expanded perlite	Visual examination and FTIR	(Alazhari et al. 2018a)
8.	Mortar	*S. pasteurii*	Direct	Optical microscopy and FTIR	(Amiri et al. 2018)
9.	Mortar	*B. sphaericus*	Direct	Visual examination, SEM-EDX and XRD	(Jongvivatsakul et al. 2019)
10.	Mortar	*S. pasteurii*	Calcium sulphoaluminate cement	Visual examination, SEM-EDX and XRD	(Xu and Wang 2018)
11.	Concrete	*B. cohnii*	Expanded perlite	Visual examination, FESEM and XRD	(Zhang et al. 2017)
12.	Mortar	*S. ureae and S. pasteurii*	Zeolite	Visual examination, SEM, EDX, XRD	(Bhaskar et al. 2017)
13.	Mortar	*S. pasteurii*	Direct	Optical analysis, SEM	(Choi et al. 2017)
14.	Concrete	*B. cohnii*	Magnesia cement	Optical analysis, SEM and XRD	(Xiao et al. 2022)
15.	Concrete	*B. subtilis*	Sugarcane bagasse	Visual examination and SEM	(Kanwal et al. 2022)

SEM: scanning electron microscopy, EDX: energy dispersive spectroscopy, XRD: x-ray diffraction, TGA: thermo-gravimetric analysis, FTIR: fourier-transform infrared spectroscopy, DSC: differential scanning calorimetry, FESEM: field emission scanning electron microscopy, UPV: ultrasonic pulse velocity

Table 2.2 (Continued): Overview of different bacteria, carriers, methodologies adopted by the researchers to study the self-healing mechanism of cracks

S.No.	Material	Bacteria	Carrier	Properties studied for crack healing	Reference
16.	Concrete	*B. sphaericus*	Hydrogel	Water absorption, Visual examination, SEM-TGA	(Wang et al. 2014)
17.	Concrete	*S. pasteurii*	Expanded glass granules	Water absorption, Visual examination, SEM-EDX, Raman spectroscopy	(Zhang et al. 2022)
18.	Mortar	*B. pasteurii*	Direct	Visual examination, water permeability, SEM-EDX	(Rong et al. 2020)
19.	Concrete	*B. pasteurii*	Recycled aggregates	Microscopic imaging, crack width reduction, SEM-EDX	(Liu et al. 2020)
20.	Concrete	*B. megaterium*	Expanded vermiculite	UPV, water permeability, visual imaging, SEM-EDX	(Soda et al. 2023)
21.	Concrete	*B. megaterium*	Expanded perlite	UPV, water permeability, visual imaging, SEM-EDX	(Ranjan et al. 2022)
22.	Concrete	*S. pasteurii* and *B. sphaericus*	Direct	Recovery in compressive strength, water absorption, SEM, XRD	(Nimafar et al. 2023)
23.	Concrete	*B. cohnii*	Magnesia cement	Water permeability, crack closure, SEM-EDX	(Xiao et al. 2023)
24.	Concrete	*B. subtilis*	Alginate	Water permeability, crack closure, SEM-EDX	(Kawaai et al. 2022)
25.	Mortar	*S. pasteurii*	Bleaching earth	Water permeability, crack closure,	(Yang et al. 2022)
26.	Concrete	*B. cohnii*	Recycled coarse aggregates	Crack closure, SEM-EDX	(Han et al. 2022)
27.	Concrete	*S. pasteurii*	Recycled concrete aggregates	Visual examination, water tightness regain, strength regain, SEM, XRD	(Wang et al. 2022)
28.	Mortar	*Diaphorobacter nitroreducens*	Expanded clay particles	Visual examination, water tightness, SEM, XRD	(Erşan et al. 2016a)

Authors simulated cracks of approximate width 1 mm in 50 × 50 × 50 mm cubic mould and monitored after 3, 7, and 28 days. They concluded the mixes prepared with a higher cell concentration and calcium lactate dosage exhibited a better performance in terms of crack healing. Jafarnia et al., (2020) induced cracks in the cylindrical specimens of height (200 mm) and diameter (100 mm) using splitting tensile test. Authors examined crack widths of healing specimens were measured after 5, 15, and 30 days of curing and reported crack width up to 0.58 mm were completely healed at 30 days by using bacteria in curing environment. Erşan et al., (2016) reported NO_3^- reduction as an alternative microbial self-healing strategy over MICCP via ureolytic. The results were found satisfactory and complete healing was achieved at 28 days of treatment in bacterial specimens. The photomicrographs crack healing of various specimens are shown in Figure 2.2.

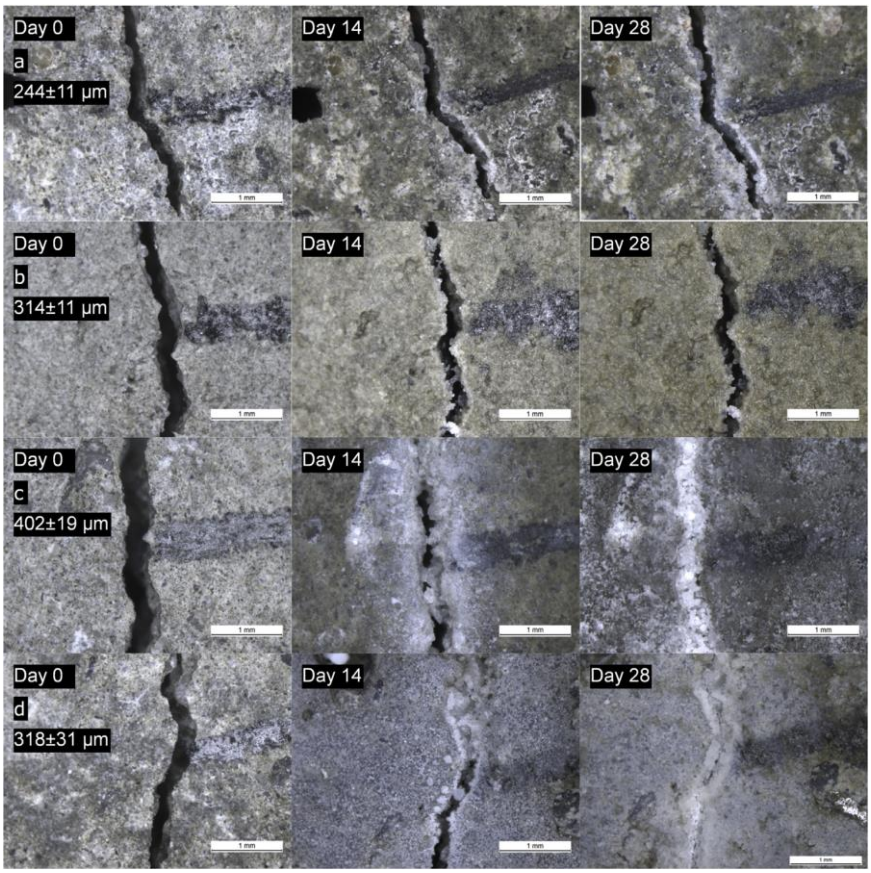

Figure 2.2: Photomicrographs of (a) Reference mortar; (b) abiotic control; (c) mortar containing *D. nitroreducens* loaded expanded clay particles (d) mortar containing *P. aeruginosa* loaded expanded clay particles (Erşan et al., 2016)

Based upon the literature survey, it can be concluded that majority of the methods for assessing healing efficiency are visual examination (Bergh et al. 2020; Jongvivatsakul et al. 2019), microstructural analysis through scanning electron microscopy (SEM) (Khushnood et al. 2020; Nain et al. 2019; Wang et al. 2019a), energy dispersive X-ray spectroscopy (EDX) (Ferrara et al. 2018), X-ray diffraction (XRD) (Kalhori and Bagherpour 2017; Ruan et al. 2019), x-ray computed tomography (Ruan et al. 2019), fourier-transform infrared spectroscopy (Wu et al. 2019), raman spectroscopy (Nguyen et al. 2019), differential scanning calorimetry (Wu et al. 2019) and thermogravimetric analysis (TGA) (Bundur et al. 2017; Khushnood et al. 2020) have been reported. All the above-mentioned techniques give qualitative information of crack healing and no quantification of crack width reduction is possible by using these techniques. Some studies employed various non-destructive techniques (NDT) for assessing the crack healing such as ultrasonic pulse velocity (UPV) (Karaiskos et al. 2016; Kaur et al. 2020) and acoustic emission (Tsangouri et al. 2016). The limitations of all these monitoring devices are that they require expertise and expensive facilities for continuous inspection of the healing process. Also, they require the continuous collection of data for which the instrument is to be continuously placed at the site where monitoring is done. Thus, there is an extensive need to develop cost-effective techniques for crack healing monitoring of real structures at different site locations.

Overall, it can be inferred that majority of the published studies used different ways to generate artificial cracks in cementitious composites in laboratory and healed using bacteria-based agent supplemented with nutrients. These findings were supported by destructive testing at laboratory scale (regain in strength and regain in water tightness). Researchers reported that non cracked concrete immobilized with bacteria could double the service life of concrete structures (De Belie 2016). This could be a sustainable solution for crack repair in concrete structures and extend the service life.

2.3.5 Remediation of cracks using bio-agent at field scale

With the development of self-healing technology, some application studies have been carried out at field scale. Wiktor and Jonkers (2015) investigated the performance of bacteria-based repair system in sealing of cracks in the concrete pavement of area 2.0 m × 0.5 m in a two-storey underground parking garage. The efficiency of repair system was evaluated in terms of water permeability on site. The treated area showed few localized dripping spots where as control area were heavily leaking. Sierra-Beltran et al., (2015) reported the application of self-healing concrete and natural fibres as lining for an irrigation in Ecuador. The use of natural fibres in concrete increases the tensile capacity of concrete and assures a controlled crack width. Also, the bacteria were incorporated in the concrete in order to seal possible cracks. Tziviloglou et al., (2016) prepared small (40 × 40 × 160 mm^3) and large (150 × 250 × 3000 mm^3) concrete beam containing 3% (weight of cement) ureolytic bacterial culture and after 28 days of curing, cracks were generated using four-point bending method. Water-spray system was installed above the cracked beam, which sprayed water for 1 min four times per day over six weeks. Authors reported that less sealing was obtained in the large-scale beam than in the smaller prisms. Araújo et al., (2018) designed the efficient capsules of wall thickness 0.7 mm to resist the mixing process of material carrying healing agents. These capsules were tested on real scale concrete beams. The results showed that cracked concrete beams with mixed-in capsules filled with water-repellent agent showed higher resistance against chloride ingress compared to plain cracked concrete beams. Davies et al., (2018) designed and tested the in-situ constructed concrete panels casted with different self-healing technologies. Self-healing arrangement of five different panels are presented in Figure 2.3. The panels were tested for crack widths, deflections, strains, permeability and applied loading. Result concluded that self-healing concrete trials have been successful in succeeding their primary aim, which was to

scale-up the healing technologies and implement them in a full-scale structure on a live construction site.

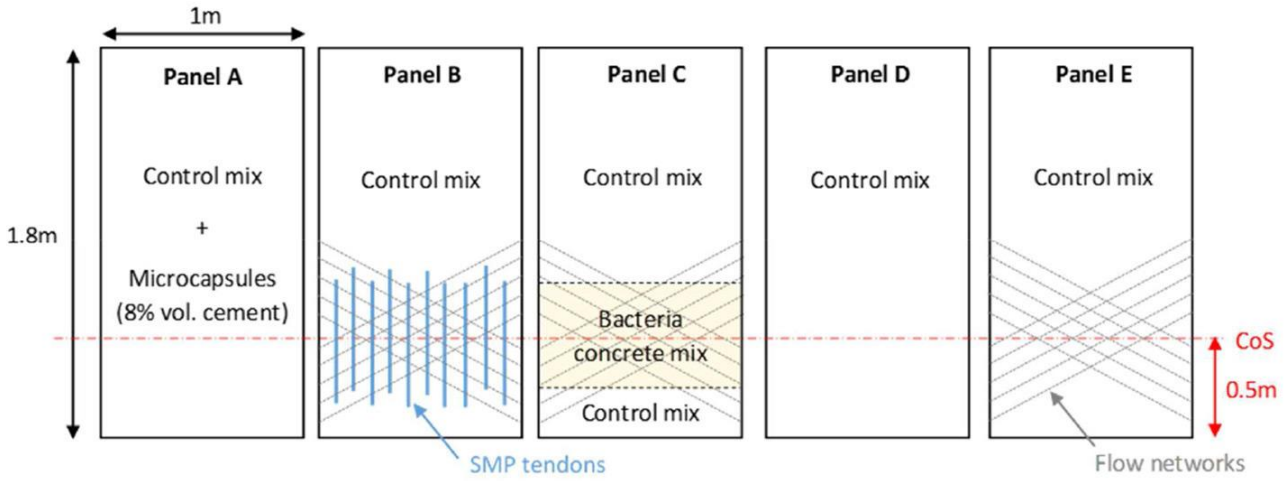

Figure 2.3: Different self-healing arrangement of panels (Davies et al. 2018)

Wang et al., (2019) applied self-healing concrete to tunnel construction in the Qianhai area, Shenzhen and concrete performance was studied in terms of strength and rapid chloride migration test. Results suggested that the self-healing system is feasible and promising for sustainable infrastructure, especially in coastal civil engineering. Al-Tabbaa et al., (2019) reported first large field trail microcapsule-based self-healing concrete in the UK and found satisfactory results in terms of low water permeability ingress. Qian et al., (2021) developed powder based and capsule based microbial self-healing agents and applied them on demonstration project (Figure 2.4). The crack sealing was monitored using ultrasonic pulse velocity. Moreover, authors suggested that powder based microbial self-healing is more efficient and suitable at field applications. The powder and capsule based material was tested in extended study from the research group (Zhang et al. 2021). The powder-based material constituted of bacteria spore powder and calcium source, which were mixed in 1:10 ratio by mass. The capsule-based material constituted of bacterial powder as core material and shell material as sulfoaluminate cement, fly ash, and iron sand powder, and the mass ratio is 3:1:1.

Authors suggested that the low cost of carrier material and preparation process are required to promote microbial self-healing concrete to the engineering applications.

Figure 2.4: Pouring process of microbial self-healing concrete (Qian et al. 2021)

Du et al., (2022) demonstrated the application of microbial self-healing concrete in sidewall of underground engineering (Figure 2.5) and tested the self-healing capabilities. Self-healing properties was monitored using ultrasonic pulse velocity at site.

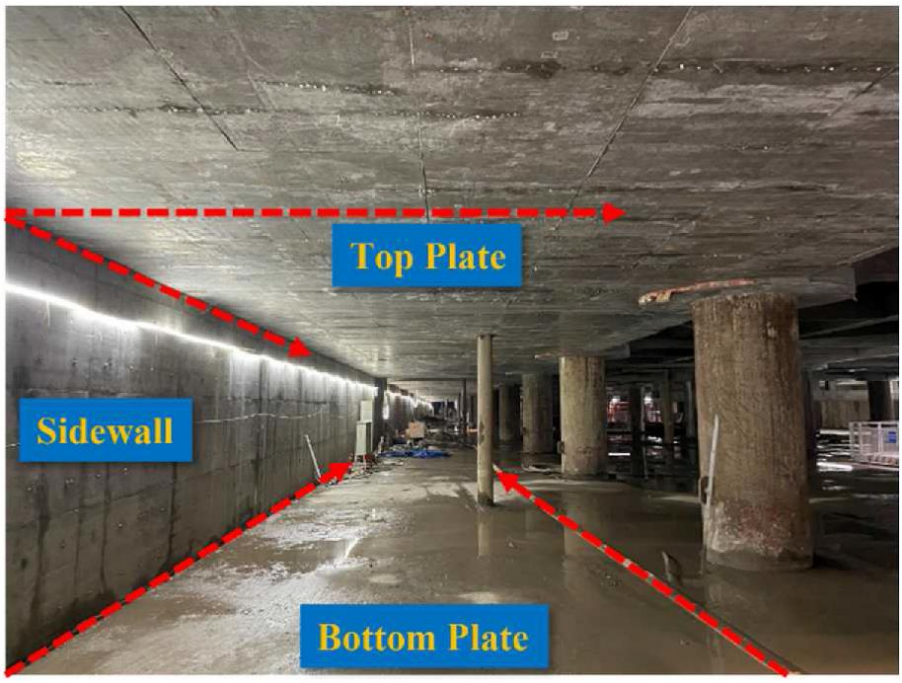

Figure 2.5: Schematic diagram of the main structure of the underground engineering (Du et al. 2022)

Moreover, authors reported that microbial healing agent (MHA) didn't have any negative effect on the workability, compressive strength and drying shrinkage. MHA can be sent to the conveyor belt along with the aggregate and directly mixed during the mixing of concrete constituents. This will help to promote self-healing technology to concrete engineering.

2.3.6 Corrosion prevention performance using bacteria as bio-agent

Presence of micro-cracks provide path for the penetration of aggressive ions inside the concrete matrix leading to early corrosion of reinforcement. Xu et al., (2020) reported application of ureolysis-based microbial $CaCO_3$ precipitation in inhibition of reinforcement corrosion. Authors prepared porous ceramsite particles as carrier material to immobilize bacteria in reinforcement concrete specimens. These prepared specimens were cracked and subjected to natural CO_2 aggressive environment. Corrosion current density (I_{corr}) were acquired at 0 and 120 days of cracking using electrochemical technique. The results indicated I_{corr} of less than $0.5\mu A/cm^2$ at 120 days of cracking in bacterial specimens suggesting a formation of layer barrier layer restricting the penetration of aggressive ions. Kanwal et al., (2023) reported *B. subtilis* and *B. safensis* were the optimum strains in developing strong and sticky biofilms during both in-vitro and in-vivo studies and appeared as excellent corrosion inhibitors of reinforcing steel bars compared to the control specimen under an exposure of 3.5% NaCl. Kanwal et al., (2022) used sugarcane bagasse as carrier material to immobilize *B. subtilis* in reinforced concrete. These specimens were subjected to accelerated current induced corrosion under chloride environment. Results indicated that the bio-inspired concrete offered larger polarization resistance, lesser corrosion rate, and highest efficiency to inhibit the corrosion in embedded rebars because of denser microstructure by biological calcite deposits in pore spaces. Osman et al., (2021) used electrochemical technique to test corrosion activity in control and bacterial specimens under chloride environment. Authors found that low I_{corr} in bacterial specimens in comparison the control specimens. Researchers also documented nitrite

producing bacteria also inhibits reinforcement corrosion under chloride environment (Erşan et al., (2016, 2018)). The denitrification mechanism produces dissolved inorganic carbon through a redox reaction between nitrate and a carbon source by the denitrifiers in an anaerobic environment, and can simultaneously inhibit steel corrosion. Based upon the above findings, it can be concluded that carrier based bacterial material can prevent the harsh alkaline environment of concrete and significantly protect the RC from aggressive ions penetration and thus extending the service life of RC structures. Immobilization of bacterial based bio-agent in RC could be a sustainable solution to prevent the corrosion in marine environment.

2.4 SUMMARY OF LITERATURE REVIEW

Microbially induced calcium carbonate precipitation (MICCP) has shown promising results in enhancing strength and durability characteristics of concrete. In long term, the survival of bacteria in high alkaline environment is of major concern. To address the survivability issue, researchers adopted suitable carrier materials and shown satisfactory results in self-healing. Some the studies reported detrimental influence on the strength properties. There is a need to select suitable mineral carrier for bacteria already known to be synergistic with the concrete. Very few or no study reported the shelf life of bacterial product before incorporating them to concrete. Longer shelf life of bacterial product is desired for upscaling MICCP application to engineering application. The goal of present work is to develop a better understanding in MICCP technique, which will facilitate the practical implementation of microbial concrete in construction sector in the near future.

CHAPTER 3: DEVELOPMENT OF CARRIER BASED INOCULUM

3.0 GENERAL

Microbially induced calcium carbonate precipitation (MICCP) has proven to be a promising technique in concrete due to its sustainability and good compatibility with concrete (De Belie et al. 2018; Hossain et al. 2022; Kan et al. 2019). The primary focus of the research on MICCP has been on the use of different microbial strains to improve the mechanical and durability properties (Achal et al. 2011a; Alazhari et al. 2018a; Nguyen et al. 2019; Tripathi et al. 2019). The survival of different bacterial strains in high alkaline environment of concrete is a major concern. Therefore, to address this concern, researchers used various carrier materials to immobilize bacteria in concrete and to increase the viability of bacterial cells in concrete. Researchers documented the use of perlite (Alazhari et al. 2018a; Zhang et al. 2017), polyurea (Zamani et al. 2020), zeolite (Bhaskar et al. 2017), diatomaceous earth (Wang et al. 2012b) and graphite nanoplatelets (Khaliq and Ehsan 2016) as potential carriers for the bacteria in concrete. These carrier materials have proven to be productive for self-healing of concrete. However, the shelf life of these bio carriers materials have not been defined and the researchers have used the freshly prepared bacterial carrier for MICCP application (Bhaskar et al. 2017), which makes them difficult to use in practical applications. Also, the detrimental influence of bacterial carriers on the mechanical properties of concrete has been reported in previous studies (Ann et al. 2006; Erşan et al. 2016b).

To tackle this concern, it is encouraged to use the carrier material that is known to be synergistic with concrete. This chapter focusses on the development of mineral inoculums using supplementary cementitious materials (SCM) as carriers which have already shown engineering benefits when used in concrete (Kunal et al. 2014; Siddique 2011; Siddique et al. 2016; Yunchao et al. 2021). For this purpose, fly ash (FA), silica fume (SF), cement kiln dust (CKD) and rice husk ash (RHA) were selected as potential carriers for bacteria. Bacterial cells

were mixed in these potential carriers separately and stored at varying temperature conditions to test the shelf life of the carrier inoculums. The mineral inoculums possessing sufficient cell count for long term were used as admixture in concrete to test its effectiveness in improving strength and permeation characteristics of the resultant concrete.

3.1 DEVELOPMENT OF CARRIER BASED INOCULUM

This section elaborates about the detailed procedure of preparation and testing of mineral inoculums. The section first discusses about the materials required for the bacterial product followed by procedure adopted to prepare carrier inoculum and finally the testing methods to define the shelf life of prepared carrier inoculums at varying temperatures.

3.1.1 Materials

This section discusses about bacterial culture cultivation process and the properties of various selected SCM for the development of mineral inoculums.

Bacterial strain and culture preparation

The bacterial strain, *Bacillus megaterium* SS3 was used in the present study because of its superior efficacy to precipitate $CaCO_3$ (Dhami et al., 2013). For growth of bacteria, the bacillus was inoculated in autoclaved Nutrient broth (NB) procured from Himedia, India as shown in Figure 3.1(a). The autoclaved NB was used to ensure the growth of bacillus cells only. The growth medium was incubated in shaker at 120 rpm at 37°C and the cell concentration was monitored by measuring its optical density (OD) at 600 nm wavelength with the help of UV-Vis spectrophotometer. UV- spectrophotometer of Shimadzu (UV-1800) was employed to measure OD of growth bacterial culture. The incubation was done until the OD_{600} of bacterial culture reaches ~ 0.5. The final grown culture is shown in Figure 3(b).

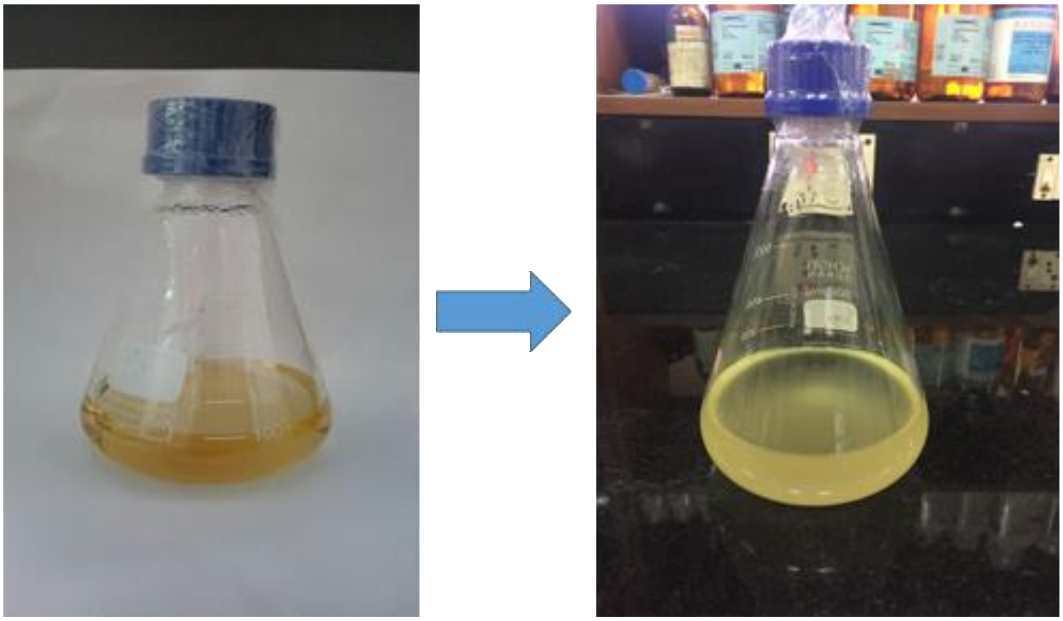

(a) (b)

Figure 3.1: (a) Autoclaved nutrient broth media and (b) Grown culture in flask

Suitable carrier materials

A suitable carrier material should create the optimum environment for bacterial growth and metabolism (Jiang et al. 2020). A good carrier material should be insoluble, non-toxic for both the immobilized material and for the environment, and easily accessible (Dzionek et al. 2016). It should not have any detrimental influence on the properties of concrete. Moreover, the potential carrier materials should be inexpensive, stable and unreactive with bacteria. In the present research, fly ash (FA), silica fume (SF), cement kiln dust (CKD) and rice husk ash (RHA) were selected as potential carriers for bacteria. These minerals have already shown positive influence on the mechanical and durability properties of concrete, when used as supplementary cementitious materials. FA was collected from Rajpura Thermal Power Plant, Punjab, India; SF was procured commercially from the vendor; CKD was collected from Ambuja Cement Plant located at Darlaghat, Himachal Pradesh, India and RHA was procured from Punjab Chemicals and Crop Protection Limited located at Derabassi, Punjab, India. The microstructural and chemical analysis of FA, SF, CKD and RHA are presented in Figure 3.2 and Table 3.1.

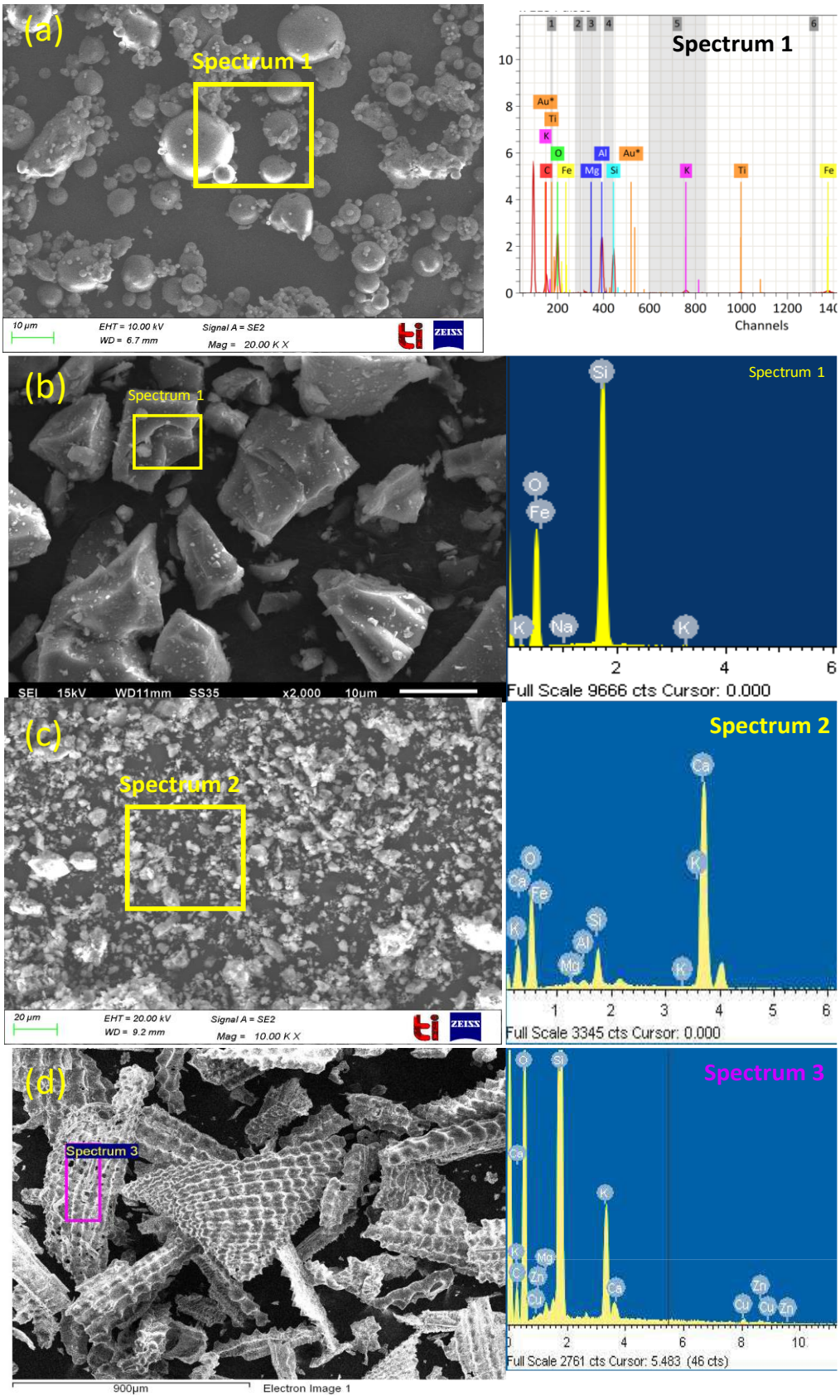

Figure 3.2: SEM-EDX analysis of (a) Fly ash (FA) (b) Silica fume (SF) (c) Cement Kiln dust (CKD) and (d) Rice husk ash (RHA)

Table 3.1: Chemical composition of selected minerals

Oxides	FA (%)	SF (%)	CKD (%)	RHA (%)
SiO_2	57.40	91.50	15	94
Al_2O_3	39.95	1	3.2	1.2
Fe_2O_3	1.05	3.46	2.3	0.37
SiO_2+ Al_2O_3+ Fe_2O_3	98.4	95.96	20.5	95.57
CaO	0.32	0.34	39.4	2.9
MgO	0.33	1.8	1.8	-
Na_2O	0.1	-	1.4	-

It can be observed from Table 3.1, that the collected FA was of class F as per IS standard (IS 3812 (Part-1): 2003) since the sum of oxides (SiO_2, Al_2O_3 and Fe_2O_3) was found to be 98.4% which is greater than 70%. The SEM micrograph of FA, as shown in Figure 3.2 (a), indicate that the particles were spherical with huge quantity of small particles attached to the larger particles. SF consists of high content of silicon dioxide (SiO_2) and small content of calcium oxide, magnesium oxide and sodium oxide. The angular shape of SF particles is observed from its SEM micrograph, as shown in Figure 3.2 (b). CKD has less content of SiO_2 and it is known to have high content of calcium oxide (CaO). CKD is fine powder material and has similar appearance as ordinary Portland cement. CKD is generally consisting of unreactive raw material of cement clinker and SEM micrograph is shown in Figure 3 (c). Whereas, RHA is a by-product of agriculture industry and is generally obtained from rice milling. It has high amount of reactive SiO_2 and has porous structure as observed from Figure 3.1 (d).

3.1.2 Preparation of carrier-based inoculums

To prepare the mineral carrier-based inoculum, the grown bacterial culture with OD_{600}~0.5 was centrifuged at 5000 rpm for 10 minutes to attain the pellet of bacillus cells. The obtained pellet was washed twice with 0.85% saline to remove adhered nutrient broth. The saline-washed cell pellets were then suspended in 20-25% sterilized distilled water to prepare the bacterial slurry.

Figure 3.3 shows the various stages involved during the preparation of carrier inoculum. The bacterial slurry was resuspended in autoclaved carrier materials separately. The carrier materials were autoclaved to ensure that other type of bacteria is not present in the material at the time of mixing of bacillus cells. It was mixed thoroughly to obtain a uniform formulation. The prepared formulations were packed in sterile petri plates of size 90 mm (Himedia, India) to retain the optimum moisture. The developed carrier-based inoculums were stored separately at 4°C and 25°C as shown in Figure 3.4 to check its viability at weekly interval.

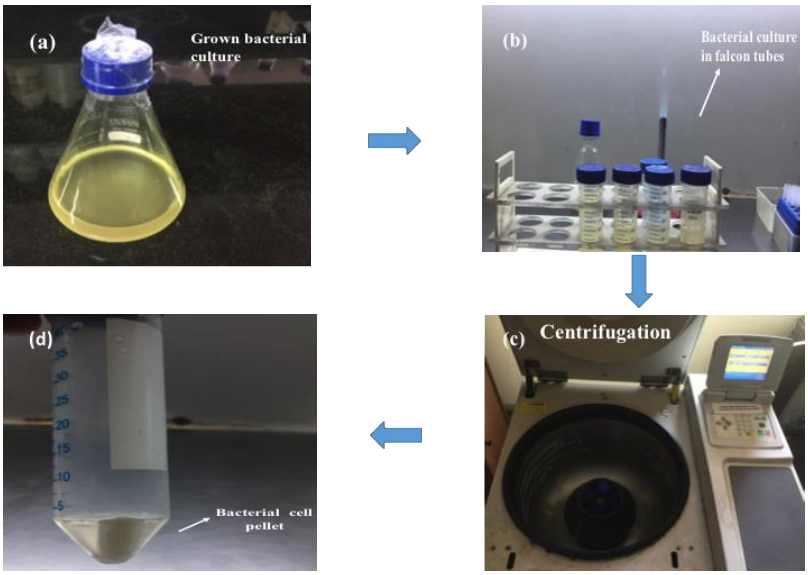

Figure 3.3: Various stages involved in the preparation of bacterial inoculum; (a) Grown bacterial culture; (b) and (c) Centrifugation of bacterial culture; (d) Bacterial cell pellet

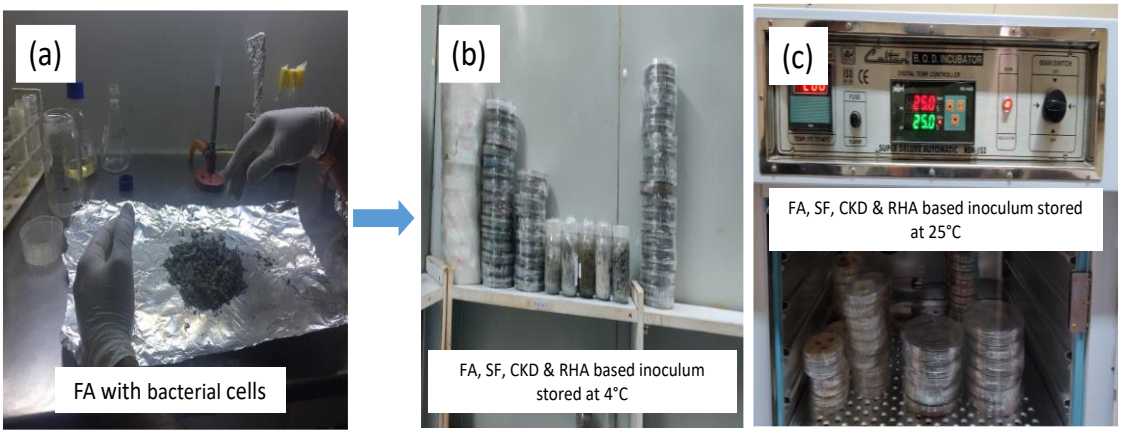

Figure 3.4: (a) Bacterial slurry suspended in FA; (b) FA, SF, CKD & RHA based inoculum stored at 4°C; (c) FA, SF, CKD & RHA based inoculum stored at 25°C

3.1.3 Testing of cell viability in the developed carrier-based inoculum

The purpose of cell viability studies was to investigate the survival rate of bacteria in FA, SF, RHA and CKD based inoculum. For this, the developed carrier-based inoculums stored at 4°C and 25°C temperature were studied separately on weekly basis until 270 days of storage. For this, one gram of the sample stored at different temperatures (4°C and 25°C) was taken weekly. To ensure the uniform distribution of cells in stored formulation, the packets were shaken well before sampling. Further, serial dilution was done by taking one gram of each carrier-based inoculum separately in 9 ml of sterile saline as shown in Figure 3.5. Serial dilution was done to reduce bacterial concertation to a required concentration level or to a concentration which is easier to count. For instance, Fig. 3.6 shows the cell viability of FA based inoculum. The cell count was made readable by serial dilution.

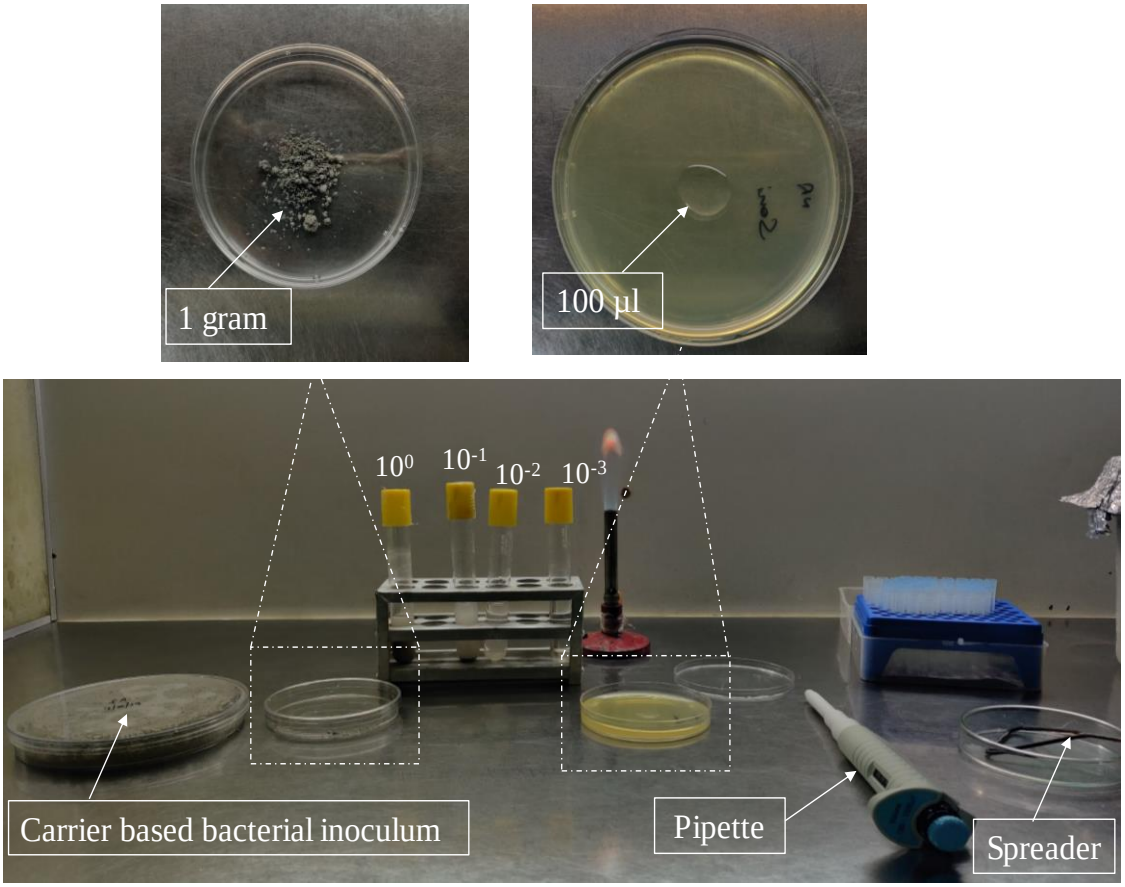

Figure 3.5: Viability studies carried out on carrier inoculums using plate count method

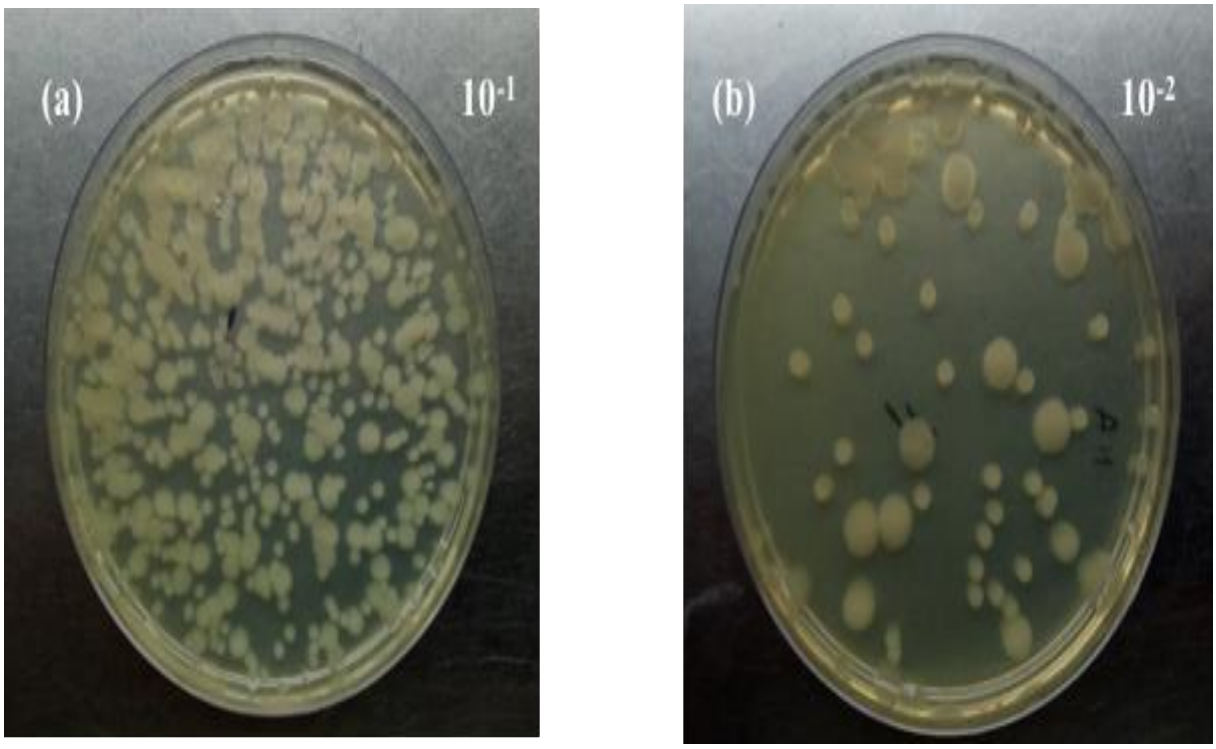

Figure 3.6: Viability test of FA carrier-based inoculum at the initial age at different dilutions

The 100-µl aliquot was taken and spread plated on the nutrient agar. The plates were then incubated at 37°C for 24-72 hours. The plate count was evaluated in triplicate and the final observation of colony-forming units (cfu/ml) was expressed as log cfu/g.

3.1.4 Results and discussion

The bacterial cell viability in terms of log cfu/g for mineral based inoculum was measured using plate count method and the test results are shown in Figure 3.7. The initial cell count of FA, SF, CKD and RHA based inoculums were observed to be 6.505, 6.53, 5.1 and 5.2 log cfu/g, respectively. The cell viability was found to be highest in SF and FA based inoculum among all the prepared inoculums at the initial age. Here initial age represents the cell viability at the time of preparation of mineral inoculums. It indicates that both the materials have similar potential for survival of the bacteria. Each mineral inoculums were then stored at 4°C and 25°C and the obtained test results are discussed individually as under.

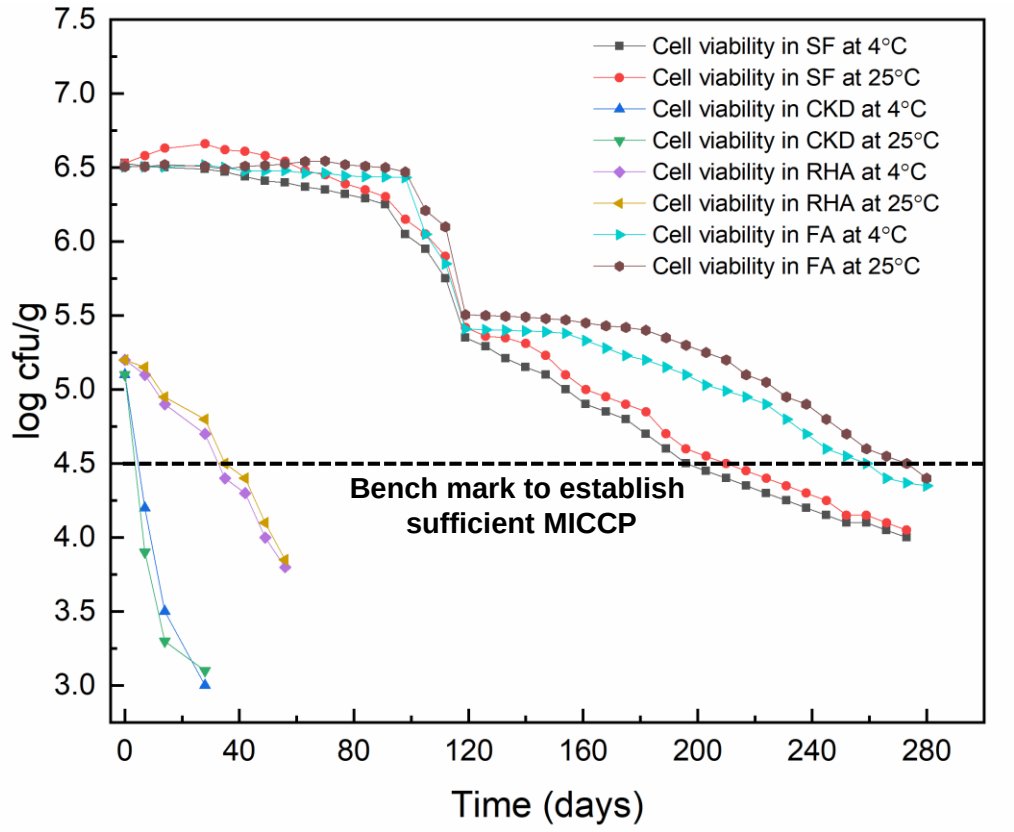

Figure 3.7: Cell viability in FA, SF, CKD and RHA based inoculum at 4°C and 25°C

In FA based inoculum, the initial cell count was observed to be 6.505 log cfu/g. The viability of FA-based inoculum showed an upward trend during the initial 28 days of storage at 4°C and 25°C, which signifies the optimum environment and nutrients in the formulation-supported bacterial multiplication. Whereas the cell viability of FA-based inoculum at 25°C showed an increasing trend after 28 days of storage, this was due to the presence of limited moisture in the bacterial formulation. Similar trend was observed up to 90 days of storage at both temperatures. However, after the 90 days of storage, the microbial load declined sharply in samples stored at 4°C and 25°C up to 120 days. Decline in the cell concentration at both temperatures after 90 days in FA-based inoculum might be due to toxicity of metabolites produced by bacteria and scarcity of nutrients. The cell concentration was in the range of 5.55 to 5.2 log cfu/g at both stored temperatures up to 180 days. The viability of all the isolates might be attributed to the formation of endospores by these isolates under unfavourable

conditions. In case of SF based inoculum, similar trend of cell viability was observed till 200 days of storage indicating potential carrier for bacteria in MICCP application in concrete structures. After that cell viability was found to be decreasing trend till the testing age of 270 days. Thus, optimum shelf life of SF based inoculum was suggested to be 180 days for efficient MICCP.

In CKD-based inoculum, the initial cell count was found to be 5.1 log cfu/g. The cell viability reduced drastically and was found to be 3 to 3.1 log cfu/g for 4°C and 25°C at 28 days of storage. It is worth mentioning that high amount of heat was released when the bacterial slurry was initially mixed with CKD to obtain a uniform formulation. The rise in temperature was monitored using laboratory based digital thermometer during mixing process of CKD and bacterial slurry. The reading indicated instant rise in temperature to 52°C and temperature shock was responsible for bacterial cell reduction. The heat released during the mixing process might have led to bacterial cell reduction, since it is known that the bacillus species of bacterial cells can survive only till the temperature of 50°C (Kaur et al. 2013; Mutitu et al. 2019). The heat was released due to the reaction of free quick lime (CaO) present in CKD with water leading to the formation of slaked lime ($Ca(OH)_2$) (Siddique 2006). It is visible from the drastic reduction in initial cell count of 5.1 log cfu/g in CKD specimens as compared to nearly 6.5 log cfu/g for SF/FA based inoculum. The cell count reduced further during storage, indicating that CKD is not suitable as a carrier material. Therefore, the cell viability test was stopped for CKD bacterial formulation after 28 days.

In case of RHA bacterial inoculum, initial cell viability was found to be 5.2 log cfu/g. The cell viability reduced linearly up to the storage of 35 days at both storage temperatures. The cell viability in RHA was found to be 3.8 log cfu/g at 56 days of storage. RHA has well known porous structure documented by various researchers (Van Tuan et al. 2011) and is visible from SEM image of RHA shown in Figure 3.2(d). Therefore, higher volume of bacterial slurry was

required for effective mixing of bacterial formulation due to high surface area in RHA. However, more bacterial slurry will indicate exponential bacterial growth that will further lead to competition among bacteria to survive. This competition leads to war among bacteria for resources and sudden cell reduction due to limited nutrients is expected (Hibbing et al. 2010). The cell count reduced further during storage, indicating that RHA was not suitable as a carrier material. The study was stopped for RHA bacterial formulation after 56 days of testing.

From the cell viability studies, it was concluded that only FA and SF based inoculum were suitable as bacterial carriers for MICCP activity. The cell count in both the inoculums was well above the 4.5 log cfu/g value till 180 days of storage. Also, the storage temperature does not have major influence on the cell viability. Therefore, FA and SF based inoculum stored at 4°C for 180 days was used as a product to precipitate calcium carbonate in the concrete matrix.

3.2 STRENGTH AND PERMEATION PROPERTIES OF BIO-CONCRETE

This section discusses about the effect of incorporation of FA and SF based bacterial product stored at 4°C in concrete. The properties of constituents of concrete are initially discussed, followed by the casting of concrete for strength and permeation properties. It is followed by the results and discussions related to the tested properties.

3.2.1 Materials

This section discusses the properties of materials used for the preparation of concrete specimens.

Cement

Ordinary Portland Cement (OPC) confirming to BIS 8112-2013 was used in the current investigation. The SEM micrograph along with energy dispersive spectroscopy (EDX) for OPC used in the study is presented in Figure 3.8.

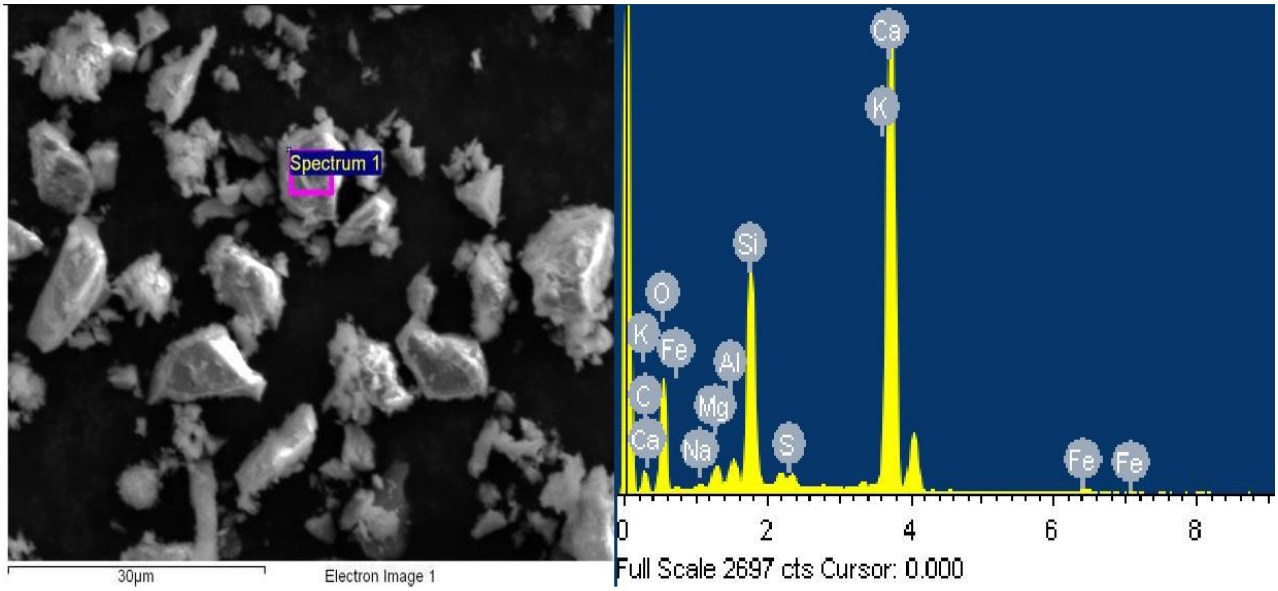

Figure 3.8: SEM-EDX analysis of OPC used in the present study

From EDX, it is clearly observed that the major constituents of OPC are calcium oxide (CaO) and silicon dioxide (SiO_2) along with the presence of other minor constituents. The chemical composition of the cement as supplied by the manufacturer is given in Table 3.2. The physical properties of cement are tabulated in Table 3.3.

Table 3.2: Chemical composition of Ordinary Portland Cement

Oxides (%)	**OPC result**	**IS Limit**
SiO_2	21.68	-
Al_2O_3	4.87	-
Fe_2O_3	3.35	-
CaO	62.79	-
MgO	1.73	<6.00
SO_3	2.43	<2.50
Na_2O	0.21	-
K_2O	0.69	-
LOI	1.94	<5.00

Table 3.3: Physical properties of cement

Properties	OPC result	IS Limit
Fineness (m^2/kg)	307	>225
Specific gravity	3.10	-
Consistency (%)	29	-
Initial setting time (min)	130	>30
Final setting time (min)	170	<600
	Compressive strength (N/mm^2)	
3 days	33.0	>23
7 days	41.3	>33
28 days	50.5	>43

Fine aggregate

Locally available river sand fulfilling the requirements of BIS 383-2016 was used as fine aggregates. The chemical composition of river sand is presented in Table 3.4. The physical properties of the aggregates were obtained by testing as per BIS codal provisions and the values are given in Table 3.5. The SEM image of the river sand is presented in Figure 3.9.

Table 3.4: Chemical composition of river sand

Constituent (%)	River Sand
CaO	5.73
SiO_2	77.39
Al_2O_3	8.38
Fe_2O_3	2.39
SO_3	-
MgO	0.70
K_2O	0.02
Na_2O	0.005

Table 3.5: Physical properties of river sand

Property	Natural River Sand	Standard followed
Specific gravity	2.63	BIS 2386 Part III- 1963
Water absorption (%)	2.1	BIS 2386 Part III- 1963
Fineness modulus	2.26	BIS 383-2016
Bulk density (kg/m^3)	1510	-
Specific surface area (m^2/g)	0.210	-
Grading Zone	Zone III	BIS 383-2016

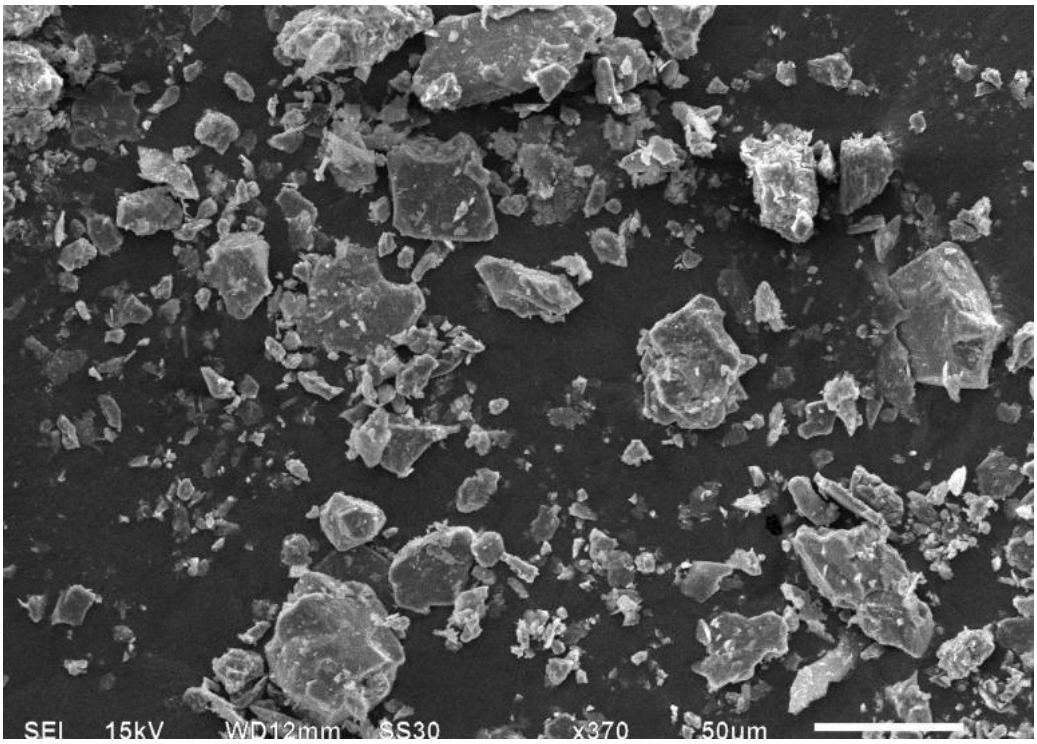

Figure 3.9: SEM image of river sand

The sieve analysis results of sand used in the present study are listed in Table 3.6. From sieve analysis results, it can be seen that the percentage passing of fine aggregates satisfied the Zone-III recommendations and codal provision. The fine aggregates (sand) used were washed and removed of any silt content followed by drying for twenty-four hours in an oven. The oven-dried aggregates are used for casting of specimens for concrete preparation.

Table 3.6: Sieve analysis results for river sand aggregates

IS-Sieve size (mm)	Weight retained (%)	Cumulative weight retained (%)	Weight passing (%)	IS limits for Zone III
10 mm	0.0	0.0	100.0	100
4.75 mm	5.2	5.2	94.8	90-100
2.36 mm	5.5	10.7	89.3	85-100
1.18 mm	8.5	19.2	80.8	75-100
600 μm	9.7	28.9	71.1	60-79
300 μm	41.0	69.9	30.1	12-40
150 μm	22.1	92.0	8.0	0-10
Pan	8	-		
Total		225.9		
Fineness modulus: 2.26, Zone III				

Coarse aggregates

Crushed gravel with nominal size of 20 mm and 10 mm was used as coarse aggregates. The physical properties of both these aggregates are listed in Table 3.7. The SEM micrograph along with EDX for crushed gravel aggregates is presented in Figure 3.10. Through EDX analysis, it was observed that crushed gravel aggregates have silica as its major composition. The exact chemical composition of the used coarse aggregates is given in Table 3.8.

Table 3.7: Physical properties of coarse aggregates

Properties	Coarse aggregates	
	20 mm	10 mm
Specific gravity	2.70	2.68
Water absorption (%)	1.38	1.4
Fineness modulus	6.82	6.18

Sieve analysis results for 20 mm and 10 mm crushed gravel aggregates are presented in Tables 3.9 and 3.10 respectively. The coarse aggregates too were washed and removed of any silt and

then dried for twenty-four hours in an oven. The oven-dried aggregates are then used for casting of specimens for concrete mix.

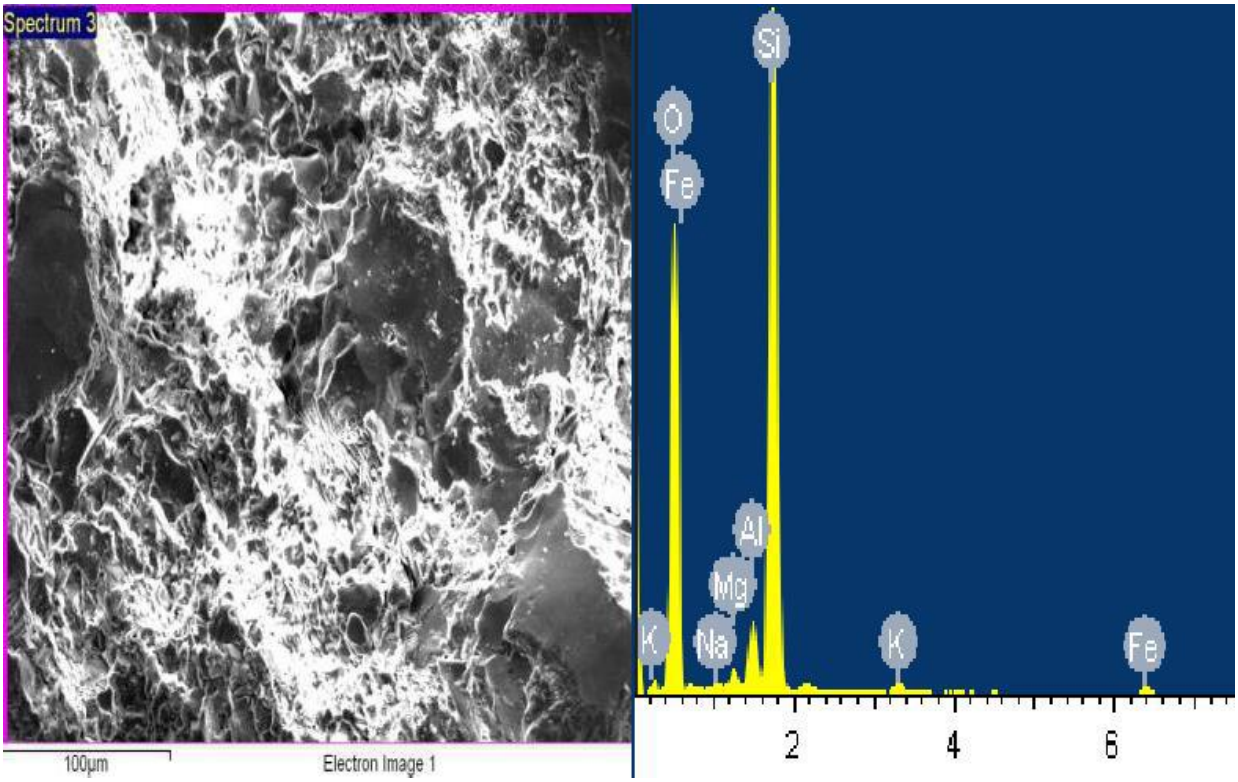

Figure 3.10: SEM-EDX image of coarse aggregates

Table 3.8: Chemical composition of coarse aggregates

Oxides (%)	**Coarse Aggregates**	
	20 mm	**10 mm**
SiO_2	85.16	86.12
CaO	-	
Al_2O_3	9.24	8.29
FeO	1.86	2.03
MgO	0.75	0.79
K_2O	2.77	2.15
Na_2O	0.23	0.65

Table 3.9: Sieve analysis of 20 mm crushed gravel coarse aggregates

IS-Sieve size (mm)	Weight retained (%)	Cumulative weight retained (%)	Weight passing (%)
40	0.00	0.00	100.00
20	3.73	3.73	96.27
12.5	79.01	82.74	17.26
10	10.64	93.38	6.62
4.75	6.58	99.96	0.04
Pan	0.04	100.00	0.00

Table 3.10: Sieve analysis of 10 mm crushed gravel coarse aggregates

IS-Sieve size (mm)	Weight retained (%)	Cumulative weight retained (%)	Weight passing (%)
20	0.0	0.0	100.0
12.5	3.63	3.63	96.37
10.0	8.41	12.04	87.96
4.75	75.63	87.67	12.33
2.36	12.31	99.98	0.02
Pan	0.02	100	0.00

Water

For the preparation of specimens, potable ground water available in laboratory tap was used throughout the investigation. The composition of the water was tested and the values are presented in Table 3.11.

Table 3.11: Properties of laboratory tap water

Substance	Concentration (mg/l)
Total dissolved solids	450
Total alkalinity	85
Total hardness	132
Chlorides	112
Sulphate	55

3.2.2 Preparation of concrete specimens

The concrete mix was prepared by following the guidelines of (BIS:10262 2009). The prepared mix was having cement: sand: coarse aggregate in the proportion of 1:1.82:3.24 (by weight) and water to cement ratio (w/c) of 0.47. Different types of specimens were cast to study strength and permeation characteristics of the resultant concrete. For strength measurement, cubes for 150 mm and prismatic specimens of 500×100×100 mm were cast as per BIS 516:1959. For permeation properties, cylindrical specimens of 100 mm (dia) × 200 mm (height) were cast and test specimens of 100 mm (dia) × 50 mm (height) was sliced as per ASTM C1585. The prepared concrete specimens were divided into three groups. The details of all three groups along with the composition of growth medium and curing mechanism is presented in Table 3.12.

Table 3.12: Outline of different sets of concrete specimen and mechanism of curing regime

Specimens	**Material used**	**Mechanism of curing**
Control	Cement: sand: coarse aggregate Water/cement = 0.47	Water Curing for 28 days
FAA	Cement: sand: coarse aggregate FA based inoculum Growth medium /cement = 0.47	Submersion in FA bacterial inoculum, growth medium for 28 days
FAS	Cement: sand: coarse aggregate Water/cement = 0.47	FA inoculum culture spray twice a day for 28 days
SFA	Cement: sand: coarse aggregate SF based inoculum Growth medium /cement = 0.47	Submersion in SF bacterial inoculum, growth medium for 28 days
SFS	Cement: sand: coarse aggregate Water/cement = 0.47	SF inoculum culture spray twice a day for 28 days

Growth medium has the following composition: Nutrient broth (1.3% w/v), 2% Urea (w/v) and 25mM Calcium chloride (w/v). All specimens were prepared in triplicate.

In 1st group, control specimen was prepared and cured using tap water for 28 days. In the 2nd group, 180 days FA/SF based bacterial carrier stored at 4°C was introduced by 5% of the weight of cement along with other ingredients during casting of the specimens. In this group, growth medium supplemented with nutrients and calcium source was used instead of tap water for preparing the mix. The specimens were cured with same growth medium and FA/SF carrier inoculum for 28 days. In the 3rd group, the specimens were fabricated same as 1st group. These specimens were then cured twice a day using the bacterial spray for 28 days.

3.2.3 Testing methods

Strength properties was studied in terms of compressive and flexural strength at the age of 7 and 28 days as per BIS 516 (1959). The compressive strength of 150 mm cubes was tested using automatic compression testing machine (AIMIL India) of 5000 KN capacity. The test setup for compression testing is shown in Figure 3.11. The flexural strength of 500 ×100 ×100 mm was tested on the flexural testing machine (AIMIL India ltd, New Delhi) of 100 KN capacity. To perform flexural strength test, concrete prism was placed on the supporting rollers of testing machine and uniform loading was applied to uppermost surface of specimen until the failure. The test setup for flexural strength is shown in Figure 3.12.

Figure 3.11: Test set for compressive strength measurement

Figure 3.12: Test setup for flexural strength measurement

Permeation characteristics was studied as per ASTM C1585 at 28 days of casting. The test was conducted on cylindrical specimens of 100 mm dia × 50 mm height. The sample was saturated by placing in vacuum dedicator for 3 hours. After saturating, samples are placed in the environmental chamber at a temperature of 50 ± 2 °C and RH of 80 ± 3 % for 3 days. After the 3 days, samples were placed inside a sealable container and stored at 23 ±2 °C for at least 15 days before testing. The conditioned samples were taken out of the container and the initial weight was recorded nearest to 0.01 gram. The average diameter of the test surface was measured to the nearest 0.1 mm. Sides of the samples were sealed with the epoxy. A pan with support device at its bottom was filled with tap water was used for water absorption mass measurement of specimens as shown in Figure 3.13. For each mass determination, the test sample was removed from the pan and excess water was blot off with a dampened paper towel or cloth. After blotting, mass to nearest 0.01 g of specimen was measured with the balance pan. The mass change was recorded at the intervals of 60 s, 5 min, 10 min, 20 min, 30 min, 60 min and every hour up to 6 hours. From the value of mass change, volume of water absorbed per unit cross sectional area was evaluated for each time interval. A plot

between the square root of time and volume of water absorbed was plotted. The slope was calculated by using least squares, linear regression analysis from the obtained plot and is called sorptivity coefficient.

Figure 3.13: Test setup for sorptivity test

3.2.4 Microstructural analysis

To assess the mineral formed during the microbial activity of microbes, mineral deposits were characterized through FESEM-EDX. For FESEM and EDX, broken samples were collected from the depth of specimens (Control, FAA and SFA) at 28 days of testing. The samples were gold coated with a sputter coating Emitech K575. The prepared samples were then analysed via FESEM (Hitachi, SU8010).

3.2.5 Results and discussion

The following section discusses about the results obtained with the incorporation of mineral inoculums on the strength and permeation characteristics of the resultant concrete.

Strength properties

The strength results obtained at 7 and 28 days of testing are shown in Figure 3.14. It can be observed that addition of 180-day old FA and SF based inoculum stored at 4°C supplemented

with nutrients significantly improved the strength as compared to control specimens. The bacterial admixed specimens made by using fly ash as carrier material (FAA) showed an average increase of 19% and 25% in compressive strength as compared to the control specimens at 7 and 28 days. The corresponding increase in strength of specimens with silica fume as a carrier material (SFA) specimen was 34% and 32% as compared to the control specimens. The dual effect of bio-deposition of calcium carbonate and early hydration of silica fume is responsible for the higher strength in SFA specimens at 7 days. Whereas, deposition of calcium carbonate is only responsible for strength improvement in FAA specimens at 7 days. At 28 days, dual effect of calcium carbonate and pozzolanic effect contributes in strength improvement in FAA and SFA specimens. Even the spray treated specimens (FAS and SFS) showed an average gain of 21% compressive strength at 28 days (Figure 3.14 (a)). The lower improvement in strength in spray treatment procedure is due to the fact that it leads to bio deposition only at surface and do not alter the bulk concrete properties to a large extent. The flexural strength results are shown in Figure 3.14 (b). It can be seen from the results that the average flexural strength improved by 8% in bacterial admixed specimen (FAA and SFA) as compared to the control at the age of 28 days. Accordingly, bacterial spray specimens (FAS and SFS) showed an average gain of 3% in flexural strength at 28 days (Figure 3.14 (b)).

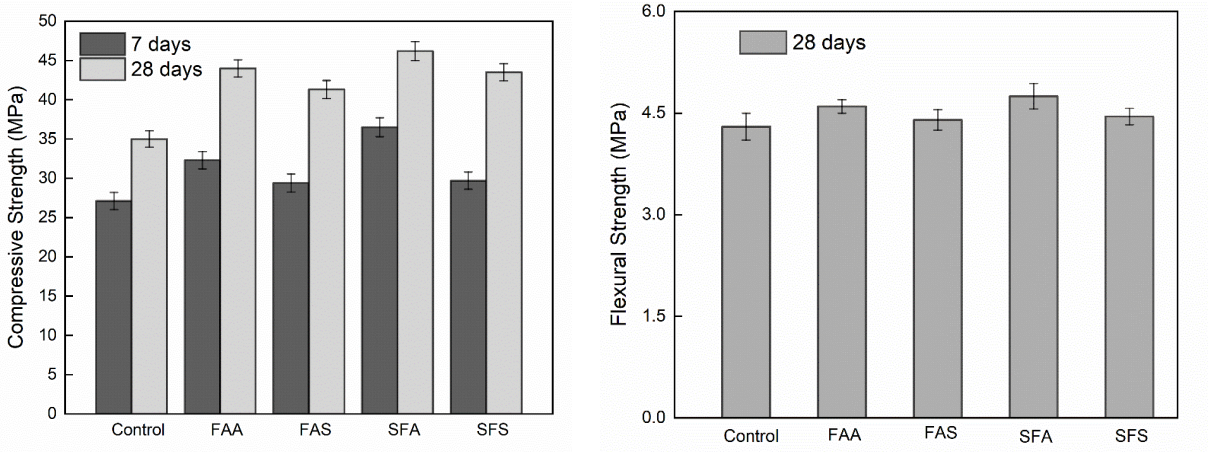

(a) (b)

Figure 3.14: (a) Compressive strength results of specimens at 7 and 28 days (b) Flexural strength results of specimens at 28 days

Permeation characteristics of resultant concrete

Along with strength properties, sorptivity test was used to study the permeation characteristics of the prepared concrete specimens and the values are presented in Table 3.13. Among the tested specimens, control specimen has higher sorptivity coefficient at 28 days of testing. The FA and SF bacterial inoculum supplemented with nutrients led to drastic reduction in sorptivity coefficient values. Even the spray treated specimens (FAS and SFS) showed significant reduction in the sorptivity coefficient. An approximate three-fold reduction in permeation can be attributed to the denser interfacial matrix formed due to the calcium carbonate precipitation between the pore structures of bacterial admixed specimens. The bio-deposition of calcium carbonate on the outer surface of specimens clogs the pores and hence acts as barrier. The results are in agreement with previous findings reported by researchers (Joshi et al. 2018a; Tripathi et al. 2019).

Table 3.13: Test results of sorptivity coefficient at 28 days of testing

Specimen	Sorptivity coefficient
Control	0.020
FAA	0.007
FAS	0.008
SFA	0.007
SFS	0.008

Microstructural analysis

FESEM-EDX analysis of the Control, FAA and SFA specimens were performed at 28 days of testing (Figure 3.15). FESEM analysis showed the presence of lamellar rhombohedral crystals of calcium carbonate in the FAA and SFA specimens (Figure 3.15 (b,c)). This morphology of mineral precipitations was confirmed to be the same as reported by researchers (Joshi et al. 2018a; Sidhu et al. 2022).

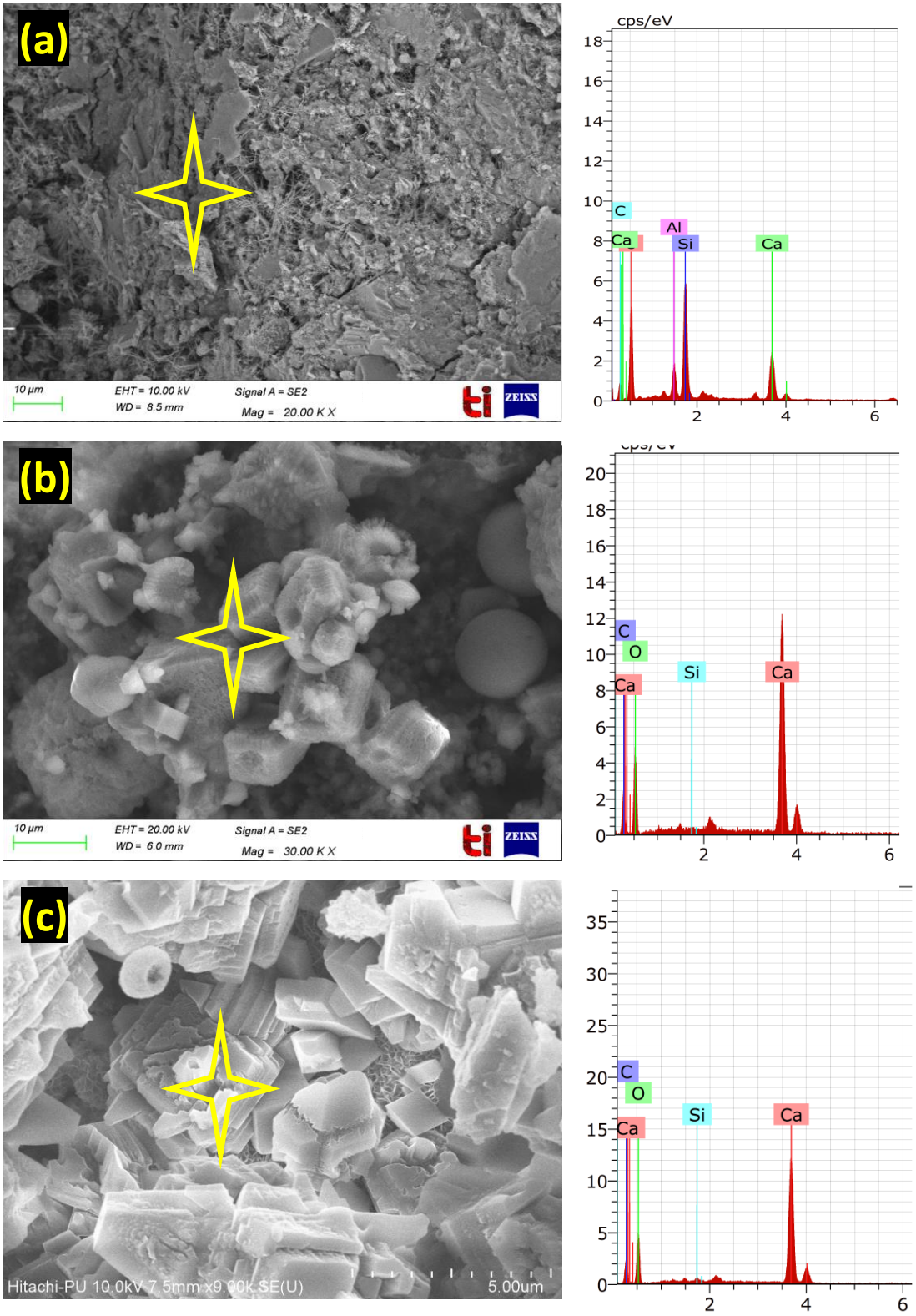

Figure 3.15: FESEM-EDX analysis of (a) Control (b) FAA and (c) SFA at 28 days of testing

The EDX analysis also confirmed the elemental composition of crystals with peaks showing high amount of calcium and carbon confirming the formation of calcium carbonate. In case of

control specimens, no formation of calcium carbonate precipitation was observed. Also, the formation of CSH and ettringite were observed in the control specimens. These findings are consistent to the previous published results (Tan et al. 2022; Yi et al. 2020).

3.3 CONCLUDING REMARKS

The aim of present study was to develop mineral based inoculums for upscaling MICCP for field scale construction and remediation of existing damages. Based upon the viability studies, it was observed that both fly ash (FA) and silica fume (SF) was good carrier materials for the bacterial inoculum. FA and SF based inoculums stored at 4°C and 25°C up to 180 days were able to sustain sufficient cells for MICCP application in concrete structures. FA and SF based inoculum stored at 4°C for 180 days stored were further immobilized in concrete and tested for strength and permeation properties. The viability/survivability of bacteria once incorporated in the concrete to establish the protective performance of the carrier material with respect to potential lifetime of concrete-incorporated bacteria can be studied in future studies. The results indicated significant improvement in strength at both 7 and 28 days of testing and reduction of permeability at 28 days of testing. FESEM-EDX analysis confirmed the presence of calcium carbonate in the bacterial carrier immobilized concrete.

CHAPTER 4: ANTI-CORROSIVE POTENTIAL OF BIO-CONCRETE

4.0 GENERAL

Reinforcement corrosion induced by chloride is one of the most common and natural phenomena accounting for structural distresses in reinforced concrete (RC) structures (Fu et al. 2021; Li et al. 2021). It is a serious problem that threatens the durability and strength of concrete structure (Rodrigues et al. 2021). These distresses may lead to premature failure, thus decreasing the service life of RC structures. Reinforcement corrosion results in loss of cross-sectional area of rebar and formation of expansive corrosion products (iron oxides and hydroxides) causing concrete cover cracking and spalling (Lin et al. 2019; Sharma et al. 2018a). To protect and mitigate RC from corrosion, denser concrete or highly impermeable surface can significantly extend the service life by resisting the ingress of aggressive agents (Dai et al. 2010). This can be achieved by microbially induced calcium carbonate precipitation (MICCP) and it is well reported by our research group in the recent publications (Achal et al. 2011a; Dhami et al. 2013c; Joshi et al. 2018a; Sidhu et al. 2022). Researchers reported that microbial urea hydrolysis and aerobic oxidation of organic carbon require O_2 as final electron acceptor to initiate and/or to keep the microbial activity (De Belie 2016). This may result in oxygen consumption in the concrete, which may pose a limitation for rebar corrosion. In this study, fly ash (FA) and silica fume (SF) based inoculums stored at 4° C for 180 days as addressed in previous chapter were immobilized in concrete mixes for MICCP activity. The prepared specimens were subjected to accelerated chloride induced corrosion for complete testing duration. These specimens were tested for corrosion using electrochemical and electromechanical impedance (EMI) technique as outlined in Figure 4.1. Initially reference specimen were cast and cured using tap water. To induce MICCP activity in specimens, two methodologies were adopted. In the first methodology, mineral inoculums were immobilized during casting with growth medium instead of water. The growth medium comprises of nutrient

broth media supplemented with urea and calcium chloride. In the second methodology, mineral inoculum was used to prepare bacterial culture supplemented with urea and calcium chloride. The prepared bacterial culture was sprayed twice a day up to 28 days on the control concrete. These prepared RC specimens in all the sets were subjected to chloride induced corrosion till the crack appeared on the surface of specimen. The changes occurred due to corrosion were assessed using electrochemical and EMI techniques during the test exposure. Therefore, the efficiency of mineral inoculums in corrosion mitigation were examined.

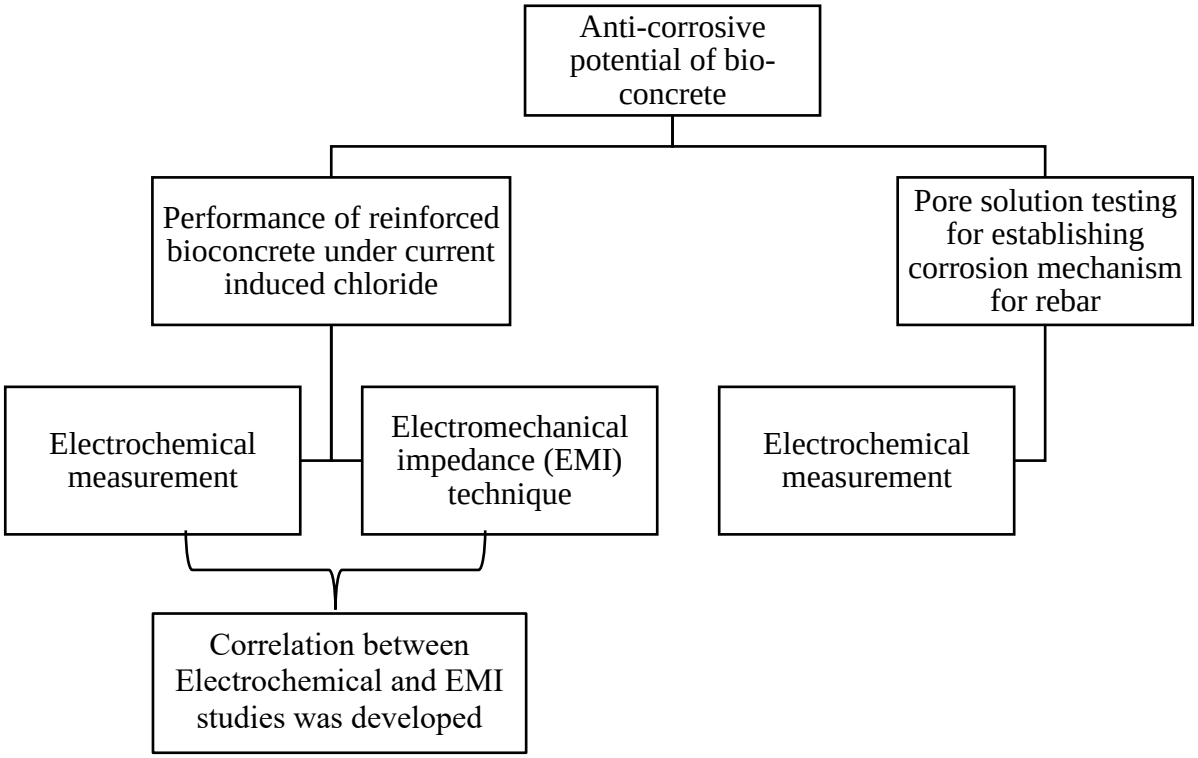

Figure 4.1: Overview of the studies conducted in exploring potential of anti-corrosive properties

4.1 MATERIALS

This section discusses about the materials used for the preparation of test specimens.

4.1.1 Mineral carrier-based inoculums

The mineral carrier-based inoculums made by using FA was used for the preparation of mixes. The detailed procedure for preparation of these inoculums is reported in previous chapter. The

inoculum was stored at 4°C for 180 days and the viability studies reported in the previous chapter confirmed that these inoculums possessed sufficient cell counts to induce MICCP even after 180 days of storage.

4.1.2 Constituents of concrete

Commercially available ordinary portland cement (43 grade) (IS 8112 2013), locally available river sand and coarse aggregates conforming to standards (IS:383 2016) was used for preparing concrete specimens. The detailed specifications of all the constituents used in the present investigation are provided in section 3.3.1.

4.1.3 Preparation of rebar

16 mm diameter - Tempcore TMT (Thermomechanically treated) steel bar conforming to IS 1786 (2008) was used in the study. The steel bar was used for two different parameters: electrochemical studies and electromechanical impedance (EMI) studies on RC specimens. The preparation procedure was different for both measurements. The procedure of cleaning the bars and removing any debris was same for all the rebars. For electrochemical measurement in RC specimens, the rebar was cut into 120 mm lengths. The rebars were cleaned and were coated with two layers of epoxy on the top 20 mm leaving 100 mm as exposed length that was embedded in concrete at the time of casting. For electrical connectivity, a threaded hole was driven on the top of the rebar (Figure 4.2(a)). For EMI studies, the bar was cut into 120 mm lengths and were cleaned thoroughly. The surface of the rebar was machined at 50 mm from the bottom to mount the piezo sensor. A lead zirconate titanate **(**PZT) patch (PIC 151) of size 10×10×0.3 mm was bonded to each machined rebar using an adhesive agent (epoxy). It was made sure that the thickness of epoxy was less than one-third of the patch thickness (Talakokula et al. 2014, 2016). A small weight was applied over the assembly to create light pressure. The setup was kept at room temperature and was left untouched for period of 24 hours so that full

curing of adhesive may be achieved. Coaxial wires were attached through the process of soldering for making connections to an impedance analyser to capture the admittance signatures. To avoid the disconnection of wires while experimenting and extra protection of PZT, a thin layer of epoxy was applied and cured for 24 hours at room temperature as shown in Figure 4.2(b). The specification of PIC 151 and epoxy are listed in Table 4.1.

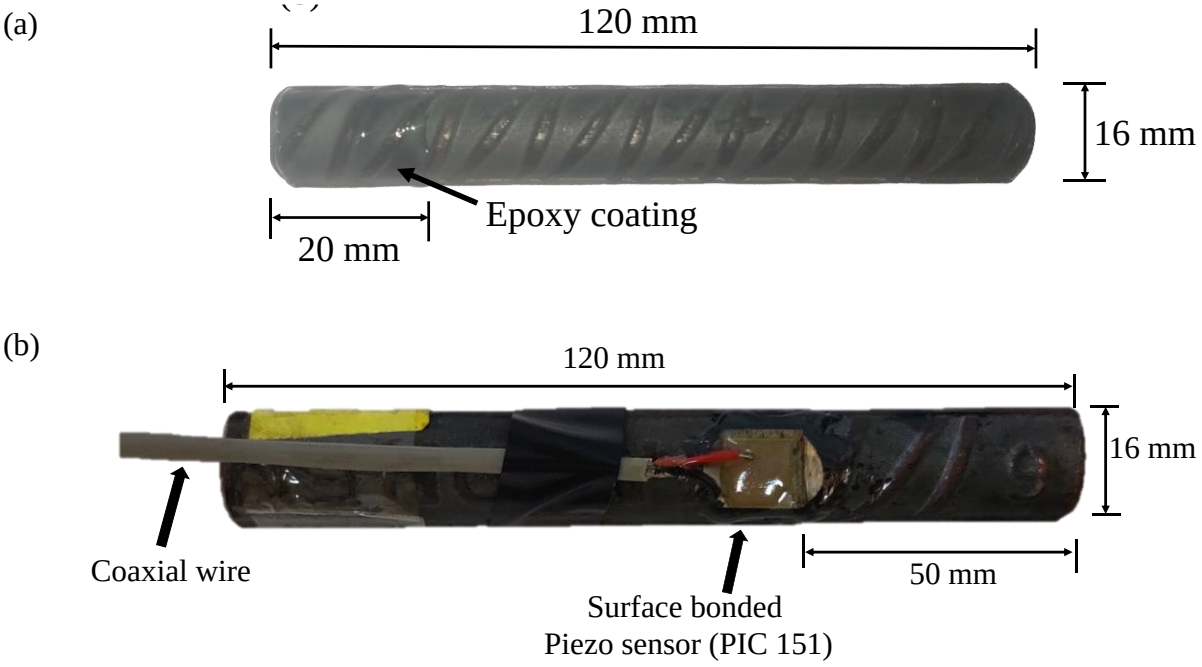

Figure 4.2: Cross sectional details of bare steel specimen (a) Electrochemical measurement; (b) EMI studies in in RC concrete

Table 4.1: Technical details of PIC-151 and epoxy

Properties	**Symbol**	**PIC 151**	**Epoxy**
Density	ρ	7800 kg/m^3	1200 kg/m^3
Relative permittivity	$\varepsilon_{33}/\ \varepsilon_0$	2400	-
Dielectric loss factor	tan δ	0.02	-
Piezo electric strain coefficient	d_{31}	-2.1×10^{-10} mV	-
	d_{13}	5.0×10^{-10} mV	-
Elastic compliance coefficient	S_{11}	1.5×10^{-11} m^2/V	-
	S_{33}	1.9×10^{-11} m^2/V	-
Young's modulus	Y^E	6.9×10^{10} N/m^2	9.79×10^{8} N/m^2

4.2 SAMPLE PREPARATION

The concrete mix used for making RC specimens was prepared using cement: sand: coarse aggregate in the proportion of 1:1.82:3.24 (by weight) and water to cement ratio (w/c) of 0.47 (BIS:10262 2009). The details about the mix are provided in Table 3.12 in the previous chapter. In these concrete mixes, bacterial inoculum was incorporated either at the casting stage or was used as a surface treatment measure during curing. Accordingly, three groups of REF, FAA and FAS specimens were created.

4.2.1 Electrochemical measurement

RC cube specimens of 150 mm were cast for each mix and prepared rebar (shown in Figure 4.2(a)) was embedded at the center inside the 150 mm during casting such that 20 mm rebar is visible outside. These prepared RC specimens were then cured for 28 days in the respective curing regime as mentioned in Table 3.12.

4.2.2 EMI studies

RC cubes of 150 mm were prepared and rebar as shown in Figure 4.2(b)) was embedded inside the cube at the centre such that a 20 mm rebar is visible outside the specimen. For concrete corrosion monitoring, ready to use packaged sensor i.e., concrete vibration sensor (CVS) procured from Central Electronics Limited, India was used in the study. The CVS was embedded inside the RC cube at a distance of 20 mm from the rebar. CVS is the encapsulated ready-to-use dynamic strain measuring sensors using PZT patches (Haq et al. 2020). The CVS is developed to utilize PZT patch in embedded form especially for concrete structures. CVS has good compatibility with the nearby concrete and can withstand harsh conditions typically encountered in the RC structures while casting (Kaur et al. 2017). The details of both piezo configurations are shown in Figure 4.3.

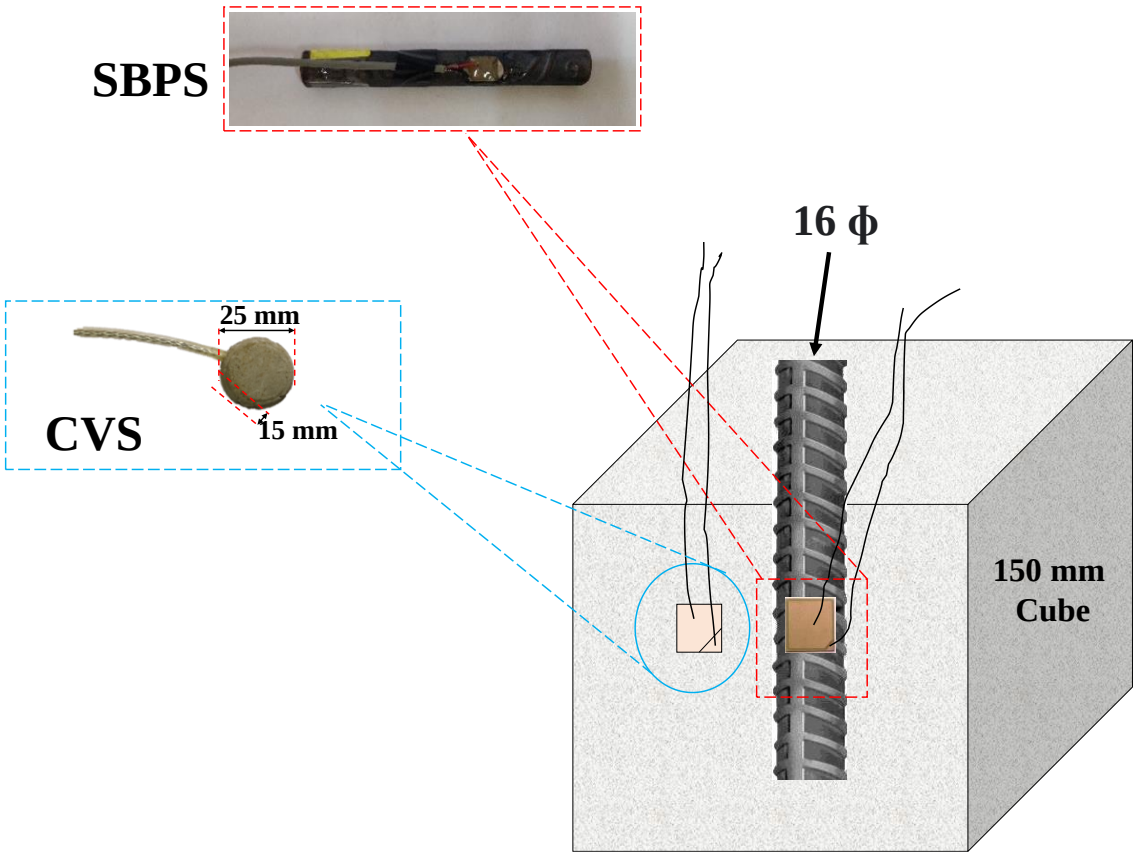

Figure 4.3: Detailed configuration of piezo sensor embedded in RC specimen (SBPS: Surface bonded piezo sensor; CVS: Concrete vibration sensor)

4.3 TEST PROCEDURES

This section elaborates all the test procedure employed for the corrosion studies on RC concrete using electrochemical and EMI technique.

4.3.1 Inducing corrosion in RC specimens

After 28 days of curing, all the test RC specimens were taken out from respective curing media and dried for 12 hours. The RC cubes were then subjected to corrosion using the impressed current method as shown in Figure 4.4. The steel mesh was wrapped onto the specimens and were positioned in a bucket containing 3.5% NaCl solution (Sharma et al. 2018b). To initiate the corrosion, an electrical loop was setup with rebar as an anode connected to the positive terminal of DC supply. Steel mesh acted as cathode and connected to negative terminal of

DC supply. An electric current was impressed to the test specimens at a constant voltage of 5 V using DC power supply, PSD3210, Scientific, India. The constant voltage was supplied to the test specimens until the specimens cracked due to corrosion. The brine solution was replaced regularly to ensure the presence of chloride ion concentration in the solution. The specimens were monitored at an interval of 7 days by electrochemical and EMI techniques.

Figure 4.4: RC specimens subjected to accelerated impressed current for corrosion studies

4.3.2 Electrochemical based corrosion monitoring

Open circuit potential (OCP), corrosion current density (I_{corr}) and corrosion potential were measured for all test specimens at an interval of 7 days till 100 days of exposure as per the guidelines of ASTM C876 (2015). ACM machine (Gill AC) was used for electrochemical measurements and experiments were programmed to polarize the specimen potential to about ±25 mV with a scan rate of 0.1 mV/s. The embedded steel bar was used as WE, steel mesh as

an auxiliary electrode (AE) and saturated calomel as a reference electrode (RE). The values of OCP, I_{corr} and corrosion potential were recorded before subjecting to chloride exposure and these values were taken as reference values. The setup for acquiring electrochemical measurement is shown in Figure 4.5. Triplicate specimens were tested for each duration and it was made ensure that the surface of RC specimen was wet for better conductivity.

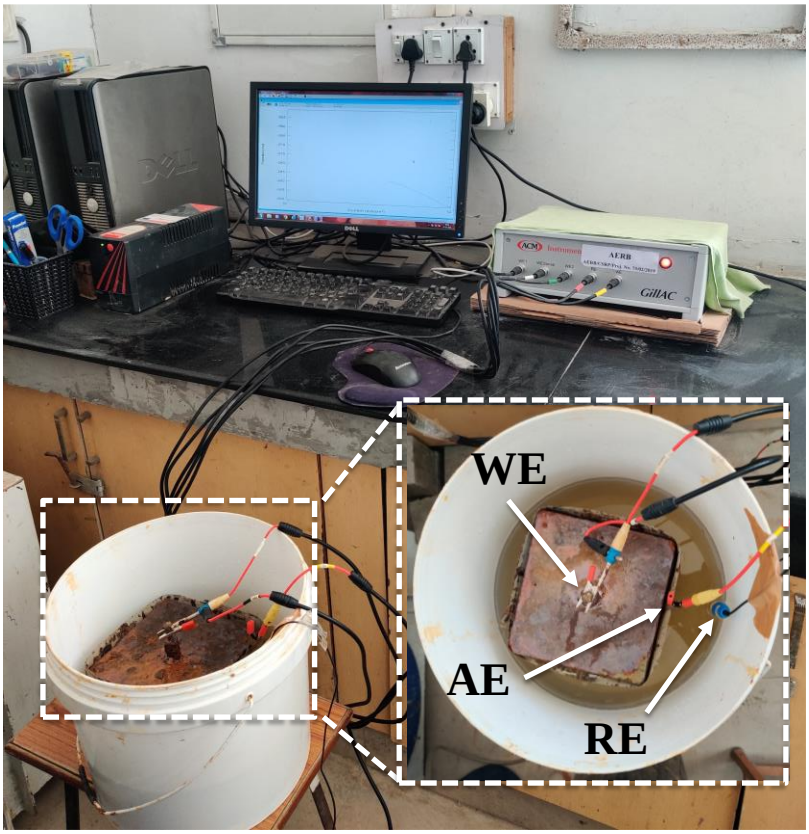

Figure 4.5: Experimental setup for electrochemical measurements of RC specimens (WE: Working electrode; AE: Auxiliary electrode; RE: Reference electrode)

4.3.3 EMI based corrosion monitoring

Prepared RC specimens were subjected to accelerated current induced chloride corrosion and monitored using EMI technique. Initially prior to the impressed corrosion, baseline EM signature was acquired. During the test exposure, EM signature were extracted at an interval of 7 days till complete testing duration. The experimental setup for corrosion monitoring is

shown in Figure 4.6. In the current study, the admittance signatures were recorded over the frequency range of 20-500 kHz for all test specimens. Admittance signature consists of real and imaginary parts i.e. conductance and susceptance respectively (Soh and Bhalla 2005). Further, the real part of admittance recorded from the EMI signature was only used in the present investigation, since it is more vulnerable to the concrete structures (Kaur et al. 2021).

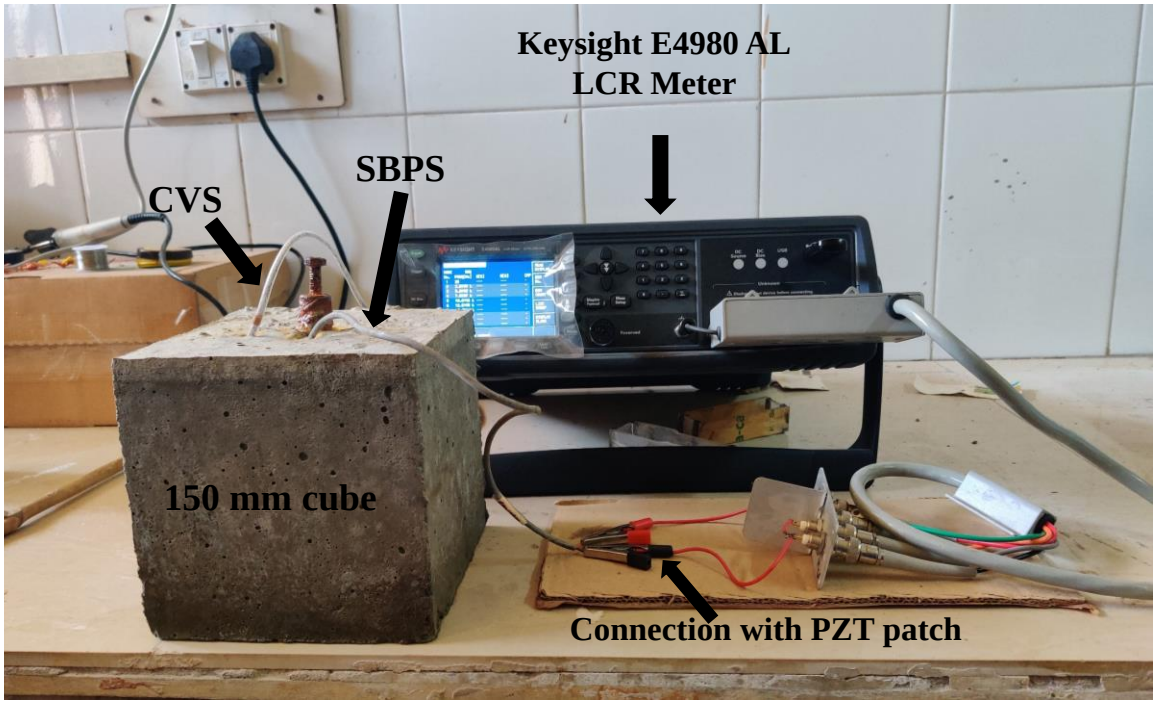

Figure 4.6: Experimental setup for corrosion monitoring using EMI technique

There are numerous indicators adopted by the researchers to study the relative change in admittance signatures. These includes root mean square deviation (RMSD), mean absolute percentage deviation and correlation coefficient deviation, out of which RMSD is extensively used (Talakokula et al. 2014). The RMSD, as denoted in Eq. (4.1), was used to assess the conductance signatures acquired at different exposure days over the considered frequency set.

$$\mathrm{RMSD}(\%) = \sqrt{\frac{\sum_{k=1}^{n}\left(G_k^L - G_k^F\right)^2}{\sum_{k=1}^{n}\left(G_k^F\right)^2}} \times 100 \qquad (4.1)$$

Here G_k^F and G_k^L are the conductance values at the k^{th} frequency for the uncorroded specimen (baseline) and corroded specimen, and $k = 1,\ldots, n$ denotes the frequencies at which the signature was recorded.

4.3.4 Evaluation using mass loss

At the end of testing, embedded rebar was extracted out from the RC specimens used in EMI studies. The extracted rebars were chemically cleaned as per ASTM G1-03 (2017) to remove all corrosion products. The mass of each treated rebar was taken to the accuracy of 0.1 gram. Percentage mass loss in rebar was computed with respect to its initial mass taken before casting of the RC specimens.

4.4 RESULTS AND DISCUSSION

This section elaborates the results obtained with the incorporation of FA based mineral inoculums in RC concrete against chloride exposure. Initially the tests of electrochemical and EMI studies are reported followed by the corrosion mechanism assessment by pore solution testing.

4.4.1 Effect of FA inoculum-based RC specimens against chloride exposure

The results obtained by various electrochemical and EMI studies are discussed here under.

4.4.1.1 Electrochemical measurements in RC specimens

Open circuit potential (OCP) and corrosion current density (I_{corr}) were monitored for all the tested specimens. Figure 4.7 shows the OCP of the rebar embedded with respect to saturated calomel electrode (SCE) for REF, FAA and FAS specimens. It can be observed from the figure that initially the potential for all the specimens is more than -125 mV_{SCE}, indicating the passive state. As the exposure durations were prolonged, potential drop was noted in all the specimens.

However, REF specimens registered higher potential drop as compared to FAA and FAS. The potential of REF remained lower than FAA and FAS specimens, till the end of testing.

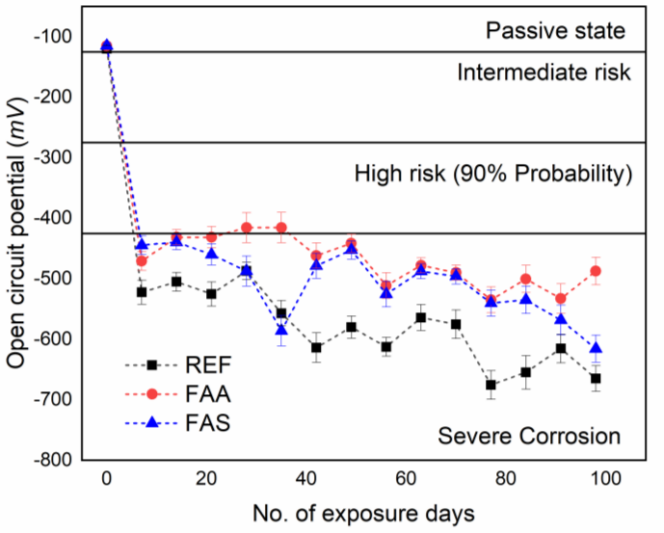

Figure 4.7: Open circuit potential versus exposure time of tested specimens

This indicates more resistive concrete matrix of bacterial treated specimens. This can be due to calcium carbonate precipitation by bacteria in FAA and FAS which reduced the penetrability of aggressive chloride ions. This bio coating acts as pore blocker and restricts the movement of aggressive agents. The reduced penetrability is also observed by lower sorptivity coefficient in FAS and FAA. Similar to the measurement of OCP, linear polarization resistance was recorded after every 7 days till the end of exposure at 100 days. Figure 4.8 shows the typical polarization curves obtained for REF, FAA and FAS specimens.

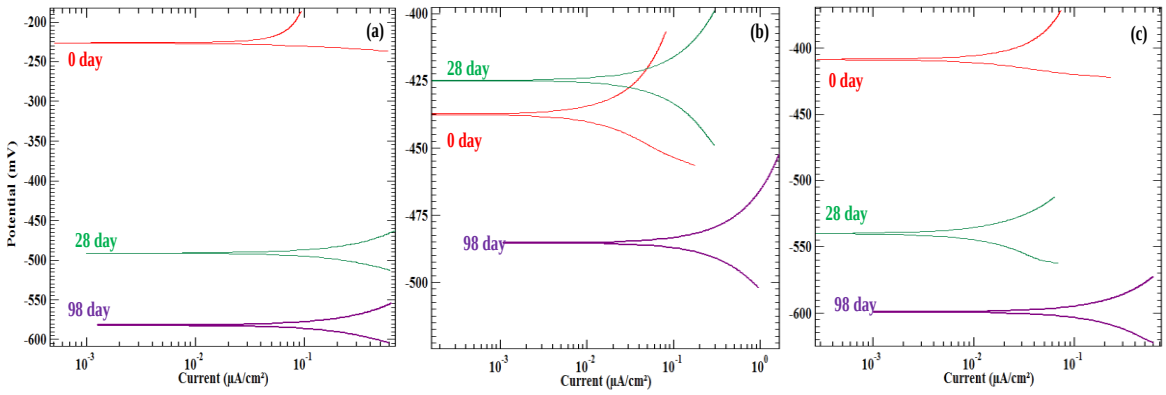

Figure 4.8: Polarization curves recorded in chloride environment at different testing age (a) REF (b) FAA (c) FAS specimens

Corrosion current density (I_{corr}) was calculated by interpolating anodic and cathodic curves of the polarization curves. Figure 4.9 shows the corrosion current density at different exposure duration for all test specimens. As can be observed, the corrosion current density increases with the increase in exposure duration and entered the active state at 20 days in REF; whereas in FAA specimen the I_{corr} was found to be stable and in passive state till 80 days of exposure. The better performance of FAA can be attributed to the denser interfacial matrix formed due to calcium carbonate precipitation between the pore structure of concrete matrix led to lower permeability of the mix, thereby hindering the ingress of aggressive chloride ions in FAA. These factors helped in achieving better corrosion protection in bacterial treated specimens. Similarly, in case of FAS, I_{corr} was found to be in passive state till 40 days of exposure. The biolayer of calcium carbonate crystals formed on the outer surface of specimens due to spray treatment helped in resisting the penetration of aggressive ions from the top surface of concrete, thereby delaying the penetration of chloride ions. After 40 days of exposure the I_{corr} increased gradually with the exposure duration and entered the active corrosion state. Even the use of bacterial spray treatment as a repair measure to reduce the surface permeability can help in application of MICCP technology in existing RC structures.

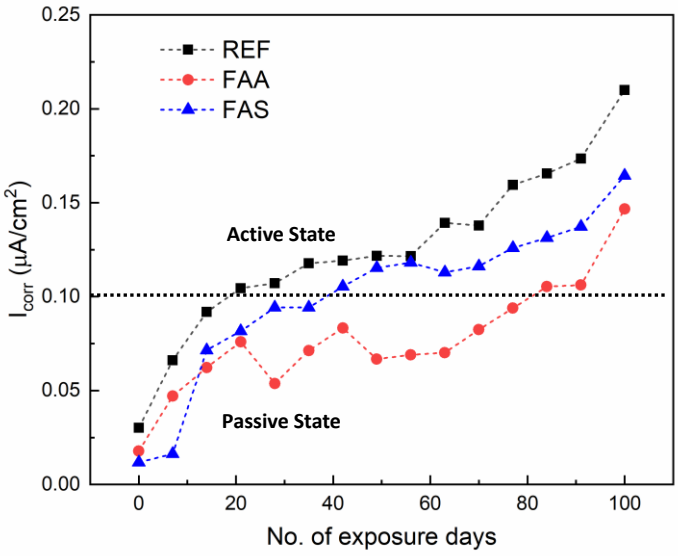

Figure 4.9: Corrosion current density versus exposure days of tested specimens

4.4.1.2 EMI based corrosion monitoring

Qualitative analysis of EMI signature

Figures 4.10-4.12 show the variation of conductance versus frequency signature for the REF, FAS and FAA samples. Conductance signatures of both CVS patch and SBPS were recorded, in the frequency range of 20 Hz to 500 kHz during the entire accelerated chloride corrosion exposure. CVS patch was embedded in concrete adjacent to rebar and was expected to monitor changes in concrete near the rebar location; while SBPS sensor was mounted on the steel surface to monitor changes in health of rebar with progressive corrosion. Conductance signature varies over the exposure time and as reported by earlier researchers (Ahmadi et al. 2021; Talakokula and Bhalla 2015), has the potential to yield useful information regarding concrete health monitoring. It can be observed that CVS and SBPS conductance signatures in the REF sample (Figure 4.10) have undergone substantial changes during testing exposure in comparison to FAA (Figure 4.11) and FAS (Figure 4.12) samples.

It was found that during the early days of chloride exposure, the conductance signatures overlapped each other in REF. With the increasing accelerated corrosion exposure after 7 days, the resonance peak shifted downward suggesting the penetration of chloride ions inside the concrete matrix. Whereas in FAA and FAS specimen, the conductance signatures overlapped each other till 40 days and the lesser shift was observed in resonance peaks with progressive chloride exposure. It can be noted that the decrease in the magnitude of the resonance peak of the corroded state is less in FAA and FAS than the REF specimen. This indicates that the lesser penetration of aggressive chloride ions occurred inside the FAA and FAS specimens. These results are also correlating with the I_{corr} results (Figure 4.16) as the corrosion observed in the FAA and FAS specimen is comparatively lower than the REF specimen. This might be due to bio-deposition formed around the outer surface of concrete due to MICCP. Various researchers

reported the lowest permeability achieved in the bacterial concrete which is majorly responsible for corrosion inhibition (Nguyen et al. 2019; Osman et al. 2021).

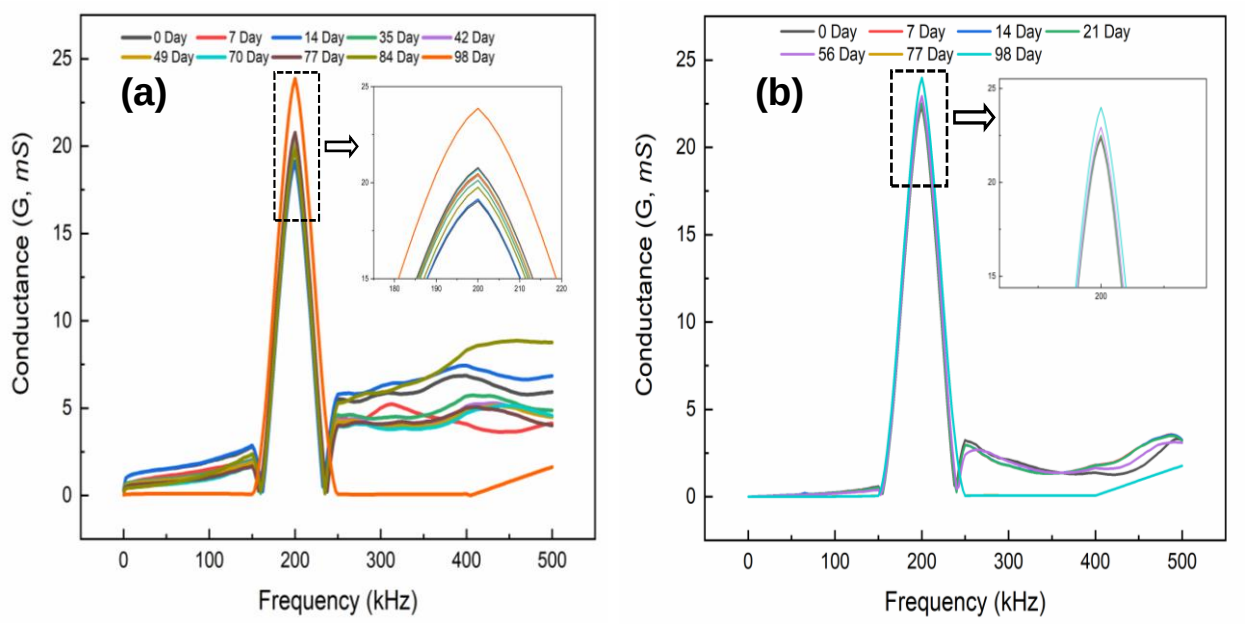

Figure 4.10: Conductance signature of patches embedded in REF specimen (a) CVS (b) SBPS

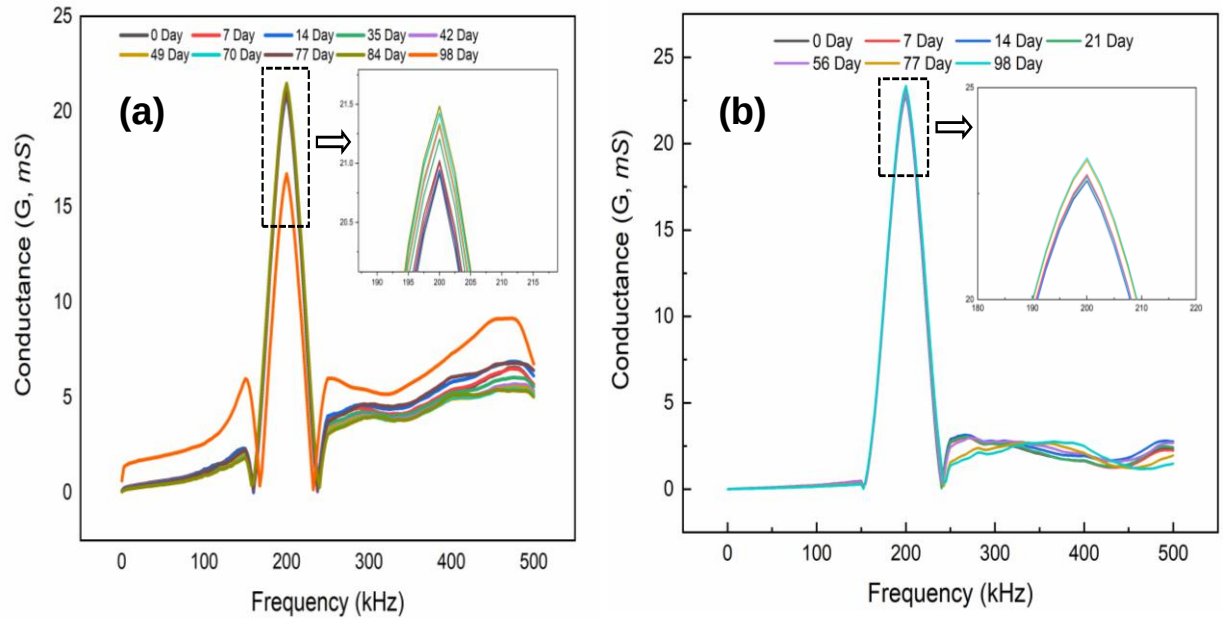

Figure 4.11: Conductance signature of patches embedded in FAA specimen (a) CVS (b) SBPS

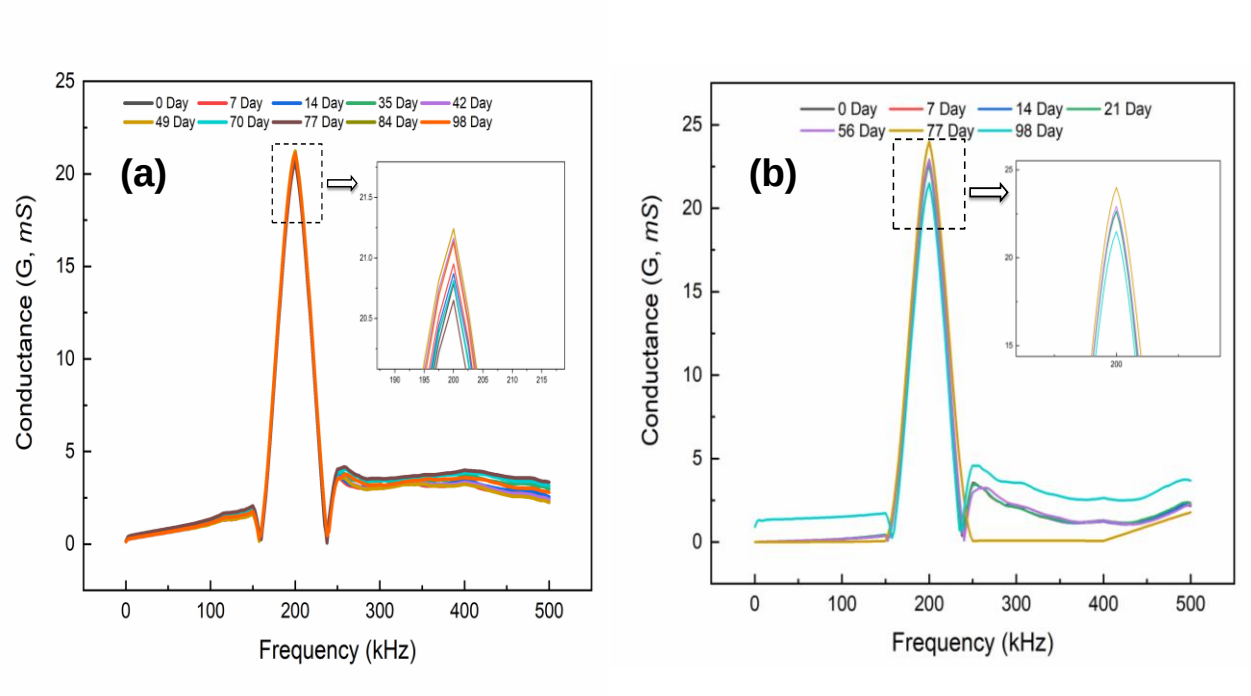

Figure 4.12: Conductance signature of patches embedded in FAS specimen (a) CVS (b) SBPS

Quantitative analysis of EMI signature

Figure 4.13 shows the variation of the RMSD index with the chloride test exposure (days) in the frequency range 20–500 kHz for CVS and SBPS. It can be found that the RMSD values in CVS were higher than SBPS in the initial days of chloride exposure, which suggests higher changes in the concrete matrix occurred during the penetration of aggressive chloride ions into the concrete as compared to the changes at the steel surface. It further suggests that CVS sensors are more senstive to the initial physical changes in the concrete matrix; and hence can detect corrosion initiation period. Similar findings were also reported by other researchers (Talakokula et al. 2014). The RMSD values recorded by CVS in FAA and FAS were lesser than the REF specimen suggesting lesser ingress of chloride ions. The RMSD values for REF shifted to higher side at 20 days of test exposure and remained in the range of 15% to 23% after this testing duration. However, the values remained in the range of 1% to 10% for both FAA and FAS throughout the testing duration.

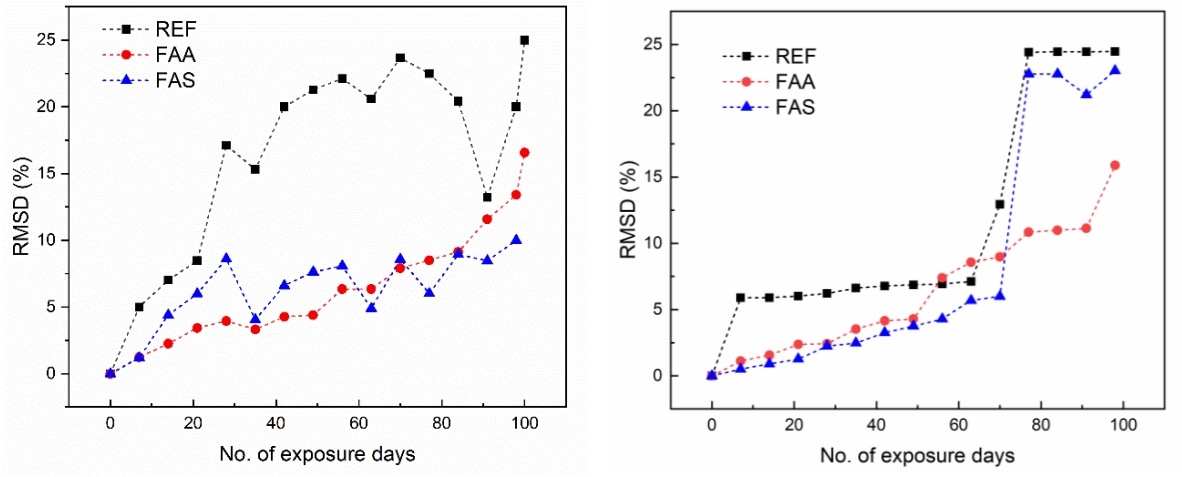

Figure 4.13: Variation of RMSD (%) extracted from (a) CVS (b) SBPS

In case of SBPS, the major shift is observed in the later days of exposure, which indicates its senstivity once the rebar is depassivated by chloride ions. After initiation of corrosion, chlorides ions destroyed the protective barrier layer and start deteriorating the rebar surface. SBPS exhibited somewhat higher sensitivity to corrosion occurrence in comparison to CVS. This is on account of the direct bonding of the piezo sensor on rebars, which is the component most affected by chloride corrosion during the post-initiation phase.

In REF, RMSD (%) became highly senstive and showed sudden shift after 60 days of test exposure, whereas similar shift was observed at 80 days in FAA and 70 days in FAS specimens. After sudden increase in RMSD values, these values got stablised till the end of testing. This might be due to appearance of crack on outer surface of the specimen, which led to release of stressses that were built up due to deposition of corrosion products. For instance, the sudden gain in RMSD was noted at 77 days of test exposure in REF specimens. The condition of REF specimen at 77 days of testing is shown in Figure 4.14, which shows major crack in concrete along the length of rebar with the corroison products oozing out of the crack. Similar observation related to stablization of RMSD values after cracking of concrete was made by other researchers (Talakokula and Bhalla 2015). In the FAA specimen, lower RMSD values of 8.96% were recorded at 77 days of exposure indicating the delay of corrosion. The constant

trend was observed in FAA upto 91 days of exposure. The denser interfacial pore refinement due to calcium carbonate deposition was responsible for the delay in the corrosion process.

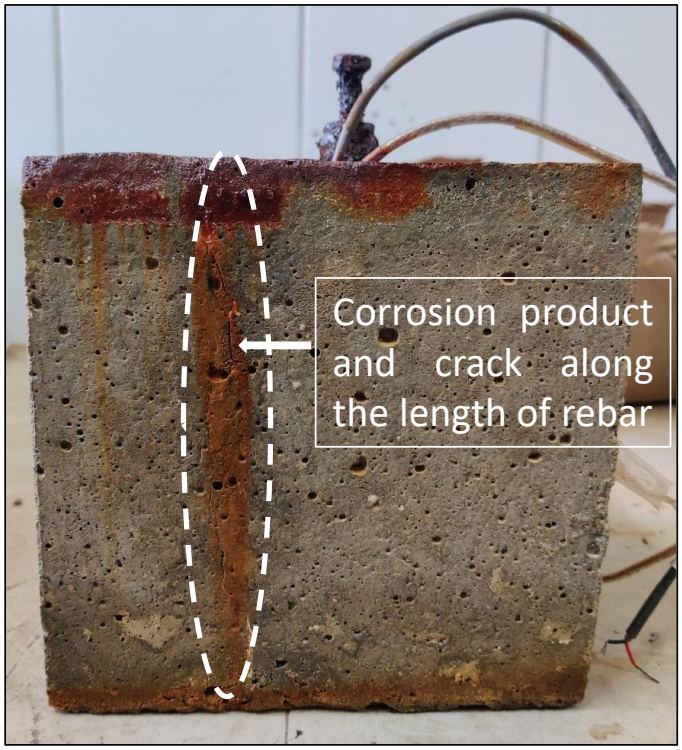

Figure 4.14: REF specimen condition in cracking phase

4.4.1.3 Mass loss

At the end of testing in EMI studies, all the specimens were damaged to extract steel rebar. The conditions of rebars extracted from the specimens after chemical cleaning are shown in Figure 4.15. General corrosion products or pitting was observed in FAA and FAS; whereas high cross-sectional loss was observed at one location in REF. The mass loss of the steel rebar was determined using gravimetric method after chemically cleaning the corrosion products as per the guidelines of ASTM G1-03 (2017). The initial mass before embedding and the final mass after extracting the rebars from RC were calculated for all the specimens as tabulated in Table 4.2. It can be noted that the mass loss is highest in the REF specimen (4.70%), whereas lowest was observed in FAA (0.70%). This observation further strengthens the positive effect of using bacterial concrete to delaying the onset and propagation of rebar corrosion.

Figure 4.15: Condition of rebar extracted from the tested specimens

Table 4.2: Gravimetric analysis of extracted rebar

Specimen	Initial mass (gram)	Final mass (gram)	Mass loss (%)
REF	185	176.3	4.70
FAA	185	183.8	0.70
FAS	185	182.0	1.62

4.4.1.4 Correlation between electrochemical and EMI technique

The parameters extracted from electrochemical and EMI techniques were correlated, in order to understand any possible correlation between the two techniques. A relation between current density (I_{corr}) and RMSD (%) obtained during exposure was attempted. The corrosion current density corresponding to 0 to 100 days of exposure for REF, FAA and FAS mixes was correlated with both types of piezo patches, viz. CVS and SBPS separately. Figure 4.16 presents relation between I_{corr} ($\mu A/cm^2$) and RMSD (%) of all three specimens. Among CVS

and SBPS sensor, SBPS has shown better level of correlation (R^2) than CVS sensor in all the specimens. Since the CVS were embedded near to the rebar, it can detect early changes occurring due to ingress of chloride ions only, whereas the SBPS sensors were able to detect and monitor the rebar corrosion in a better way.

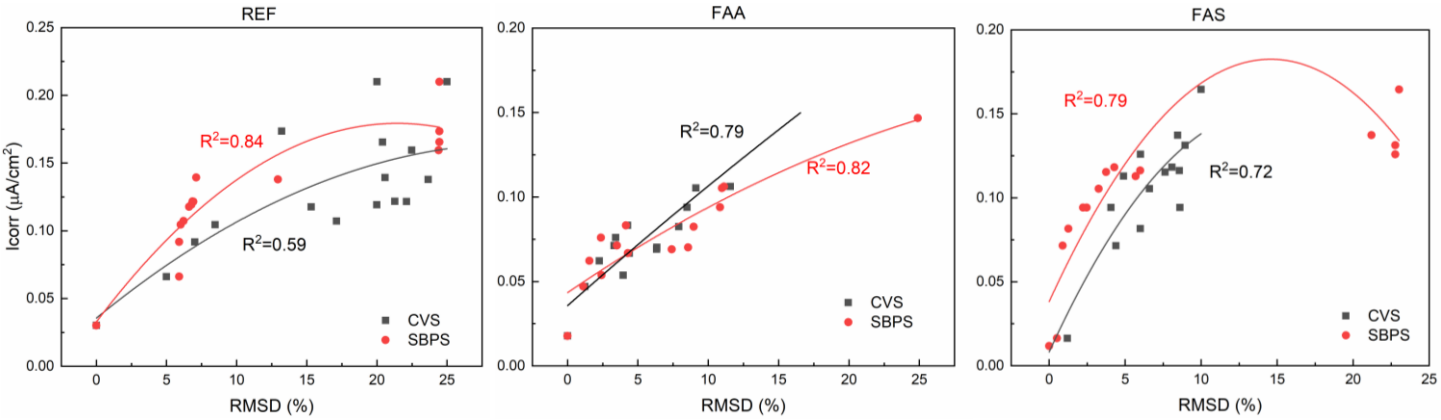

Figure 4.16: Correlation between I_{corr} and RMSD of all specimens

The other major observation, w.r.t RMSD values (%) by SBPS for both FAA and FAS are sudden increase in values once the I_{corr} is nearly 0.1 μA/cm^2. This reflects a sudden rise in RMSD once the corrosion state shifts from passive to active state. In FAA, the RMSD values had a sudden shift from 10% to 25%; whereas the corresponding shift in FAS was from 7% to 23%. It suggests that initiation of active state of corrosion can be clearly detected by the SBPS. It further suggests that SBPS will be able to detect any changes occurring in the rebar due to corrosion in RC structures. However, no such sudden shift was observed in REF specimens. This can be due to an unusual phenomenon that occurred in REF specimen and is visible from the condition of the rebar as shown in Figure 4.15. It can be seen that the corrosion occurred almost uniformly throughout the rebar length extracted from both the FAA and FAS specimen. However, larger cross-sectional loss occurred at a particular location that was away from the SBPS bonding location making it lesser responsive to the ongoing corrosion process in REF specimen. Conclusively, SBPS can effectively monitor the progressive corrosion on the rebar in both FAA and FAS specimen.

4.5 PORE SOLUTION TESTING FOR ESTABLISHING CORROSION MECHANISM FOR REBAR IN FA INOCULUM IMMOBILIZED REINFORCED CONCRETE

Above findings clearly suggested the application of MICCP played a significant role in restricting the penetration of chloride ions under impressed current induced corrosion. Therefore, it is worthy to study and define the corrosion mechanism responsible for inhibition on rebar interface. The materials and experimental techniques used for pore solution testing are as follows.

4.5.1 Materials and solution preparation

16 mm diameter - Tempcore TMT (Thermomechanically treated) steel bar conforming to IS 1786 (2008) was used in this investigation. Steel bars were cut to a length of 60 mm and drilled and threaded at one end. The rebars were rubbed with emery papers of grade 600 and washed with double distilled water, then degreased with hexane to remove debris from the surface of bars. After this, the bars were coated with two layers of epoxy leaving an exposed length of 4 mm at the opposite portion of the drilled end for active corrosion process. The exposed area of the bare steel specimen was 401.92 mm^2. The finally prepared test specimen is shown in Figure 4.17.

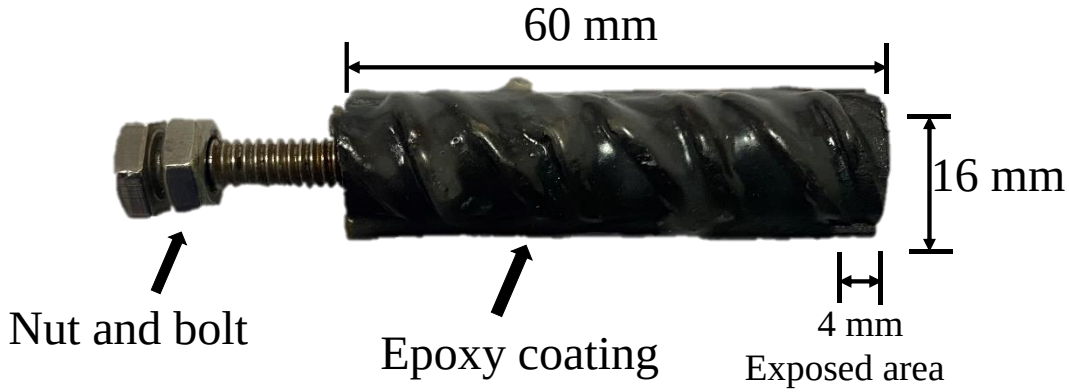

Figure 4.17: Cross sectional details of bare steel specimen for electrochemical measurements

In order to prepare pore solution for electrochemical measurements, the concrete mix was prepared using cement: sand: coarse aggregate in the proportion of 1:1.82:3.24 (by weight) and water to cement ratio (w/c) of 0.47 (BIS:10262 2009). The details about the mix are provided in Table 3.12 in the previous chapter.

In these concrete mixes, bacterial inoculum was incorporated either at the casting stage or was used as a surface treatment measure during curing. Accordingly, three groups of specimens were created. After 28 days of respective curing, one concrete specimen from each group was taken out and air-dried for 24 hours. The concrete cubes were then drilled from two levels: upto 10 mm and between 40-50 mm from the top surface using rotary hammer drill machine. The obtained concrete powder was stored separately in air tight packets and were used to prepare aqueous solution (AQS) for electrochemical investigation. For preparing AQS, the concrete powder was blended with autoclaved distilled water in the 1:20 proportion by mass and then stirred for 1 day. Then this solution was filtered through Whatman no. 1 filter paper. The procedure was adopted from Shaheen and Pradhan (2017).

The study was conducted on the non-chloride as well as chloride contaminated solution to assess the role of bacterial treatment. The details with nomenclature are given in Table 4.3. It is to mention that for FAA specimens, only concrete powder extracted from 40-50 mm depth was used for AQS study.

Table 4.3: Nomenclature of prepared AQS

S.No.	Sample	Non-chloride contaminated solution	Chloride contaminated solution
1.	Reference	P_{REF}	P_{REF}(Cl)
2.	FAA	P_{FAA}M	P_{FAA}M(Cl)
3.	FAS	P_{FAS}T, P_{FAS}M	P_{FAS}T(Cl), P_{FAS}M(Cl)

M: concrete powder used of 40-50 mm depth; T: concrete powder used of 10 mm depth from top

This is because admixed bacterial procedure was adopted followed by bacterial curing supplemented with nutrients to prepare concrete specimens which resulted in uniform $CaCO_3$ precipitation in the concrete matrix.

4.5.2 Testing methods

The electrochemical behaviour of bare steel specimens in different types of electrolytic concrete powder AQS contaminated with 0.1M chloride was evaluated by conducting potentiodynamic polarization test. The electrochemical measurements were acquired using ACM Gill AC corrosion analyser (S.No. 1924) and three-electrode cell system setup as shown in Figure 4.18. The steel bar immersed in the AQS was treated as working electrode (WE); while platinum electrode and saturated calomel was used as counter electrode and reference electrode respectively.

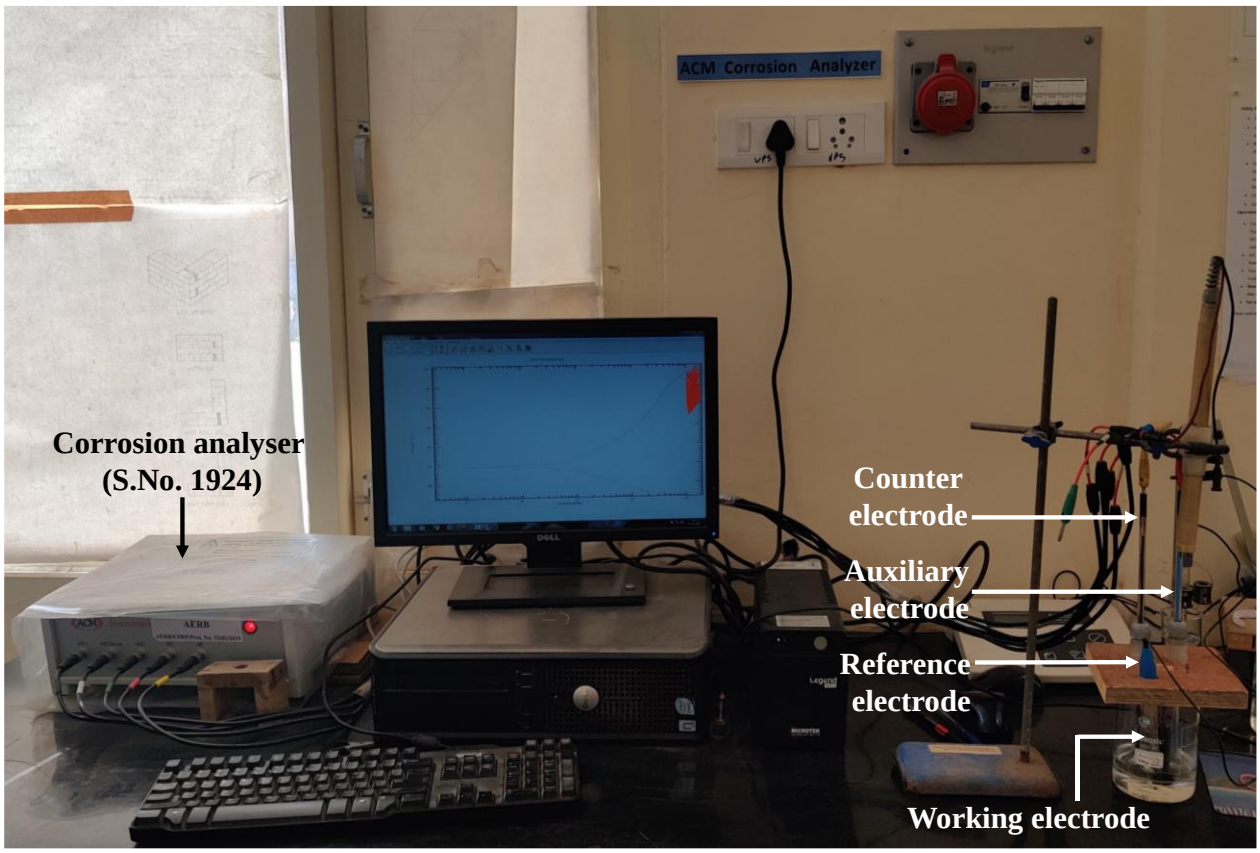

Figure 4.18: Experimental setup for electrochemical measurements of bare steel immersed in electrolytic concrete powder aqueous solution (AQS)

For obtaining the curves, the specimens were immersed in the prepared AQS, and the reading were obtained at 3, 5 and 10 days of immersion. One set was also made in which AQS was not contaminated with chlorides to serve as a reference. At any testing age, polarization curve was measured at a scan rate of 0.5 mv/sec over a potential ranging from -0.25 V to 1.50 V. The high scan range makes the test highly disturbed to the electrodes, and hence every time, the readings were taken on the undisturbed specimens. The testing duration till 10 days was taken based on the literature that suggests that this duration is sufficient for the formation of any protective film and for understanding the passivation mechanism (Poursaee and Hansson 2007; Tiwari et al. 2021). All the measurements were conducted at room temperature around 28 ± 5°C.

To study the product formation on the steel surface due to chloride environment, steel tablets of 10×10×2 mm were prepared and were kept in chloride contaminated AQS for 5 days (Figure 4.19). After 5 days, the tablets were taken out of the AQS.

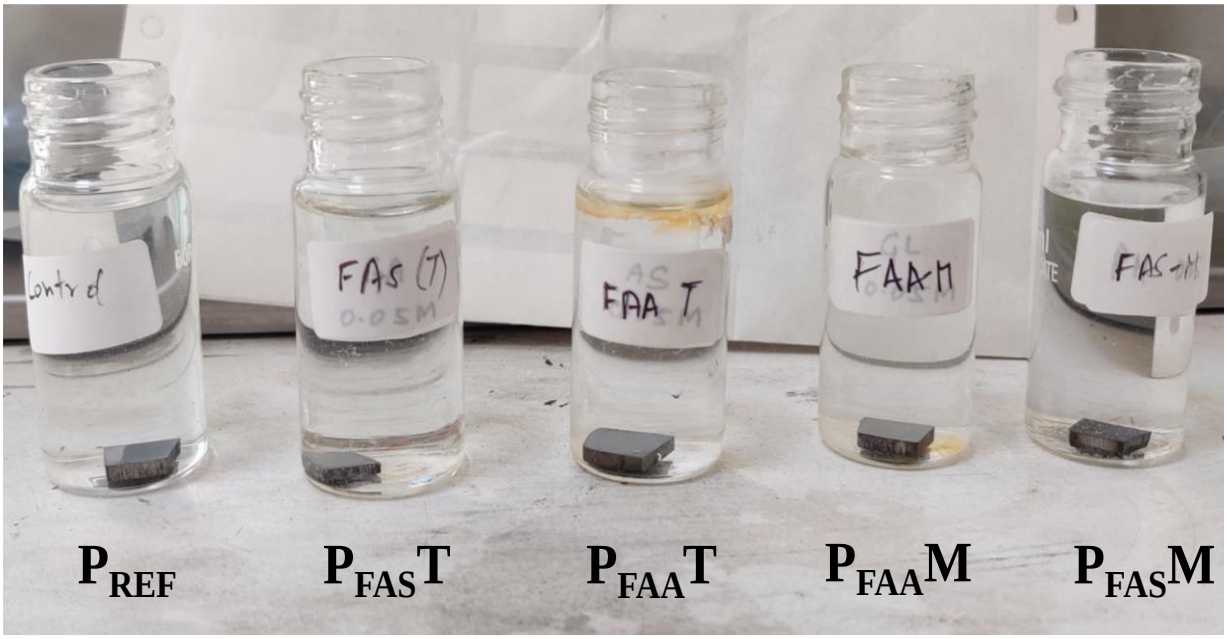

Figure 4.19: Steel tablets immersed in electrolytic concrete powder aqueous solution (AQS)

One set of steel tables were washed using distilled water and the surface was closely investigated by optical imaging; while the other set of tablets were used without any surface cleaning for FESEM-EDX analysis.

4.5.3 Effect of FA based inoculum against chloride exposure

The results obtained of FA based inoculum pore solution by electrochemical studies are discussed here under.

4.5.3.1 Potentiodynamic polarization curves in concrete powder aqueous solution (AQS)

The bare steel was immersed in the prepared AQS and corrosion activity was tested at 3, 5 and 10 days of immersion by conducting potentiodynamic polarization test. Tafel extrapolation of polarization curves was performed to obtain corrosion current density of the specimens. The polarization curves obtained at 5 days of immersion for the set without aggressive chloride ions are shown in Figure 4.20. It can be observed from the figure that all the specimens showed similar kind of potentiodynamic behaviour, that is formation of a passive layer followed by a transpassive zone. The recorded potentiodynamic curves suggested that the bacterial precipitates facilitated the formation of passive layer.

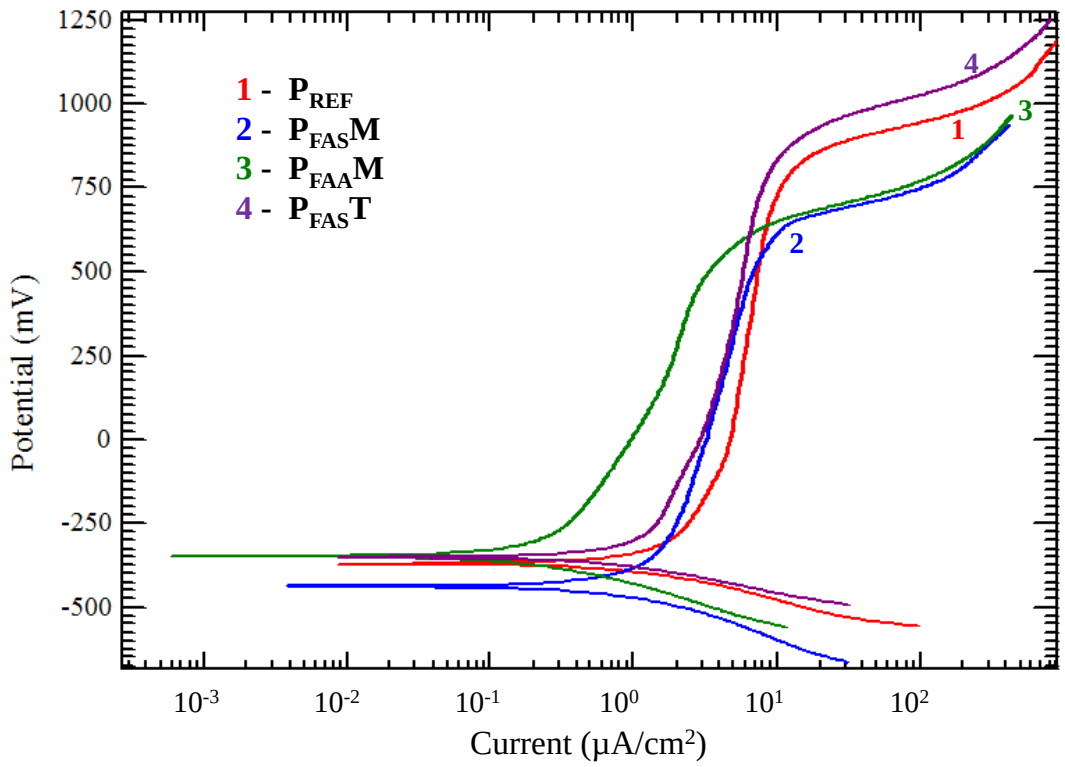

Figure 4.20: Polarization curve recorded on steel in non-chloride contaminated solution

The obtained E_{corr} and I_{corr} values are presented in Table 4.4. It can be inferred that the I_{corr} was found to be one order less in $P_{FAA}M$ and $P_{FAS}T$ than P_{REF}. The preliminary results clearly showed the deposition of stable protective layer over the exposed area of steel bar in $P_{FAA}M$, $P_{FAS}T$ and $P_{FAS}M$.

Table 4.4: Electrochemical parameter of samples in non-chloride contaminated solution

Solution	**I_{corr} ($\mu A/cm^2$)**	**E_{corr} (mV)**
P_{REF}	1.4	-350
$P_{FAS}M$	1.1	-425
$P_{FAA}M$	0.19	-325
$P_{FAS}T$	0.87	-330

The corrosion activity of all specimens was then tested in the presence of 0.1 M NaCl. The polarization curves obtained at 3, 5 and 10 days of immersion are shown in Figure 4.21. The obtained E_{corr} and I_{corr} values are presented in Table 4.5.

(a)

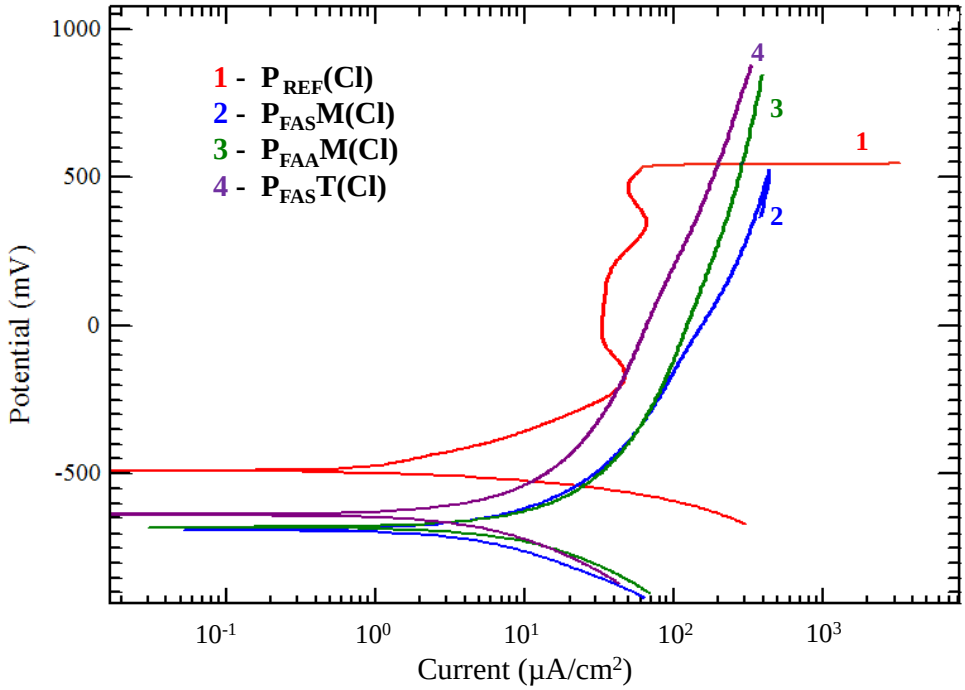

(b)

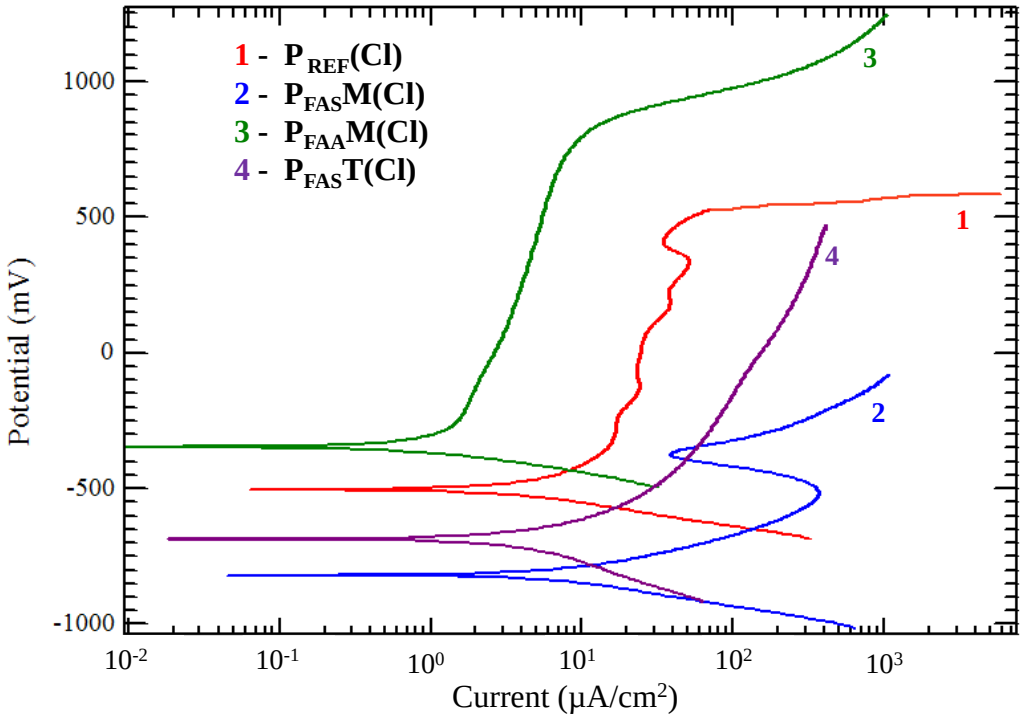

(c)

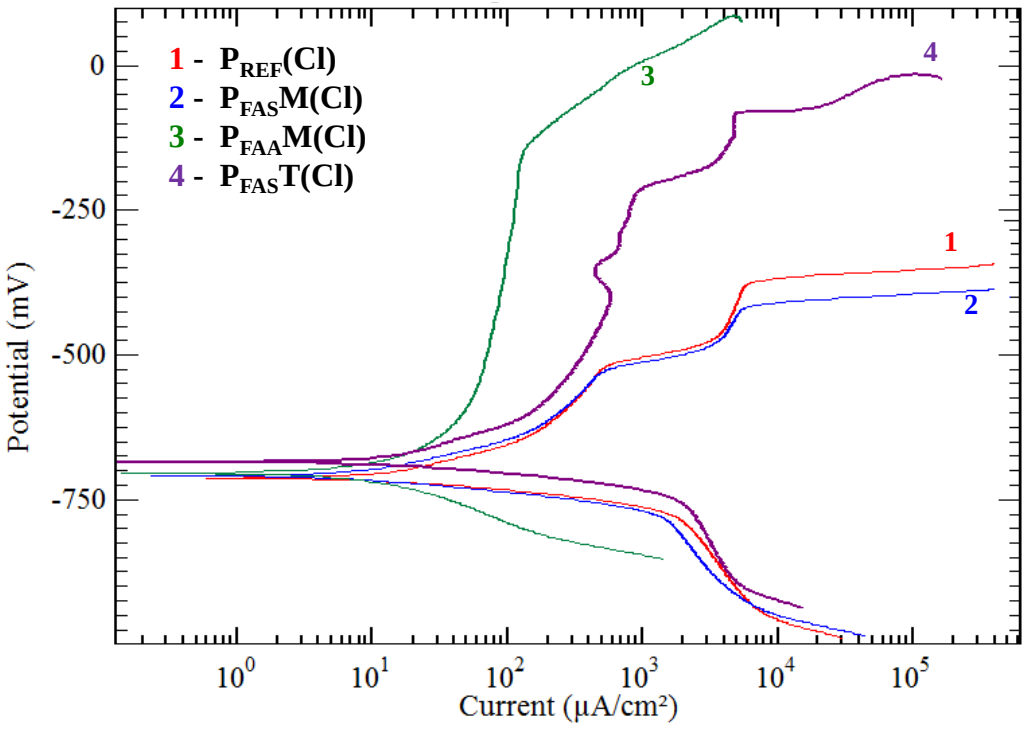

Figure 4.21: Polarization curve recorded on steel in chloride contaminated solution after (a) 3 day (b) 5 day (c) 10 day

Table 4.5: Electrochemical parameter of tested samples in chloride contaminated solution

Solution	Test duration					
	3 days		5 days		10 days	
	I_{corr} ($\mu A/cm^2$)	E_{corr} (mV)	I_{corr} ($\mu A/cm^2$)	E_{corr} (mV)	I_{corr} ($\mu A/cm^2$)	E_{corr} (mV)
P_{REF}(Cl)	10.22	-500	16.78	-500	48.9	-700
P_{FAS}M(Cl)	8.5	-545	17.2	-750	54.9	-715
P_{FAA}M(Cl)	8.7	-540	9.5	-350	29.1	-700
P_{FAS}T(Cl)	7.4	-650	8.5	-700	55.2	-670

It can be observed from Figure 4.21(a), due to the addition of 0.1 M NaCl, the unstable passive layer was observed along with pitting potential at 500 mV in P_{REF}(Cl). The addition of Cl ions weaken the passive layer over the steel surface. Whereas in other specimens, stable passive layer was noted at 3 days of exposure. Also, the I_{corr} values were recorded to be 10.22, 8.5, 8.7 and 7.4 $\mu A/cm^2$ in P_{REF}(Cl), P_{FAS}M(Cl), P_{FAA}M(Cl) and P_{FAS}T(Cl). This clearly represents the I_{corr} is one order magnitude lower than P_{REF}(Cl). The results recorded at 5 days of immersion demonstrates meta stable pitting P_{REF}(Cl) which signifies the active corrosion reaction on the steel surface (Figure 4.21(b)). While in P_{FAS}M(Cl), active passive transition was recorded in the polarization curve. However, in P_{FAA}M(Cl), noble shift in E_{corr} along with decrease in I_{corr} value was observed. Also, a stable passive region was noted followed transpassive dissolution of passive layer. In case of P_{FAS}T(Cl), pseudo passive behaviour was observed with no change in I_{corr} as compared to 3 day of exposure. It clearly represents formation of protective layer that could resist the progressive action of chloride ions on steel surface. The results at 10 days of immersion indicate active corrosion in all the specimens (Figure 4.21(c)). Still, the values of I_{corr} recorded in P_{FAA}M(Cl) is lower than the corresponding reference specimen. It can be inferred from the overall polarization curves that passive layer in P_{FAS}M(Cl), P_{FAA}M(Cl) and P_{FAS}T(Cl) were stable and efficient upto 5 days of exposure. However continuous action of

active chloride ions in solution at 10 days of immersion destroyed the protective layer over the steel surface causing the active corrosion in all specimens.

The condition of the exposed surface of steel bar was also inspected after immersing the steel tablets in chloride contaminated AQS for 5 days. Figure 4.22 shows the optical imaging of steel tablets taken at 50x magnification. The images clearly show indicate large number of red coloured pits formed on the steel surface in P_{REF}(Cl); which can be linked to the formation of FeOOH (Tiwari et al. 2021). The amount of corrosion pits was small in number in P_{FAS}M(Cl); whereas no corrosion products/pits was observed in the P_{FAA}M(Cl) and P_{FAS}T(Cl). It clearly indicated that bacterial treatment to concrete helped in providing better protection to the steel rebar.

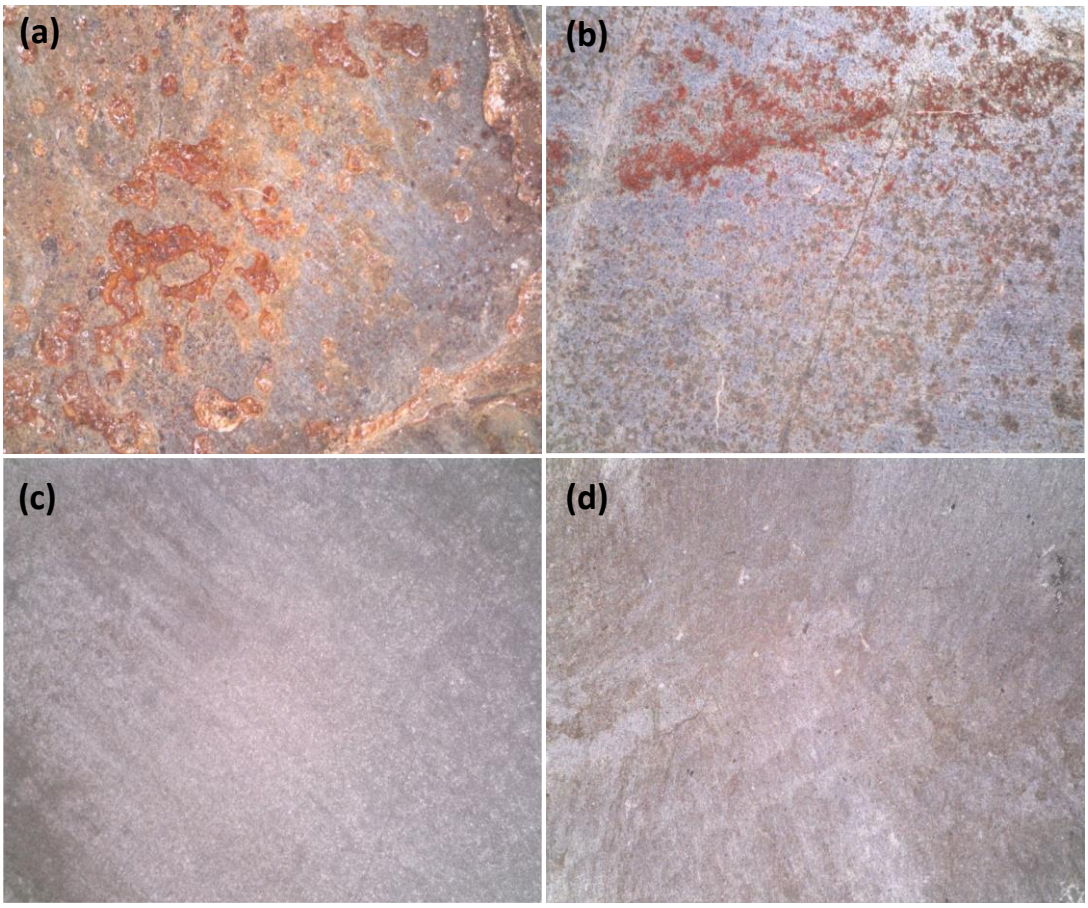

Figure 4.22: Optical imaging of steel tablets immersed in (a) P_{REF}(Cl); (b) P_{FAS}M(Cl); (c) P_{FAA}M(Cl); (d) P_{FAS}T(Cl) at 5 days

FESEM was conducted to examine the morphology of product precipitated on the steel surface, while EDX was done for elemental analysis at the select locations. The FESEM-EDX results obtained of all the immersed specimens are shown in Figure 4.23.

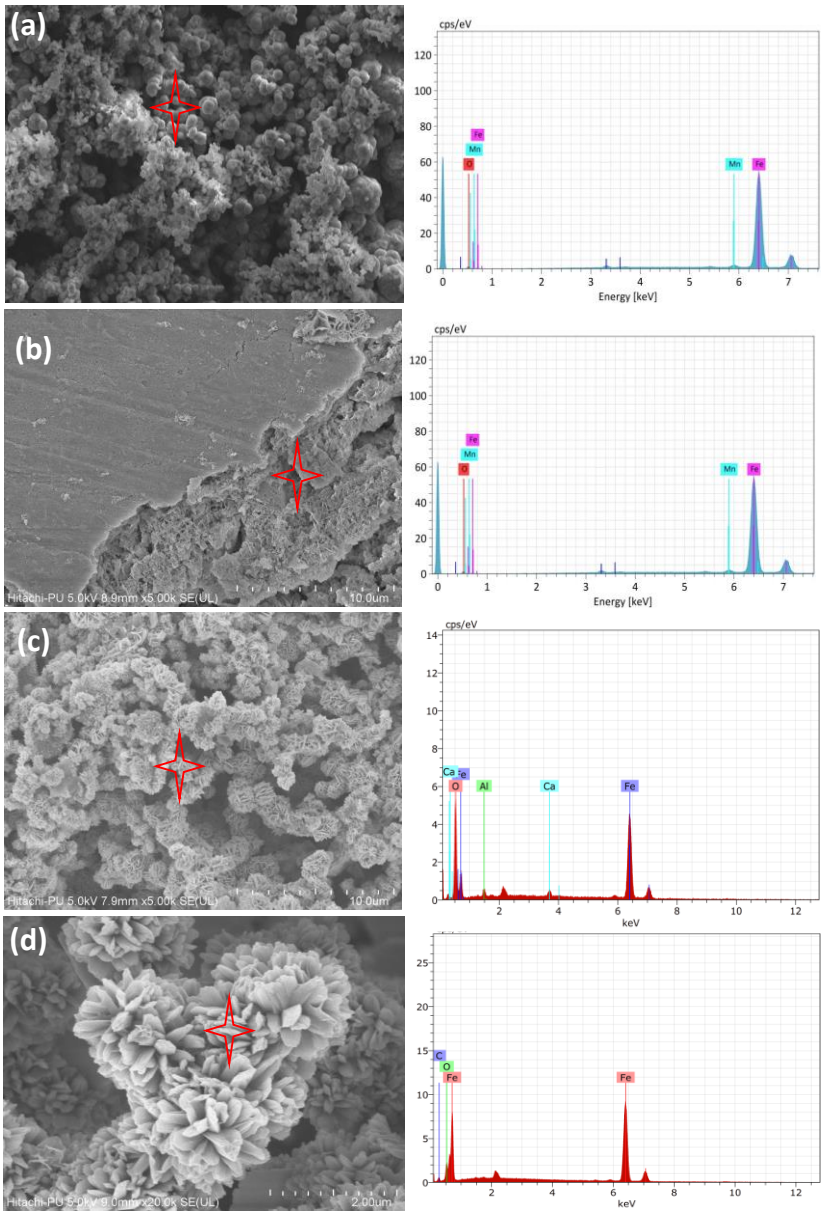

Figure 4.23: FESEM-EDX analysis of steel tablets immersed in (a) P_{REF}(Cl) (b) P_{FAS}M(Cl) (c) P_{FAA}M(Cl) (d) P_{FAS}T(Cl) for 5 days

The considerable corrosion product was notable on the surface of P_{REF}(Cl), which is clear evidence of pitting corrosion due to chlorides (Figure 4.22(a)). EDX spectra also confirmed the presence of Fe and O elements associated with corrosion products.

Similar observation was made in FESEM-EDX analysis of $P_{FAS}M(Cl)$. However, in $P_{FAA}M(Cl)$ and $P_{FAS}T(Cl)$, flower shaped cluster was observed on the surface of steel tablet. EDX analysis in $P_{FAA}M(Cl)$ confirmed the presence of Fe, O, Ca and C. This indicated the formation of $CaCO_3$ layer on the steel surface which resisted the attack of chloride ions on the steel surface.

4.6 EFFECT OF SF INOCULUM-BASED RC SPECIMENS AGAINST CHLORIDE EXPOSURE

In this section, the anti-corrosive potential of SF based inoculum in RC specimens was assessed under chloride exposure. The stored SF inoculum at 4°C for 180 days was immobilized in the 150 mm cube RC specimens as tabulated in Table 3.12. 16 mm diameter steel bar conforming to IS 1786 (2008) and described previously in section 4.1.3 was used. SFA and SFS specimens were prepared for electrochemical and EMI studies with rebar embedded at centre. These RC specimens were subjected to accelerated current induced chloride corrosion. At the end of testing of RC specimens, rebars were only extracted from EMI studies for evaluating the mass loss. Further, the corrosion mechanism was examined using pore solution testing. The powder samples were extracted from SFA and SFS specimens at different depth and AQS was prepared as described in 4.5.1. The details of various AQS are given in Table 4.6.

Table 4.6: Nomenclature of prepared AQS

S.No.	Sample	Non-chloride contaminated solution	Chloride contaminated solution
1.	Reference	P_{REF}	$P_{REF}(Cl)$
2.	SFA	$P_{SFA}M$	$P_{SFA}M(Cl)$
3.	SFS	$P_{SFS}T$, $P_{SFS}M$	$P_{SFS}T(Cl)$, $P_{SFS}M(Cl)$

M: concrete powder used of 40-50 mm depth; T: concrete powder used of 10 mm depth from top

The bare steel specimens were immersed in AQS and electrochemical analysis was conducted as discussed in 4.5.2.

4.6.1 Electrochemical measurements in RC specimens

Figure 4.24 shows the OCP of the rebar embedded with respect to saturated calomel electrode (SCE) for REF, SFA and SFS specimens.

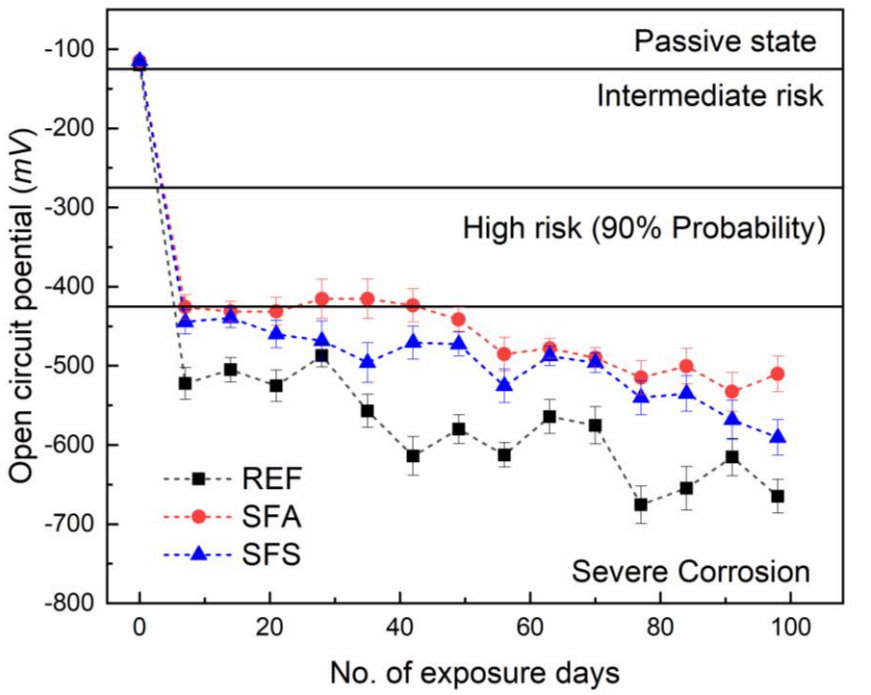

Figure 4.24: Open circuit potential versus exposure time of tested specimens

It can be observed from the figure that initially the potential for all the specimens is more than -125 mV_{SCE}, indicating the passive state. As the exposure durations were prolonged, potential drop was noted in all the specimens. However, REF specimens registered higher potential drop as compared to SFA and SFS. The potential of REF remained lower than SFA and SFS specimens, till the end of testing. This indicates more resistive concrete matrix of bacterial treated specimens. This can be due to calcium carbonate precipitation by bacteria in SFA and SFS which reduced the penetrability of aggressive chloride ions. This bio coating acts as pore blocker and restricts the movement of aggressive agents. Similar to the measurement of OCP, linear polarization resistance was recorded after every 7 days till the end of exposure at 100 days. Figure 4.25 shows the typical polarization curves obtained for REF, SFA and SFS specimens.

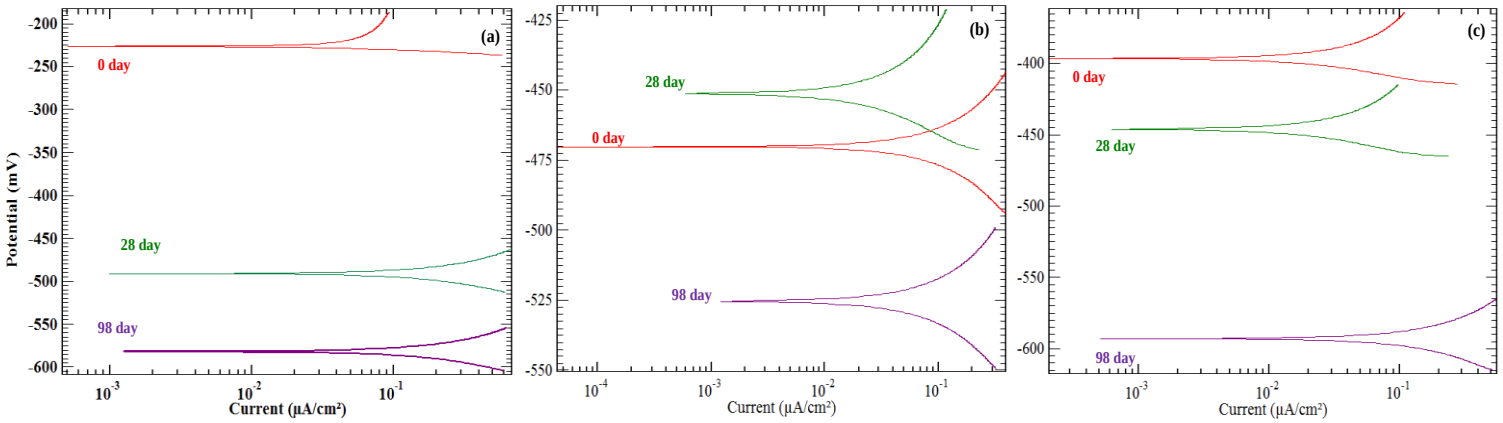

Figure 4.25: Polarization curves recorded in chloride environment at different testing age (a) REF (b) SFA (c) SFS specimens

I_{corr} was calculated by interpolating anodic and cathodic curves of the polarization curves. Figure 4.26 shows the corrosion current density at different exposure duration for all test specimens. As can be observed, the corrosion current density increases with the increase in exposure duration and entered the active state at 20 days in REF; whereas in SFA specimen the I_{corr} was found to be stable and in passive state till 80 days of exposure. The better performance of SFA can be attributed to the denser interfacial matrix formed due to calcium carbonate precipitation between the pore structure of concrete matrix led to lower permeability of the mix, thereby hindering the ingress of aggressive chloride ions in SFA. Also, the protective layer at the steel-concrete interface was observed to be more stable and passive in potentiodynamic behaviour on bare steel specimen in $P_{SFA}M(Cl)$.

Both these factors helped in achieving better corrosion protection in bacterial treated specimens. Similarly, in case of SFS, I_{corr} was found to be in passive state till 40 days of exposure. The biolayer of calcium carbonate crystals formed on the outer surface of specimens due to spray treatment helped in resisting the penetration of aggressive ions from the top surface of concrete, thereby delaying the penetration of chloride ions. After 40 days of exposure the I_{corr} increased gradually with the exposure duration and entered the active corrosion state.

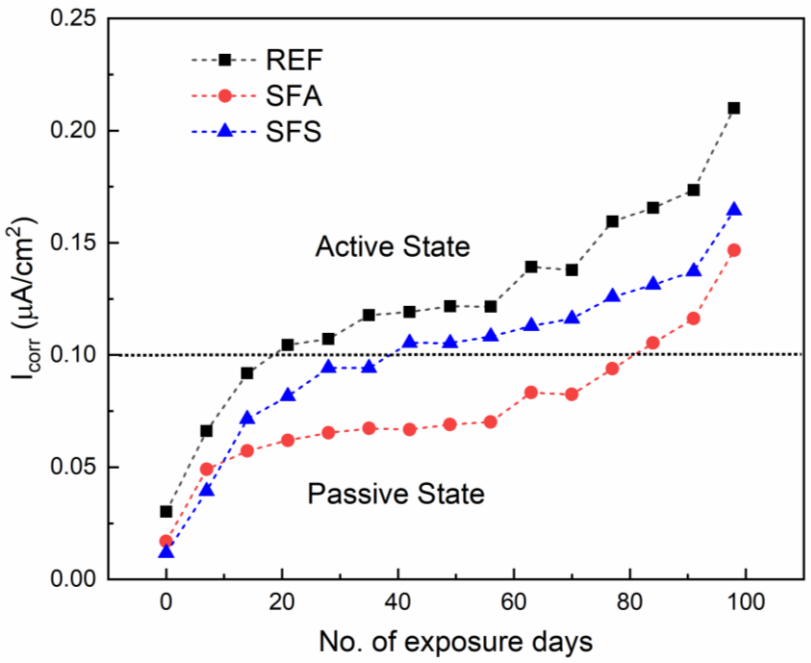

Figure 4.26: Corrosion current density versus exposure days of tested specimens

4.6.2 EMI based corrosion monitoring

Qualitative analysis of EMI signature

Figures 4.27-4.29 show the variation of conductance versus frequency signature for the REF, SFA and SFS samples. Conductance signatures of both CVS patch and SBPS were recorded, in the frequency range of 20 Hz to 500 kHz during the entire accelerated chloride corrosion exposure. It can be observed that CVS and SBPS conductance signatures in the REF sample (Figure 4.27) have undergone substantial changes during testing exposure in comparison to SFA (Figure 4.28) and SFS (Figure 4.29) samples.

It was found that during the early days of chloride exposure, the conductance signatures overlapped each other in REF. With the increasing accelerated corrosion exposure after 7 days, the resonance peak shifted downward suggesting the penetration of chloride ions inside the concrete matrix. Whereas in SFA and SFS specimen, the conductance signatures overlapped each other till 40 days and the lesser shift was observed in resonance peaks with progressive chloride exposure.

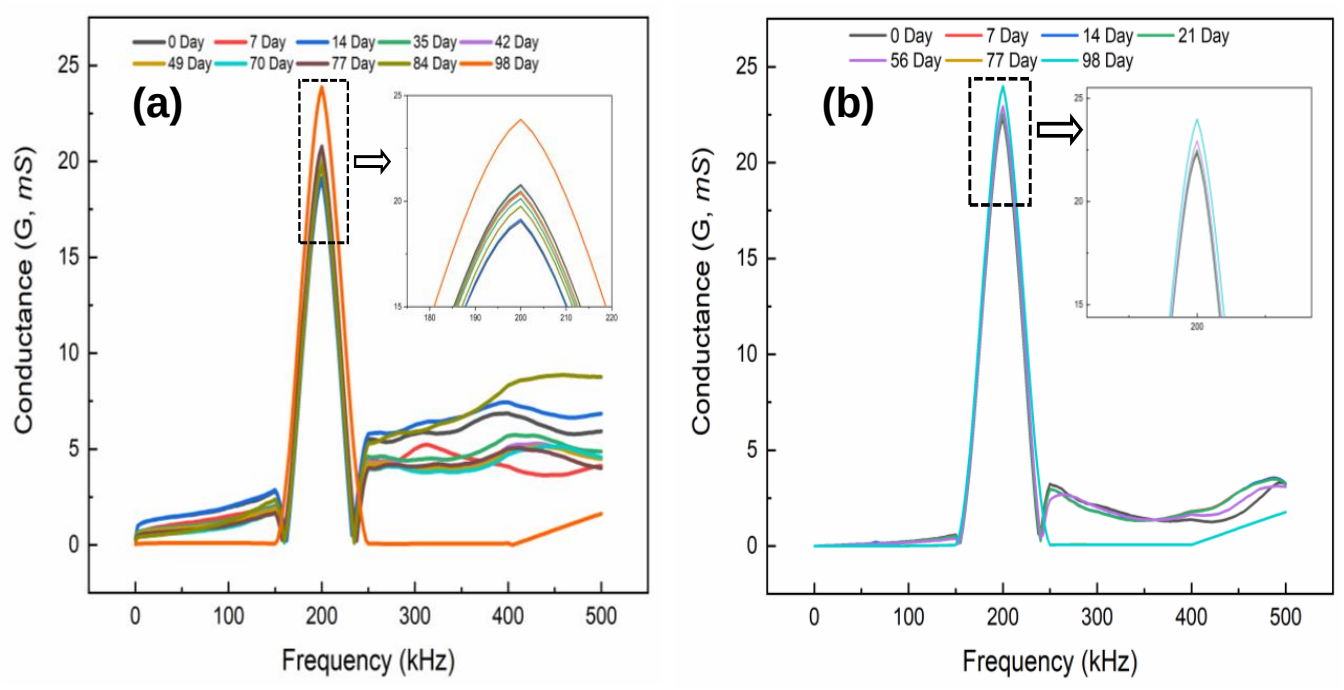

Figure 4.27: Conductance signature of patches embedded in REF specimen (a) CVS (b) SBPS

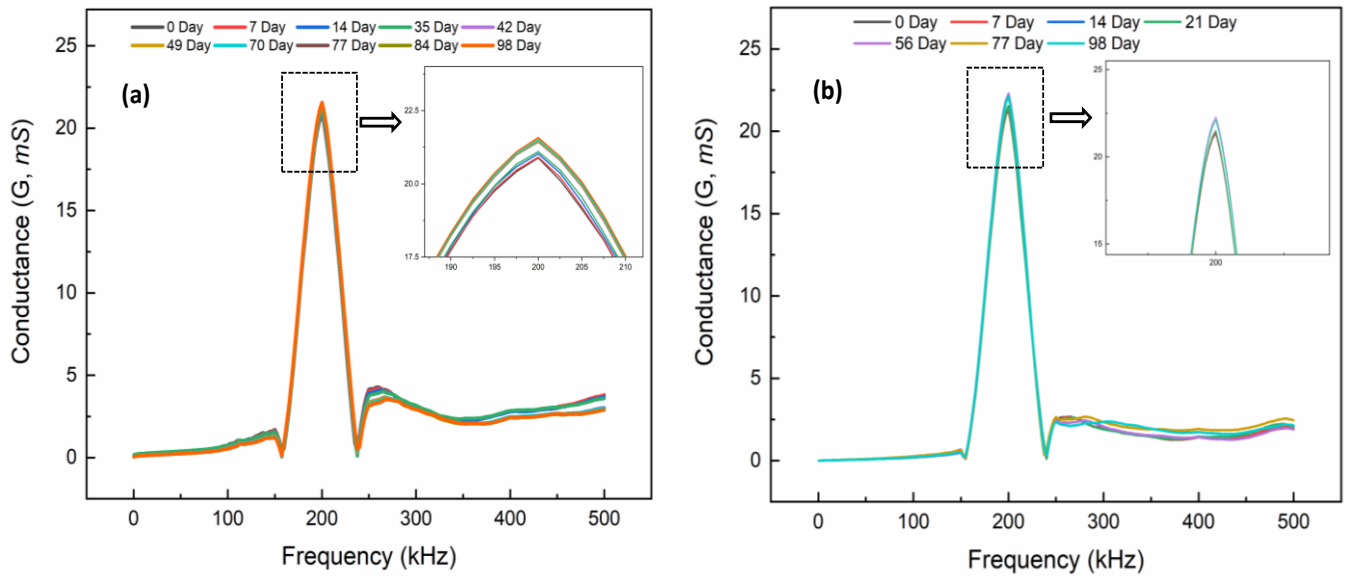

Figure 4.28: Conductance signature of patches embedded in SFA specimen (a) CVS (b) SBPS

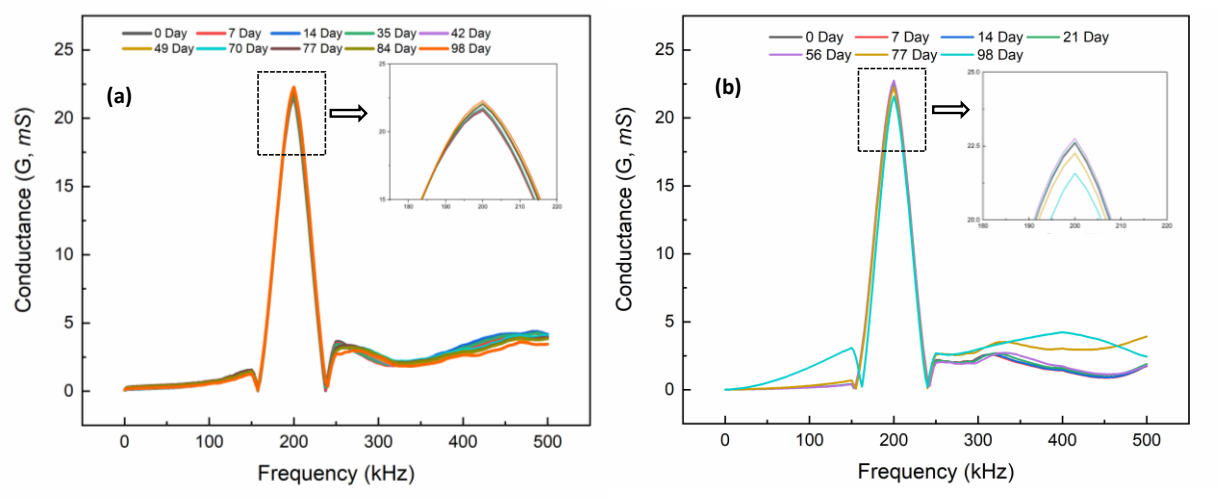

Figure 4.29: Conductance signature of patches embedded in SFS specimen (a) CVS (b) SBPS

It can be noted that the decrease in the magnitude of the resonance peak of the corroded state is less in SFA and SFS than the REF specimen. This indicates that the lesser penetration of aggressive chloride ions occurred inside the SFA and SFS specimens. These results are also correlating with the I_{corr} results (Figure 4.33) as the corrosion observed in the SFA and SFS specimen is comparatively lower than the REF specimen. This might be due to bio-deposition formed around the outer surface of concrete due to MICCP.

Quantitative analysis of EMI signature

Figure 4.30 shows the variation of the RMSD index with the chloride test exposure (days) in the frequency range 20–500 kHz for CVS and SBPS. It can be found that the RMSD values in CVS were higher than SBPS in the initial days of chloride exposure, which suggests higher changes in the concrete matrix occurred during the penetration of aggressive chloride ions into the concrete as compared to the changes at the steel surface. It further suggests that CVS sensors are more senstive to the initial physical changes in the concrete matrix; and hence can detect corrosion initiation period. Similar findings were also reported by other researchers (Talakokula et al. 2014). The RMSD values recorded by CVS in SFA and SFS were lesser than the REF specimen suggesting lesser ingress of chloride ions. The RMSD values for REF shifted to higher side at 20 days of test exposure and remained in the range of 15% to 23% after this

testing duration. However, the values remained in the range of 1% to 14.5% for both SFA and SFS throughout the testing duration.

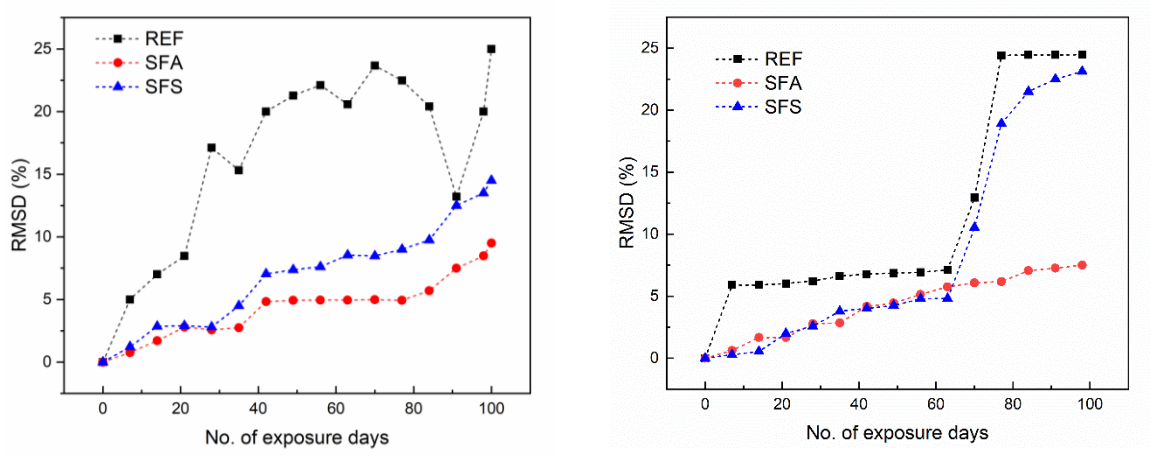

(a) (b)

Figure 4.30: Variation of RMSD (%) extracted from (a) CVS (b) SBPS

In case of SBPS, the major shift is observed in the later days of exposure, which indicates its senstivity once the rebar is depassivated by chloride ions. After initiation of corrosion, chlorides ions destroyed the protective barrier layer and start deteriorating the rebar surface. SBPS exhibited somewhat higher sensitivity to corrosion occurrence in comparison to CVS. This is on account of the direct bonding of the piezo sensor on rebars, which is the component most affected by chloride corrosion during the post-initiation phase. In REF, RMSD (%) became highly senstive and showed sudden shift after 60 days of test exposure, whereas similar shift was observed at 90 days in SFA and 70 days in SFS specimens. After sudden increase in RMSD values, these values got stablised till the end of testing. This might be due to appearance of crack on outer surface of the specimen, which led to release of stressses that were built up due to deposition of corrosion products. For instance, the sudden gain in RMSD was noted at 77 days of test exposure in REF specimens. The condition of REF specimen at 77 days of testing is shown in Figure 4.31, which shows major crack in concrete along the length of rebar with the corroison products oozing out of the crack. Similar observation related to stablization of RMSD values after cracking of concrete was made by other researchers (Talakokula et al.

2016; Talakokula and Bhalla 2015). In the SFA specimen, lower RMSD values of 6.1% were recorded at 77 days of exposure indicating the delay of corrosion . The constant trend was observed in SFA upto 100 days of exposure. The denser interfacial pore refinement due to calcium carbonate deposition was responsible for the delay in the corrosion process.

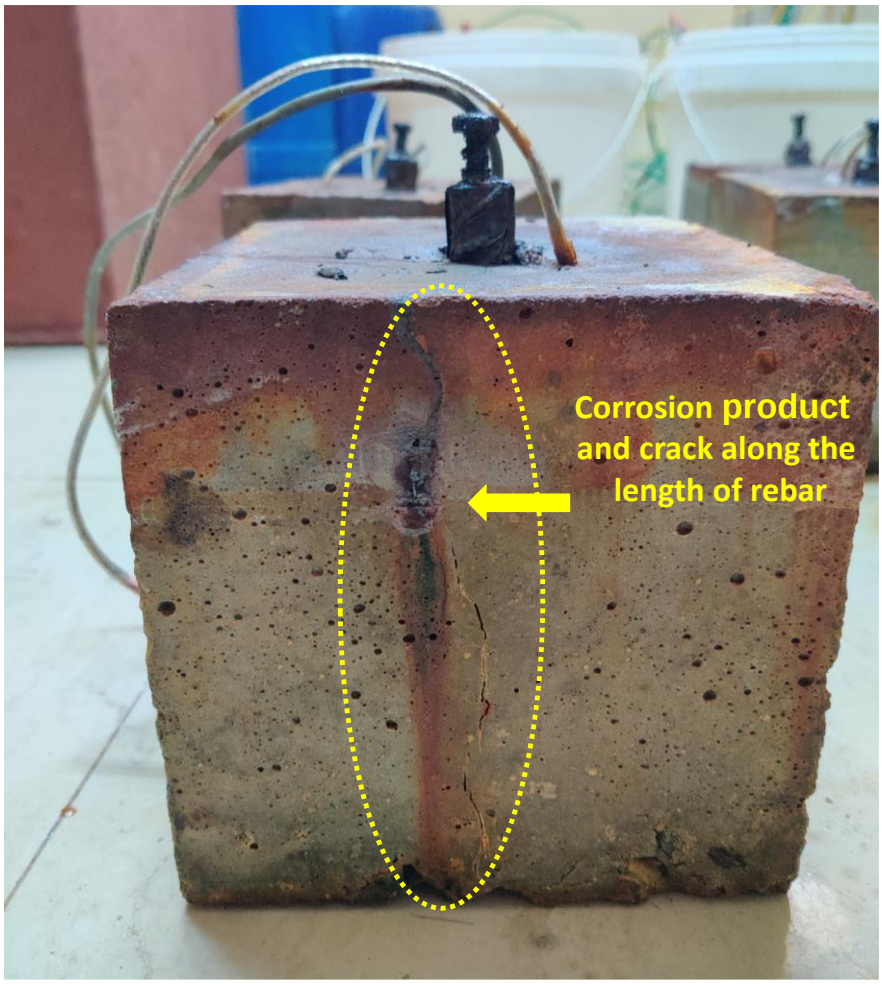

Figure 4.31: REF specimen condition in cracking phase

4.6.3 Mass loss

At the end of testing in EMI studies, all the specimens were damaged to extract steel rebar. The conditions of rebars extracted from the specimens after chemical cleaning are shown in Figure 4.32. General corrosion products or pitting was observed in SFA and SFS; whereas high cross-sectional loss was observed at one location in REF. The mass loss of the steel rebar was determined using gravimetric method after chemically cleaning the corrosion products as per

the guidelines of ASTM G1-03 (2017). The initial mass before embedding and the final mass after extracting the rebars from RC were calculated for all the specimens as tabulated in Table 4.7. It can be noted that the mass loss is highest in the REF specimen (4.70%), whereas lowest was observed in SFA (0.82%). This observation further strengthens the positive effect of using bacterial concrete to delaying the onset and propagation of rebar corrosion.

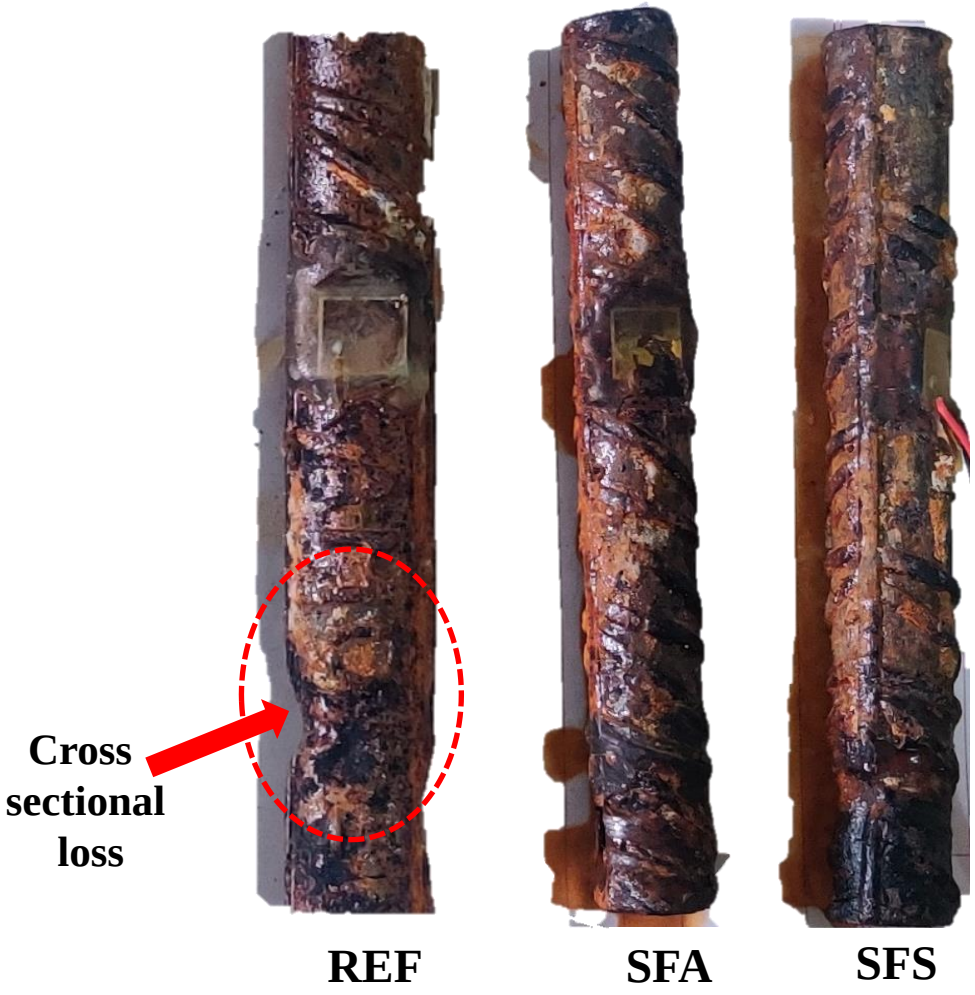

Figure 4.32: Condition of rebar extracted from the tested specimens

Table 4.7: Gravimetric analysis of extracted rebar

Specimen	Initial mass (gram)	Final mass (gram)	Mass loss (%)
REF	185.0	176.3	4.70
SFA	185.0	183.4	0.82
SFS	185.0	182.0	1.58

4.6.4 Correlation between electrochemical and EMI technique

The parameters extracted from electrochemical and EMI techniques were correlated, in order to understand any possible correlation between the two techniques. A relation between current density (I_{corr}) and RMSD (%) obtained during exposure was attempted. The corrosion current density corresponding to 0 to 100 days of exposure for REF, SFA and SFS mixes was correlated with both types of piezo patches, viz. CVS and SBPS separately. Figure 4.33 presents relation between I_{corr} ($\mu A/cm^2$) and RMSD (%) of all three specimens. Among CVS and SBPS sensor, SBPS has shown better level of correlation (R^2) than CVS sensor in REF specimens. Since the CVS were embedded near to the rebar, it can detect early changes occurring due to ingress of chloride ions only, whereas the SBPS sensors were able to detect and monitor the rebar corrosion in a better way. The other major observation, w.r.t RMSD values (%) by SBPS for both REF and SFS are sudden increase in values once the I_{corr} is nearly 0.1 $\mu A/cm^2$. This reflects a sudden rise in RMSD once the corrosion state shifts from passive to active state.

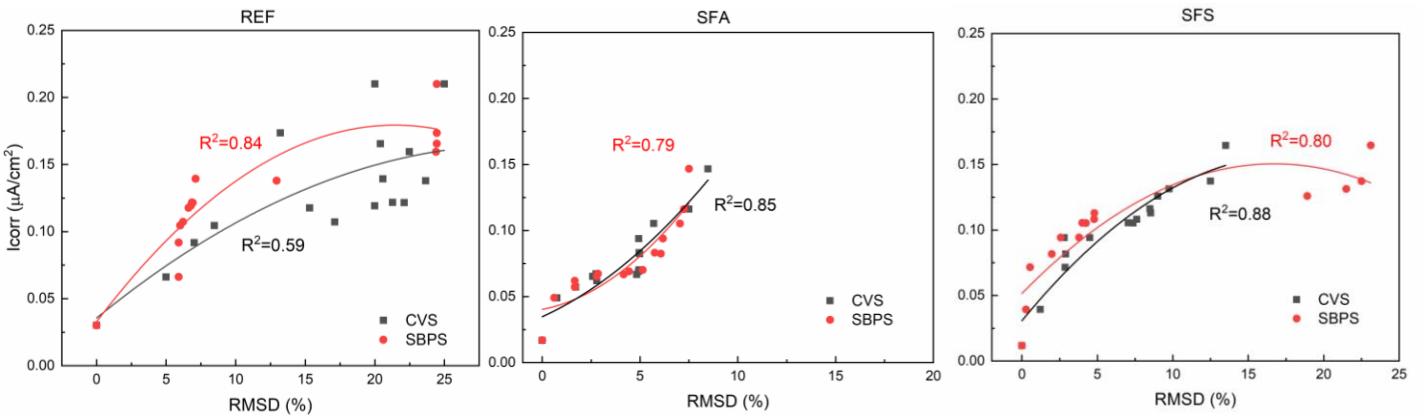

Figure 4.33: Correlation between I_{corr} and RMSD of tested specimens

In the SFA specimens no sudden rise in RMSD (%) values was observed suggesting delay in corrosion. Also, the values of R^2 were found to be 0.79 and 0.85 for SBPS and CVS. The higher values of R^2 signifies the EMI-RMSD can be used to assess the corrosion initiation process in RC structures. In case of REF specimens, R^2 were found to be 0.84 and 0.59 for SBPS and CVS. Lower value of R^2 in REF can be attributed to an unusual phenomenon that occurred in

REF specimen and is visible from the condition of the rebar as shown in Figure 4.32. In REF specimen, larger cross-sectional loss occurred at a particular location on the rebar suggesting lesser responsive to the ongoing corrosion process in the REF specimen. This observation can be better detected by SBPS in REF. It can be seen that the corrosion occurred almost uniformly throughout the rebar length extracted from both the SFA and SFS specimen. Both SBPS and CVS sensor were able to detect the corrosion process in SFA and SFS specimens.

4.6.5 Exploring the corrosion mechanism using pore solution testing SF inoculum-based specimens against chloride exposure

The results obtained of SF based inoculum pore solution by electrochemical studies are discussed here under.

4.6.5.1 Potentiodynamic polarization curves in concrete powder aqueous solution (AQS)

The AQS was admixed with 0.1 M NaCl to simulate aggressive chloride environment. The bare steel was immersed in the prepared AQS and corrosion activity was tested at 3, 5 and 10 days of immersion. The polarization curves obtained at 5 days of immersion for the set without aggressive chloride ions are shown in Figure 4.34.

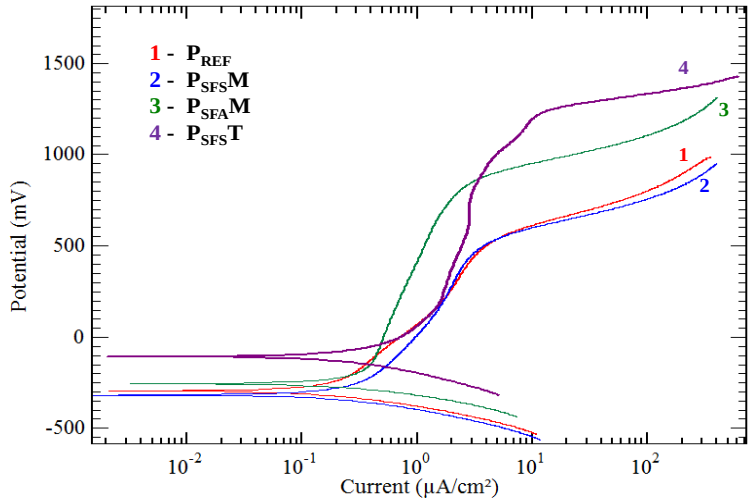

Figure 4.34: Polarization curve recorded on steel in non-chloride contaminated solution

It can be observed from the figure that all the specimens showed similar kind of potentiodynamic behaviour, that is formation of a passive layer followed by a transpassive zone. The recorded potentiodynamic curves suggested that the bacterial precipitates facilitated the formation of passive layer. The obtained E_{corr} and I_{corr} values are presented in Table 4.8. The preliminary results clearly showed the deposition of stable protective layer over the exposed area of steel bar in $P_{SFA}M$, $P_{SFS}T$ and $P_{SFS}M$.

Table 4.8: Electrochemical parameter of samples in non-chloride contaminated solution

Solution	**I_{corr} ($\mu A/cm^2$)**	**E_{corr} (mV)**
P_{REF}	0.24	-306.16
$P_{SFS}M$	0.14	-332.51
$P_{SFA}M$	0.16	-351.63
$P_{SFS}T$	0.41	-107.2

The corrosion activity of all specimens was then tested in the presence of 0.1 M NaCl. The polarization curves obtained at 3, 5 and 10 days of immersion are shown in Figure 4.35. The obtained E_{corr} and I_{corr} values are presented in Table 4.9. It can be observed from Figure 4.35(a), due to the addition of 0.1 M NaCl, the unstable passive layer was observed along with pitting potential at 500 mV in P_{REF}(Cl). The addition of Cl ions weaken the passive layer over the steel surface. Whereas in other specimens, stable passive layer was noted at 3 days of exposure. Also, the I_{corr} values were recorded to be 10.22, 8.15, 8.06 and 6.9 $\mu A/cm^2$ in P_{REF}(Cl), $P_{SFS}M$(Cl), $P_{SFA}M$(Cl) and $P_{SFS}T$(Cl). This clearly represents the I_{corr} is one order magnitude lower than P_{REF}(Cl). The results recorded at 5 days of immersion demonstrates meta stable pitting P_{REF}(Cl) which signifies the active corrosion reaction on the steel surface (Figure 4.35(b)). However, in $P_{SFA}M$(Cl) and $P_{SFS}T$(Cl), stable passive region was observed at 5 days of immersion. Uniform increase anodic current density along with potential shows the sign of active corrosion in $P_{SFS}M$(Cl). It can be concluded that the $P_{SFA}M$(Cl) and $P_{SFS}T$(Cl) performed better in comparison to P_{REF}(Cl) and $P_{SFS}M$(Cl).

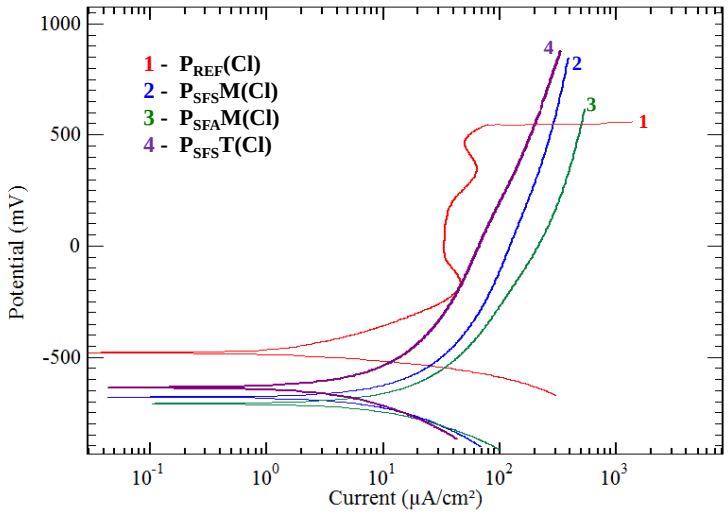

(a)

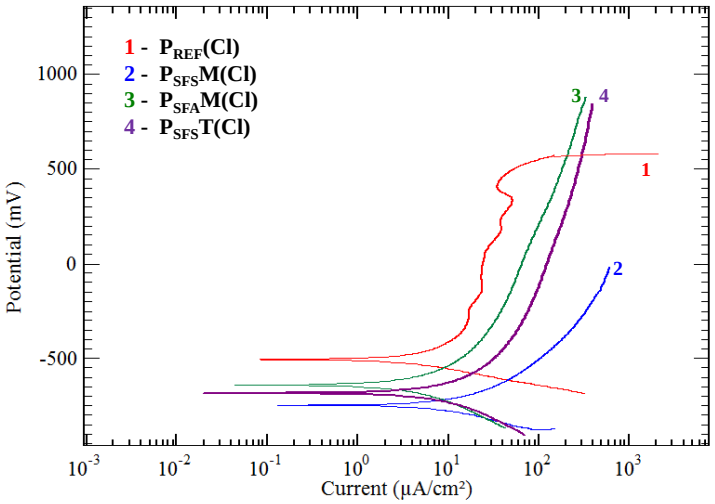

(b)

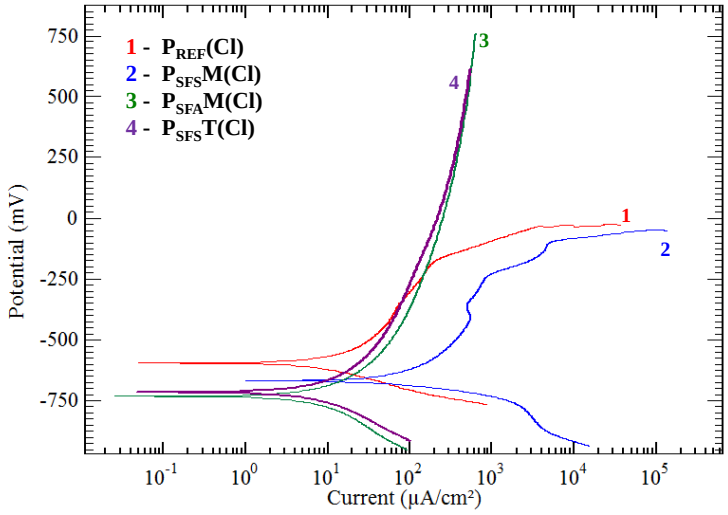

(c)

Figure 4.35: Polarization curve recorded on steel in chloride contaminated solution after (a) 3 day (b) 5 day (c) 10 day

Table 4.9: Electrochemical parameter of tested samples in chloride contaminated solution

Solution	Test duration					
	3 days		5 days		10 days	
	I_{corr} ($\mu A/cm^2$)	E_{corr} (mV)	I_{corr} ($\mu A/cm^2$)	E_{corr} (mV)	I_{corr} ($\mu A/cm^2$)	E_{corr} (mV)
P_{REF}(Cl)	10.22	-500	16.78	-500	48.9	-700
P_{SFS}M(Cl)	8.15	-680.31	17.1	-741.25	47.35	-723
P_{SFA}M(Cl)	8.06	-710.17	9.5	-638	18.2	-724
P_{SFS}T(Cl)	6.9	-640.51	7.9	-682.72	21.91	-715.29

The results at 10 days of immersion indicate active corrosion in all the specimens (Figure 4.35(c)). Still, the values of I_{corr} recorded in P_{SFA}M(Cl) is lower than the corresponding P_{REF}(Cl) specimen. It can be inferred from the overall polarization curves that passive layer in P_{SFS}M(Cl), P_{SFA}M(Cl) and P_{SFS}T(Cl) were stable and efficient upto 5 days of exposure. However continuous action of active chloride ions in solution at 10 days of immersion destroyed the protective layer over the steel surface causing the active corrosion in all specimens. The condition of the exposed surface of steel bar was also inspected after immersing the steel tablets in chloride contaminated AQS for 5 days. Figure 4.36 shows the optical imaging of steel tablets taken at 50x magnification.

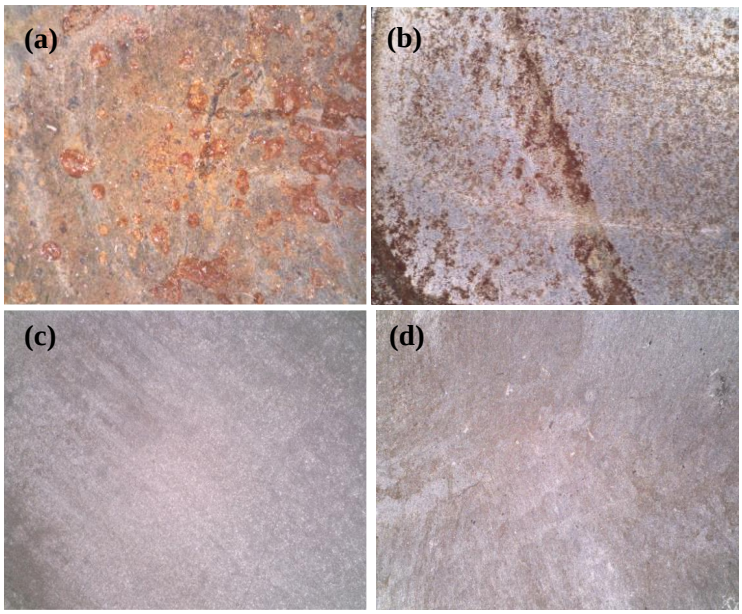

Figure 4.36: Optical imaging of steel tablets immersed in (a) P_{REF}(Cl); (b) P_{SFS}M(Cl); (c) P_{SFA}M(Cl); (d) P_{SFS}T(Cl) at 5 days

The images clearly show indicate large number of red coloured pits formed on the steel surface in P_{REF}(Cl); which can be linked to the formation of FeOOH (Tiwari et al. 2021). The amount of corrosion pits was small in number in P_{SFS}M(Cl); whereas no corrosion products/pits was observed in the P_{SFA}M(Cl) and P_{SFS}T(Cl). It clearly indicated that bacterial treatment to concrete helped in providing better protection to the steel rebar. The FESEM-EDX results obtained of all the immersed specimens are shown in Figure 4.37.

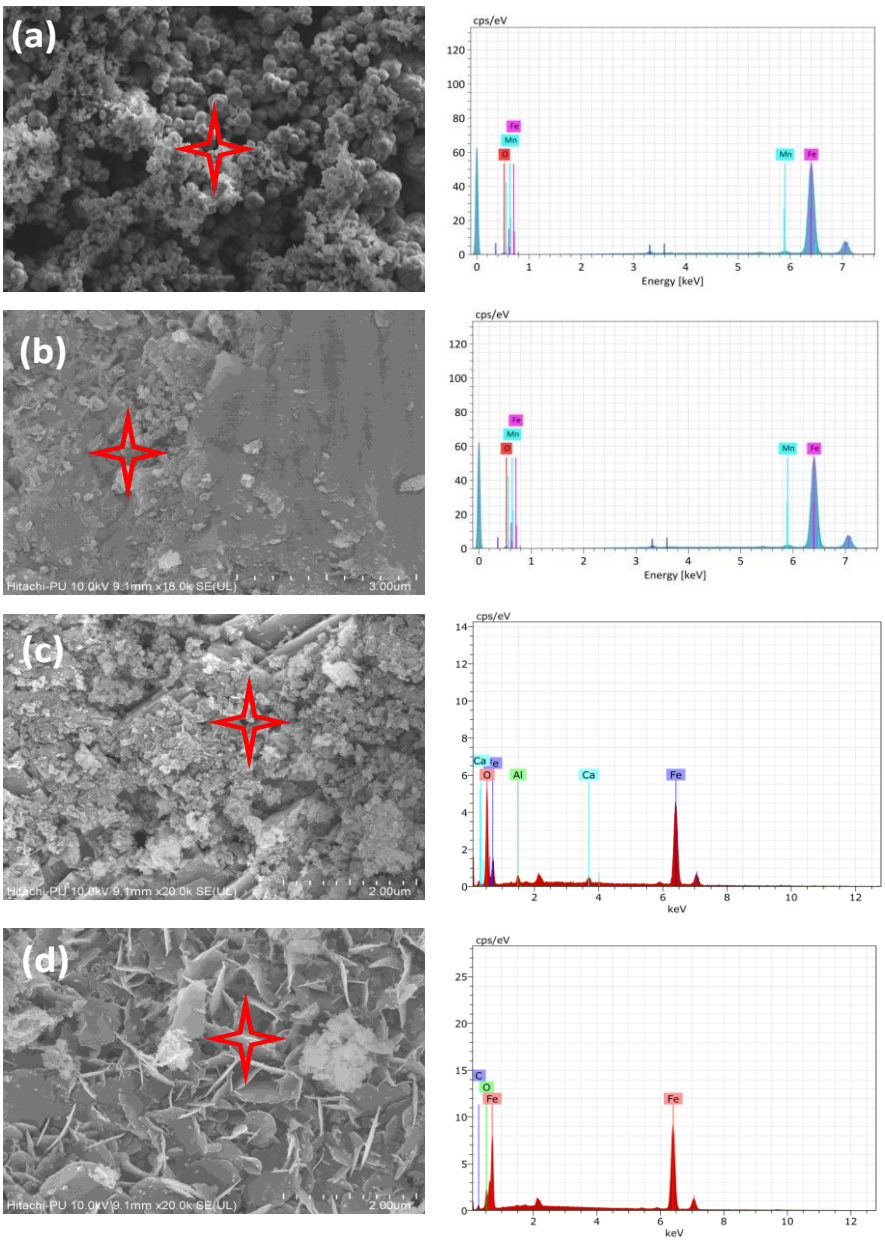

Figure 4.37: FESEM-EDX analysis of steel tablets immersed in (a) P_{REF}(Cl) (b) P_{SFS}M(Cl) (c) P_{SFA}M(Cl) (d) P_{SFS}T(Cl) for 5 days

The considerable corrosion product was notable on the surface of P_{REF}(Cl), which is clear evidence of pitting corrosion due to chlorides (Figure 4.36(a)). EDX spectra also confirmed the presence of Fe and O elements associated with corrosion products. Similar observation was made in FESEM-EDX analysis of P_{SFS}M(Cl). However, in P_{SFA}M(Cl) and P_{SFS}T(Cl), flower shaped cluster was observed on the surface of steel tablet. EDX analysis in P_{SFA}M(Cl) confirmed the presence of Fe, O, Ca and C. This indicated the formation of $CaCO_3$ layer on the steel surface which resisted the attack of chloride ions on the steel surface.

4.7 PERFORMANCE COMPARISON OF FA AND SF INOCULUMS BASED ON CORROSION STUDIES

Based upon the obtained test results of RC specimen under chloride environment, it can be concluded that mineral inoculums were able to restrict the entry of aggressive chloride ions inside the concrete. The obtained results are shown in Figure 4.38 to compare the performance of mineral inoculums in corrosion inhibition. At 91 days of electrochemical testing, I_{corr} recorded in REF specimen was 0.18 µA/cm^2 where as in FAA and SFA was nearly 0.1 µA/cm^2.

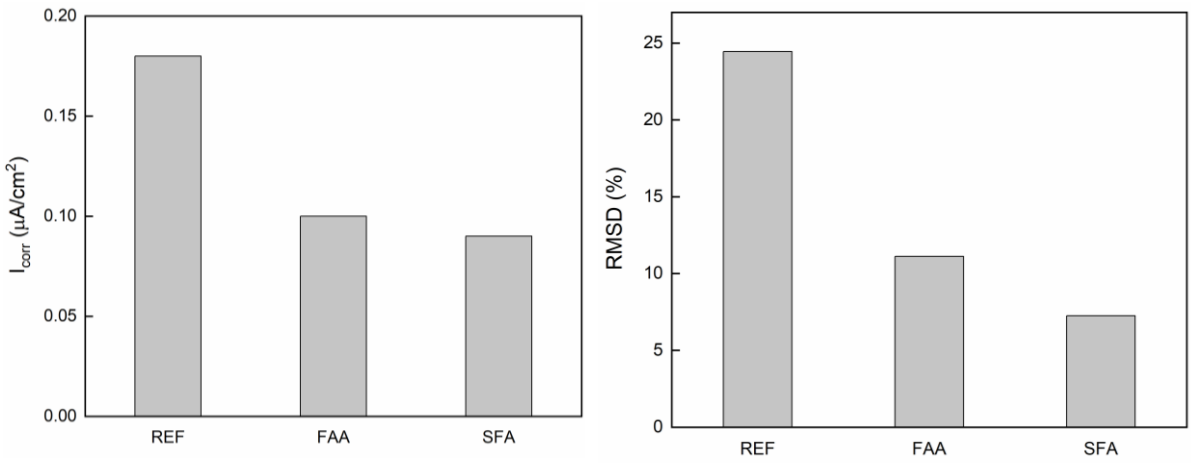

(a) (b)

Figure 4.38: Comparison of mineral inoculums (a) Electrochemical studies; (b) EMI studies at the end of testing exposure

At 91 days of EMI studies, RMSD (%) recorded by SBPS in REF was 24.45% where as in FAA and SFA specimen were 11.12% and 7.25%. Both FA and SF based inoculums were able to restrict the aggressive penetration of chloride ions.

4.8 CONCLUDING REMARKS

The aim of present study was to test the effectiveness of developed mineral (FA and SF) inoculums resistance against the ingress of aggressive chloride ions. FA and SF based inoculums were immobilized in RC concrete and subjected to accelerated chloride exposure. The corrosion monitoring was done using electrochemical and electromechanical impedance techniques. Corrosion current density (I_{corr}) and admittance signatures were acquired over the test exposure. Lower (I_{corr}) and low RMSD (%) were observed in the bacterial specimens. The results clearly indicated the effectiveness of mineral inoculums in restricting the penetration of chloride ions.

CHAPTER 5: MINERAL INOCULUMS AS CRACK REPAIR MEASURE IN CONCRETE

5.0 GENERAL

Several investigators have used bacteria as a measure of eco-friendly crack healing agent in concrete structures (De Belie and Wang 2015; Bergh et al. 2020; Jiang et al. 2020; Rong et al. 2020; Son et al. 2022). The results revealed that bacteria could produce calcium carbonate ($CaCO_3$) precipitation inside the cracks and block them, thus the mechanical properties of the concrete could be restored to a certain extent (Ramachandran et al. 2001). In the current investigation, fly ash (FA) and silica fume (SF) based inoculums stored at 4°C for 180 days as reported in chapter 3 was immobilized in concrete to study their self-healing capabilities. The remediation methodologies were developed for new concrete structures as well as for the damages in the existing concrete structures.

Regarding self-healing capabilities, developed mineral inoculums were immobilized in concrete and tested for their self-healing abilities. An artificial crack of 0.5 mm width was generated during the casting and healed using a bacteria-based healing agent (nutrient broth, urea and $CaCl_2$). Crack healing efficiency was monitored using a non-destructive technique, visual examination and regain in strength. At the end of testing, the mineral precipitated inside the healed crack was assessed through field emission scanning electron microscopy (FESEM), energy dispersive x-ray (EDX), x-ray diffraction (XRD) and thermogravimetric analysis (TGA) to evaluate its physicochemical attributes.

In context to repair damages in the existing concrete structures, bio-inspired cementitious grouts containing mineral inoculums, as reported in chapter 3 were designed and tested for fresh and hardened properties of grouts. The best performing bio-cementitious grout was used to repair existing cracks in the concrete structures. The performance of the repaired surface was assessed in terms of recovery in flexural strength and water tightness. The mineral composition

of the healing product was also examined for FESEM-EDX and XRD at the end of treatment. Also, to quantify the calcium carbonate precipitation in the bio-repaired specimens during curing, a non-destructive technique was employed. And finally, the efficient cementitious bio-grouts were applied in field application to repair cracks in concrete structures.

5.1 SELF-HEALING OF CRACKS BY MINERAL INOCULUMS

In the present study, a crack of 0.5 mm width was generated during the casting and healed using a bacteria-based healing agent (nutrient broth, urea and $CaCl_2$). The electromechanical impedance (EMI) technique was used to monitor the crack healing potential of selected inoculum through microbially induced calcium carbonate precipitation (MICCP) to restore the integrity of cracked concrete. The monitoring was done until the complete healing of the cracked surface was achieved. The healed cracked surface was also examined through optical imaging to monitor the crack width reduction. At the end of the test, the healed specimens were subjected to bending failure to assess the strength regain. The healing mineral precipitated inside the cracks was examined through FESEM-EDX, XRD and TGA to evaluate its physicochemical attributes.

5.1.1 Material and methods

This section discusses the detailed properties of materials used for the preparation of test specimens and methods for testing.

5.1.1.1 Mineral carrier-based inoculums

The mineral carrier-based inoculums made by FA or SF were used to prepare mixes. The detailed procedure for preparing these inoculums is reported in the previous chapter. The inoculums were stored at 4°C for 180 days and the viability studies reported in the last chapter confirmed that these inoculums possessed sufficient cell counts to induce MICCP even after 180 days of storage.

5.1.1.2 Constituents of concrete

Commercially available ordinary portland cement (43 grade) (IS 8112 2013), locally available river sand and coarse aggregates *conforming to standards (IS:383 2016)* were used for preparing concrete specimens. The detailed specifications of all the constituents used in the present investigation are provided in section 3.3.1.

5.1.1.3 Preparation of concrete specimen and creation of cracks

The concrete mix was prepared and cast using cement: fine aggregate: coarse aggregate in the proportion of 1:1.82:3.24 and water to cement ratio (w/c) of 0.47. In this study, prismatic concrete specimens of 500×100×100 mm were prepared and divided into three sets.

In set 1, the control specimens were prepared using tap water. In set 2, FA-based inoculum was added by 5% of the weight of cement along with other constituents during the casting of the prismatic specimens. In this set, growth media supplemented with nutrient broth (1.3% weight (w)/volume (v)), urea (2% w/v) and 25mM $CaCl_2$ was used instead of tap water during casting. Here calcium chloride was used within the permissible limits of 0.4% of cement weight (Angst et al. 2009; Paine 2016). The alternative calcium sources such as calcium acetate and calcium lactate can also be used as it is free from chloride ions. In set 3, SF-based inoculum was added by 5% of the weight of cement along with other constituents during the casting of the prismatic specimens. Growth medium as discussed in set 2 was used instead of water during casting. The specimens were cast immediately after preparation of the concrete mixture. Triplicate specimens of all sets were cast to check the data's repeatability.

The cracks were generated while casting prismatic specimens in all the sets. The cracks were created by inserting a steel plate of 60 mm width, 20 mm depth and 0.5 mm thickness while casting, as shown in Figure 5.1. The steel plate was removed after 3 hours from casting. The prepared prismatic specimens were placed in a room environment of (25-27°C) for one day.

After one day, the specimens for both sets were demolded and water cured for 28 days. At 28th day, hardened samples were taken out and air-dried for further study. These cracked specimens were then healed using a bacterial healing agent (nutrient broth (1.3% w/v), urea (2% w/v) and 25mM $CaCl_2$) to assess the MICCP for crack healing. The outline and mechanism of the curing regime of the prepared specimens are mentioned in Table 5.1.

Figure 5.1: Artificial cracks generated in prismatic specimens during casting

Table 5.1: Outline of specimen and mechanism of curing regime

Specimens	**Material used**	**Mechanism of curing**
Control	Cement: sand: coarse aggregate Water/cement = 0.47	Water Curing for 28 days
FAA	FA based bacterial inoculum**: cement: sand: coarse aggregate Growth medium /cement = 0.47	Water Curing for 28 days
SFA	SF based bacterial inoculum$^{\#\#}$: cement: sand: coarse aggregate Growth medium /cement = 0.47	Water Curing for 28 days

Growth medium has the following composition: Nutrient broth (1.3% w/v), 2% Urea (w/v) and 25mM Calcium chloride (w/v). All specimens were prepared in triplicate.

**FA based inoculum stored at 4°C & 180 days storage age.

$^{\#\#}$SF based inoculum stored at 4°C & 180 days storage age.

5.1.1.4 Installation of PZT

To monitor the crack healing process, a thin PZT transducer (PIC 151) of dimensions 10×10×0.3 mm was mounted to each prismatic specimen (host structure) using an adhesive mix (epoxy). The PZT patch was installed 30 mm away from the center of the cracked specimen (Kim et al. 2019). It was ensured that epoxy thickness was less than one-third of the patch thickness (Bansal and Talakokula 2021). A small weight was applied over the assembly to create light pressure. At room temperature, the setup was left untouched for a period of 24 hours so that complete curing of adhesive may be achieved. Coaxial wires were attached through the process of soldering for making connections to an impedance analyser (E4980Al, Keysight) to capture the admittance signatures. To avoid the disconnection of wires while experimenting and extra protection of PZT, a thin layer of epoxy was applied and cured for 24 hours at room temperature. Details of the experimental setup is shown in Figure 5.2, while the specification of PIC 151 and epoxy are listed in Table 4.1.

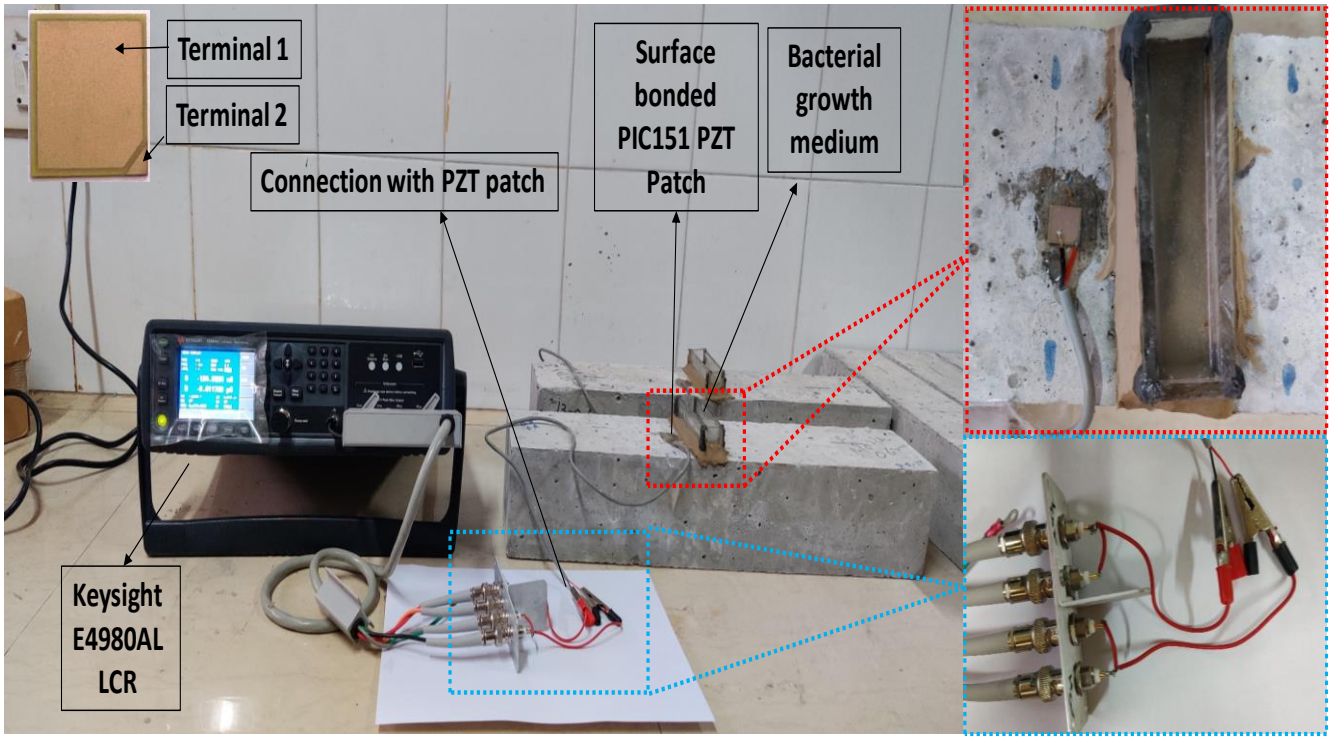

Figure 5.2: Experimental setup for monitoring of crack healing using LCR (L-Inductance, C-Capacitance & R-Resistance) meter

5.1.1.5 Non-destructive monitoring of crack healing process

To study the entire crack healing process, two non-destructive techniques were employed. This includes visual examination and recording admittance signature using EMI technique. After the instrumentation of the PZT patch on specimens, a small pond was created with the acrylic frame around the artificial cracked area of the specimens. A growth medium comprising nutrient broth (1.3% w/v), urea (2% w/v) and 25mM $CaCl_2$ was then ponded on the cracked area. For each specimen, 50 ml growth medium supplemented with $CaCl_2$ and urea was prepared and poured on the cracked site once a day. The cracked area of the specimen was treated until 100% healing was achieved. For comparison, all sets were supplied with the same medium. Crack width reduction was monitored through a stereomicroscope (SMZ1500) during the healing process at five days intervals until 100% healing. Obtained images were further studied for $CaCO_3$ crystal formation within cracks using image analysis software (NIS-Element). The percentage of crack healing was computed from the given expression (Eq. 5.1).

$$\text{Percentage of crack healing} = \left(\frac{w_i - w_0}{w_0}\right) \times 100 \tag{5.1}$$

where w_0 is the crack width measured at the start of the experiment and w_i is the crack width measured at any time during the healing process.

The crack healing process was monitored by recording the EMI signatures at regular intervals. In the previous studies reported, the EMI technique was successfully utilized to evaluate the performance of cementitious repair material before and after the repair process in concrete (Kim et al. 2019). In context to crack healing, biomineralization through MICCP is a continuous process until the calcifying bacteria is supplemented with nutrients (NB, urea and Ca source) under the optimum conditions. Capturing the continuous healing process is difficult

and require progressive monitoring. EMI technique has shown promising results in real time monitoring of surface cracks (Feng et al. 2018).

While monitoring through the EMI technique, selecting a frequency interval for the EM signatures is essential, as the statistical indicators are computed from the selected frequency range (Kim et al. 2019). Park et al. 2003 suggested a frequency range of 40-300 kHz for piezo-based SHM of concrete structures because it contains more structural information about the health of a structure. Therefore, before the start of the monitoring process, the admittance signature was captured over the range of 20 Hz to 500 kHz for all prismatic specimens. From the captured EMI signature, it was noted that the structural peaks were in the range of 100 kHz to 250 kHz. Therefore, the frequency range of 100 kHz to 250 kHz was chosen for monitoring the EMI signatures throughout the healing process. Further, the real part of admittance acquired from the EMI signature was only considered in the present study since it is more prone to changes in the concrete specimen (Kaur et al. 2021). Moreover, the imaginary part of conductance is generally avoided as it is sensitive to temperature variations (Park et al. 2003). To correlate the signatures with physical interpretation for crack sealing efficiency of the bacterial agent, changes in the measured impedance and admittance were directly explored with the various statistical indices. Root mean square deviation (RMSD), correlation coefficient deviation (CCD) and mean absolute percentage deviation (MAPD) were employed to study the deviation in the EM signatures during the healing process (Jothi Saravanan et al. 2017; Kim et al. 2019). RMSD was calculated using Eq. (4.1), CCD and MAPD were calculated by using the following Eq. (5.2) and (5.3) as below.

$$\mathrm{CCD}\,(\%) = 100 - \left\{ \frac{1}{N\,\eta_{G_k^L}\;\eta_{G_k^F}} \sum_{k=1}^{n} \left[(G_k^L - \overline{G}_k^L)(G_k^F - \overline{G}_k^F) \right] \right\} \tag{5.2}$$

$$\text{MAPD}\ (\%) = \frac{1}{N}\sum_{k=1}^{n}\left|\frac{G_k^L - G_k^F}{G_k^L}\right| \tag{5.3}$$

Where, G_k^F and G_k^L are the conductance values at the k^{th} frequency for the cracked specimen (baseline) and healed specimen, and $k = 1,\ldots, n$ signifying the frequencies at which the conductance signature was obtained.

At the end of testing, the correlation in terms of the percentage of crack healing and RMSD (%) extracted during the healing process of the FAA and SFA specimens was attempted separately.

5.1.1.6 Strength regain

A measure of recovery in strength properties is reported as an indirect method for assessing self-healing efficiency in pre-cracked specimens (Khushnood et al. 2020). After 45 days of healing treatment, the prismatic samples were subjected to four-point bending test to assess the strength regained due to crack sealing. The bending strength test of all prismatic specimens were carried out using the flexural testing machine (AIMIL India Ltd, New Delhi) as per BIS 516 (1959) as discussed in section 3.2.3.

5.1.1.7 Characterization of healing mineral

The crack healing process results from $CaCO_3$ deposition instigated by microbial activity in the cracked region. To assess the mineral formed during the microbial activity of microbes, healing mineral deposits were characterized through FESEM-EDX, XRD and TGA. For FESEM and EDX, broken samples were collected from the upper depth of 0-10 mm of the treated crack of the FAA, SFA specimen and were gold coated with a sputter coating Emitech K575. The prepared samples were then analysed via FESEM (Hitachi, SU8010). Similarly, for XRD, samples were collected from the top surface of the FAA and SFA specimen and at a

depth of 10 mm of healed FAA, SFA and control specimen. The collected samples were sieved through 90 µm sieve. XRD spectrum was obtained using Bruker D8 X-ray diffractometer with a Cu anode (40 kV and 30 mA) and scanning from 10° to 80° (2θ). TGA analysis was carried out on 20 mg of concrete powder collected from a depth of 10 mm of the healed crack portion of the FAA, SFA and control specimen. The analysis was conducted on Perkin-Elmer. The sample was placed in a TGA holder and the temperature was elevated constantly from 100°C to 900°C at a heating rate of 10°C/min. The analysis was done from 100°C to neglect any water loss from the tested sample.

5.1.2 Results and discussion

To monitor the crack healing process by bacterial inoculums, visual examination and admittance signatures were recorded using LCR meter during the entire healing period.

5.1.2.1 Visual examination

After 28 days of water curing, all the specimens were microscopic examined to measure the initial crack width. The crack width of control, FAA and SFA specimens were found to be 509 µm, 507 µm and 549 µm. Figure 5.3 and 5.4 shows the stereo-microscopic observation of crack healing process of FAA and SFA specimen during 45 days of MICCP precipitation.

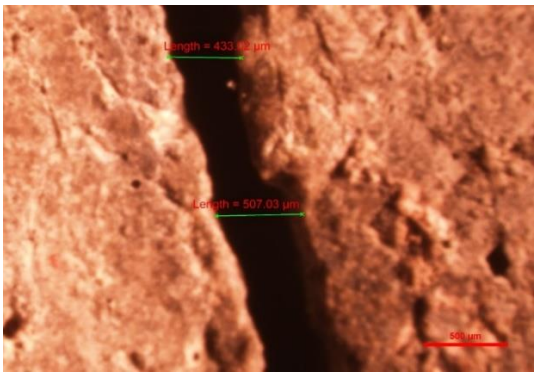

(a)

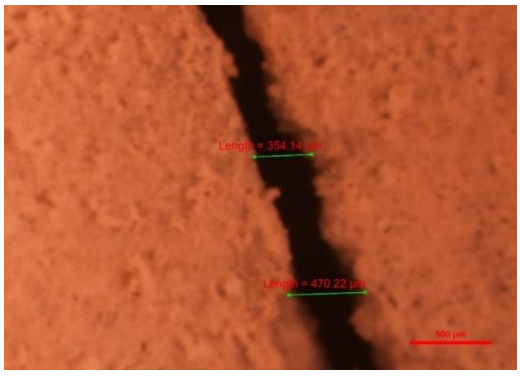

(b)

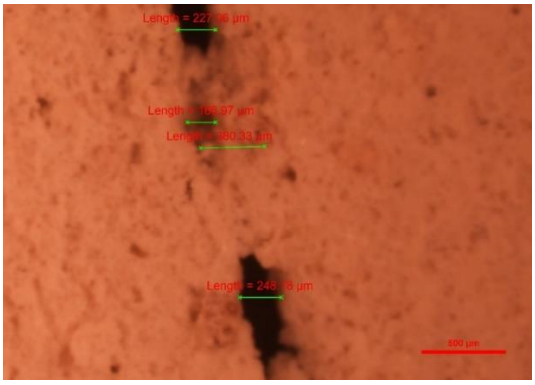

(c)

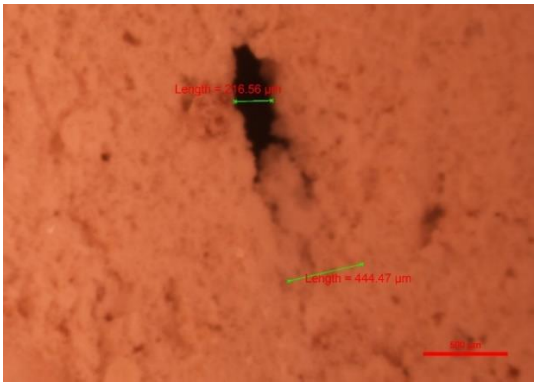

(d)

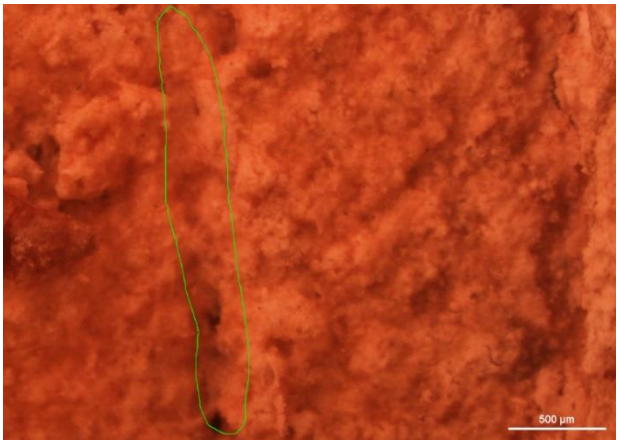

(e)

Figure 5.3: Stereomicroscopic images showing the healing of cracks in FAA specimen (a) 0 Day (b) 10 Day (c) 15 Day (d) 30 Day (e) 45 Day

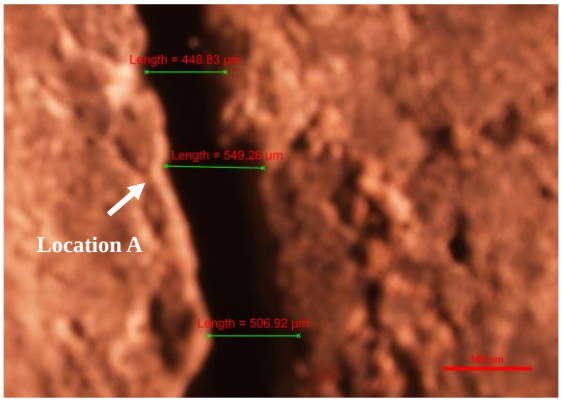

(a)

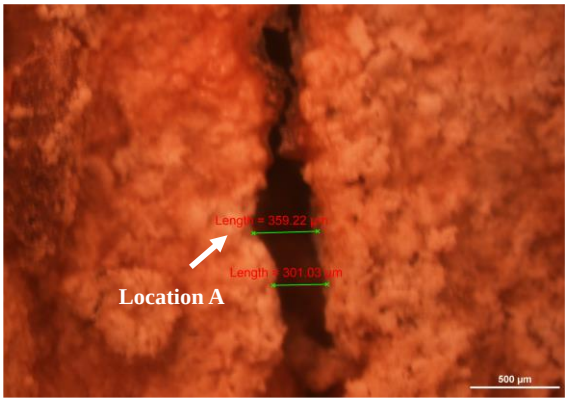

(b)

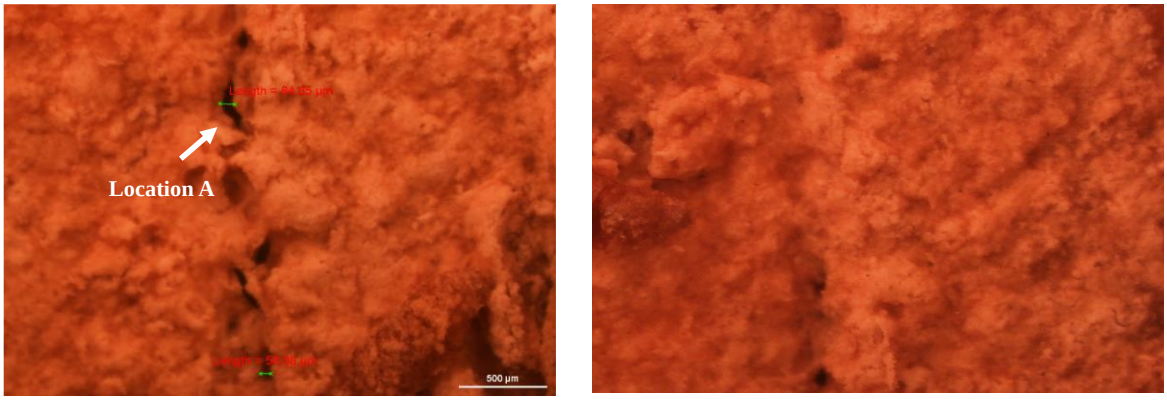

(c) (d)

Figure 5.4: Stereomicroscopic images showing the healing of cracks in SFA specimen (a) 0 Day (b) 15 Day (c) 30 Day (d) 45 Day

During the periodic visual observations, it was seen that the simulated crack on the specimen surface showed no signs of healing during the first 5 days of treatment. In fact, during the initial five days of healing, the growth medium supplemented with urea and calcium chloride was absorbed by the crack surface. A similar observation regarding absorption of growth media during initial days of treatment was made by Jongvivatsakul et al., (2019) during the remediation of cracks in cement concrete.

In FAA specimen, after 10 days of healing treatment, the crack width reduced from 507 µm to 470 µm. Average 10% crack width healing was observed during 10 days of treatment. Similar observation was noted in the SFA specimens. After 15 days of healing treatment in SFA, the crack width was reduced to 359 µm from 549 µm. Average 34% crack width healing was observed during 15 days of treatment. White mineral products were noticed on the cracked surface in repaired specimens. Continued activity of crack healing treatment caused the reduction of crack width. After 30 days of healing, the width was reduced to 84.65 µm resulting in a significant crack width repair of 84.5%. At 45 days, 549 µm crack surface width was filled by microbial carbonate precipitations. Similar observation of substantial crack width repair in FAA specimen was also noted. In FAA and SFA specimen, the crack healing ratio was calculated using Eq. 5.1 and shown in Figure 5.5. No sign of healing was observed in control specimen at the end of curing period.

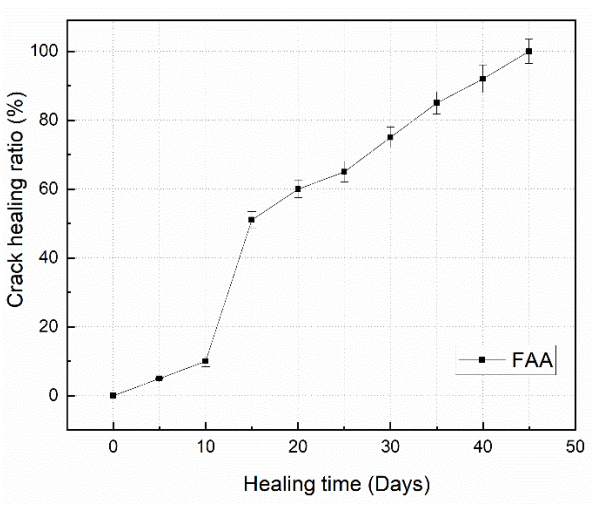

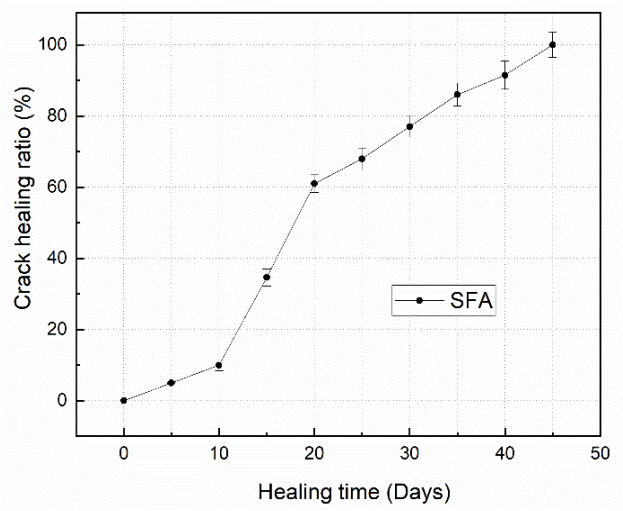

(a) (b)

Figure 5.5: Crack healing ratio vs No. of healing days in (a) FAA (b) SFA specimens

5.1.2.2 EMI monitoring

The conductance versus frequency plot of control, FAA and SFA specimens over the healing period are shown in Figure 5.6. During the progressive healing process, the gradual vertical and lateral shift is observed in the conductance plot of FAA and SFA specimens. With the increasing number of days of the healing process, the metabolic activity of microbes leads to the formation of calcium carbonate inside the cracks of the specimens (Rong et al. 2020).

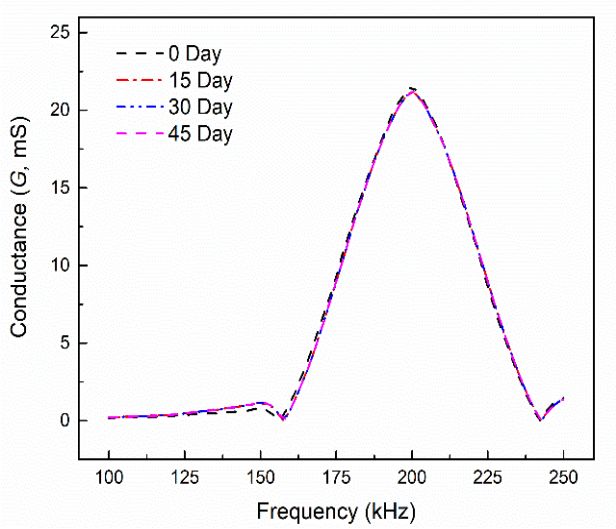

(a)

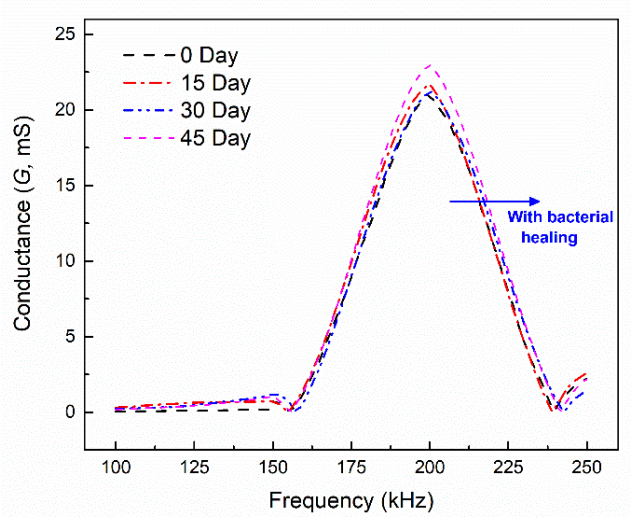

(b)

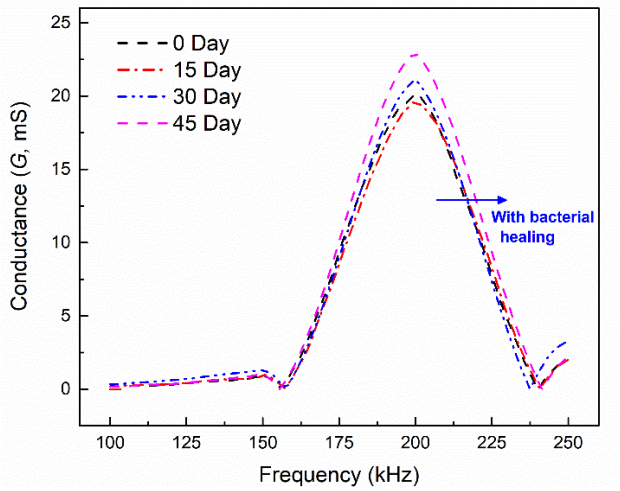

(c)

Figure 5.6: Conductance plot of (a) Control (b) FAA and (c) SFA specimens

It can be noted that in FAA and SFA specimens, with crack sealing, the peak shifts rightwards and at the same time is getting sharper. Soh and Bhalla (2005) reported the shifting of the resonance peak towards the right indicates that the stiffness (strength) of the monitored structure increases with time. It can be noticed from the captured EMI signatures that regain in strength and stiffness due to calcite precipitation was achieved during progressive crack healing. Whereas in the case of control specimen, it can be concluded that up to 45 days,

deviation in the EM signatures were minimal suggesting less crack healing. The calculated statistical indices in control, FAA and SFA specimens are presented in Figure 5.7.

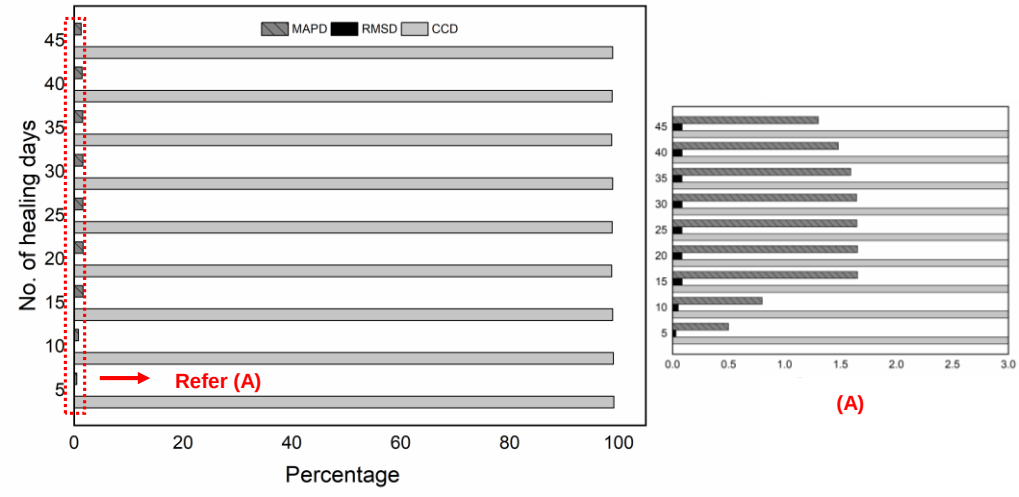

(a)

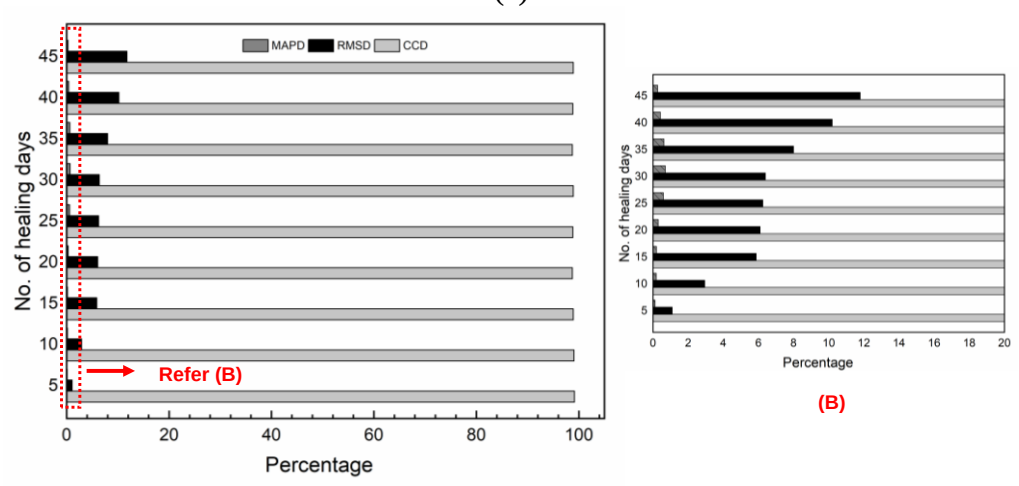

(b)

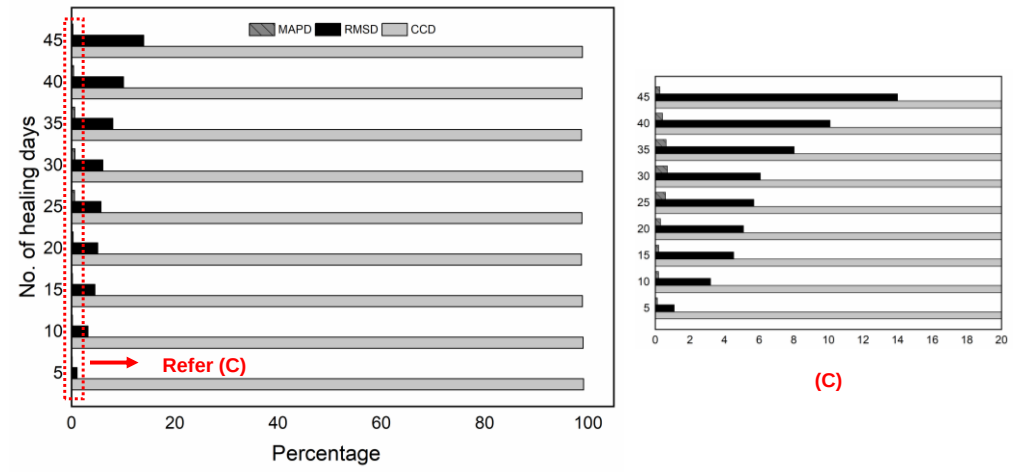

(c)

Figure 5.7: Calculated statistics indices (a) Control (b) FAA (c) SFA specimens

On comparing the values of various indices between control, FAA and SFA specimens, it can be seen that out of the three indicators, MAPD and CCD exhibited less variation and lack of clear trend was recorded by these two statistical indices (Figure 5.7 (b) and (c)). The CCD values remained in the range of 98-99% same for all the specimens; while MAPD was found to be in the range of 0.1% to 1.65% for all tested specimens. On the other hand, RMSD reflected an increasing trend from 1% to 11.8% in FAA and 1% to 14% in SFA specimens with progressive healing with subsequent treatment duration as shown in Figure 5.8.

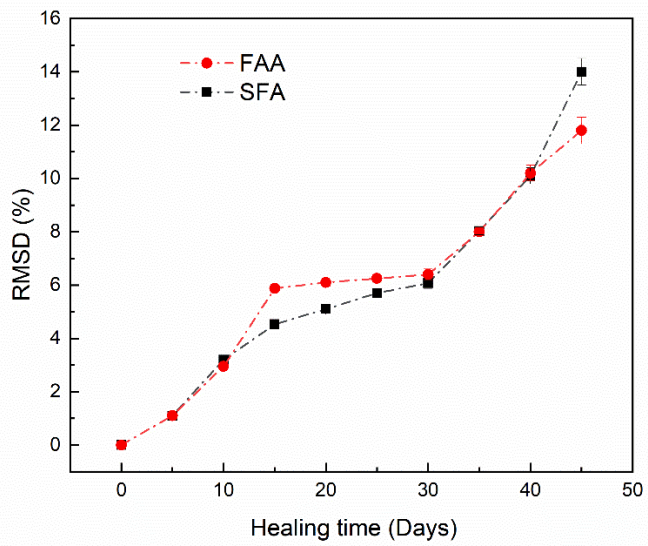

Figure 5.8: Calculated RMSD (%) values for healing days in SFA specimens

The results suggested that RMSD can be a promising parameter in explaining the physical changes that occurred due to the precipitations inside the crack of the SFA specimen. RMSD proved to be a good measure of indicator of healing crack in this study and found to be sensitive to the extracted EM signatures. Therefore, the obtained RMSD values was further used in the study.

In FAA and SFA specimens, the RMSD values increased sharply up to 15 days (from 1 to 6%) of healing treatment which signifies the crack sealing activity in the specimen. This might be attributed to the availability of more nucleation sites i.e. bacteria present in SFA specimen for calcium carbonate precipitation leading to gain in stiffness. The urease activity is majorly

influenced by four different parameters such as pH, dissolved inorganic carbon concentration, calcium concentration and the availability of nucleation sites (Dhami et al. 2013c). It can be noted that the crack was initially healed at the depth, having concrete at the bottom and both sides of the cracks. Later, for the period of 15 to 30 days of healing, RMSD values showed limited improvement in comparison to the initial 15 days of healing treatment. This might be due to the influence of carbonate ion concentration by available bacteria reaching the saturation state (Anbu et al. 2016). Between 30 to 45 days of healing treatment, it can be concluded from Figure 5.3(b) and (c); a rightward shift in EM signature was observed suggesting gain in stiffness in concrete. Continuously media incorporated with 25 mM $CaCl_2$ and 2% urea was provided to pace up the ureolytic reaction by the bacteria inside the crack. High content of precipitated carbonate is visible over the top surface of the crack depicting crack healing over the surface too. The full healing of crack in FAA and SFA was achieved at 45 days of healing treatment. It can be concluded that during the crack healing process of the structure using MICCP, the basic characteristics of the structure such as mass and stiffness changed. Thus, suggesting the formation of additional crystals inside the cracked portion.

5.1.2.3 Relation between crack sealing and RMSD

It can be noted from Figure 5.5 and 5.8 that obtained crack healing ratio and RMSD showed increasing trend during the healing treatment of FAA and SFA specimen. Therefore, crack width reduction can be correlated to the RMSD values obtained from EM signatures of repaired specimens at different healing days. A relation between crack sealing (%) and the RMSD (%) obtained during the healing process was attempted and shown in Figure 5.9. The data set corresponding to 0 to 45 days of healing treatment of FAA and SFA specimens were correlated. The results showed that the crack sealing (%) is directly proportional to RMSD (%) values. In FAA specimen, the level of correlation is good with regression coefficient (R^2) value of 0.91 as shown in Figure 5.9(a). Also, the higher R^2 value indicates the predicted linear equation can

estimate the crack sealing (%) within 95% of the prediction band. The predicted correlation Eq. (5.4) is given below.

$$y = (9.47 \pm 1.11)\, x + (-0.60 \pm 7.9) \tag{5.4}$$

Where, 'y' denotes crack sealing (%) obtained at any day of treatment and 'x' represents the RMSD (%) calculated at any day of healing process. In SFA specimen, the level of correlation was found to be 0.92. Also, the higher R^2 value indicates the predicted quadratic equation can estimate the crack sealing (%) within 95% of the prediction band. The predicted correlation Eq. (5.5) is given below.

$$y = (-0.59 \pm 0.2)x^2 + (16.35 \pm 2.84)x + (-10.4 \pm 8.79) \tag{5.5}$$

Where, y = crack sealing (%) at any day and x = RMSD (%) calculated at any day of the healing process. It can be observed from Figure 5.9(b) that variation of RMSD values (%) lowers down once the crack healing is in 90 to 100%. It indicates that the RMSD values saturate near full crack healing. The proposed correlation can be utilized for the assessment of crack sealing in real RC structures and can be a possible low-cost monitoring solution.

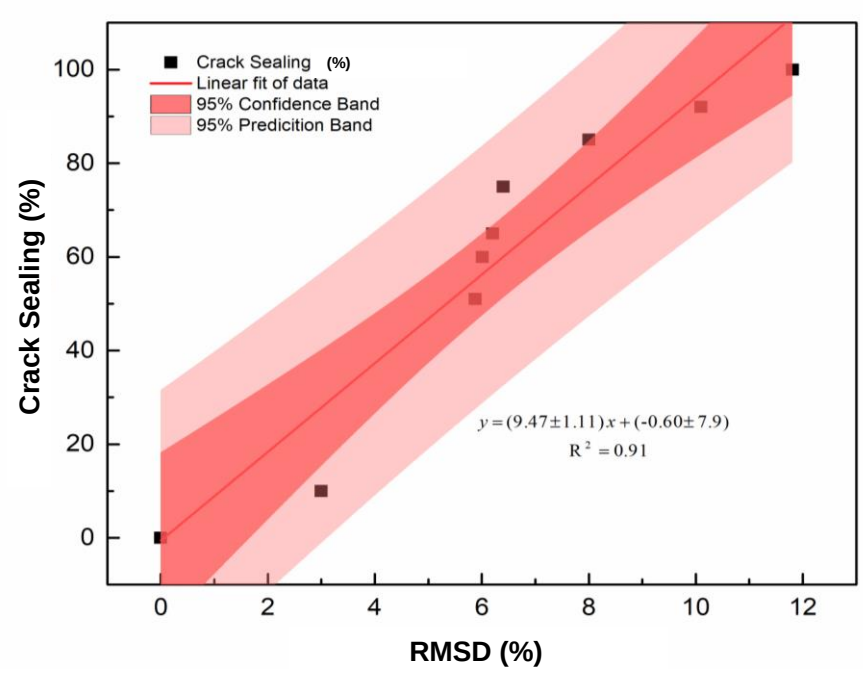

(a)

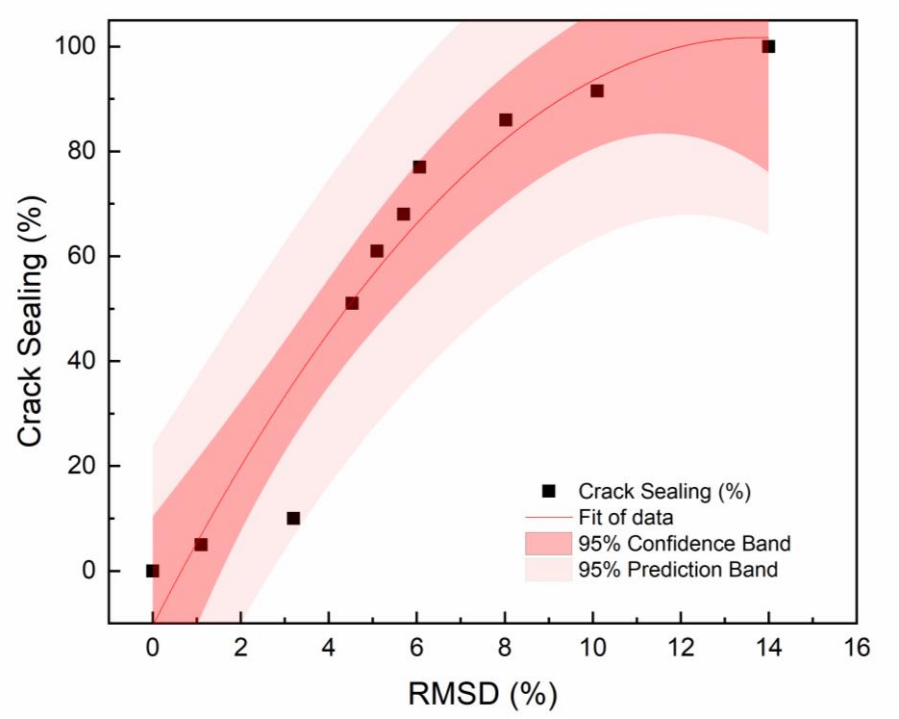

(b)

Figure 5.9: Relation between crack sealing (%) and RMSD (%) (a) FAA (b) SFA specimens

5.1.2.4 Strength regain

The strength regain due to crack healing with FA and SF immobilized cells were evaluated by investigating flexural strength at the end of healing treatment. The results obtained from the flexural strength are shown in Figure 5.10. The flexural strength in treated FAA and SFA specimens were found to be 4.2 and 4.3 MPa. The significant gain in strength (approximately 30%) was achieved in FAA and SFA in comparison to control (3.25 MPa) specimen.

To get the better clarity of strength regain, flexural strength of treated FAA, treated SFA and control specimens were further compared with uncracked control, uncracked FAA specimens and uncracked SFA specimens. The prismatic specimens after bending test in SFA is shown in Figure 5.11. The comparable results in healed bacterial specimens and uncracked bacterial specimens were observed, indicating an effective crack healing and capability of biomineralization precipitates to effectively resist the bending failure.

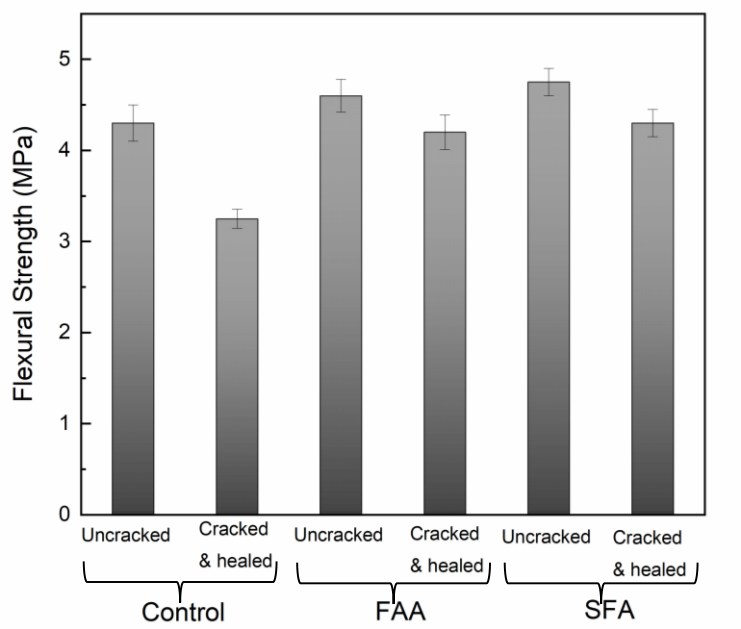

Figure 5.10: Flexural strength of prismatic specimens

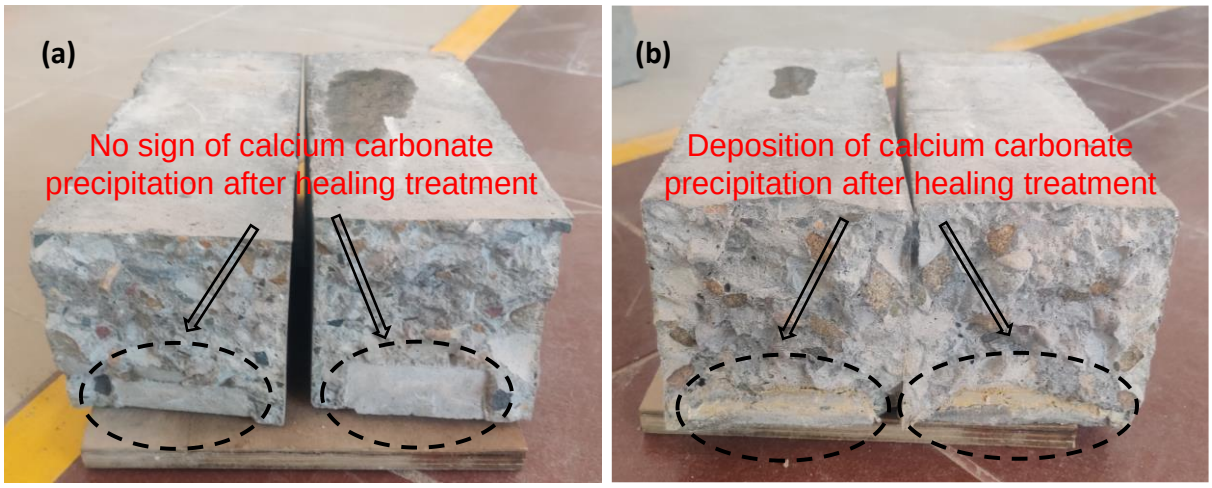

Figure 5.11: Damaged prismatic specimens (a) Healed control (b) Healed SFA specimens

5.1.2.5 Characterization of healing mineral

The healing product precipitated inside the cracks were analysed through TGA, FESEM-EDX and XRD at the end of full healing. The samples were collected from the treated crack surface of the control, FAA and SFA specimen at an upper depth of 10 mm. The TGA results of the specimens are shown in Figure 5.12 and 5.13. The major weight loss appears around 600-800°C, which is linked with the endothermic breakdown of $CaCO_3$ into CaO and CO_2 (Chaurasia et al. 2019; Joshi et al. 2018a). The FAA and SFA specimens exhibited weight loss

of 6.58% and 6.2% associated to decomposition of $CaCO_3$ in the range of 600-800°C; whereas weight loss of 4% was observed in control specimen.

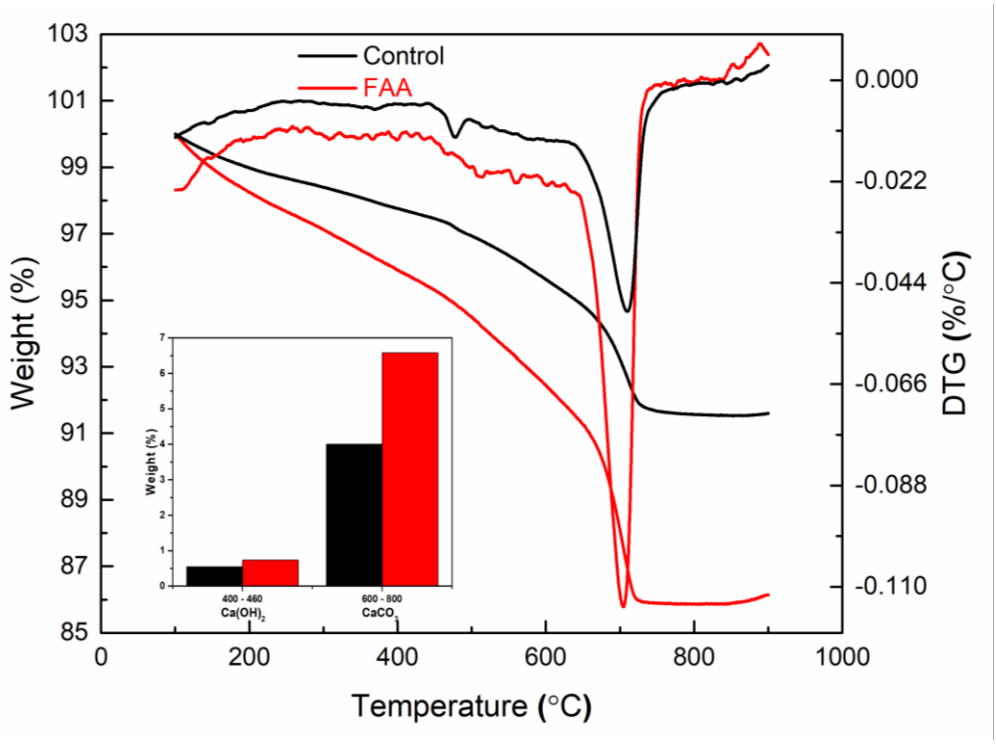

Figure 5.12: TG and DTG graphs of Control and FAA specimens

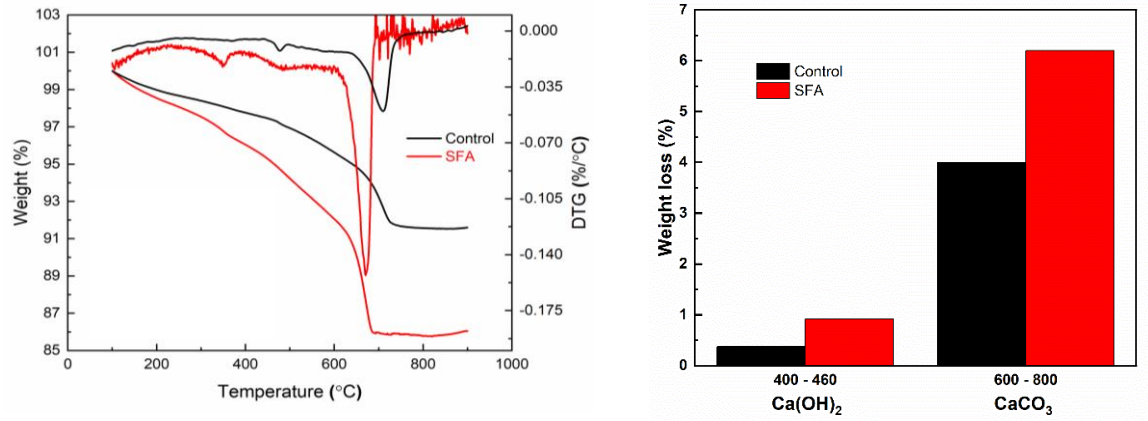

(a) (b)

Figure 5.13: (a) TG and DTG graphs of Control and SFA specimens; (b) Weight loss (%) associated with decomposition of different volatiles in TGA

The second major weight loss occurred between 400-460°C which is related to the decomposition of $Ca(OH)_2$ (Sharma and Goyal 2020). The weight loss of 0.74% and 0.92% associated with $Ca(OH)_2$ was noted in the FAA and SFA specimen while 0.37% was observed

in the control specimen. The results were in agreement with the findings of researchers regarding TGA in bio-based concrete (Amiri and Bundur 2018; Bundur et al. 2017).

The FESEM analysis was conducted to study the precipitation produced at the crack surface. Figure 5.14 and 5.15 shows the FESEM-EDX images of the FAA and SFA specimen. Healed FAA and SFA specimens showed the presence of lamellar rhombohedral crystals of calcium carbonate. This morphology of mineral precipitations was confirmed to be the same as one of those reported by researchers (Wiktor and Jonkers 2011; Zhang et al. 2017). The EDX analysis of SFA specimen confirmed the high amount of calcium. The observed results were in agreement with the effect of bacteria on the microstructural development of concrete reported by researchers (Ersan et al. 2018; Vaezi et al. 2020).

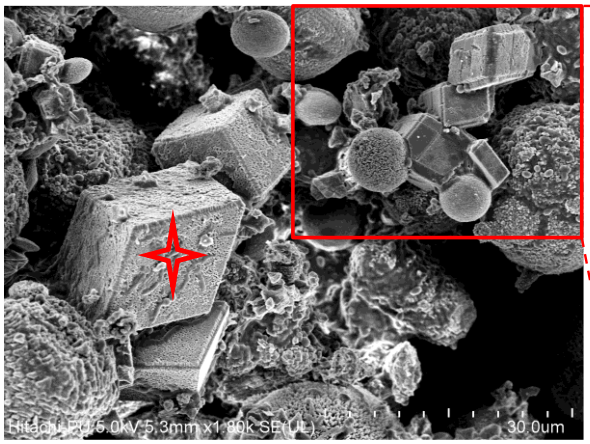

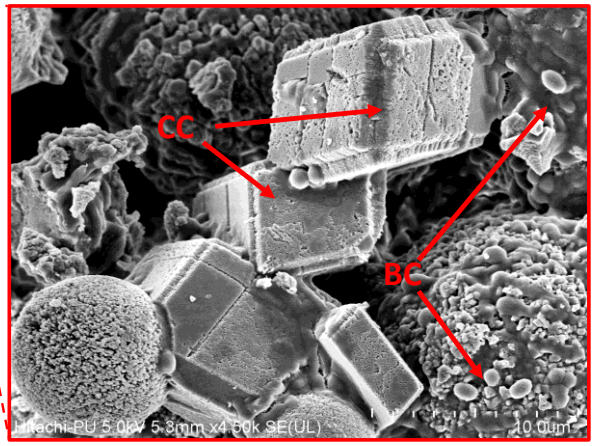

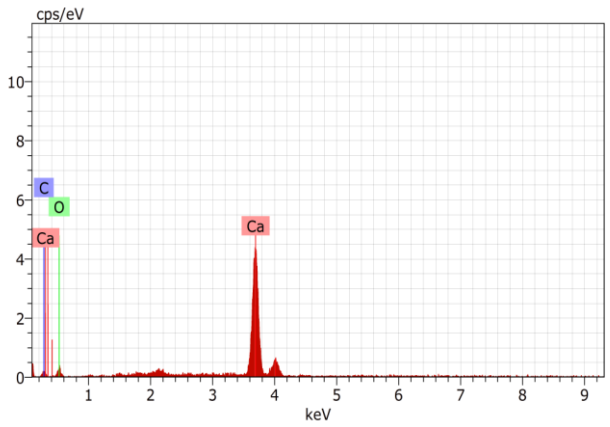

Element	Atomic weight (%)	Weight (%)
Ca	58.51	78.49
O	36.18	19.38
C	5.31	2.13

Figure 5.14: FESEM-EDX images of FAA specimen. Square shows the spot of EDX analysis (BC: Bacterial Cells, CC: Calcium Carbonate)

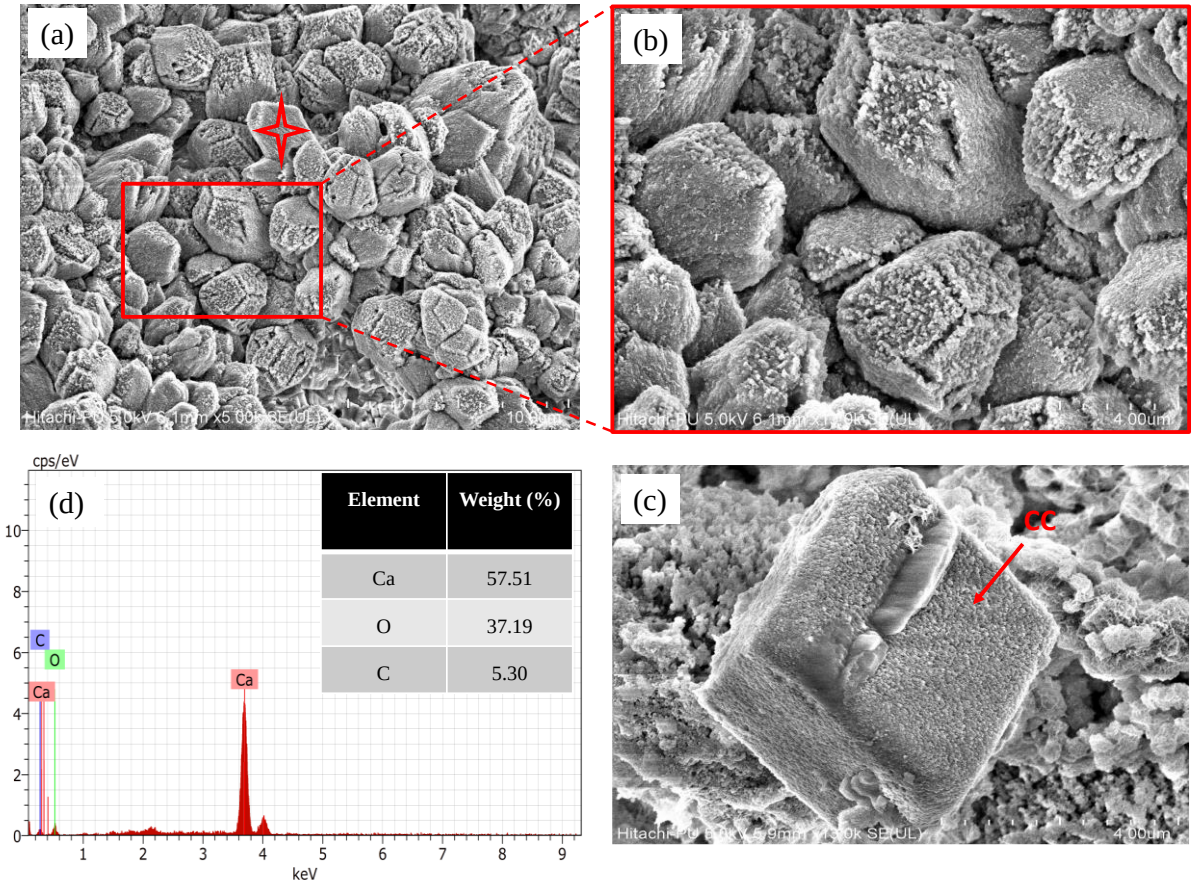

Figure 5.15: FESEM-EDX images of SFA specimen. Star shows the spot of EDX analysis; (CC: Calcium Carbonate)

To study the mineralogy of crystal precipitates, XRD test was performed. For XRD the samples were extracted from the top surface of FAA and SFA and at a depth of 10 mm from the control, FAA and SFA specimens. The results of XRD are shown in Figure 5.16. XRD analysis indicated the precipitates generated on the top surface of crack of FAA specimens at 45 days of the treatment is calcite ($CaCO_3$) (Figure 5.16 (a)). Similar results were observed in sample in SFA sample. Therefore, XRD analysis of only FAA is shown here. Moreover, it can be observed from XRD analysis (Figure 5.16 (b)), the high-intensity peak occurred at $2\theta = 29.2°$ in FAA and SFA specimen in comparison to control which approves that the precipitation generated in the cracks is calcium carbonate. This observation is consistent with the finding of other researchers (Chaerun et al. 2020; Kalhori and Bagherpour 2017). Overall, it can be concluded the MICCP is responsible for filling the cracks.

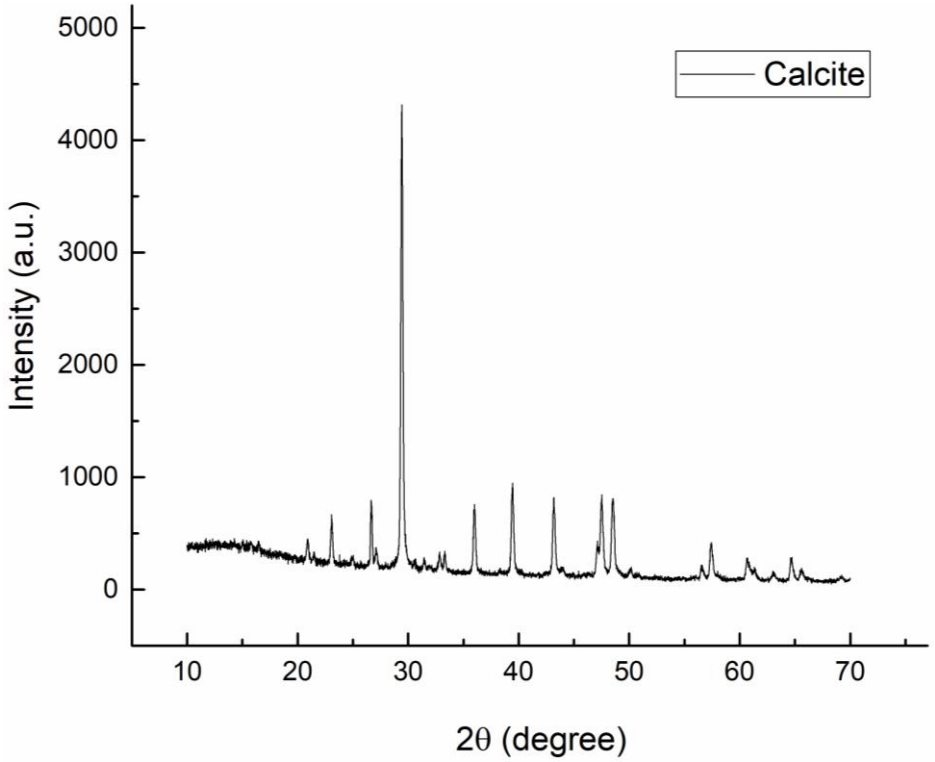

(a)

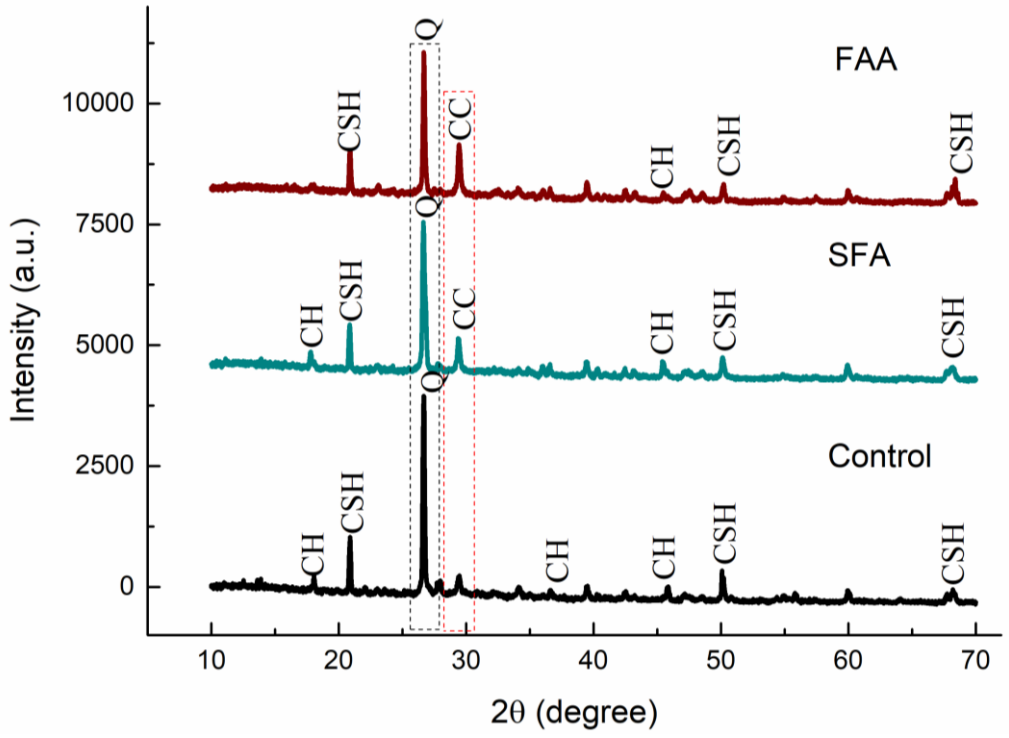

(b)

Figure 5.16: XRD of specimen (a) Sample collected from top surface from FAA (b) At a depth of 10 mm from top surface; (CSH: Calcium silicate hydrate, CH: Calcium hydroxide, CC: Calcium carbonate and Q: Quartz)

5.2 PREPARATION OF BIO-INSPIRED CEMENTITIOUS GROUT

This study targets the developing efficient bio cementitious grout to repair existing cracks in concrete structure. In the current investigation, FA and SF based inoculums of shelf life 180 days at 4°C of effective cell count was used to develop bio-inspired cementitious grouts to repair existing damages in concrete structures. Various bio-inspired grouts were prepared and tested for flowability, mini-slump and bleeding. Selected bio-inspired grouts based on fresh properties were further tested for setting time, mechanical strength and drying shrinkage. The best bio-inspired grout was selected to repair cracks in the horizontal, vertical and inverted orientation of concrete.

5.2.1 Material and methods

This section discusses the detailed properties of materials used for the preparation of grout mixes and methods for testing.

5.2.1.1 Mineral carrier-based inoculums

The mineral carrier-based inoculums made by FA or SF were used to prepare mixes. The detailed procedure for preparing these inoculums is reported in chapter 3. The inoculums were stored at 4°C for 180 days, and the viability studies reported in chapter 3 confirmed that these inoculums possessed sufficient cell counts to induce MICCP even after 180 days.

5.2.1.2 Constituents of grout

Ordinary portland cement (OPC) (43 grade) (IS 8112 2013) was utilized for preparing the grout mixture. Many researchers reported the use of fine sand with particle size ranging between 75-600µm to prepare efficient cement grout (Shannag 2002; Vasumithran et al. 2020). The present study used fine sand of less than 600µm to develop stable grout.

5.2.1.3 Preparation of bio-inspired cementitious grout

Bio-inspired cementitious grout was prepared to remediate cracks in artificially cracked concrete specimens to mimic fractures in existing concrete structures. Initially, the control grout (referred as CW) was prepared using cement and fine sand in proportion of 70:30, by weight. The water (w)/cement (c) ratio of (0.5) was used to prepare the control grout. To develop bio-inspired cementitious grout, cement was substituted with FA and SF based inoculum separately by weight, the proportions systemically varied from 10%, 15% and 20%. Further, growth media supplemented with nutrient broth (1.3% weight (w)/volume (v)), urea (2% w/v) and 25mM $CaCl_2$ was used instead of water during the preparation of both the bio-based grouts. Also, to study the effect of only growth media along with urea and $CaCl_2$ in the absence of bacteria, another grout was prepared using growth media instead of water and the grout was designated as CM. The detailed mix proportion for the prepared grouts and the corresponding nomenclature is given in Table 5.2.

Table 5.2: Mix proportion details of all grout mixtures

Nomenclature	**Mix proportion (FA/SF based inoculum: Cement: Sand)**	**Water (or growth media)/cement ratio**
CW	0:70:30	0.5[#]
CM	0:70:30	0.5*
BFA10	10:60:30	0.5*
BFA15	15:55:30	0.5*
BFA20	20:40:30	0.5*
SFA10	10:60:30	0.5*
SFA15	15:55:30	0.5*
SFA20	20:40:30	0.5*

[#] Water was used for preparing control grout

*Growth media has used instead of water and has following composition: Nutrient broth (1.3% w/v), Urea (2% w/v) and 25mM $CaCl_2$.

For preparation of cementitious grout, a Hobart-type laboratory mixer (AIMIL India) was used to mix constituents of grout. A standard procedure was followed in which sand, cement and

mineral inoculum were mixed for 1 minute at a speed of 140 rpm. After that water (or growth medium) was added in the dry cementitious mix and operated at same speed of 140 rpm for 1 minute. Then the rotational speed was increased for the next 30 seconds. The mixer was stopped for 90 seconds and the cementitious grout was hand-mixed properly. Further, the mixer was operated at high speed (285 ± 5 rpm) for the last 1 min to obtain final grout slurry. The detailed standard procedure of mixing is reported in (Joshi et al. 2021).

5.2.1.4 Fresh properties of grout

High early strength and sufficient workability are vital requirements to design effective cementitious grout (Shu et al. 2022). Therefore, investigation of fresh properties for optimizing efficient grout is required. The fresh properties include marsh flow time, mini-slump, bleeding and setting time. The outline of various parameters tested for fresh grout is shown in Figure 5.17.

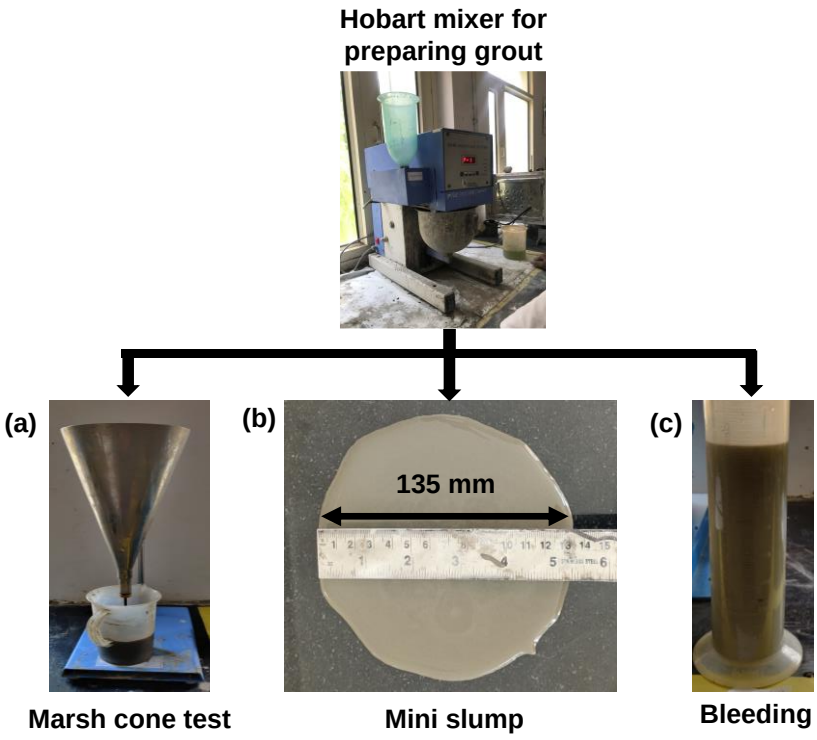

Figure 5.17: Outline of tests conducted for the fresh properties of cementitious grout (a) Marsh cone flow time (b) Mini slump (c) Bleeding

The flow time of all the prepared grout mixes were studied as per ASTM:C939 (2010). Initially, the marsh cone apparatus was placed on the leveled surface along with a measuring container. The bottom orifice was closed and a prepared slurry of 1000 ml was poured inside the marsh cone. The time required to accumulate 800 ml of grout slurry in measuring jar was recorded and it was termed as flow time.

The mini-slump was noted on the cone having a bottom diameter as 38.1 mm, upper diameter as 19 mm and vertical height of 57 mm (Kantro 1980). The grout slurry was poured inside the mini cone and gently stirred to remove the air bubbles. The mini cone was then lifted slowly and the spread diameter in orthogonal directions was measured.

The bleeding test was performed as per guidelines of ASTM:C940 (2010). The grout slurry (800ml) was poured inside the measuring cylinder and was left undisturbed. After 180 mins, the volume of water gathered on the top surface was collected in the separate cylinder. The bleed water volume was noted and the total volume percentage change was calculated.

5.2.1.5 Hardened properties of grout mixtures

The selected grouts based on the fresh properties were further tested for setting time and hardened properties of grouts. The initial and final setting of all the prepared grouts were studied as per ASTM:C953 (2010). The grout slurry was poured in vicat apparatus to assess the setting times of all grouts. The initial and final setting time starts immediately after adding water to the grout mix.

50 mm cubical specimens were cast as per ASTM C109 for compressive strength measurement of grout (ASTM C109/C109M-20 2020). Prismatic specimens of 160×40×40 mm were cast for flexural strength and drying shrinkage as per ASTM standards (ASTM:C348 2020; ASTM C 157 2014). For flexural strength, three-point bending test was conducted on the prismatic specimens using flexural testing machine.

For testing the drying shrinkage of selected grouts, prismatic specimens upon removal from molds after casting, were immersed in lime-saturated solution (having pH=12.4) for 15 minutes. The specimens were taken out and immediately initial reading was taken in length comparator as per ASTM C 157 (2014). After this, specimens were dipped in lime saturated water for 28 days for curing. The specimens were then air dried and shrinkage was noted at 3, 7, 14 and 28 days using length comparometer. The average of the three shrinkage readings (expressed as microstrains) was taken at different testing age for selected grout. All the strength tests were performed in triplicate at each testing durations and the average of three specimens was taken as the strength of the cementitious grout.

5.2.2 Results and discussion

Marsh cone flow time and Mini-Slump

These tests were performed to study the effect of addition of FA and SF based inoculum on the fluidity of prepared cementitious grout.

Figure 5.18 shows the flow time and mini slump results for various grout mixes prepared in the study. It can be observed that with the inclusion of FA and SF based inoculum, marsh cone flow time reduces. The flow time was found to be 120 seconds in CW grout mix; where as in case of BFA10, BFA15, BFA20, BSF10, BSF15 and BSF20, the flow time was recorded to be 98, 92, 86, 97, 91 and 87 seconds, respectively. The fluidity and mini-slump of any cementitious grout is dependent on the type of filler used and percentage of cement substitution (Vasumithran et al. 2020). Substitution of cement with 20% FA and SF based inoculum showed the highest mini-slump diameter reflecting more workability of grout. Grout mixes prepared with growth media comprising of NB, urea and $CaCl_2$ in the absence of bacteria (CM) instead of water also showed higher fluidity in comparison to grout prepared with tap water. Similar findings was noted by other researchers (Joshi et al. 2021).

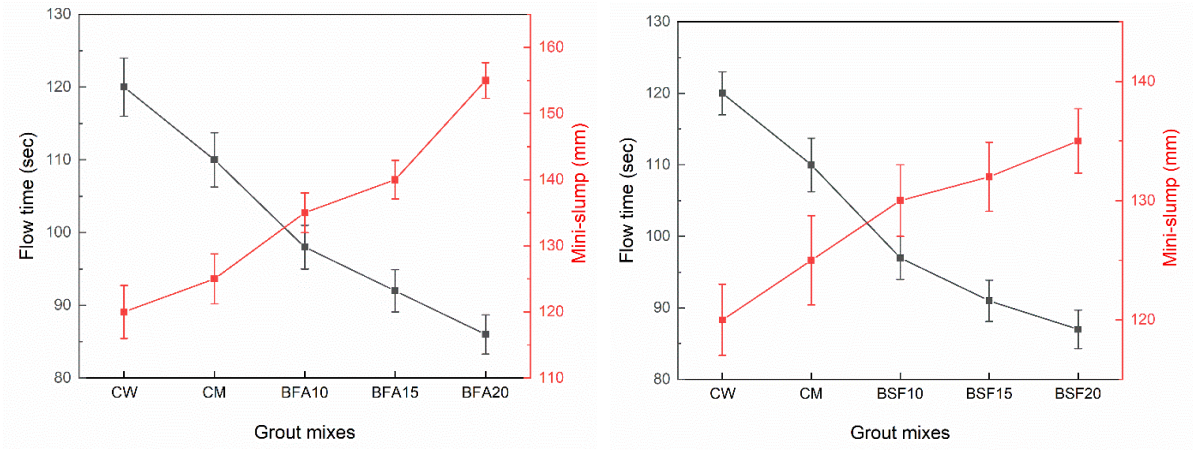

(a) (b)

Figure 5.18: Influence of (a) FA (b) SF based inoculum on flow time (seconds) and mini-slump (mm) of prepared grout mixes

In case of mini-slump test, it can be noted that with the incorporation of FA and SF based inoculum supplemented with growth media, the spreading ability of grout increased in respect to CW and CM. The mini-slump in BFA10, BFA15, BFA20, BSF10, BSF15 and BSF20 was found to be 135 mm, 140 mm, 155 mm, 130 mm, 132 mm and 135 mm. The spreading ability was recorded to be higher in all BFA grout mixes than BSF grouts. This is due to the ball effects of FA, which enhanced the fluidity attributes of the resultant grout (Sha et al. 2018). The mini-slump diameter of CW was found to be 120 mm where as in CM diameter was observed to be 125 mm. The use of growth media supplemented with nutrients instead of tap water increased the spreading ability of the resultant grout (CM). Initially it was expected that due to high viscosity of growth media supplemented with nutrients, a decrease in mini-slump could be observed. This is due to presence of organic matter which offers high fluidity by decreasing yield stress. Similar observation of increasing fluidity with the addition of organic matter was reported by other researchers (Beddaa et al. 2019; Uchikawa et al. 1997).

Bleeding

Bleeding is an important characteristic of efficient and stable grout for remediation of concrete structures. Excessive bleeding may weaken the cement grout which ultimately affects the

strength and durability of the grout (Sowmini and Anand 2018). The percentage water bleeding results of all grout mixes after 180 mins of sedimentation is shown in Figure 5.19.

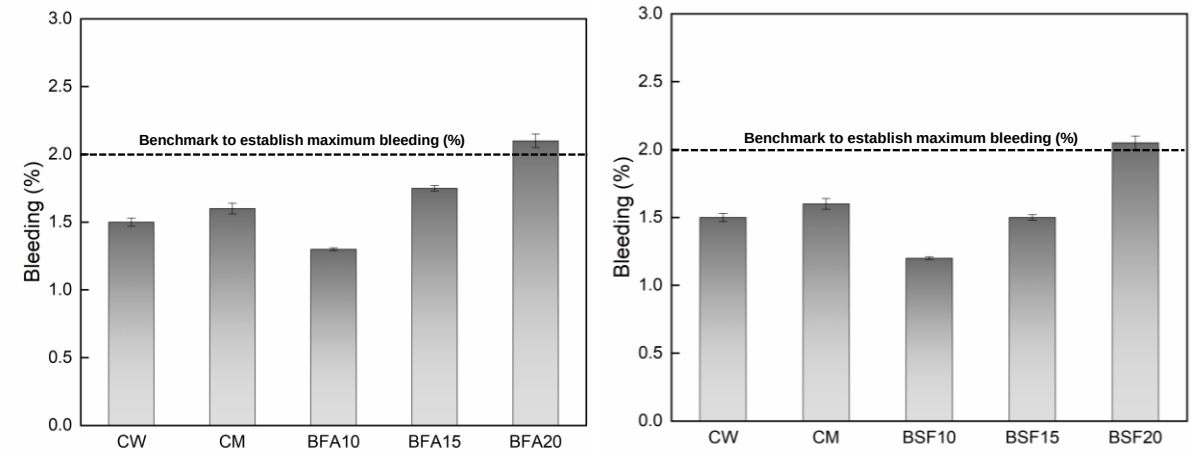

(a) (b)

Figure 5.19: Bleeding (%) results noted in grout mixes prepared using (a) FA based inoculum (b) SF based inoculum

The percentage bleed was found to be in the range of 1% to 2% for all grout mixes except BFA20 and BSF20. The higher value of bleed was noted in BFA20 and BSF20 mixes in comparison to other FA and SF based inoculum incorporated bio-grouts. The presence of additional optimum moisture in FA and SF inoculum could be responsible for the excessive bleeding. As per ASTM guidelines, allowable bleeding of 2% is recommended for a stable grout (ASTM:C940 2010). The BFA20 and BSF20 grout mixes did not conform to above guideline, therefore BFA20 and BSF20 were eliminated from the further study. However in case of BFA10, BFA15, BSF10 and BSF15 lesser bleeding can be attributed to denser pore structure and enhanced packing density (Shannag 2002). Previous studies reported the use of natural pozzolan for preparation of highly durable cementitious grouts (Sha and Liu 2021).

Setting time

Initial setting time (IST) and final setting time (FST) of the selected grouts are shown in Figure 5.20. IST and FST of all the selected grout mixes were in the range of 4 to 5 hours and 7 to 9

hours, respectively. ASTM standard recommends IST of at least 4 hours and FST of maximum 24 hours for a stable cementitious grout (ASTM:C937 2016). All the selected grouts mixes performed satisfactorily as their initial and final setting times are within the acceptable limits.

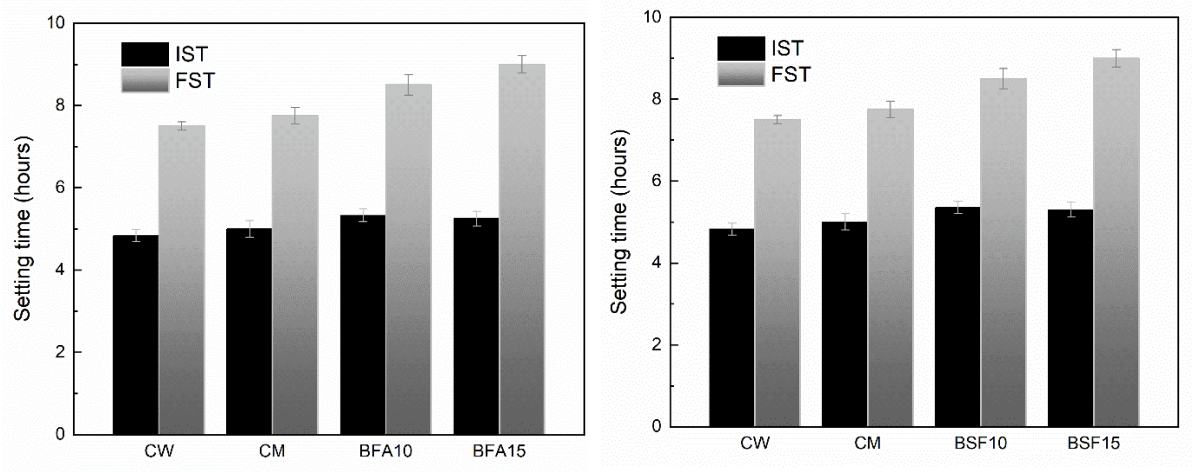

(a) (b)

Figure 5.20: Setting time of selected grout mixes (a) FA based (b) SF based inoculums

Compressive and flexural strength of grouts

The compressive and flexural strength test results of the selected grouts obtained at 7 and 28 days of testing are shown in Figures 5.21 and 5.22. The compressive and flexural strength of CW was found to be 21 MPa and 2.9 MPa respectively, at 7 days of testing. The test results of CM indicated lower mechanical strength at 7 days testing. This may be attributed to inadequate hydration of cementitious material due to the presence of organic matter, urea and calcium chloride. Researchers reported the lower compressive strength due to the presence of organic matter and other nutrients in the absence of bacteria (Ersan et al. 2015; Joshi et al. 2018a). The bacterial admixed grout specimens registered a considerable increase in mechanical strength at both testing durations compared to CW specimens. Among all the prepared specimens, BFA15 observed 15% higher compressive strength at 28 days than CW; where as BSF15 observed 25% higher compressive strength at 28 days than CW as shown in Figure 5.21 (a). Similar

findings of improvement in compressive strength was observed in BSF10 and BSF20 at 28 days of testing in comparison to CW as shown in Figure 5.21 (b). The approximate improvement of 8% was noticed in the flexural strength at 28 days in BFA10 and BFA15 than CW specimens as shown in Figure 5.22 (a). Similar findings were observed in the flexural strength results at 7 and 28 days in SF immobilized cell cementitious grout as shown in Figure 5.22 (b). Other major obervation was noted among BFA10 and BFA15. The BFA15 showed higher strength at both testing duration in comparison to BFA10. Similar findings noted in higher strength in BSF15 was recorded than BSF10 mixes.

The high dosage of FA and SF based inoculums are responsible for higher strength compared to the BFA10 and BSF10. The addition of bacteria in the presence of nutrients is accountable for the deposition of $CaCO_3$ in the pores of grout specimens (Tripathi et al. 2019). This biogenic deposition help in densification of the pores in the bio-grout. The FA and SF based inoculums were admixed during the preparation of grout; this suggests the uniform precipitation of $CaCO_3$, hence densifying cement matrix.

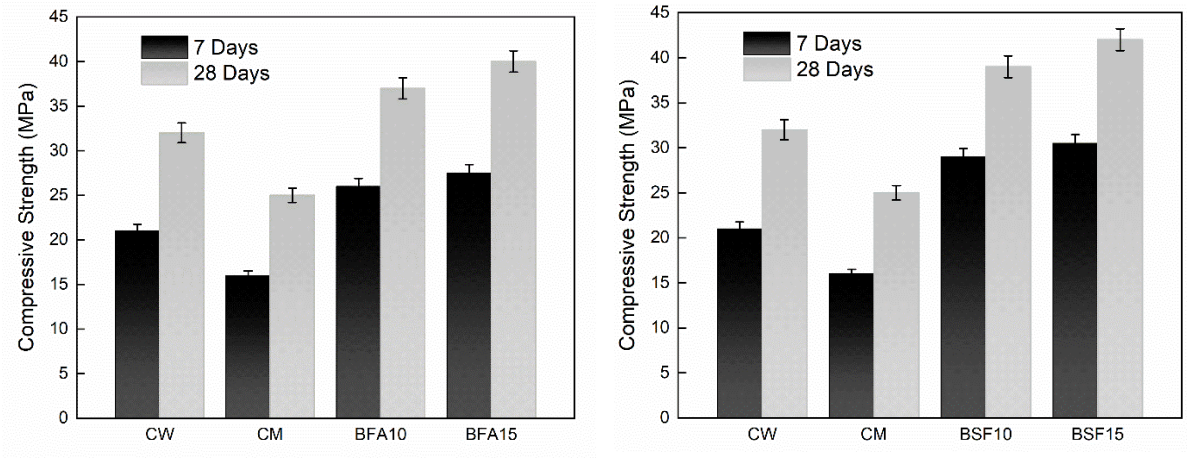

(a) (b)

Figure 5.21: Compressive strength of selected cementitious containing (a) FA based (b) SF based inoculums grouts at 7 and 28 days

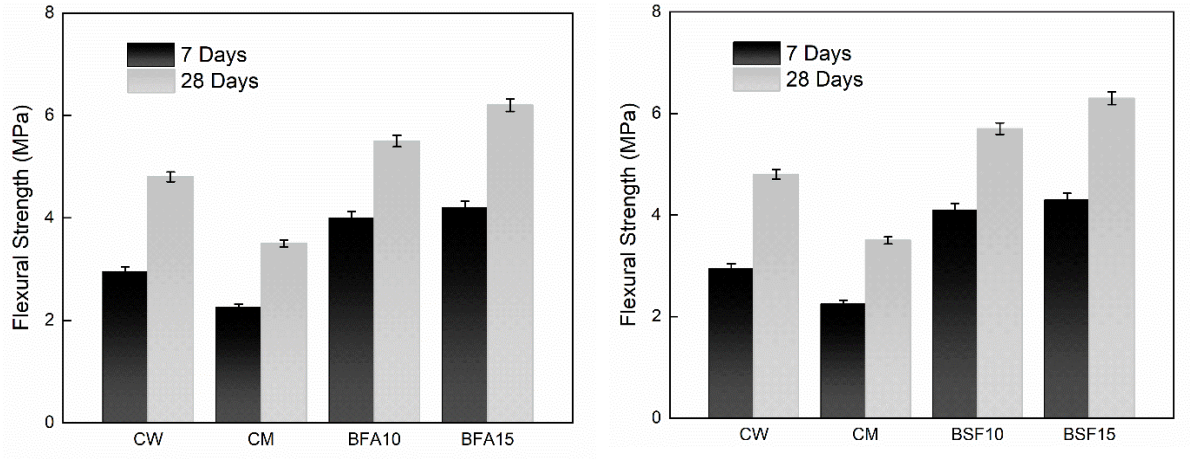

(a) (b)

Figure 5.22: Flexural strength of selected cementitious containing (a) FA based (b) SF based inoculums grouts at 7 and 28 days

Drying shrinkage

Shrinkage is a crucial aspect mostly encountered in cement-based grout due to moisture loss in dry environments, which further leads to lower bonding strength and reopening of repaired cracks (Li et al. 2017). Figure 5.23 shows drying shrinkage results of all the selected grouts at different testing durations.

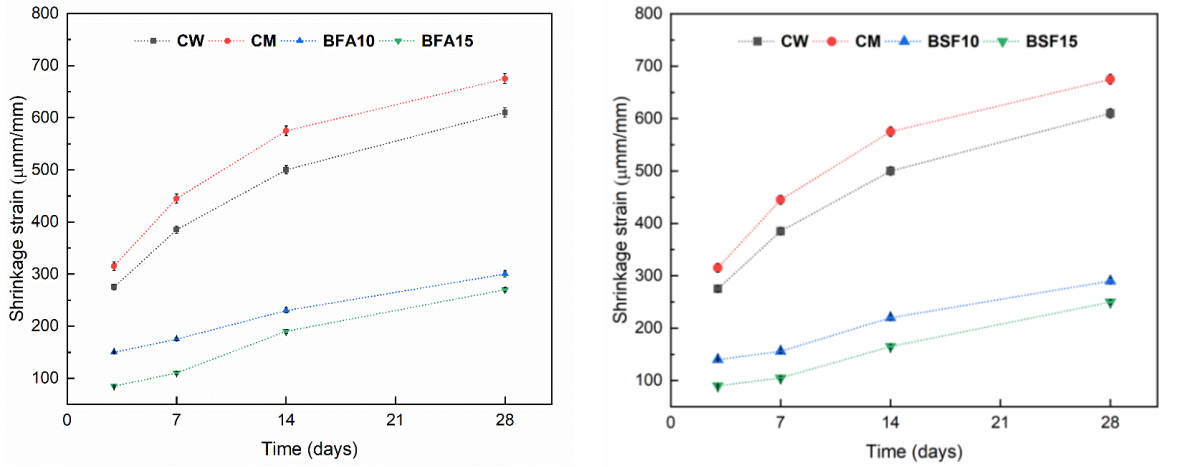

(a) (b)

Figure 5.23: Shrinkage strain of selected grout (a) FA based (b) SF based inoculums at different testing age

It can be noted that CM has the highest drying shrinkage among all the grout mixes. It indicates that the organic matter and other supplementary nutrients in the absence of bacteria have

retarding effect on the chemical setting of cementitious material (Ersan et al. 2015). The higher shrinkage in CM can be attributed to the presence of nutrient broth (1.3% w/v), urea (2% w/v) and 25mM $CaCl_2$. CW also showed higher shrinkage in comparison to BFA10 and BFA 15 specimens. It is known fact that higher shrinkage is associated with OPC grouts (Atiş et al. 2004). Drying shrinkage reduces as the amount of cement decreases for a unit volume of a mixture. With the incorporation of FA and SF based inoculums in the cementitious grout, remarkable reduction in drying shrinkage was noted at all testing age.

The synergetic effect of FA and SF and activity of bacteria by MICCP could be responsible for the reduction in drying shrinkage. Both BFA10 and BFA15 showed lower drying shrinkage than CW and CM. BFA15 showed lowest shrinakge among all the tested grout mixtures. Similar findings were observed in BSF10 and BSF 15 grout mixtures. Higher micro filler mineral inoculum present in BFA15 and BSF15 are accountable for the lowest drying shrinkage. The results obtained in this study are in agreement with other studies incorporating micronized supplementary cementitious materials to refine the cement grout (Sha and Liu 2021; Zhang et al. 2019).

5.3 APPLICATION OF BIO-GROUTS FOR REPAIR OF CRACKS

Based upon the obtained test results in the previous section, BFA15 and BSF15 cementitious grout mixed were used to repair existing cracks in the concrete structures. In this study, an artifical crack of approximately 1.0 mm was created during the preparation of prismatic concrete specimens using steel plate and cured using tap water for 28 days.

5.3.1 Material and methods

This section discusses the detailed properties of materials used for the preparation of concrete mixes and methods for testing.

5.3.1.1 Constituents of concrete

Commercially available ordinary portland cement (43 grade) (IS 8112 2013), locally available river sand and coarse aggregates *conforming to standards (IS:383 2016)* were used for preparing concrete specimens. The detailed specifications of all the constituents used in the present investigation are provided in section 3.3.1.

5.3.1.2 Preparation of concrete specimens with artificial crack

The cracked prismatic specimens of 500 mm × 100 mm ×100 mm and cylindrical disc of 100 mm (dia) × 50 mm (height) were cast using cement: fine aggregate: coarse aggregate in the proportion of 1: 1.82: 3.24 and water/cement of 0.47. The artificial cracks were created in both prismatic and cylindrical specimens at the time of casting by embedding a metal plate of 60 mm length, 20 mm depth and 1.0 mm thickness. The metal plate was taken out after 3 hours from casting. The crack width of 1.0 mm was selected based on the damages occurred because of variable environmental and loading conditions during service life in concrete structures. The specimens were demoulded after 24 hours and water cured for 28 days.

5.3.1.3 Instrumentation of PZT

A PZT patch (PIC 151) of size 10×10×0.3 mm was bonded on cracked prismatic concrete specimen using an adhesive mix (epoxy). The PZT patch was instrumented at a distance of 30mm from the crack surface. The detailed specification of PIC 151 and the procedure of soldering coaxial wires for creating connection to an impedance analyser (E4980 AI Keysight) is discussed in section 5.1.1.4.

5.3.1.4 Crack repair using grouting

After 28 days of water curing of cracked concrete specimens, the specimens were taken out and dried for 6 hours. The specimens were divided into three sets, to create three different

orientations of crack. The first set of specimens were placed in such a way that the crack orientation is horizontal, the second set represented vertical orientation of crack and the third set was supported such that the crack was in the inverted orientation. The detailed representations of varying orientations are shown in Figure 5.24. Further, in each orientation, the sets were repaired using either control (CW) grout or best performing bio-inspired grouts (BFA15 and BSF15). All the tests were performed in triplicate and nine specimens were tested for each orientation. The prismatic specimens were used for studying improvement in flexural strength after bio-grouting procedure; while cylindrical specimens were used for measuring permeation properties of concrete. Along with this, prismatic specimens were used for continuous monitoring using EMI technique. Injection based technique was adopted for remediation of cracks using CW and bio-inspired cementitious grouts. After repairing, all the bio-inspired cementitious grouts were to be supplied with growth media comprising of nutrient broth (1.3% w/v), urea (2% w/v) and 25mM $CaCl_2$. For supplying the growth media in the set having crack in the horizontal orientation, a small pond was created around the crack with the acrylic frame and the pond was filled with the growth media. For each specimen 50 ml growth media was prepared and poured once a day. In the second set, having cracks in vertical orientation, the growth media supplemented with nutrients was supplied by spray treatment twice a day for 28 days. In the third set, the same growth media and curing procedure was adopted as mentioned in second set. The challenge of growth media retention on the inverted surface was observed in the initial days. Therefore, a foam was mounted below the repaired surface so as to have retention of the growth media for longer duration. Additionally, one set of cracked prismatic and cylindrical specimens was repaired using CW grout in all three orientations. In horizontal orientation, water was ponded around the repaired surface whereas in vertical and inverted orientation cracks, water spray twice a day for 28 days was adopted to cure the repaired surface.

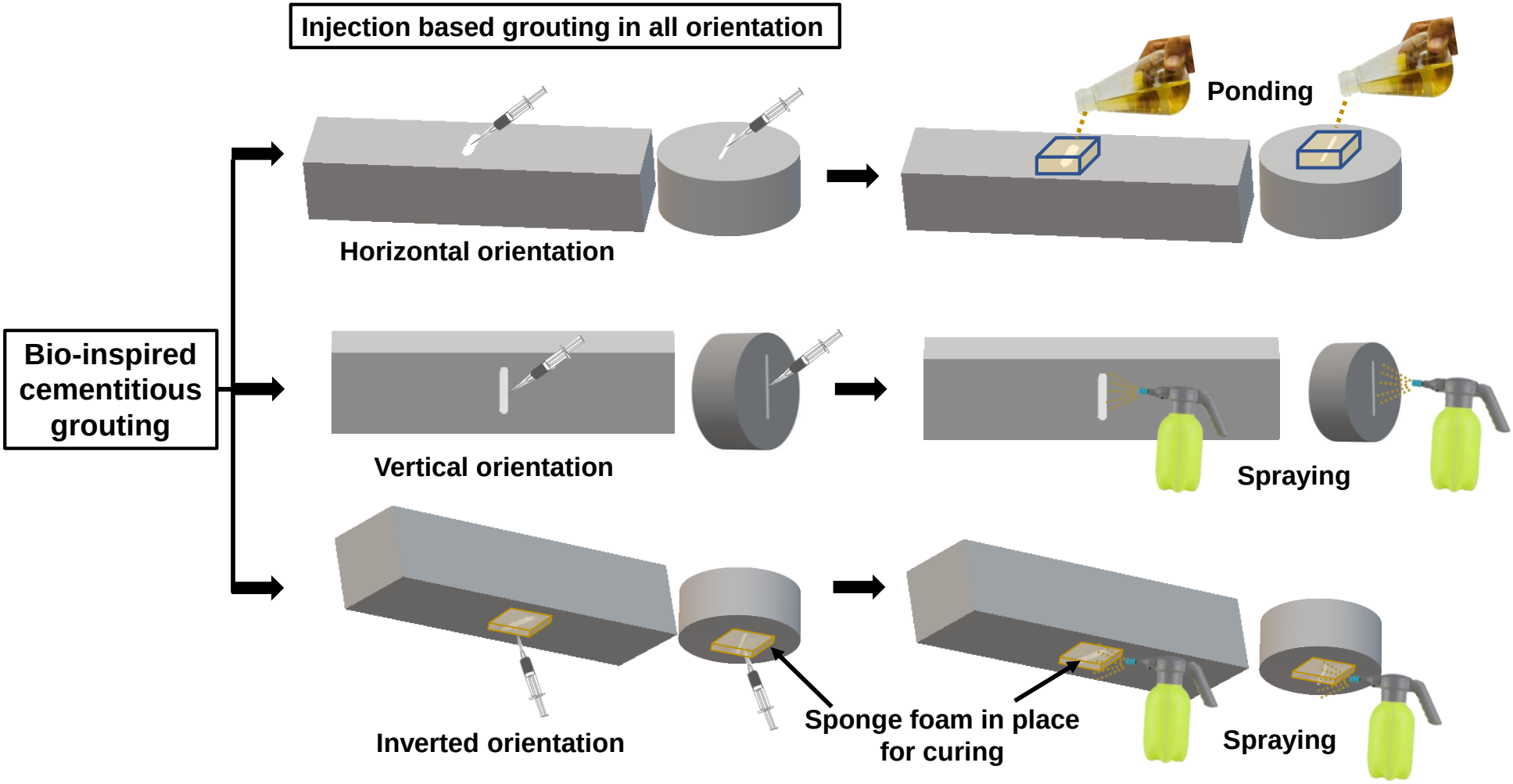

Figure 5.24: Schematic representation of repair of cracks with injectable bio-inspired grout and curing with growth media supplemented with nutrients

Details of all the sets along with their nomenclature is outlined in Table 5.3. Moreover, to assess the improvement in strength and permeation characteristics by bio-inspired and CW grout on concrete structures, the values were compared with the corresponding uncracked prismatic and cylindrical specimens.

Table 5.3: Outline of various sets of concrete specimens and curing treatment

Specimens	**Nomenclature**	**Grouting mix**	**Curing regime**
Reference	REF	-	-
Untreated Crack	UT	-	-
Treated horizontal crack	HCW	CW	Water ponding
Treated vertical crack	VCW	CW	Water spraying
Treated inverted crack	ICW	CW	Water spraying
FA bio-treated horizontal crack	HBFA	BFA15*	Growth media ponding#
FA bio-treated vertical crack	VBFA	BFA15*	Growth media spraying#
FA bio-treated inverted crack	IBFA	BFA15*	Growth media spraying#
SF bio-treated horizontal crack	HBSF	BSF15*	Growth media ponding#
SF bio-treated vertical crack	VBSF	BSF15*	Growth media spraying#
SF bio-treated inverted crack	IBSF	BSF15*	Growth media spraying#

*Bio-inspired grout selected based on fresh and hardened properties

#Growth media comprising of nutrient broth (1.3% w/v), urea (2% w/v) and 25mM $CaCl_2$

5.3.1.5 EMI monitoring of repaired crack surface

The MICCP process was monitored continuously by extracting the EMI signatures at an interval of seven days. The frequency range of 100 kHz to 250 kHz was selected for capturing the EMI signatures. The experimental setup for acquiring EMI signatures is shown in Figure 5.25. In the present study, the changes in real part of admittance were observed and was correlated with the healing process. RMSD, MAPD and CCD are statistical parameters to describing the physical changes happened due to the MICCP activity inside the crack. It was noted from section 5.1.2.2 that RMSD is most promising parameter to study the deviation in

the admittance signature acquired during the curing treatment. Therefore, RMSD was adopted only in this study and is calculated by using Eq. (4.1).

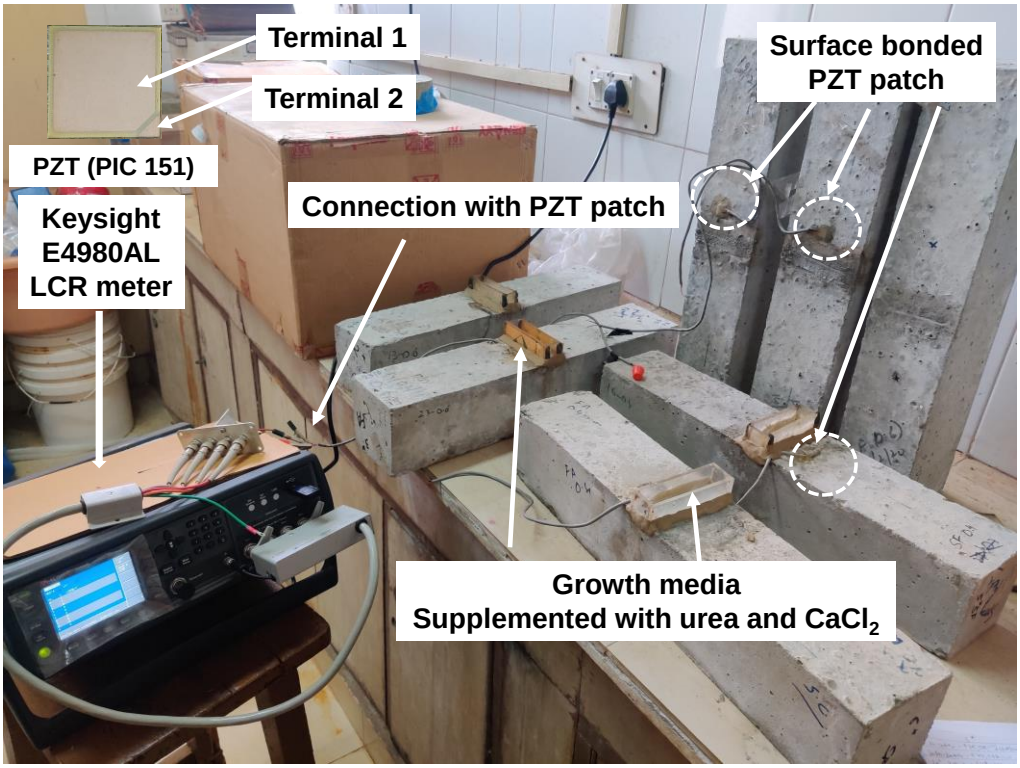

Figure 5.25: Experimental setup for acquiring EM signatures

5.3.1.6 Water tightness

The effectiveness of bacterial grouting procedure in resisting water ingress into concrete was conducted on 100 (dia) × 50 (height) cylindrical specimens after the complete bio-treatment of 28 days. The test was conducted as per (ASTM C1585 2020). In order to ensure that the water ingress takes place only through the repaired surface, epoxy sealant was applied on the top surface leaving only 80 mm × 20 mm area around the crack uncovered. The similar procedure of covering the adjacent area with epoxy was adopted by other researchers (Joshi et al. 2021). The water absorption was determined by dividing change in mass by area of test specimen and density of water. Since the water ingress was allowed only through repaired area, the test area of (80 mm × 20 mm) was used for calculating water absorption by the treated surface. The reading of mass change at different intervals was taken as per ASTM C1585 (2020).

5.3.1.7 Regain in flexural strength in concrete

The repaired specimens were subjected to four point bending after the completion of healing process to assess the strength gain due to MICCP. REF, HCW and UT prismatic specimens were also tested for the flexural strength in order to compare the flexural strength recovery. The test was conducted on flexural testing machine (AIMIL India Ltd, New Delhi) as per BIS 516 (1959) as discussed in 5.1.1.6.

5.3.1.8 Microstructural analysis

To examine the mineral product formed during the microbial activity of microbes, FESEM-EDX and XRD were performed at the end of healing procedure of 28 days. For FESEM-EDX, the grout samples were taken from depth of 10-20 mm of repaired prismatic specimens after subjecting to bending failure. The sample was collected at a depth of 10-20 mm to assess presence of calcium carbonate precipitation inside the repaired crack. For XRD, the collected grout samples were powdered and sieved through 90 μm sieve. The detailed procedure for sample preparation for analysis is discussed in section 5.1.1.7.

5.3.2 Results and discussion

Water tightness

Water tightness test was conducted on the CW, BFA15 and BSF15 repaired 50×100 mm cylindrical specimens after 28 days of respective curing. Figure 5.26 presents the cumulative water absorption against square root of time of repaired concrete specimens with cracks in different orientations. It is evident from the figure that water absorption is least in bio treated specimens irrespective of the orientation of crack. It clearly indicates that bio inspired cementitious grouts helped in remediating the cracks and provided an impermeable surface. Among the various orientations of the cracks, the best water tightness was achieved in the case of horizontal, followed by vertical and inverted repaired locations. The slope of water

absorption versus square root of time graph is further used to obtain sorptivity coefficient of the specimens and the values are tabulated in Table 5.4. The values indicate that UT specimens registered highest sorptivity coefficient of 0.035. In all grout repaired concrete specimens, low values of sorptivity coefficient were observed. Lowest sorptivity coefficient was observed in HBFA among all the repaired specimens.

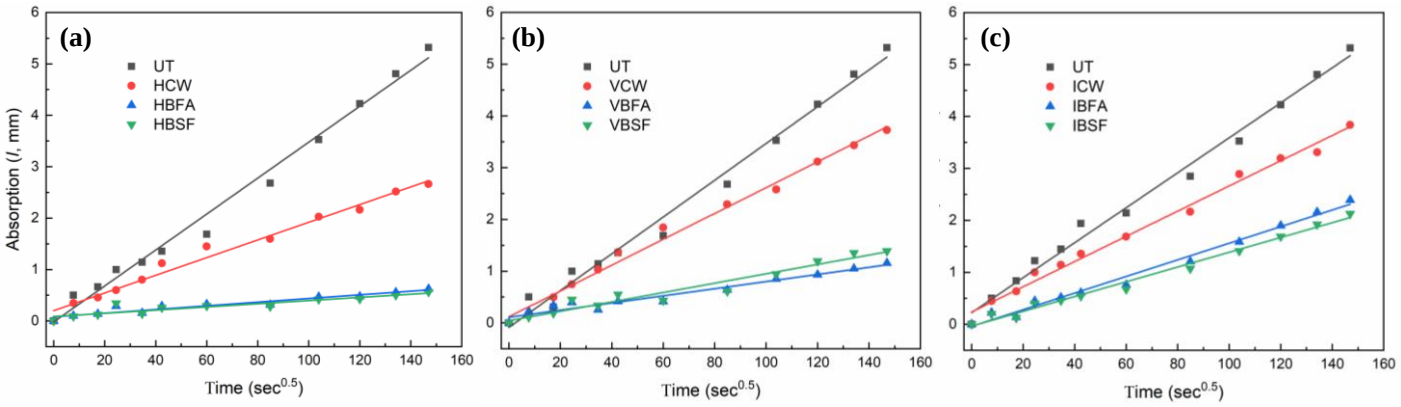

Figure 5.26 Cumulative water absorption of repaired specimen using CW, BFA15 and BSF15

Table 5.4: Sorptivity coefficient of various tested concrete specimens

Specimens	Orientation	Sorptivity cofficient
UT		0.0351
HCW	Horizontal	0.0171
HBFA		0.0035
HBSF		0.0031
VCW	Vertical	0.0249
VBFA		0.0068
VBSF		0.0090
ICW	Inverted	0.0242
IBFA		0.0159
IBSF		0.0140

The lower value of sorptivity in bio inspired grouts was mainly due to the bio-deposition of calcium carbonate precipitated inside in the repaired crack. The formation of stable form of calcium carbonate (calcite) was observed in the pores of cementitious matrix which helps in clogging the pores resulting in low permeability of repaired surface (Amiri et al. 2018; Mohammed et al. 2020; Sidhu et al. 2022).

Among the various orientations of cracks, highest improvement in sorptivity was observed in horizontal location of crack; followed by vertical and inverted locations. It clearly suggests that higher amount of calcium carbonate was precipitated in location where the growth media along the nutrients could ingress into the depth of crack due to capillary effect. The bacterial precipitation was found to be satisfactory even in the vertical and inverted orientations. It further indicated that a modified procedure of retaining the growth media by using foam worked appropriately in achieving calcium carbonate precipitation. The procedure of curing in the inverted orientation can be upgraded with suitable arrangement to get more productive results of bacterial precipitation by MICCP. This is first study successfully implementing the bio-inspired cementitious grout in the inverted direction. Inverted cracks are generally visible in the roof slabs (Jędrzejewska et al. 2020; Venkateshwaran et al. 2021). The bio-inspired cementitious grout can be employed to repair the roof slab cracks.

EMI based monitoring of repaired concrete

To monitor the bacterial precipitation inside the repaired surface, EMI signatures were extracted in the range of 100-250 kHz during the whole curing period for repaired prismatic specimens. The PZT patches were bonded to the control cementitious (CW) and bio-inspired cementitious grouts (BFA15 and BSF15) repaired prismatic concrete specimens only. The conductance versus frequency plots of HCW, HBFA, VBFA, IBFA, HBSF, VBSF and IBSF are shown in Figure 5.27 and 5.28.

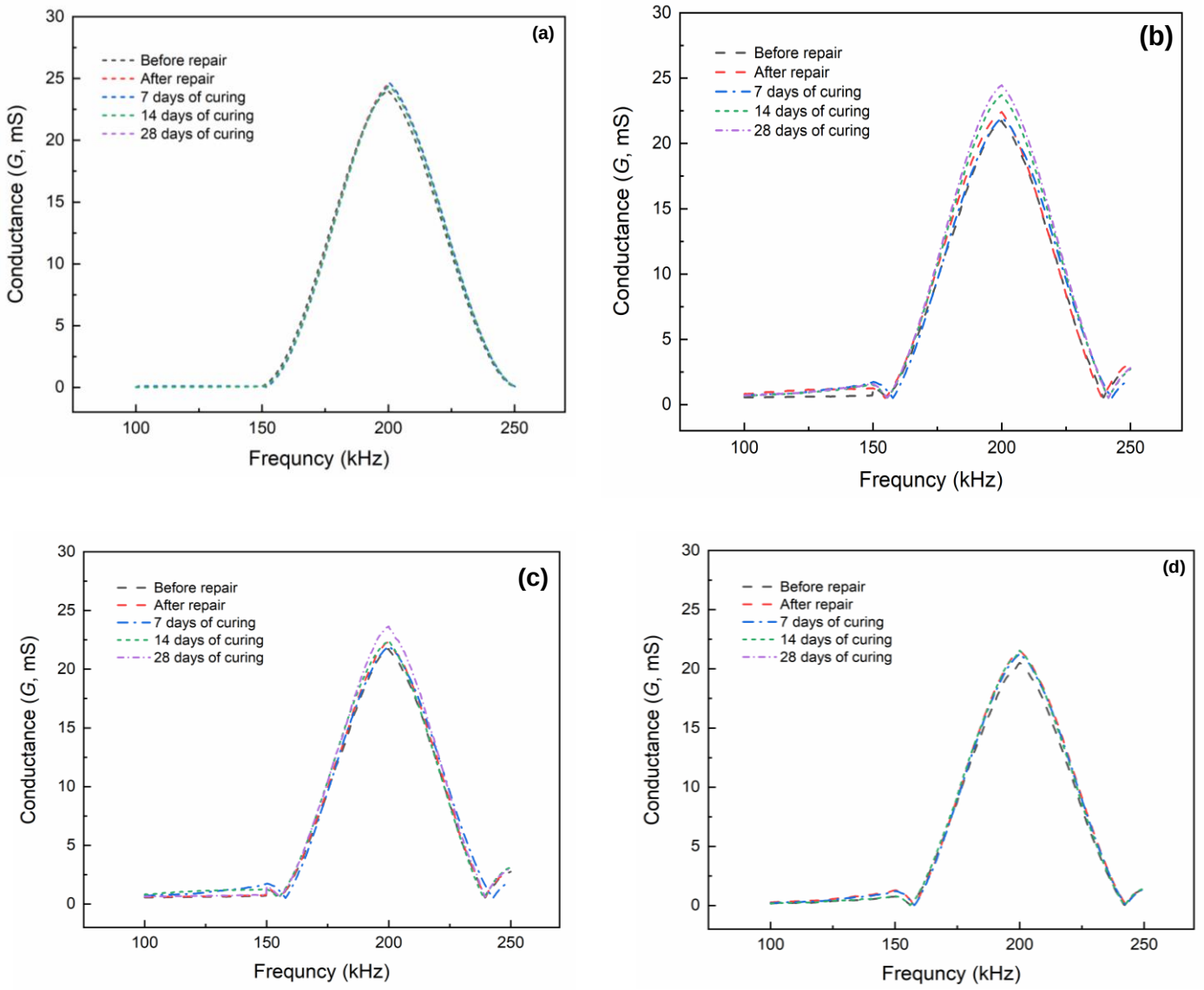

Figure 5.27: Conductance versus frequency plots of (a) HCW (b) HBFA (c) VBFA and (d) IBFA

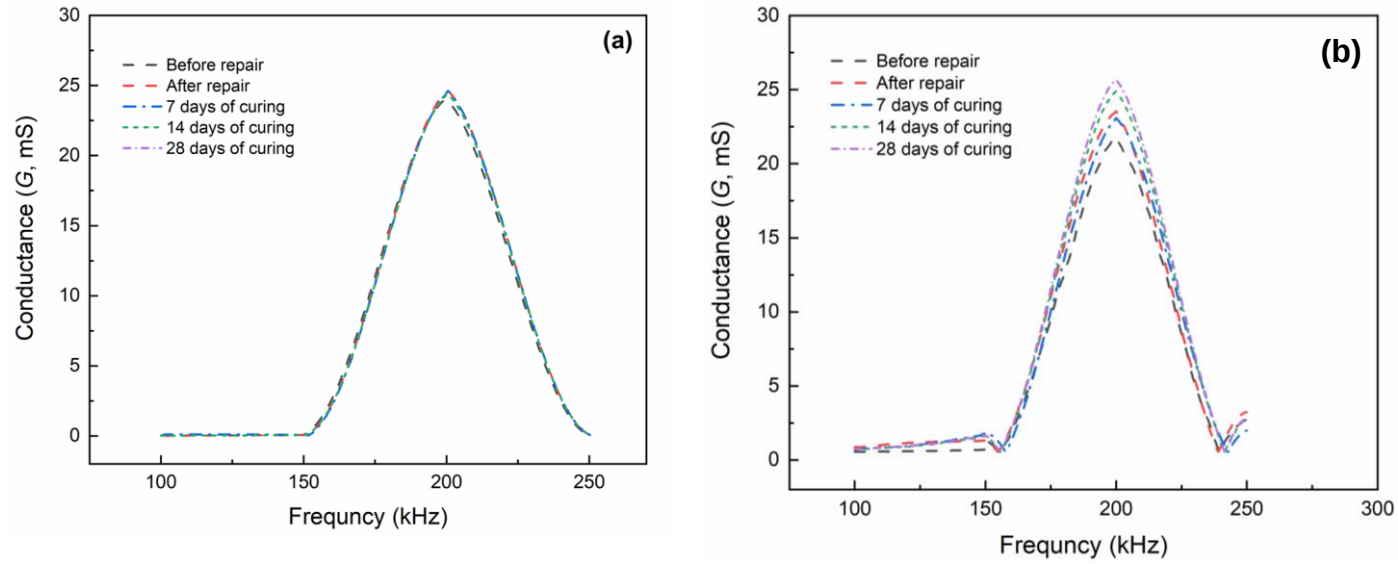

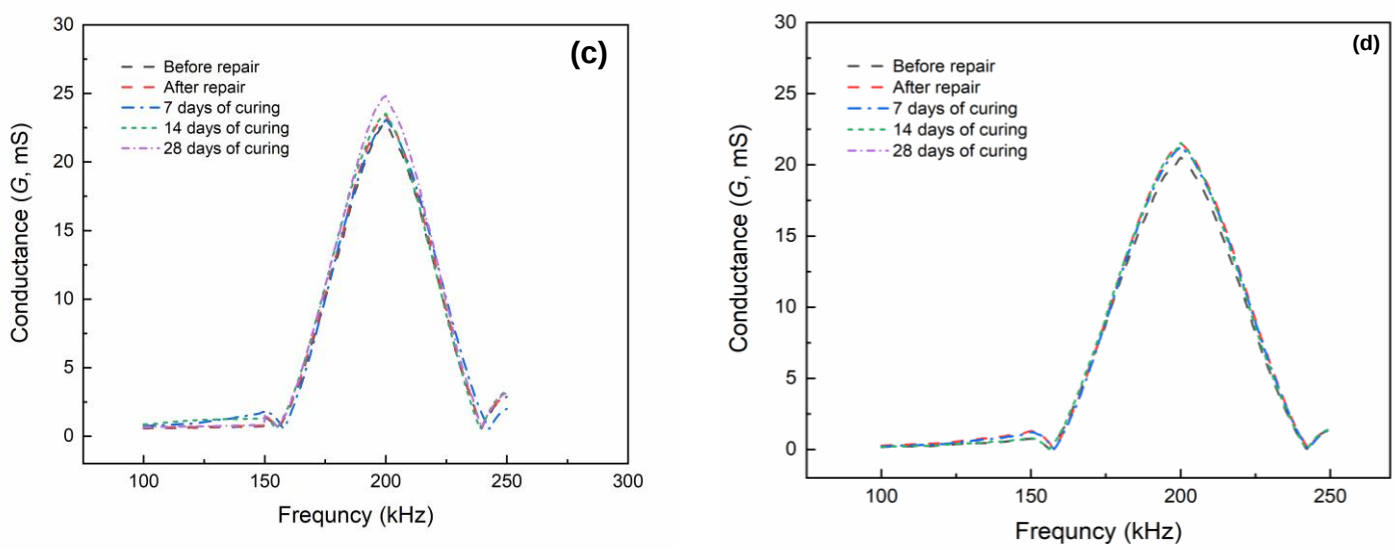

Figure 5.28: Conductance versus frequency plots of (a) HCW (b) HBSF (c) VBSF and (d) IBSF

It can be seen from conductance plots of all the repaired specimens that there was a shift on the resonance peak after the application of grout in the repaired surface, irrespective of the type of grout. The shifting of the resonance peak can be linked with the gain in stiffness of the monitored structure with time (Soh and Bhalla 2005). With the progressive curing of repaired surface, the gradual and vertical shift was observed more predominantly in all the bio-grout repaired specimens. However, minor shift was observed in HCW specimens after 7, 14 and 28 days of water curing indicating no additional stiffness gain in the system. Among the three orientations, maximum shift in resonance peak was observed in the HBFA and HBSF specimens followed by VBFA, VBSF, IBFA and IBSF. This is primarily due to the significant percolation of growth media on the repaired horizontal surface. This leads to maximum calcium carbonate precipitation inside the repaired region. The lateral shift in resonance peaks of VBFA, VBSF, IBFA and IBSF also suggested the application of spray treatment of growth media was adequate in promoting MICCP.

In order to further quantify the pore densification of cementing grout by MICCP, root mean square deviation (RMSD) was employed to study the relative changes in the EM signatures

during the curing process. RMSD values are calculated using Eq. (4.1) over the frequency range of 100-250 kHz. The RMSD plots of various repaired specimens are shown in Figure 5.29.

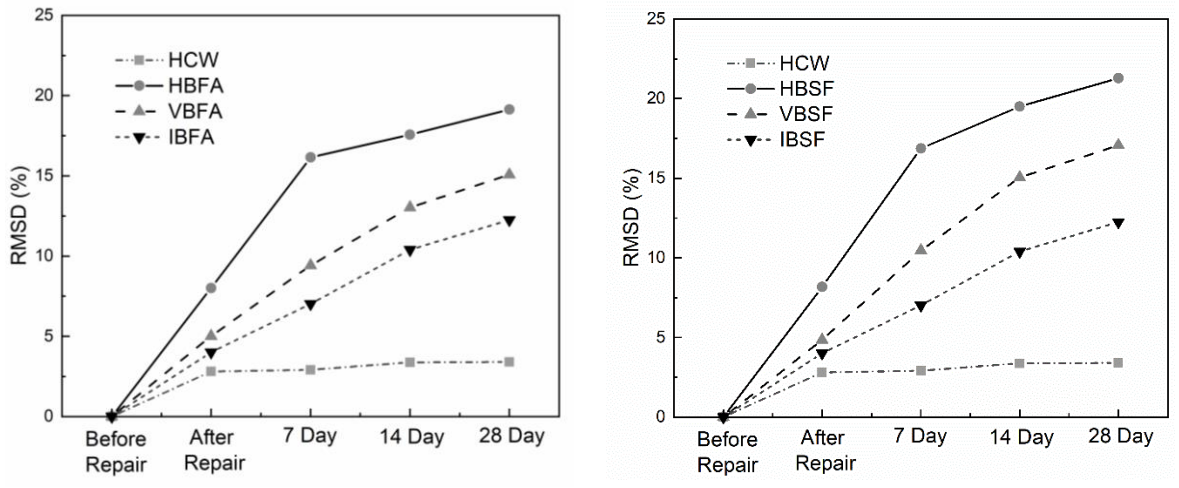

(a) (b)

Figure 5.29: RMSD (%) values of repaired specimens acquired at various curing duration

First major observation from the RMSD plot is regarding the changes observed before and after the application of grout. In HCW specimen, a small change was noted once the CW grout was injected in the fractured surface. The relative change in RMSD (%) values were significantly higher in HBFA and HBSF followed by VBFA, VBSF, IBFA and IBSF after repair. This can be due to higher fluidity of BFA15 and BSF15 as compared to the CW in the cracked surface, which facilitated in superior penetration of the bio-grout slurry inside the fractured surface.

Second observation is regarding progressive changes in RMSD value upon curing till 28 days. No significant change was observed up to 28 days of curing in HCW. Limited change in RMSD value signifies limited gain in stiffness. The RMSD (%) values were found to be higher and progressively improving in the bio-inspired repaired cementitious prismatic specimens, regardless of the orientation of the crack. This signifies better gain in strength and stiffness in prismatic specimens repaired using bio-inspired grouts. After 14 days of respective curing of repaired surface, RMSD (%) values were found to be maximum in HBFA and HBSF specimens. This is obviously due to the better percolation of growth media inside the repaired surface; ultimately leading to higher calcite precipitation inside as well as the top surface of

repaired surface. The RMSD (%) values exhibited little improvement between 14 to 28 days in HBFA and HBSF. This indicates saturation of MICCP activity towards the end of 28 days curing. High content of mineral precipitated was visible over the top of repaired area depicting crack sealing over the surface too. This might be due to the influence of CO_3^{2-} concentration by available bacteria reaching the saturation state as documented by researchers (Anbu et al. 2016). In contrast to HBFA and HBSF after 14 days of curing, lower RMSD (%) values were observed in VBFA, VBSF, IBFA and IBSF. This implies that the orientation of crack plays a key role in the efficiency of proposed methodology. Whereas in VBFA, VBSF, IBFA and IBSF, the RMSD (%) values were found to be in an increasing trend up to 28 days of curing. RMSD (%) values does not saturate at the end of curing treatment (28 days) which signifies bacteria present in bio-repaired surface still has potential to yield the MICCP. Continuous spray of growth media along with other nutrients on the repaired surface after 28 days may result in additional MICCP activity. This is first study implementing EMI technique in crack repairing using bio-inspired cementitious grout. EMI technique was able to capture admittance signature due to the biomineralization by bacteria and EMI technique can be implemented for monitoring of crack sealing in actual RC structures.

Regain in flexural strength

The results obtained in flexural testing are shown in Figure 5.30. It can be noted from the figure that there was significant improvement in strength as compared to UT. Among the various orientations, highest increase in flexural strength was observed in HBFA and HBSF, followed by VBFA, VBSF, IBFA and IBSF. This is due to effective bio-densification of pores and potential of biomineralization precipitates to withstand the bending failure. These findings were in accordance with the earlier observations noted by researchers (Van Tittelboom et al. 2016).

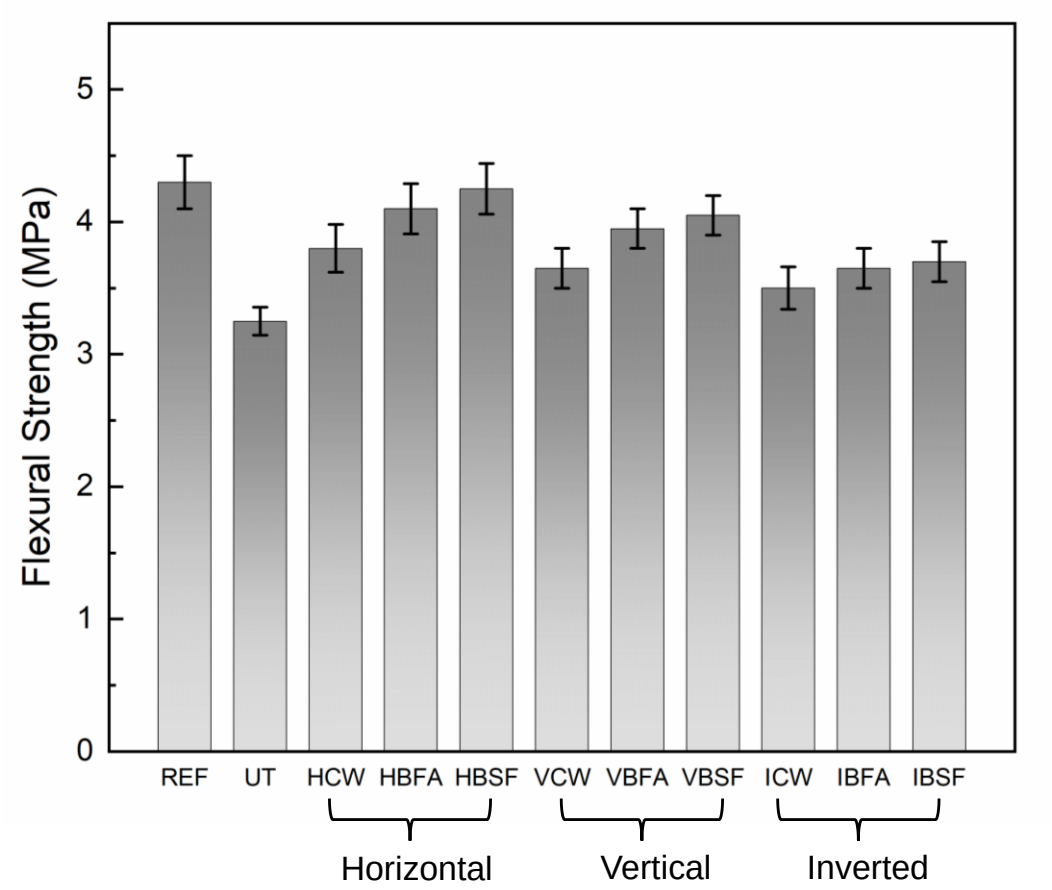

Figure 5.30: Flexural strength results of various prismatic concrete specimens

The lower strength gain in IBFA and IBSF indicates comparably lesser bacterial precipitation in this orientation as compared to the bio deposition possible in horizontal and vertical orientations. It further suggests that more curing of growth media spray supplemented with nutrients will be required to get better regain in strength gain in vertical and inverted orientation. Moreover, HCW and VCW showed marginal gain in strength recovery in contrast to UT specimens. It can be inferred that strength gain in bio-inspired repaired specimens was higher than those repaired with CW grout mix.

Microstructural analysis

For microstructural analysis, samples were collected from HCW, HBFA, HBSF, VBFA, VBSF, IBFA and IBSF repaired prismatic specimen at depth of 10-20mm after bending failure. Figure 5.31 and 5.32 shows the FESEM-EDX images of all tested samples.

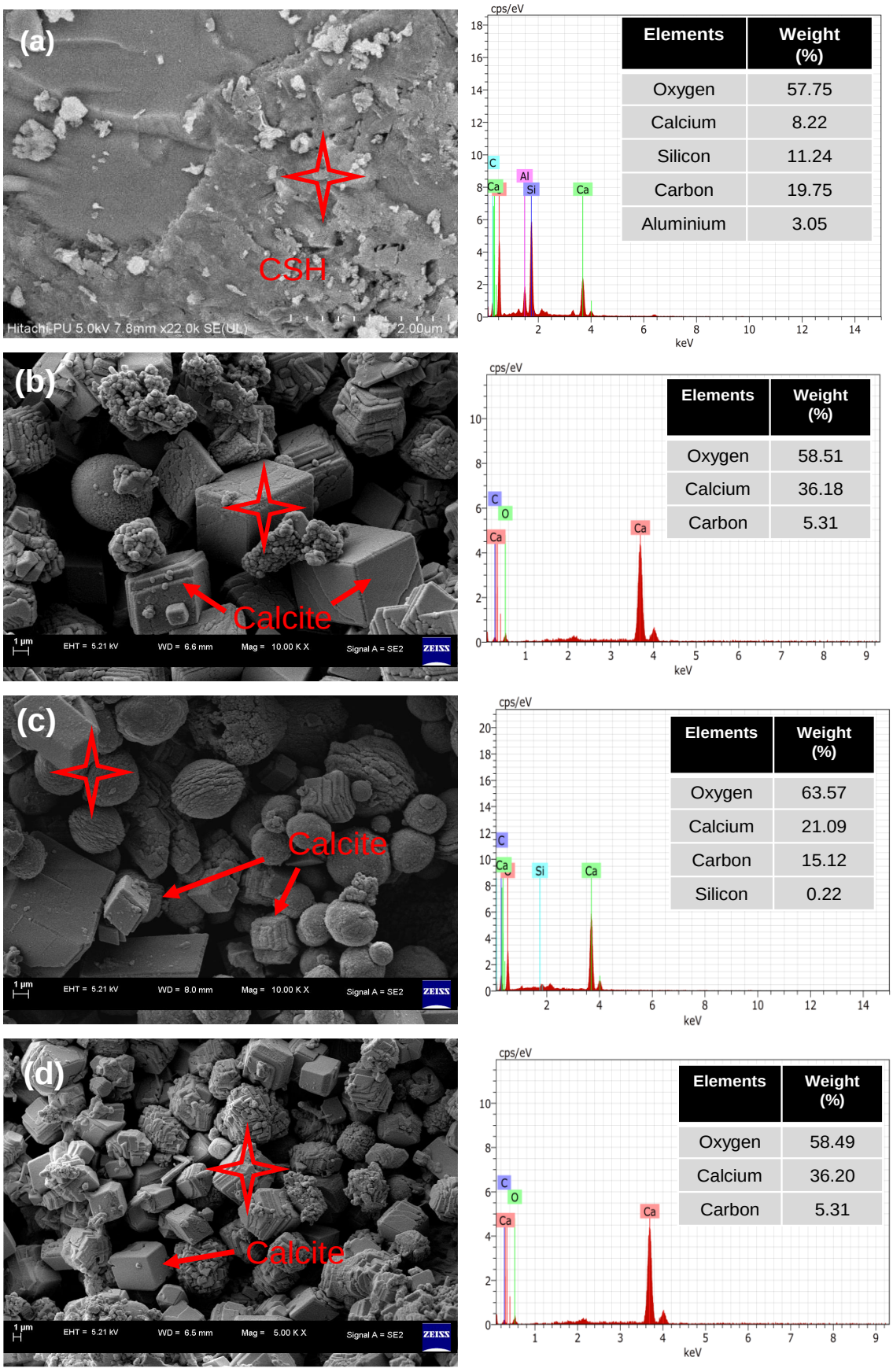

Figure 5.31: FESEM-EDX results of (a) HCW (b) HBFA (c) VBFA (d) IBFA

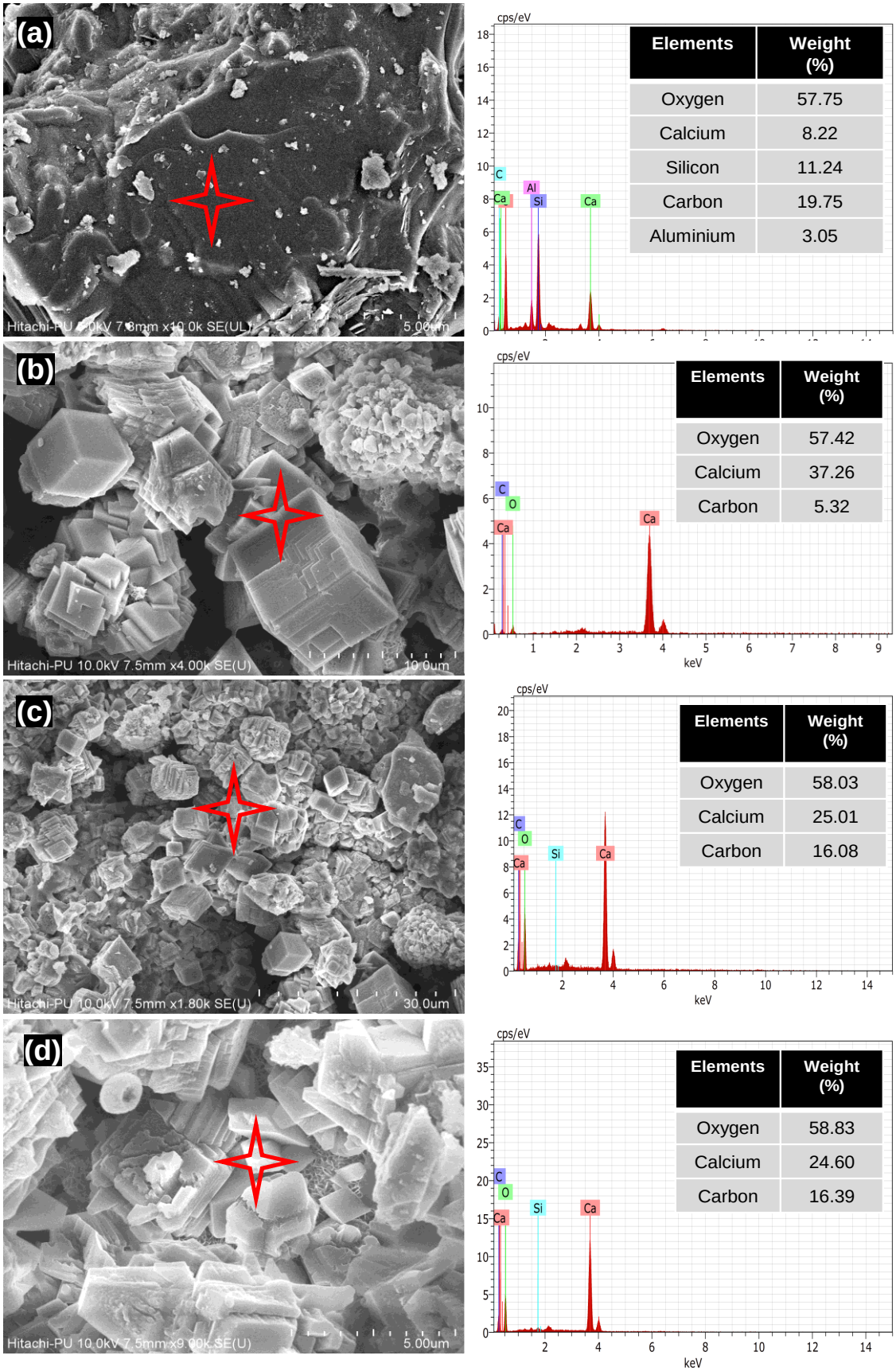

Figure 5.32 FESEM-EDX results of (a) HCW (b) HBSF (c) VBSF (d) IBSF

The results clearly indicate the precipitation of rhombohedral crystals of $CaCO_3$ in bio-cementitious grouts specimens. The size of calcite crystals as observed in Figure 5.31 (b) and (c) are in the range of 3-5 µm, regardless of the orientation of repaired cracks. Researchers also documented the calcite crystals of size (less than 10 µm) are responsible for improved strength of bio-inspired cementing materials (Choi et al. 2016). In the FESEM examination, similar calcite particles were found in all bio-cementitious repaired specimens. Therefore, the presence of calcite provides clear evidence of strength improvement and reduction in permeation characteristics of repaired concrete surface. The results observed in EDX analysis of all bio-cementitious repaired specimens suggested the high amount of calcium, carbon and oxygen which is linked in bacterial precipitation of calcium carbonate. Similar findings were reported by other researchers (Yazdi et al. 2021).

XRD analysis was conducted on the samples collected from HCW, HBFA, VBFA, IBFA, HBSF, VBSF and IBSF specimens. The XRD results are shown in Figure 5.33 and 5.34.

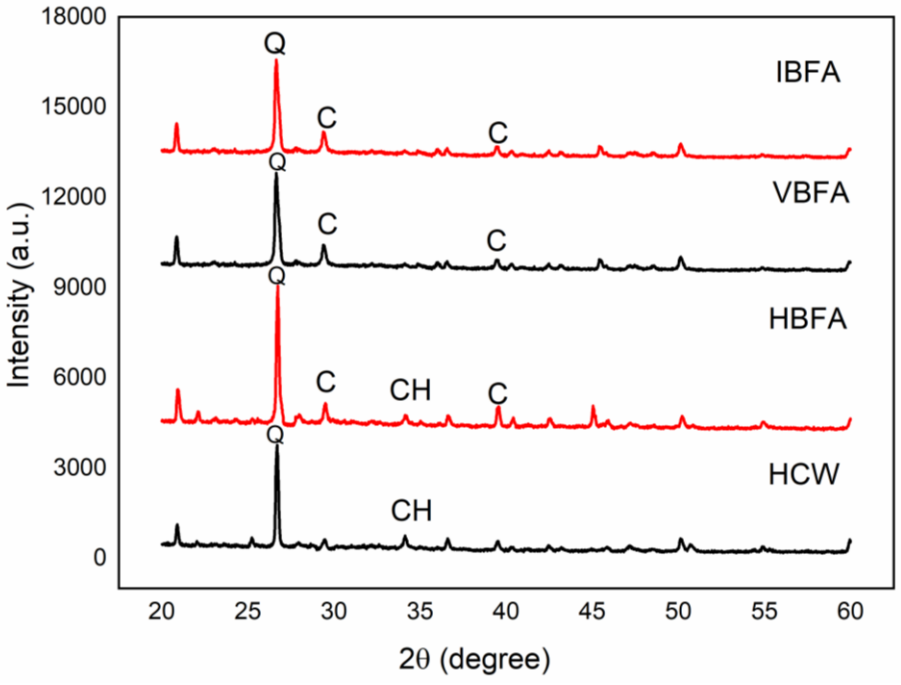

Figure 5.33: XRD results of control, HBFA, VBFA and IBFA specimens (Q: Quartz, CSH: Calcium silicate hydrate, CH: Calcium hydroxide, C: Calcite)

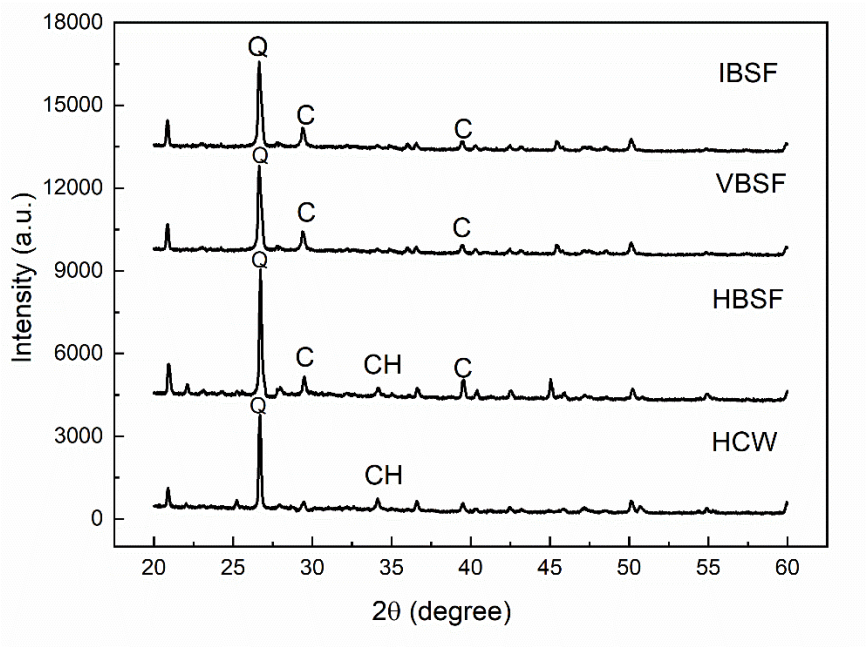

Figure 5.34: XRD results of control, HBSF, VBSF and IBSF specimens (Q: Quartz, CSH: Calcium silicate hydrate, CH: Calcium hydroxide, C: Calcite)

The highest intensity of peak occurred at 2 Theta = 29.2° in all bio-cementitious repaired specimens in comparison to HCW, which is associated to calcite produced in the repaired surface. The findings observed are consistent with other researchers (Tripathi et al. 2019).

5.4 ONSITE REMEDIATION OF CRACKS USING BIO-GROUTS

The efficient BFA15 and BSF15 cementitious grouts as addressed in previous section was employed to repair onsite cracks in concrete structures. Various damaged locations within the institute campus were identified and remediated using the best performing bio-grouts (Figure 5.35). The damaged locations were repaired using injection-based technique and spray cured for 28 days. The growth medium supplemented with urea and calcium chloride were sprayed on the repaired area twice a day till 28 days of curing. During the curing process, to assess the efficiency of bio-grout for MICCP activity, PZT sensor was instrumented near the repaired area and admittance signatures acquired at an interval of 7 days till 28 days.

Figure 5.35: Identified damaged location for application bio-cementitious grout

5.4.1 Material and methods

Installation of PZT and visual examination

To assess the efficiency of bio-cementitious grout for MICCP activity, a PZT sensor was mounted near the damaged location. The experimental set up for the acquiring admittance signature is shown in Figure 5.36.

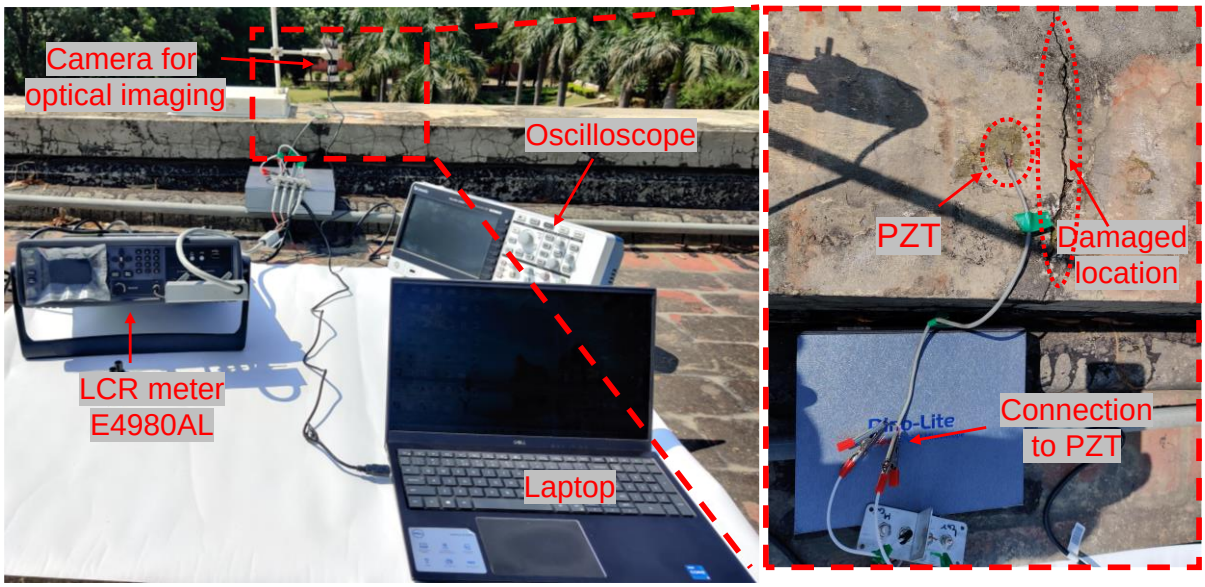

Figure 5.36: Experimental setup for acquiring EMI signatures and optical imaging

PZT (PIC151) sensor was instrumented at distance of 30 mm to the damaged location. Coaxial wires were attached through the process of soldering for making connections to an impedance analyser (E4980Al, Keysight) to capture the admittance signatures. To avoid the disconnection

of wires while experimenting and extra protection of PZT, a thin layer of epoxy was applied and cured for 24 hours. Visual examination was conducted to assess the crack width of the damaged location using Dino-Lite portable camera.

Crack repair using bio-grouting

The fractured surface was repaired using best performing bio-cementitious grouts (BFA15 and BSF15). The injection-based technique was adopted to inject bio-grout inside the cracked surface. The repaired surface was then spray cured using growth medium supplemented with urea and calcium chloride as discussed in section 5.1.1.2. The growth medium was sprayed twice a day till 28 days. The pictorial representation of the damaged surface before and after the application of bio-cementitious grout is shown in Figure 5.37.

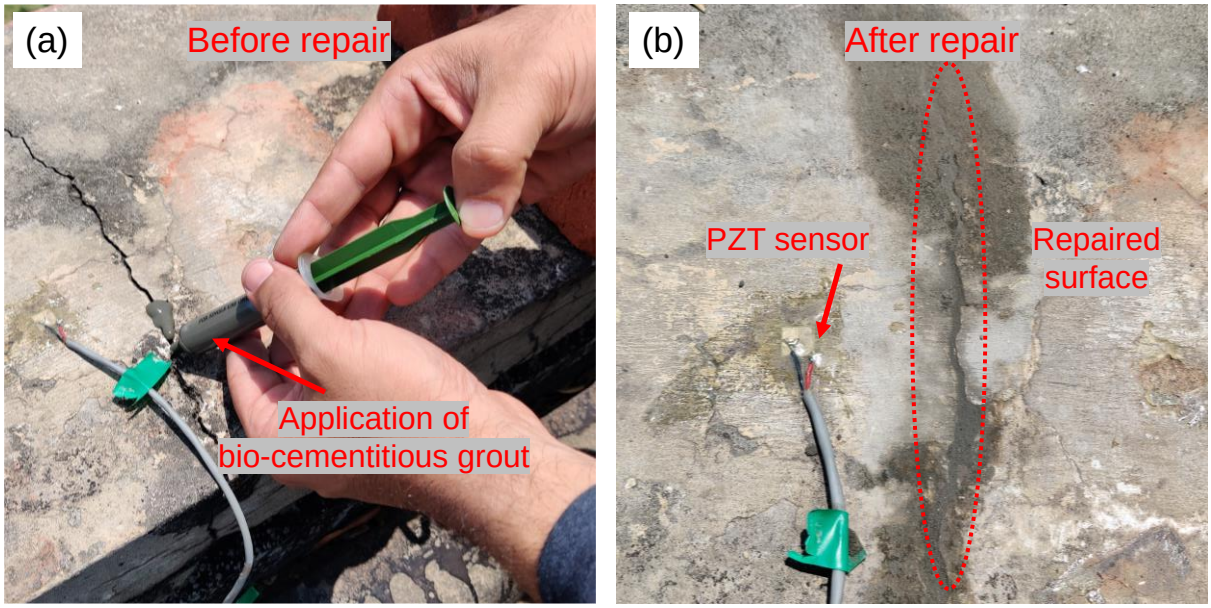

Figure 5.37: Pictorial representation of damaged location (a) Before repair (b) After repair

Microstructure analysis

The sample was collected from the surface of repaired area at the end of curing treatment. The samples were analysed for FESEM-EDX analysis. The same methodology for coating was adopted as discussed in 5.2.1.12.

5.4.2 Results and discussion

EMI monitoring and visual examination

EM signatures was recorded using impedance analyser as discussed before in the frequency range of 100-250 kHz. The acquired EM signatures is shown in Figure 5.38. The vertical shift was observed in the EM admittance signatures before and after repaired the fractured surface. This shift can be correlated to the MICCP activity due to the bacterial inoculum. Further to quantify the changes in EM signatures at various stages, statistical indicator RMSD was employed. The calculated RMSD results are shown in Figure 5.39.

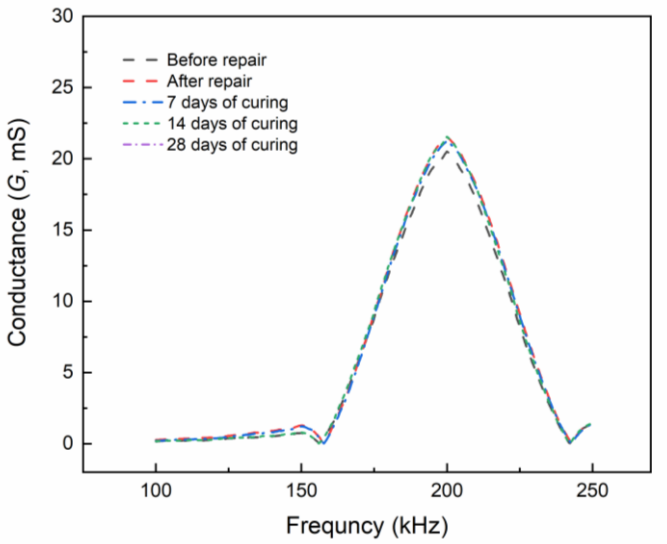

Figure 5.38: EM admittance signatures versus frequency plot

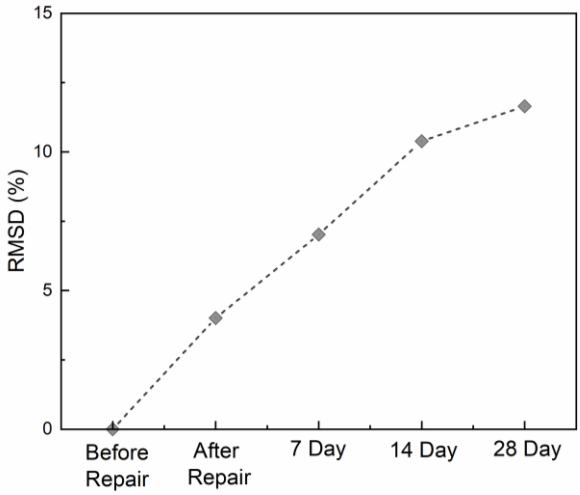

Figure 5.39: RMSD result obtained at various stages of repair to study MICCP activity

Rise in RMSD clearly indicates the bacterial precipitation of calcium carbonate which is responsible for crack sealing. The RMSD value was found to stable after days of bacterial growth media. This suggest adequate calcium carbonate which is effective in clogging the pores. Also, visual examination of the repaired area is shown in Figure 5.40. It clearly indicated the formation of white mineral on the surface of the repaired area.

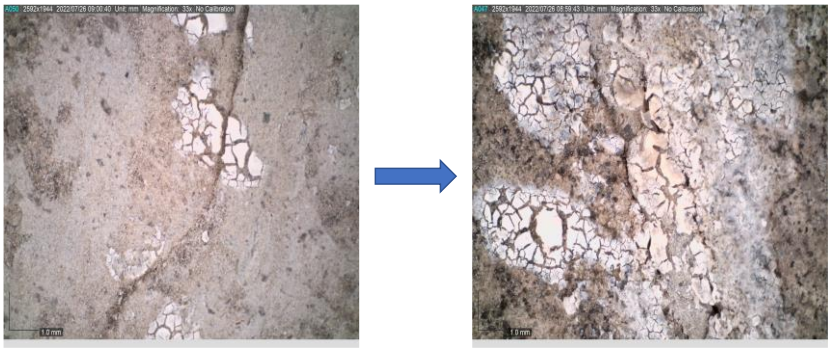

Figure 5.40: Visual examination of repaired surface during curing treatment

The sample from the top surface was collected and assessed for the microstructure using FESEM-EDX. The obtained results are shown in Figure 5.41 and formation of rhombohedral crystal was observed which is stable form of calcium carbonate. These formed crystals helped in clogging the voids which help in reduction of permeability.

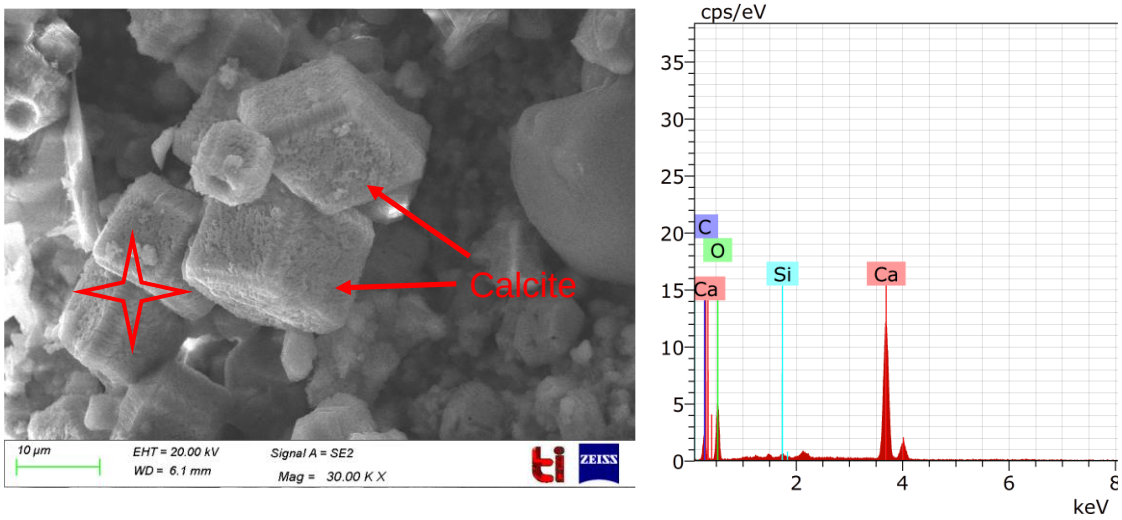

Figure 5.41: FESEM-EDX analysis of the sample collected from the repaired cementitious surface

5.5 CONCLUDING REMARKS

The aim of the present study is to test the effectiveness of mineral inoculums in crack healing for concrete structures. Initially the mineral inoculums were immobilized separately in the concrete elements and crack width of 0.5 mm was healing and monitoring using EMI technique. This targets the self-healing measure in the new concrete structures. Also, to repair the damages in the existing concrete structures, bio-cementitious grouts were developed based on the fresh and hardened properties of the grout. The best performing bio-grouts was used to repair damages in the existing concrete structures.

CHAPTER 6: SUMMARY AND CONCLUSIONS

6.0 GENERAL

The present study aims to develop various mineral inoculums containing efficient bacteria to upscale the microbially induced calcium carbonate precipitation (MICCP) technology for field scale construction. The developed mineral inoculums of sufficient shelf life were immobilized in concrete to study strength, permeation properties, self-healing capabilities and corrosion mitigation. Further to remediate cracks in the existing concrete structures of variable orientations, bio-cementitious grouts were developed and employed to repair cracks in actual concrete structures.

6.1 DEVELOPMENT OF MINERAL CARRIER BASED INOCULUMS

In the present research, fly ash (FA), silica fume (SF), cement kiln dust (CKD) and rice husk ash (RHA) based inoculums were developed and stored at two temperatures (4°C & 25°C). The stored inoculums were tested at an interval of seven days till eleven months to define the shelf life of bacterial product using plate count methods. In CKD and RHA based inoculums, cell count reduced drastically within 28 days of storage indicating that CKD and RHA were not suitable as a carrier material. In FA and SF based inoculums, cell concentration was in the range of 4.5 to 5.2 log cfu/g at both storage temperatures even till 180 days. Based on the cell viability studies, only FA and SF based mineral inoculums were extended as bacterial product to induce MICCP activity in concrete.

6.2 STRENGTH AND PERMEATION PROPERTIES OF BIO-CONCRETE

The selected FA and SF inoculum of 180 days at 4°C were immobilized in concrete supplemented with urea and calcium chloride. The prepared specimens were cured and tested as per BIS 516 (1959). The bacterial admixed specimens made by using fly ash as carrier material (FAA) showed an average increase of 19% and 25% in compressive strength as

compared to the control specimens at 7 and 28 days. The corresponding increase in strength of specimens with silica fume as a carrier material (SFA) specimen was 34% and 32% as compared to the control specimens. Similar observations were observed in improvement of flexural strength at both the testing age. Permeation characteristics was studied as per ASTM C1585 at 28 days of casting. The FA and SF bacterial inoculum (FAA and SFA) supplemented with nutrients led to drastic reduction in sorptivity coefficient values. Even the spray treated specimens (FAS and SFS) showed significant reduction in the sorptivity coefficient. An approximate three-fold reduction in permeation can be attributed to the denser interfacial matrix formed due to the calcium carbonate precipitation between the pore structures of bacterial admixed specimens.

6.3 ANTI-CORROSION ASPECT OF REINFORCED BIO-CONCRETE

In order to study the anti-corrosive potentiol of the developed mineral inoculums, the reinforced concrete (RC) specimens were prepared and cured using FA and SF based inoculum for 28 days respectively. After requisite curing procedure, the test specimens were subjected to accelerated chloride induced corrosion till the crack appeared on the surface of specimens. The changes occurred due to corrosion were assessed using electrochemical and electromechanical impedance (EMI) techniques during the complete test exposure. Along with this, in order to assess the inhibition mechanism of bacterial concrete, concrete powder samples were extracted from the specimens after 28 days of respective curing and was used to prepare electrolytic concrete powder aqueous solution (AQS). The performance of bare steel specimns in AQS contaminated with and without 0.1M NaCl was evaluated by conducting potentiodynamic polarization test. Following conclusions were drawn based on the tests results:

6.3.1 Potentiodynamic polarization curves in concrete powder AQS

The bare steel was immersed in the prepared AQS and corrosion activity was tested at 3, 5 and 10 days of immersion by conducting potentiodynamic polarization test. The preliminary results

without 0.1M NaCl clearly showed the deposition of stable protective layer over the exposed area of steel bar in bacterial concrete powder AQS. The AQS was admixed with 0.1 M NaCl to simulate aggressive chloride environment. Results clearly showed formation of bacterial protective layer that could resist the progressive action of chloride ions on steel surface at 5 days of testing. These results were supported by FESEM-EDX analysis, in which flower shaped cluster was observed on the surface of steel surface. EDX analysis confirmed the presence of Fe, O, Ca and C. This indicated the formation of $CaCO_3$ layer on the steel surface which resisted the attack of chloride ions on the steel surface.

6.3.2 Electrochemical measurements in RC specimens

Open circuit potential and corrosion current density (I_{corr}) were monitored for all the tested specimens. The corrosion current density increased with the exposure duration and entered the active state at 20 days in reference specimen; whereas in bacterial specimens (FAA and SFA) the I_{corr} were found to be stable and in passive state till 80 days of exposure. The better performance of admixed specimens can be attributed to the denser interfacial matrix formed due to $CaCO_3$ between the pore structure of concrete matrix led to lower permeability of the mix, thereby hindering the ingress of aggressive chloride ions. I_{corr} was found to be in passive state till 40 days of exposure in spray treated specimens (FAS and SFS). After 40 days of exposure the I_{corr} increased gradually with the exposure and entered the active corrosion state.

6.3.3 EMI based monitoring

Prepared RC specimens were subjected to accelerated current induced chloride corrosion and monitored using EMI technique. To assess the corrosion on rebar and concrete corrosion, surface bonded piezo sensors (SBPS) and concrete vibration sensor (CVS) were employed. Conductance signatures of both CVS patch and SBPS were recorded, in the frequency range of 20 Hz to 500 kHz during the entire accelerated chloride corrosion exposure. In reference specimen, with the increasing accelerated corrosion exposure after 7 days, the resonance peak

shifted downward suggesting the penetration of chloride ions inside the concrete matrix. Whereas, in FAA, FAS, SFA and SFS specimens, the conductance signatures overlapped each other till 40 days and the lesser shift was observed in resonance peaks with progressive chloride exposure. This is due to bio-deposition formed around the outer surface of concrete due to MICCP. To study the deviation in conductance signatures, root mean square values (RMSD) values were calculated for both SBPS and CVS. RMSD (%) values were found to higher in reference specimen over the complete testing duration. Whereas, lower RMSD (%) values were observed in the bacterial admixed (FAA and SFA) and bacterial spray treated (FAS and SFS) specimens. Among all the tested specimens, lowest RMSD (%) values were noted in the FAA and SFA specimens. The denser interfacial pore refinement due to calcium carbonate deposition was responsible for the delay in the corrosion process.

6.3.4 Correlation between electrochemical and EMI studies

The parameters extracted from electrochemical and EMI techniques were correlated, to understand any possible correlation between the two techniques. A correlation between I_{corr} and RMSD (%) obtained from SBPS and CVS sensors over complete exposure was attempted for all specimens separately. Among CVS and SBPS sensor, SBPS showed better level of correlation (R^2) than CVS sensor in all the specimens. Since the CVS were embedded near to the rebar, it can detect early changes occurring due to ingress of chloride ions only, whereas the SBPS sensors were able to detect and monitor the rebar corrosion in a better way.

6.4 MINERAL INOCULUMS AS SELF-HEALING MEASURE IN CONCRETE

The FA and SF based mineral inoculums were immobilized in concrete and tested for their self-healing abilities. An artificial crack of 0.5 mm width was generated during the casting and healed using a bacteria-based healing agent (nutrient broth, urea and $CaCl_2$). Crack healing efficiency was monitored using EMI technique, visual examination and regain in strength. At the end of testing, the mineral precipitated inside the healed crack was assessed to evaluate its

physicochemical attributes. Full crack healing was achieved at 45 days of treatment and conductance signatures were obtained at an interval of 7 days to assess changes due to MICCP activity. It was noted that in FAA and SFA specimens, with crack sealing, the peak shifts rightwards and at the same time is getting sharper. RMSD showed promising results and only considered for the further studies. Moreover, results indicated that crack width reduction and RMSD were linearly increasing over the test exposure. Significant gain in flexural strength (approximately 30%) was achieved in FAA and SFA in comparison to control specimen. Healed FAA and SFA specimens showed the presence of lamellar rhombohedral crystals of calcium carbonate. This finding was also verified by TGA and XRD results.

6.5 DEVELOPMENT OF BIO-INSPIRED CEMENTITIOUS GROUTS

To repair damages in the existing concrete structures, bio-inspired cementitious grouts containing FA and SF based mineral inoculums were designed. Various bio-grouts were prepared and tested for flowability as per ASTM:C939 (2010), mini-slump as per (Kantro 1980) and bleeding as per ASTM:C940 (2010). Selected bio-inspired grouts based on fresh properties were further tested for setting time (ASTM C953, 2010), mechanical strength (ASTM C109 (2020); ASTM C348, (2020) and drying shrinkage (ASTM C 157 2014). To develop grouts, cement was substituted with FA and SF based inoculum separately by weight, the proportions systemically varied from 10%, 15% and 20%. Based upon fresh and hardened properties, the best results were obtained in 15% cement replacement grout mix. The best performing cementitious bio-grouts were further used for crack repair in existing concrete structures.

6.6 APPLICATION OF BIO-GROUTS FOR REPAIR OF CRACKS

The prepared bio-grout was used to repair an artifical crack of approximately 1.0 mm width. Further, in order to develop the remeditation procedure for variable oritentations of crack, the specimens were placed in such a way that the cracks were oriented in horizontal, vertical and

inverted locations. All the cracks were repaired using ither the control grout (CW) and best performing grouts (BFA15 and BSF15). For supplying the growth media/water in the horizontal orientation, a small pond was created around the crack with the acrylic frame and the pond was filled with 50 ml growth media/water. For vertical orientation, spray treatment was employed in which growth media/water was sprayed twice a day till 28 days. In case of inverted orientation, a foam was mounted below the repaired surface so as to have retention of the growth media/water for longer duration. The effectiveness of bacterial grouting procedure was tested using water tightness test as per ASTM C1585 (2020), EMI monitoring, regain in strength and microstructural analysis. Results indicated that the bio-inspired repaired procedure helped in improving the flexural strength and water tightness in all the tested orientations. Maximum improvement was observed in horizontal, followed by vertical and inverted orientations in comparison to untreated specimens. RMSD was found to be promising measure to quantify the pore densification of cementing grout by MICCP. Moreover, microstructure analysis clearly indicated the presence of rhombohedral calcite in the bio-repaired cracks. The presence of calcite crystals was majorly responsible for the densification of pores and effective sealing of the cracked surface. The best performing bio-grout was then used to repair cracks in actual concrete structures. The cracked location were identified and bio-grout was injected inside the cracked surface. The repaired surface was then cured using growth media supplemented with nutrients. To assess the MICCP activity, EMI technique was employed during the curing period and at the end samples were extracted for microstructural analysis. Results indicated the presence of calcite crystals responsible for the densification of pores.

6.7 FUTURE PERSPECTIVES

The outcomes of current study clearly demonstrates that the developed and tested bacterial carrier inoculums will promote MICCP to field implementation. Calcium chloride was used in the present study as food for calcifying bacteria to precipitate calcium carbonate, if the dosage

of calcium chloride exceeds the permissible limit of 0.4% of cement weight. This will surely have detrimental effect on the reinforcement. Therefore, alternative calcium sources such as calcium acetate, calcium lactate can be used as food for bacteria to precipitate calcium carbonate. Moreover, to reduce cost of preparing bacterial product, industrial based growth medium such as corn steep liquor can be used over the laboratory based nutrient broth. More studies with the consideration of abovementioned concerns will facilitate the practical implementation of MICCP in construction sector in the near future.

REFERENCES

Achal, V., Mukherjee, A., Goyal, S., and Reddy, M. S. (2012). "Corrosion prevention of reinforced concrete with microbial calcite precipitation." *ACI Materials Journal*, 109(2), 157–164.

Achal, V., Mukherjee, A., and Reddy, M. S. (2011a). "Microbial concrete: Way to enhance the durability of building structures." *Journal of Materials in Civil Engineering*, 23(6), 730–734.

Achal, V., Mukherjee, A., and Sudhakara Reddy, M. (2010). "Characterization of two urease-producing and calcifying Bacillus spp. isolated from cement." *Journal of Microbiology and Biotechnology*, 20(11), 1571–1576.

Achal, V., Mukherjee, A., and Zhang, Q. (2016). "Unearthing ecological wisdom from natural habitats and its ramifications on development of biocement and sustainable cities." *Landscape and Urban Planning*, Elsevier B.V., 155, 61–68.

Achal, V., Pan, X., and Özyurt, N. (2011b). "Improved strength and durability of fly ash-amended concrete by microbial calcite precipitation." *Ecological Engineering*, Elsevier B.V., 37(4), 554–559.

Ahmadi, J., Feirahi, M. H., Farahmand-Tabar, S., and Keshvari Fard, A. H. (2021). "A novel approach for non-destructive EMI-based corrosion monitoring of concrete-embedded reinforcements using multi-orientation piezoelectric sensors." *Construction and Building Materials*, Elsevier Ltd, 273, 121689.

Al-Tabbaa, A., Litina, C., Giannaros, P., Kanellopoulos, A., and Souza, L. (2019). "First UK field application and performance of microcapsule-based self-healing concrete."

Construction and Building Materials, Elsevier Ltd, 208(2019), 669–685.

Alazhari, M., Sharma, T., Heath, A., Cooper, R., and Paine, K. (2018a). "Application of expanded perlite encapsulated bacteria and growth media for self-healing concrete." *Construction and Building Materials*, The Authors, 160, 610–619.

Alazhari, M., Sharma, T., Heath, A., Cooper, R., and Paine, K. (2018b). "Application of expanded perlite encapsulated bacteria and growth media for self-healing concrete." *Construction and Building Materials*, The Authors, 160, 610–619.

Amer Algaifi, H., Abu Bakar, S., Rahman Mohd. Sam, A., Ismail, M., Razin Zainal Abidin, A., Shahir, S., and Ali Hamood Altowayti, W. (2020). "Insight into the role of microbial calcium carbonate and the factors involved in self-healing concrete." *Construction and Building Materials*, Elsevier Ltd, 254, 119258.

Amiri, A., Azima, M., and Bundur, Z. B. (2018). "Crack remediation in mortar via biomineralization: Effects of chemical admixtures on biogenic calcium carbonate." *Construction and Building Materials*, 190, 317–325.

Amiri, A., and Bundur, Z. B. (2018). "Use of corn-steep liquor as an alternative carbon source for biomineralization in cement-based materials and its impact on performance." 165, 655–662.

Anbu, P., Kang, C. H., Shin, Y. J., and So, J. S. (2016). "Formations of calcium carbonate minerals by bacteria and its multiple applications." *SpringerPlus*, Springer International Publishing, 5(1), 1–26.

Angst, U., Elsener, B., Larsen, C. K., and Vennesland, Ø. (2009). "Critical chloride content in reinforced concrete - A review." *Cement and Concrete Research*, Elsevier Ltd, 39(12),

1122–1138.

Ann, K. Y., Jung, H. S., Kim, H. S., Kim, S. S., and Moon, H. Y. (2006). “Effect of calcium nitrite-based corrosion inhibitor in preventing corrosion of embedded steel in concrete.” *Cement and Concrete Research*, 36(3), 530–535.

Araújo, M., Chatrabhuti, S., Gurdebeke, S., Alderete, N., Van Tittelboom, K., Raquez, J. M., Cnudde, V., Van Vlierberghe, S., De Belie, N., and Gruyaert, E. (2018). “Poly(methyl methacrylate) capsules as an alternative to the proof-of-concept’’ glass capsules used in self-healing concrete.” *Cement and Concrete Composites*, Elsevier Ltd, 89, 260–271.

ASTM:C348. (2020). “Flexural strength of hydraulic-cement mortars.” *American Society for Testing and Material*, 04, 1–6.

ASTM:C937. (2016). “Standard Specification for Grout Fluidifier for Preplaced-Aggregate Concrete.” *ASTM International*, i(c), 10–12.

ASTM:C939. (2010). “Standard Test Method for Flow of Grout for Preplaced-Aggregate Concrete (Flow Cone Method).” *ASTM International*, 04(c), 9–11.

ASTM:C940. (2010). “Standard Test Method for Expansion and Bleeding of Freshly Mixed Grouts for Preplaced-Aggregate Concrete in the Laboratory.” *ASTM International*, i(c), 1–3.

ASTM:C953. (2010). “Standard Test Method for Time of Setting of Grouts for Preplaced-Aggregate Concrete in the Laboratory.” *ASTM International*, 87(c), 1–2.

ASTM C 157. (2014). “Standard Test Method for Length Change of Hardened Hydraulic-Cement Mortar and Concrete.” *ASTM International*, 04, 1–7.

ASTM C109/C109M-20. (2020). “Standard Test Method for Compressive Strength of Hydraulic Cement Mortars.” *Annual Book of ASTM Standards*, 04, 11.

ASTM C1585. (2020). “Standard Test Method for Measurement of Rate of Absorption of Water by Hydraulic-Cement Concretes ASTM C 1585:2007.” *American Society for Testing and Materials.*, 1–6.

ASTM C876. (2015). “Corrosion Potentials of Uncoated Reinforcing Steel in Concrete.” 1–7.

ASTM G1-03. (2017). *Standard Practice for Preparing, Cleaning, and Evaluating Corrosion Test Specimens*.

Atiş, C. D., Kiliç, A., and Sevim, U. K. (2004). “Strength and shrinkage properties of mortar containing a nonstandard high-calcium fly ash.” *Cement and Concrete Research*, 34(1), 99–102.

Bains, A., Dhami, N. K., Mukherjee, A., and Reddy, M. S. (2015). “Influence of Exopolymeric Materials on Bacterially Induced Mineralization of Carbonates.” *Applied Biochemistry and Biotechnology*, 175(7), 3531–3541.

Bansal, T., and Talakokula, V. (2021). “Deterioration of structural parameters due to corrosion in prestressed concrete identified by smart probe-based piezo sensor.” *Engineering Research Express*, IOP Publishing, 3(1), 015011.

Basheer, L., Kropp, J., and Cleland, D. J. (2001). “Assessment of the durability of concrete from its permeation properties: A review.” *Construction and Building Materials*, 15(2–3), 93–103.

Beatty, D. N., Williams, S. L., and Iii, W. V. S. (2022). “Biomineralized Materials for Sustainable and Durable Construction.” *Annual Review of Materials Research*.

Beddaa, H., Ben Fraj, A., Lavergne, F., and Torrenti, J. M. (2019). “Effect of potassium humate as humic substances from river sediments on the rheology, the hydration and the strength development of a cement paste.” *Cement and Concrete Composites*, Elsevier, 104(April), 103400.

De Belie, N. (2016). “Application of bacteria in concrete: a critical evaluation of the current status.” *RILEM Technical Letters*, 1, 56.

De Belie, N., Gruyaert, E., Al-Tabbaa, A., Antonaci, P., Baera, C., Bajare, D., Darquennes, A., Davies, R., Ferrara, L., Jefferson, T., Litina, C., Miljevic, B., Otlewska, A., Ranogajec, J., Roig-Flores, M., Paine, K., Lukowski, P., Serna, P., Tulliani, J. M., Vucetic, S., Wang, J., and Jonkers, H. M. (2018). “A Review of Self-Healing Concrete for Damage Management of Structures.” *Advanced Materials Interfaces*, 5(17), 1–28.

De Belie, N., and Wang, J. (2015). “Bacteria-based repair and self-healing of concrete.” *Journal of Sustainable Cement-Based Materials*, 5(1), 35–56.

Bergh, J. M. van der, Miljević, B., Šovljanski, O., Vučetić, S., Markov, S., Ranogajec, J., and Bras, A. (2020). “Preliminary approach to bio-based surface healing of structural repair cement mortars.” *Construction and Building Materials*, 248(x).

Bhaskar, S., Anwar Hossain, K. M., Lachemi, M., Wolfaardt, G., and Otini Kroukamp, M. (2017). “Effect of self-healing on strength and durability of zeolite-immobilized bacterial cementitious mortar composites.” *Cement and Concrete Composites*, Elsevier Ltd, 82, 23–33.

BIS:10262. (2009). “Indian Standard Guidelines for concrete mix design proportioning.” *Bureau of Indian Standards, New Delhi*, New Delhi,India.

BIS 516. (1959). “Method of Tests for Strength of Concrete.” *Bureau of Indian Standards*, 1–30.

Bundur, Z. B., Amiri, A., Erşan, Y. Ç., Boon, N., and De Belie, N. (2017). “Impact of air entraining admixtures on biogenic calcium carbonate precipitation and bacterial viability.” *Cement and Concrete Research*, 98(April), 44–49.

Castro-Alonso, M. J., Montañez-Hernandez, L. E., Sanchez-Muñoz, M. A., Macias Franco, M. R., Narayanasamy, R., and Balagurusamy, N. (2019). “Microbially induced calcium carbonate precipitation (MICP) and its potential in bioconcrete: Microbiological and molecular concepts.” *Frontiers in Materials*, 6(June), 1–15.

Chaerun, S. K., Syarif, R., and Wattimena, R. K. (2020). “Bacteria incorporated with calcium lactate pentahydrate to improve the mortar properties and self-healing occurrence.” *Scientific Reports*, Nature Publishing Group UK, 10(1), 1–10.

Chahal, N., Siddique, R., and Rajor, A. (2012). “Influence of bacteria on the compressive strength, water absorption and rapid chloride permeability of fly ash concrete.” *Construction and Building Materials*, Elsevier Ltd, 28(1), 351–356.

Chaurasia, L., Bisht, V., Singh, L. P., and Gupta, S. (2019). “A novel approach of biomineralization for improving micro and macro-properties of concrete.” *Construction and Building Materials*, Elsevier Ltd, 195, 340–351.

Choi, S. G., Wang, K., and Chu, J. (2016). “Properties of biocemented, fiber reinforced sand.” *Construction and Building Materials*, Elsevier Ltd, 120, 623–629.

Choi, S. G., Wang, K., Wen, Z., and Chu, J. (2017). “Mortar crack repair using microbial induced calcite precipitation method.” *Cement and Concrete Composites*, Elsevier Ltd,

83, 209–221.

Dai, J. G., Akira, Y., Wittmann, F. H., Yokota, H., and Zhang, P. (2010). “Water repellent surface impregnation for extension of service life of reinforced concrete structures in marine environments: The role of cracks.” *Cement and Concrete Composites*, Elsevier Ltd, 32(2), 101–109.

Davies, R., Teall, O., Pilegis, M., Kanellopoulos, A., Sharma, T., Jefferson, A., Gardner, D., Al-Tabbaa, A., Paine, K., and Lark, R. (2018). “Large scale application of self-healing concrete: Design, construction, and testing.” *Frontiers in Materials*, 5(September), 1–12.

Dhami, N. K., Mukherjee, A., and Reddy, M. S. (2013a). “Viability of calcifying bacterial formulations in fly ash for applications in building materials.” *Journal of Industrial Microbiology and Biotechnology*, 40(12), 1403–1413.

Dhami, N. K., Reddy, M. S., and Mukherjee, A. (2013b). “Bacillus megaterium mediated mineralization of calcium carbonate as biogenic surface treatment of green building materials.” *World Journal of Microbiology and Biotechnology*, 29(12), 2397–2406.

Dhami, N. K., Reddy, M. S., and Mukherjee, M. S. (2013c). “Biomineralization of calcium carbonates and their engineered applications: A review.” *Frontiers in Microbiology*, 4(OCT), 1–13.

Du, W., Qian, C., and Xie, Y. (2022). “Demonstration application of microbial self-healing concrete in sidewall of underground engineering: A case study.” *Journal of Building Engineering*, Elsevier Ltd, 63(PA), 105512.

Dzionek, A., Wojcieszyńska, D., and Guzik, U. (2016). “Natural carriers in bioremediation: A review.” *Electronic Journal of Biotechnology*, 23, 28–36.

Erşan, Y. Ç., Hernandez-Sanabria, E., Boon, N., and De Belie, N. (2016a). “Enhanced crack closure performance of microbial mortar through nitrate reduction.” *Cement and Concrete Composites*, 70, 159–170.

Ersan, Y. C., Palin, D., Yengec Tasdemir, S. B., Tasdemir, K., Jonkers, H. M., Boon, N., and De Belie, N. (2018). “Volume fraction, thickness, and permeability of the sealing layer in microbial self-healing concrete containing biogranules.” *Frontiers in Built Environment*, 4(November), 1–11.

Ersan, Y. Ç., Silva, F. B. Da, Nico Boon, Willy Verstraete, and Nele De Belie. (2015). “Screening of bacteria and concrete compatible protection materials.” *Construction and Building Materials*, 88, 196–203.

Erşan, Y. Ç., Van Tittelboom, K., Boon, N., and De Belie, N. (2018). “Nitrite producing bacteria inhibit reinforcement bar corrosion in cementitious materials.” *Scientific Reports*.

Erşan, Y. Ç., Verbruggen, H., De Graeve, I., Verstraete, W., De Belie, N., and Boon, N. (2016b). “Nitrate reducing CaCO3 precipitating bacteria survive in mortar and inhibit steel corrosion.” *Cement and Concrete Research*, 83, 19–30.

Feng, Q., Cui, J., Wang, Q., Fan, S., and Kong, Q. (2018). “A feasibility study on real-time evaluation of concrete surface crack repairing using embedded piezoceramic transducers.” *Measurement*, 122, 591–596.

Ferrara, L., Van Mullem, T., Alonso, M. C., Antonaci, P., Borg, R. P., Cuenca, E., Jefferson, A., Ng, P. L., Peled, A., Roig-Flores, M., Sanchez, M., Schroefl, C., Serna, P., Snoeck, D., Tulliani, J. M., and De Belie, N. (2018). “Experimental characterization of the self-healing capacity of cement based materials and its effects on the material performance: A state of the art report by COST Action SARCOS WG2.” *Construction and Building*

Materials, Elsevier Ltd, 167, 115–142.

Fu, C., Fang, D., Ye, H., Huang, L., and Wang, J. (2021). "Bond degradation of non-uniformly corroded steel rebars in concrete." *Engineering Structures*, Elsevier Ltd, 226(May 2020), 111392.

Gupta, S., Kua, H. W., and Pang, S. D. (2018). "Healing cement mortar by immobilization of bacteria in biochar: An integrated approach of self-healing and carbon sequestration." *Cement and Concrete Composites*, Elsevier Ltd, 86, 238–254.

Gupta, S., Pang, S. D., and Kua, H. W. (2017). "Autonomous healing in concrete by bio-based healing agents – A review." *Construction and Building Materials*, Elsevier Ltd, 146, 419–428.

Han, R., Xu, S., Zhang, J., Liu, Y., and Zhou, A. (2022). "Insights into the effects of microbial consortia-enhanced recycled concrete aggregates on crack self-healing in concrete." *Construction and Building Materials*, Elsevier Ltd, 343(April), 128138.

Haq, M., Bhalla, S., and Naqvi, T. (2020). "Fatigue damage and residual fatigue life assessment in reinforced concrete frames using PZT-impedance transducers." *Cement and Concrete Composites*, Elsevier Ltd, 114(August), 103771.

Hibbing, M. E., Fuqua, C., Parsek, M. R., and Peterson, S. B. (2010). "Bacterial competition: surviving and thriving in the microbial jungle." 8(JaNuary), 15–25.

Hossain, M. R., Sultana, R., Patwary, M. M., Khunga, N., Sharma, P., and Shaker, S. J. (2022). "Self-healing concrete for sustainable buildings. A review." *Environmental Chemistry Letters*, Springer International Publishing, 20(2), 1265–1273.

IS:383. (2016). "Indian Standard Coarse and Fine aggregate for Concrete- Specification."

Bureau of Indian Standards, New Delhi, India, (January), 1–21.

IS 1786. (2008). "High Strength Deformed Steel Bars and Wires for Concrete reinforcement-Specification." *Bureau of Indian Standards, New Delhi*, 1–12.

IS 3812 (Part-1): 2003. (2003). "Pulverized fuel ash — specification. Part 1: For use as Pozzolana in cement, Cement Mortar and Concrete (Second Revision)." *Bureau of Indian Standards, New*.

IS 8112. (2013). *Ordinary Portland Cement, 43 Grade- Specification*. *Bureau of Indian Standards, New Delhi*.

Issa, C. A., and Debs, P. (2007). "Experimental study of epoxy repairing of cracks in concrete." *Construction and Building Materials*, 21(1), 157–163.

Jafarnia, M. S., Khodadad Saryazdi, M., and Moshtaghioun, S. M. (2020). "Use of bacteria for repairing cracks and improving properties of concrete containing limestone powder and natural zeolite." *Construction and Building Materials*, Elsevier Ltd, 242, 118059.

Jędrzejewska, A., Kanavaris, F., Zych, M., Schlicke, D., and Azenha, M. (2020). "Experiences on early age cracking of wall-on-slab concrete structures." *Structures*, 27, 2520–2549.

Jiang, L., Jia, G., Jiang, C., and Li, Z. (2020). "Sugar-coated expanded perlite as a bacterial carrier for crack-healing concrete applications." *Construction and Building Materials*, Elsevier Ltd, 232, 117222.

Jiang, L., Xue, X., Zhang, W., Yang, J., Zhang, H., Li, Y., Zhang, R., Zhang, Z., Xu, L., Qu, J., Song, J., and Qin, J. (2015). "The investigation of factors affecting the water impermeability of inorganic sodium silicate-based concrete sealers." *Construction and Building Materials*, Elsevier Ltd, 93, 729–736.

Jongvivatsakul, P., Janprasit, K., Nuaklong, P., Pungrasmi, W., and Likitlersuang, S. (2019). "Investigation of the crack healing performance in mortar using microbially induced calcium carbonate precipitation (MICP) method." *Construction and Building Materials*, Elsevier Ltd, 212, 737–744.

Jonkers, H. M., and Schlangen, E. (2006). "Self-healing of cracked concrete : A bacterial approach."

Jonkers, H. M., Thijssen, A., Muyzer, G., Copuroglu, O., and Schlangen, E. (2010). "Application of bacteria as self-healing agent for the development of sustainable concrete." *Ecological Engineering*, 36, 230–235.

Joshi, S., Goyal, S., Mukherjee, A., and Reddy, M. S. (2017). "Microbial healing of cracks in concrete: a review." *Journal of Industrial Microbiology and Biotechnology*, Springer Berlin Heidelberg, 44(11), 1511–1525.

Joshi, S., Goyal, S., Mukherjee, A., and Reddy, M. S. (2019). "Protection of concrete structures under sulfate environments by using calcifying bacteria." *Construction and Building Materials*, Elsevier Ltd, 209, 156–166.

Joshi, S., Goyal, S., and Reddy, M. S. (2018a). "Influence of nutrient components of media on structural properties of concrete during biocementation." *Construction and Building Materials*, Elsevier Ltd, 158, 601–613.

Joshi, S., Goyal, S., and Reddy, M. S. (2018b). "Corn steep liquor as a nutritional source for biocementation and its impact on concrete structural properties." *Journal of Industrial Microbiology and Biotechnology*, Springer International Publishing, 45(8), 657–667.

Joshi, S., Goyal, S., and Sudhakara Reddy, M. (2021). "Bio-consolidation of cracks with fly

ash amended biogrouting in concrete structures." *Construction and Building Materials*, Elsevier Ltd, 300, 124044.

Jothi Saravanan, T., Balamonica, K., Bharathi Priya, C., Gopalakrishnan, N., and Murthy, S. G. N. (2017). "Piezoelectric EMI–Based Monitoring of Early Strength Gain in Concrete and Damage Detection in Structural Components." *Journal of Infrastructure Systems*, 23(4), 04017029.

Kalhori, H., and Bagherpour, R. (2017). "Application of carbonate precipitating bacteria for improving properties and repairing cracks of shotcrete." *Construction and Building Materials*, Elsevier Ltd, 148, 249–260.

Kan, L. li, Lv, J. wei, Duan, B. bei, and Wu, M. (2019). "Self-healing of Engineered Geopolymer Composites prepared by fly ash and metakaolin." *Cement and Concrete Research*, Elsevier, 125(July), 105895.

Kantro, D. (1980). "Influence of Water-Reducing Admixtures on Properties of Cement Paste-A Miniature Slump Test." *Cement, Concrete and Aggregates*, 2(2), 95.

Kanwal, M., Khushnood, R. A., Adnan, F., Wattoo, A. G., and Jalil, A. (2023). "Assessment of the MICP potential and corrosion inhibition of steel bars by biofilm forming bacteria in corrosive environment." *Cement and Concrete Composites*, Elsevier Ltd, 137, 104937.

Kanwal, M., Khushnood, R. A., Shahid, M., and Wattoo, A. G. (2022). "An integrated and eco-friendly approach for corrosion inhibition and microstructural densification of reinforced concrete by immobilizing Bacillus subtilis in pyrolytic sugarcane-bagasse." *Journal of Cleaner Production*, Elsevier Ltd, 355(April), 131785.

Karaiskos, G., Tsangouri, E., Aggelis, D. G., Van Tittelboom, K., De Belie, N., and Van

Hemelrijck, D. (2016). “Performance monitoring of large-scale autonomously healed concrete beams under four-point bending through multiple non-destructive testing methods.” *Smart Materials and Structures*, IOP Publishing, 25(5).

Kaur, N., Goyal, S., Anand, K., and Sahu, G. K. (2021). “A cost-effective approach for assessment of pre-stressing force in bridges using piezoelectric transducers.” *Measurement*, Elsevier Ltd, 168(August 2020), 108324.

Kaur, N., Li, L., Bhalla, S., Xia, Y., and Ni, P. (2017). “Integration and evaluation of multiple piezo configurations for optimal health monitoring of reinforced concrete structures.”

Kaur, N. P., Majhi, S., Dhami, N. K., and Mukherjee, A. (2020). “Healing fine cracks in concrete with bacterial cement for an advanced non-destructive monitoring.” *Construction and Building Materials*, Elsevier Ltd, 242, 118151.

Kaur, N., Reddy, M. S., and Mukherjee, A. (2013). “Biomineralization of calcium carbonate polymorphs by the bacterial strains isolated from calcareous sites.” *Journal of Microbiology and Biotechnology*, 23(5), 707–714.

Kawaai, K., Nishida, T., Saito, A., and Hayashi, T. (2022). “Application of bio-based materials to crack and patch repair methods in concrete.” *Construction and Building Materials*, Elsevier Ltd, 340(December 2021), 127718.

Khaliq, W., and Ehsan, M. B. (2016). “Crack healing in concrete using various bio influenced self-healing techniques.” *Construction and Building Materials*, Elsevier Ltd, 102, 349–357.

Khushnood, R. A., Ali, A. M., Faraz Bhatti, M., and Ahmed Khan, H. (2022). “Self-healing fungi concrete using potential strains Rhizopus oryzae and Trichoderma

longibrachiatum." *Journal of Building Engineering*, Elsevier Ltd, 50(January), 104155.

Khushnood, R. A., Qureshi, Z. A., Shaheen, N., and Ali, S. (2020). "Bio-mineralized self-healing recycled aggregate concrete for sustainable infrastructure." *Science of the Total Environment*, Elsevier LTD, 703, 135007.

Kim, H., Liu, X., Ahn, E., Shin, M., Shin, S. W., and Sim, S. H. (2019). "Performance assessment method for crack repair in concrete using PZT-based electromechanical impedance technique." *NDT and E International*, Elsevier Ltd, 104(November 2018), 90–97.

Krishnapriya, S., Babu, D. L. V., and G, P. A. (2015). "Isolation and identification of bacteria to improve the strength of concrete." *Microbiological Research*, Elsevier GmbH., 174, 48–55.

Ksara, M., Newkirk, R., Langroodi, S. K., Althoey, F., Sales, C. M., Schauer, C. L., and Farnam, Y. (2019). "Microbial damage mitigation strategy in cementitious materials exposed to calcium chloride." *Construction and Building Materials*, Elsevier Ltd, 195, 1–9.

Kumari, C., Das, B., Jayabalan, R., Davis, R., and Sarkar, P. (2017). "Effect of nonureolytic bacteria on engineering properties of cement mortar." *Journal of Materials in Civil Engineering*, 29(6), 1–9.

Kunal, Siddique, R., and Rajor, A. (2014). "Influence of bacterial treated cement kiln dust on the properties of concrete." *Construction and Building Materials*, Elsevier Ltd, 52, 42–51.

Lee, Y. S., and Park, W. (2018). "Current challenges and future directions for bacterial self-

healing concrete." *Applied Microbiology and Biotechnology*, Applied Microbiology and Biotechnology, 102(7), 3059–3070.

Li, S., Sha, F., Liu, R., Li, W., Li, Z., and Wang, G. (2017). "Properties of Cement-Based Grouts with High Amounts of Ground Granulated Blast-Furnace Slag and Fly Ash." *Journal of Materials in Civil Engineering*, 29(11), 1–11.

Li, Z., Jin, Z., Wang, P., and Zhao, T. (2021). "Corrosion mechanism of reinforced bars inside concrete and relevant monitoring or detection apparatus: A review." *Construction and Building Materials*, Elsevier Ltd, 279, 122432.

Lin, H., Zhao, Y., Yang, J. Q., Feng, P., Ozbolt, J., and Ye, H. (2019). "Effects of the corrosion of main bar and stirrups on the bond behavior of reinforcing steel bar." *Construction and Building Materials*, Elsevier Ltd, 225, 13–28.

Liu, C., Xu, X., Lv, Z., and Xing, L. (2020). "Self-healing of Concrete Cracks by Immobilizing Microorganisms in Recycled Aggregate." *Journal of Advanced Concrete Technology*, 18(4), 168–178.

Luo, M., Qian, C., and Li, R. (2015). "Factors affecting crack repairing capacity of bacteria-based self-healing concrete." *Construction and Building Materials*, Elsevier Ltd, 87, 1–7.

Mohammed, H., Ortoneda-Pedrola, M., Nakouti, I., and Bras, A. (2020). "Experimental characterisation of non-encapsulated bio-based concrete with self-healing capacity." *Construction and Building Materials*, Elsevier Ltd, 256, 119411.

Mondal, S., and Ghosh, A. (Dey). (2018). "Investigation into the optimal bacterial concentration for compressive strength enhancement of microbial concrete." *Construction and Building Materials*, Elsevier Ltd, 183, 202–214.

Monteiro, P. J. M., Miller, S. A., and Horvath, A. (2017). “Towards sustainable concrete.” *Nature Materials*, Nature Publishing Group, 16(7), 698–699.

Mutitu, K. D., Munyao, M. O., Wachira, M. J., Mwirichia, R., Thiong’o, K. J., and Marangu, M. J. (2019). “Effects of biocementation on some properties of cement-based materials incorporating Bacillus Species bacteria–a review.” *Journal of Sustainable Cement-Based Materials*, Taylor & Francis, 8(5), 309–325.

De Muynck, W., De Belie, N., and Verstraete, W. (2010). “Microbial carbonate precipitation in construction materials: A review.” *Ecological Engineering*, 36(2), 118–136.

De Muynck, W., Cox, K., Belie, N. De, and Verstraete, W. (2008). “Bacterial carbonate precipitation as an alternative surface treatment for concrete.” *Construction and Building Materials*, 22(5), 875–885.

Nain, N., Surabhi, R., Yathish, N. V., Krishnamurthy, V., Deepa, T., and Tharannum, S. (2019). “Enhancement in strength parameters of concrete by application of Bacillus bacteria.” *Construction and Building Materials*, Elsevier Ltd, 202, 904–908.

Nguyen, T. H., Ghorbel, E., Fares, H., and Cousture, A. (2019). “Bacterial self-healing of concrete and durability assessment.” *Cement and Concrete Composites*, Elsevier, 104(June), 103340.

Nimafar, M., Hosseini, S. J., Akhlaghi, A., Samali, B., and Soltaninia, S. (2023). “Effect of Bacterial Carbonate Precipitation on the Durability of Concrete Specimens Exposed to High Temperatures.” *Journal of Materials in Civil Engineering*, 35(1).

Nosouhian, F., Mostofinejad, D., and Hasheminejad, H. (2016). “Concrete Durability improvement in a sulfate environment using bacteria.” *Journal of Materials in Civil*

Engineering, 28(1), 1–12.

Osman, K. M., Taher, F. M., El-tawab, A. A., and Faried, A. S. (2021). "Role of different microorganisms on the mechanical characteristics , self-healing efficiency , and corrosion protection of concrete under different curing conditions." *Journal of Building Engineering*, Elsevier Ltd, 41(January), 102414.

Paine, K. (2016). "Bacteria-based self-healing concrete: Effects of environment, exposure and crack size. in V Wiktor, H Jonkers & A Bertron (eds)." *Proceedings of the RILEM Conference on Microorganisms-Cementitious Materials Interactions., 10, RILEM publications S.A.R.L, Paris, RILEM Conference on Microorganisms- Cementitious Materials Interactions, Delft, Netherlands, 23/06/16*, 3457–3466.

Pan, X., Shi, C., Jia, L., Zhang, J., and Wu, L. (2016). "Effect of Inorganic Surface Treatment on Air Permeability of Cement-Based Materials." *Journal of Materials in Civil Engineering*, 28(3).

Pan, X., Shi, Z., Shi, C., Ling, T. C., and Li, N. (2017). "A review on concrete surface treatment Part I: Types and mechanisms." *Construction and Building Materials*, Elsevier Ltd, 132, 578–590.

Park, G., Sohn, H., Farrar, C. R., and Inman, D. J. (2003). "Overview of piezoelectric impedance-based health monitoring and path forward." *Shock and Vibration Digest*, 35(6), 451–463.

Pei, R., Liu, J., Wang, S., and Yang, M. (2013). "Use of bacterial cell walls to improve the mechanical performance of concrete." *Cement and Concrete Composites*, Elsevier Ltd, 39, 122–130.

Poursaee, A., and Hansson, C. M. (2007). “Reinforcing steel passivation in mortar and pore solution.” *Cement and Concrete Research*, 37(7), 1127–1133.

Pungrasmi, W., Intarasoontron, J., Jongvivatsakul, P., and Likitlersuang, S. (2019). “Evaluation of Microencapsulation Techniques for MICP Bacterial Spores Applied in Self-Healing Concrete.” *Scientific Reports*, 9(1), 1–10.

Qian, C., Zheng, T., Zhang, X., and Su, Y. (2021). “Application of microbial self-healing concrete: Case study.” *Construction and Building Materials*, Elsevier Ltd, 290, 123226.

Rajczakowska, M., Habermehl-Cwirzen, K., Hedlund, H., and Cwirzen, A. (2019). “Autogenous Self-Healing: A Better Solution for Concrete.” *Journal of Materials in Civil Engineering*, 31(9), 1–19.

Ramachandran, S. K., Ramakrishnan, V., and Bang, S. S. (2001). “Remediation of Concrete Using Micro-organisms.” *ACI Material Journal*, 98, 3–9.

Ramdas, V. M., Mandree, P., Mgangira, M., Mukaratirwa, S., Lalloo, R., and Ramchuran, S. (2020). “Establishing miniaturised structural testing techniques to enable high-throughput screening of microorganisms and microbial components for unpaved road stabilisation application.” *Journal of Advanced Research*, Cairo University, 21, 151–159.

Ranjan, P., Soda, K., Chakravarthi, E. K., Mogal, A., Mini, K. M., Soda, P. R. K., Chakravarthi, E. K., Mogal, A., Mini, K. M., Ranjan, P., Soda, K., Chakravarthi, E. K., Mogal, A., and Mini, K. M. (2022). “Statistical and experimental investigation on self-healing of microcracks in cement mortar by encapsulation of calcite precipitating bacteria into expanded perlite.” *Construction and Building Materials*, Elsevier Ltd, 342(PA), 127985.

Rodrigues, R., Gaboreau, S., Gance, J., Ignatiadis, I., and Betelu, S. (2021). “Reinforced

concrete structures: A review of corrosion mechanisms and advances in electrical methods for corrosion monitoring." *Construction and Building Materials*, Elsevier Ltd, 269, 121240.

Rong, H., Wei, G., Ma, G., Zhang, Y., Zheng, X., Zhang, L., and Xu, R. (2020). "Influence of bacterial concentration on crack self-healing of cement-based materials." *Construction and Building Materials*, Elsevier Ltd, 244, 118372.

Ruan, S., Qiu, J., Weng, Y., Yang, Y., Yang, E. H., Chu, J., and Unluer, C. (2019). "The use of microbial induced carbonate precipitation in healing cracks within reactive magnesia cement-based blends." *Cement and Concrete Research*, Elsevier, 115(June 2018), 176–188.

Seifan, M., and Berenjian, A. (2019). "Microbially induced calcium carbonate precipitation: a widespread phenomenon in the biological worldSeifan, M., Berenjian, A., 2019. Microbially induced calcium carbonate precipitation: a widespread phenomenon in the biological world. Appl. Microbiol. Bio." *Applied Microbiology and Biotechnology*, Applied Microbiology and Biotechnology, 103(12), 4693–4708.

Seifan, M., Samani, A. K., and Berenjian, A. (2016). "Bioconcrete: next generation of self-healing concrete." *Applied Microbiology and Biotechnology*, 100(6), 2591–2602.

Sha, F., Li, S., Liu, R., Li, Z., and Zhang, Q. (2018). "Experimental study on performance of cement-based grouts admixed with fly ash, bentonite, superplasticizer and water glass." *Construction and Building Materials*, 161, 282–291.

Sha, F., and Liu, P. (2021). "Development of High-Performance Microfine Cementitious Grout with High Amount of Fly Ash, Silica Fume, and Slag." *Journal of Materials in Civil Engineering*, 33(10), 04021270.

Shaheen, F., and Pradhan, B. (2017). “Influence of sulfate ion and associated cation type on steel reinforcement corrosion in concrete powder aqueous solution in the presence of chloride ions.” *Cement and Concrete Research*, Elsevier Ltd, 91, 73–86.

Shannag, M. J. (2002). “High-performance cementitious grouts for structural repair.” *Cement and Concrete Research*, 32(5), 803–808.

Sharma, A., Sharma, S., Sharma, S., and Mukherjee, A. (2018a). “Investigation of deterioration in corroding reinforced concrete beams using active and passive techniques.” *Construction and Building Materials*, Elsevier Ltd, 161, 555–569.

Sharma, A., Sharma, S., Sharma, S., and Mukherjee, A. (2018b). “Monitoring invisible corrosion in concrete using a combination of wave propagation techniques.” *Cement and Concrete Composites*, Elsevier Ltd, 90, 89–99.

Sharma, B., Singh, A., Joshi, S., and Reddy, M. S. (2022). “Utilization of sandstone waste in cement mortar for sustainable production of building materials through biomineralization.” *Journal of Sustainable Cement-Based Materials*, Taylor & Francis, 0(0), 1–9.

Sharma, D., and Goyal, S. (2020). “Effect of accelerated carbonation curing on near surface properties of concrete.” *European Journal of Environmental and Civil Engineering*, Taylor & Francis, 0(0), 1–22.

Shu, X., Zhao, Y., Liu, Z., and Zhao, C. (2022). “A study on the mix proportion of fiber-polymer composite reinforced cement-based grouting material.” *Construction and Building Materials*, Elsevier Ltd, 328(February), 127025.

Siddique, R. (2006). “Utilization of cement kiln dust (CKD) in cement mortar and concrete-an

overview.” *Resources, Conservation and Recycling*, 48(4), 315–338.

Siddique, R. (2011). “Utilization of silica fume in concrete: Review of hardened properties.” *Resources, Conservation and Recycling*, Elsevier B.V., 55(11), 923–932.

Siddique, R., Singh, K., Kunal, P., Singh, M., Corinaldesi, V., and Rajor, A. (2016). “Properties of bacterial rice husk ash concrete.” *Construction and Building Materials*, Elsevier Ltd, 121, 112–119.

Sidhu, N., Goyal, S., and Reddy, M. S. (2022). “Biomineralization of cyanobacteria Synechocystis pevalekii improves the durability properties of cement mortar.” *AMB Express*, Springer Berlin Heidelberg.

Sidiq, A., Gravina, R., and Giustozzi, F. (2019). “Is concrete healing really efficient? A review.” *Construction and Building Materials*, Elsevier Ltd, 205, 257–273.

Sierra-Beltran, M. G., Jonkers, H. M., and Ortiz, M. (2015). “Field application of self--healing concrete with natural fibres as linings for irrigation canals in Ecuador.” *Fifth International Conference on Self-Healing Materials*, 32.

Sierra-Beltran, M. G., Jonkers, H. M., and Schlangen, E. (2014). “Characterization of sustainable bio-based mortar for concrete repair.” *Construction and Building Materials*, Elsevier Ltd, 67(PART C), 344–352.

Sisomphon, K., Copuroglu, O., and Koenders, E. A. B. (2012). “Self-healing of surface cracks in mortars with expansive additive and crystalline additive.” *Cement and Concrete Composites*, Elsevier Ltd, 34(4), 566–574.

Snoeck, D., Wang, J., Bentz, D. P., and De Belie, N. (2018). “Applying a biodeposition layer to increase the bond of a repair mortar on a mortar substrate.” *Cement and Concrete*

Composites, Elsevier Ltd, 86, 30–39.

Soda, P. R. K., Chakravarthi, K., and Mini, K. M. (2023). "Experimental and statistical investigation on strength and microcracks remediation in cement mortar using expanded vermiculite as a bacterial carrier." *Journal of Building Engineering*, Elsevier Ltd, 63(PB), 105567.

Soh, C. K., and Bhalla, S. (2005). "Calibration of piezo-impedance transducers for strength prediction and damage assessment of concrete." *Smart Materials and Structures*, 14(4), 671–684.

Son, Y., Min, J., Jang, I., Yi, C., and Park, W. (2022). "Development of a novel compressed tablet-based bacterial agent for self-healing cementitious material." *Cement and Concrete Composites*, Elsevier Ltd, 129(February), 104514.

Sowmini, G., and Anand, K. B. (2018). "Properties of cement grout modi fi ed with ultra- fine slag." *Frontiers of Structural and Civil Engineering*, 12(1), 58–66.

Su, Y., Feng, J., Zhan, Q., Zhang, Y., and Qian, C. (2019). "Non-ureolytic microbial self-repairing concrete for low temperature environment." *Smart Materials and Structures*, IOP Publishing, 28(7).

Talakokula, V., and Bhalla, S. (2015). "Reinforcement corrosion assessment capability of surface bonded and embedded piezo sensors for reinforced concrete structures." *Journal of Intelligent Material Systems and Structures*, 26(17), 2304–2313.

Talakokula, V., Bhalla, S., Ball, R. J., Bowen, C. R., Pesce, G. L., Kurchania, R., Bhattacharjee, B., Gupta, A., and Paine, K. (2016). "Diagnosis of carbonation induced corrosion initiation and progression in reinforced concrete structures using piezo-impedance

transducers.” *Sensors and Actuators, A: Physical*, Elsevier B.V., 242, 79–91.

Talakokula, V., Bhalla, S., and Gupta, A. (2014). “Corrosion assessment of reinforced concrete structures based on equivalent structural parameters using electro-mechanical impedance technique.” *Journal of Intelligent Material Systems and Structures*, 25(4), 484–500.

Tan, L., Ke, X., Li, Q., Gebhard, S., Ferrandiz-Mas, V., Paine, K., and Chen, W. (2022). “The effects of biomineralization on the localised phase and microstructure evolutions of bacteria-based self-healing cementitious composites.” *Cement and Concrete Composites*, Elsevier Ltd, 128(August 2021), 104421.

Van Tittelboom, K., Adesanya, K., Dubruel, P., Van Puyvelde, P., and De Belie, N. (2011). “Methyl methacrylate as a healing agent for self-healing cementitious materials.” *Smart Materials and Structures*, 20(12).

Van Tittelboom, K., De Belie, N., De Muynck, W., and Verstraete, W. (2010). “Use of bacteria to repair cracks in concrete.” *Cement and Concrete Research*, Elsevier Ltd, 40(1), 157–166.

Van Tittelboom, K., Wang, J., Araújo, M., Snoeck, D., Gruyaert, E., Debbaut, B., Derluyn, H., Cnudde, V., Tsangouri, E., Van Hemelrijck, D., and De Belie, N. (2016). “Comparison of different approaches for self-healing concrete in a large-scale lab test.” *Construction and Building Materials*, Elsevier Ltd, 107, 125–137.

Tiwari, A., Goyal, S., Luxami, V., Chakraborty, M. K., and Prabhakar, G. (2021). “Assessment of corrosion inhibition efficiency of generic compounds having different functional groups in carbonated pore solution with chlorides and migration ability in concrete.” *Construction and Building Materials*, Elsevier Ltd, 290, 123275.

Tripathi, E., Anand, K., Goyal, S., and Reddy, M. S. (2019). “Bacterial based admixed or spray treatment to improve properties of concrete.” *Sadhana - Academy Proceedings in Engineering Sciences*, Springer India, 44(1), 1–8.

Tsangouri, E., Karaiskos, G., Deraemaeker, A., Van Hemelrijck, D., and Aggelis, D. (2016). “Assessment of Acoustic Emission localization accuracy on damaged and healed concrete.” *Construction and Building Materials*, Elsevier Ltd, 129, 163–171.

Van Tuan, N., Ye, G., Van Breugel, K., and Copuroglu, O. (2011). “Hydration and microstructure of ultra high performance concrete incorporating rice husk ash.” *Cement and Concrete Research*, Elsevier Ltd, 41(11), 1104–1111.

Tziviloglou, E., Van Tittelboom, K., Palin, D., Wang, J., Sierra-Beltrán, M. G., Erşan, Y. Ç., Mors, R., Wiktor, V., Jonkers, H. M., Schlangen, E., and De Belie, N. (2016). “Bio-based self-healing concrete: From research to field application.” *Advances in Polymer Science*, 273, 345–386.

Uchikawa, H., Hanehara, S., and Sawaki, D. (1997). “The role of steric repulsive force in the dispersion of cement particles in fresh paste prepared with organic admixture.” *Cement and Concrete Research*, 27(1), 37–50.

Vaezi, M., Zareei, S. A., and Jahadi, M. (2020). “Recycled microbial mortar: Effects of bacterial concentration and calcium lactate content.” *Construction and Building Materials*, Elsevier Ltd, 234, 117349.

Vahabi, A., Ramezanianpour, A. A., and Akbari Noghabi, K. (2015). “A preliminary insight into the revolutionary new line in improving concrete properties using an indigenous bacterial strain Bacillus licheniformis AK01, as a healing agent.” *European Journal of Environmental and Civil Engineering*, 19(5), 614–627.

Vasumithran, M., Anand, K. B., and Sathyan, D. (2020). “Effects of fillers on the properties of cement grouts.” *Construction and Building Materials*, Elsevier Ltd, 246, 118346.

Venkateshwaran, A., Krishnan, P., and Liew, J. Y. R. (2021). “Fiber-reinforced mortar for secondary roofing slabs.” *Structural Concrete*, 22(3), 1873–1887.

Wang, J. Y., De Belie, N., and Verstraete, W. (2012a). “Diatomaceous earth as a protective vehicle for bacteria applied for self-healing concrete.” *Journal of Industrial Microbiology and Biotechnology*, 39(4), 567–577.

Wang, J. Y., Belie, N. De, and Verstraete, W. (2012b). “Diatomaceous earth as a protective vehicle for bacteria applied for self-healing concrete.” *J Ind Microbiol Biotechnol*, 39, 567–577.

Wang, J. Y., Snoeck, D., Van Vlierberghe, S., Verstraete, W., and De Belie, N. (2014). “Application of hydrogel encapsulated carbonate precipitating bacteria for approaching a realistic self-healing in concrete.” *Construction and Building Materials*, Elsevier Ltd, 68, 110–119.

Wang, X. F., Yang, Z. H., Fang, C., Han, N. X., Zhu, G. M., Tang, J. N., and Xing, F. (2019a). “Evaluation of the mechanical performance recovery of self-healing cementitious materials – its methods and future development: A review.” *Construction and Building Materials*, Elsevier Ltd, 212, 400–421.

Wang, X., Huang, Y., Huang, Y., Zhang, J., Fang, C., Yu, K., Chen, Q., Li, T., Han, R., Yang, Z., Xu, P., Liang, G., Su, D., Ding, X., Li, D., Han, N., and Xing, F. (2019b). “Laboratory and field study on the performance of microcapsule-based self-healing concrete in tunnel engineering.” *Construction and Building Materials*, Elsevier Ltd, 220, 90–101.

Wang, X., Xu, J., Wang, Z., and Yao, W. (2022). “Use of recycled concrete aggregates as carriers for self-healing of concrete cracks by bacteria with high urease activity.” *Construction and Building Materials*, Elsevier Ltd, 337(December 2021), 127581.

Wiktor, V., and Jonkers, H. M. (2011). “Quantification of crack-healing in novel bacteria-based self-healing concrete.” *Cement and Concrete Composites*, Elsevier Ltd, 33(7), 763–770.

Wiktor, V., and Jonkers, H. M. (2015). “Field performance of bacteria-based repair system: Pilot study in a parking garage.” *Case Studies in Construction Materials*, Elsevier Ltd., 2, 11–17.

Wu, M., Hu, X., Zhang, Q., Xue, D., and Zhao, Y. (2019). “Growth environment optimization for inducing bacterial mineralization and its application in concrete healing.” *Construction and Building Materials*, Elsevier Ltd, 209, 631–643.

Xiao, X., Tan, A. C. Y., Unluer, C., and Yang, E. (2023). “Development of a functionally graded bacteria capsule for self-healing concrete.” *Cement and Concrete Composites*, Elsevier Ltd, 136(October 2022), 104863.

Xiao, X., Unluer, C., and Yang, E. (2022). “Study on the viability of unprotected bacterial spores directly embedded in a reactive magnesia cement matrix for potential crack healing.” *Construction and Building Materials*, Elsevier Ltd, 346(May), 128424.

Xu, J., Tang, Y., Wang, X., Wang, Z., and Yao, W. (2020). “Application of ureolysis-based microbial CaCO3 precipitation in self-healing of concrete and inhibition of reinforcement corrosion.” *Construction and Building Materials*, Elsevier Ltd, 265, 120364.

Xu, J., and Wang, X. (2018). “Self-healing of concrete cracks by use of bacteria-containing low alkali cementitious material.” *Construction and Building Materials*, Elsevier Ltd,

167, 1–14.

Yang, D., Xu, G., Duan, Y., and Dong, S. (2022). “Self-healing cement composites based on bleaching earth immobilized bacteria.” *Journal of Cleaner Production*, Elsevier Ltd, 358(December 2021), 132045.

Yang, Z., Hollar, J., He, X., and Shi, X. (2010). “Laboratory assessment of a self-healing cementitious composite.” *Transportation Research Record*, (2142), 9–17.

Yazdi, M. A., Gruyaert, E., Van Tittelboom, K., Boon, N., and De Belie, N. (2021). “Treatment with nano-silica and bacteria to restore the reduced bond strength between concrete and repair mortar caused by aggressive removal techniques.” *Cement and Concrete Composites*, Elsevier Ltd, 120, 104064.

Yi, Y., Zhu, D., Guo, S., Zhang, Z., and Shi, C. (2020). “A review on the deterioration and approaches to enhance the durability of concrete in the marine environment.” *Cement and Concrete Composites*, Elsevier Ltd, 113(May), 103695.

Yunchao, T., Zheng, C., Wanhui, F., Yumei, N., Cong, L., and Jieming, C. (2021). “Combined effects of nano-silica and silica fume on the mechanical behavior of recycled aggregate concrete.” *Nanotechnology Reviews*, 10(1), 819–838.

Zamani, M., Nikafshar, S., Mousa, A., and Behnia, A. (2020). “Bacteria encapsulation using synthesized polyurea for self-healing of cement paste.” *Construction and Building Materials*, Elsevier Ltd, 249, 118556.

Zhang, J., Liu, Y., Feng, T., Zhou, M., Zhao, L., Zhou, A., and Li, Z. (2017). “Immobilizing bacteria in expanded perlite for the crack self-healing in concrete.” *Construction and Building Materials*, Elsevier Ltd, 148, 610–617.

Zhang, L. V, Suleiman, A. R., Mehdizadeh, M., Marani, A., Tuyan, M., and Nehdi, M. L. (2022). “Crack self-healing in alkali-activated slag composites incorporating immobilized bacteria.” *Construction and Building Materials*, Elsevier Ltd, 326(February), 126842.

Zhang, S., Qiao, W. G., Chen, P. C., and Xi, K. (2019). “Rheological and mechanical properties of microfine-cement-based grouts mixed with microfine fly ash, colloidal nanosilica and superplasticizer.” *Construction and Building Materials*, Elsevier Ltd, 212, 10–18.

Zhang, X., Jin, Z., Li, M., and Qian, C. (2021). “Effects of carrier on the performance of bacteria-based self-healing concrete.” *Construction and Building Materials*, Elsevier Ltd, 305(September), 124771.